Dictyostelium discoideum as a Model for the Evaluation of Teratogenic Compounds

A thesis submitted to University College London for the degree of Doctor of Philosophy

Robert P. Baines

2020

University College London

Declaration of Ownership

I, Robert Phillip Baines confirm that the work presented in this thesis is my own. Where information has been derived from other sources, I confirm that this has been indicated in the thesis.

Abstract

Before new chemicals can be put on the market, they must be evaluated for toxicological safety. Evaluating the safety of new chemicals, for either medical, cosmetic or environmental application, is tightly regulated by worldwide legislation. A critical aspect of toxicity evaluation is developmental and reproductive toxicity (DART) testing. Traditionally, DART testing has been conducted *in vivo* in mammalian model systems. In fact, current EU DART testing guidelines accounts for the majority of animals used and the financial costs of new compound compliance testing. Therefore, because of the need to reduce the financial and animal costs associated with DART testing, there is a growing demand for new alternative model systems for toxicity evaluation.

Dictyostelium discoideum is a eukaryotic amoeba which due to its unique developmental cycle has the potential to serve as a non-animal alternative model in DART testing. However, for a new alternative model to be proven effective it must allow for high-throughput screening, whilst maintaining biological complexity; allowing developmental toxicity results to be predictive of mammalian systems. To address these concerns, we developed new high-throughput *D. discoideum* growth and developmental toxicity assays. We use the assays to characterise toxicity across a broad range of test compounds, thereby revealing a significant relationship between *D. discoideum* and mammalian toxicity values. Our data demonstrates that *D. discoideum* has the biological complexity necessary to be predictive of mammalian toxicity. We further assess whether *D. discoideum* could be used to genetically characterise developmentally toxic compounds. Using next generation functional genomic screens, we show how the developmentally toxicity compounds, lithium and VPA can be globally genetically phenotyped. Using this genetic phenotyping approach, we were also able to identify the biological targets and processes that mediate lithium and VPA toxicity. Together, these studies illustrate the potential of *D. discoideum* to be developed as a new alternative model in DART testing.

Impact Statement

Compliance in developmental toxicity testing represents a major obstacle for new compounds to reach the market. During the early stages of a new compound's development alternative models to *in vivo* testing are critical for toxicity evaluation. However, many alternative models are still based on animal systems which contradicts the drive for the 3R's. Additionally, current alternative models generally cannot deliver high-throughput screening with the biological complexity required to assess the underlying mode of action of developmentally toxic compounds. In this research, the validity of developing a *D. discoideum* based teratogen evaluation system was assessed. To our knowledge, this work is the most thorough evaluation of *D. discoideum* for this purpose to date. The results presented here establish a significant correlation between *D. discoideum* and mammalian toxicity values across a large, well-defined cohort of test compounds. Additionally, establishing a parallel phenotyping approach as a compound evaluation assay establishes a concise methodology for global toxicological profiling. This is the first study of significance to demonstrate the efficacy of *D. discoideum* in developmental toxicity evaluation. The ability to screen compounds for developmental toxicity in a fully realised *D. discoideum* system will both increase throughput and reduce financial costs. Furthermore, the *D. discoideum* system also functions as a model in which the molecular targets and biological process affect by developmental toxicity compounds can be screened. The future of developmental toxicity testing is the increased use of non-mammalian alternatives to *in vivo* screening. An operational *D. discoideum* based system will contribute to a reduction in unnecessary mammalian *in vivo* screening. By further developing and refining the *D. discoideum* evaluation system proposed in this study, its integration within a battery of toxicity testing models will become achievable.

Novel high-throughput growth and developmental toxicity assays were constructed and validated in this work, increasing the capacity at which compounds can be screened in *D. discoideum.* The growth assay can (and has been) adapted to assess the growth rate in different research projects involving *D. discoideum.* The high-throughput method adds value to *D. discoideum* research, particularly in compound characterisation, an area of increasing interest in the model. Both of the assays have been developed to be capably performed with simple toxicity endpoint readouts and without the need for extensive *D. discoideum* research experience, thereby demonstrating the capacity to translate the results of this study into an industrial setting.

Table of contents

List of figures

List of tables

List of abbreviations

3R's – Replacement, Reduction and Refinement (of *in vivo* animal testing)

BP – Biological process (GO term category)

cAMP – Cyclic adenosine monophosphate

CAR1 – Cyclic AMP Receptor 1

CLP – Classification, labelling and packaging regulation

DAG – Diacylglycerol

DART – Developmental and reproductive toxicity

DDDC – *Dictyostelium discoideum* developmental cycle assay

DES – Diethylstilbestrol

DGKA – Diacylglycerol kinase

DIF-1 – Differentiation inducing factor 1

DMSO – Dimethyl sulfoxide

DpoA – Prolyl oligopeptidase

dTPns – Developmental toxicological pathway networks

ecmA – Extracellular Matrix protein A

ecmB – Extracellular Matrix protein B

ECVAM – European centre for the validation of alternative methods

EPA – U.S. Environmental protection agency

ESC – Embryonic stem cell

EU – European Union

FACs – Fluorescence-activated cell sorting

FDA – U.S. Food and drugs agency

FETAX – Frog embryo teratogenesis assay

FPR – Fluorescence multiwell plate reader

GFP – Green fluorescent protein

GHS – Globally harmonised system

GO – Gene ontology

GSK-3 – Glycogen synthase kinase 3

GWAS – Genome wide association studies

HDAC – Histone deacetylase

hESC – Human embryonic stem cells

hEST – Human embryonic stem cell test

HTP – High-throughput

IP – Inositol-3-phosphate

IP – Intraperitoneal

IP_3 – Inositol-1,4,5-triphosphate

IV – Intravenous

LC_{50} – Median lethal dose

LD_{50} – Median lethal dose

LOAEL – Lowest observable adverse effect level

mEST – Mouse embryonic stem cell test

MF – Molecular function (GO term category)

MOA – Mode of action

NOAEL – No observable adverse effect level

OECD – Organisation for Economic Co-operation and Development

PI – Phosphatidylinositol

PIP – Phosphatidylinositol - 4 - phosphate

PIP_2 – Phosphatidylinositol 4,5 - bisphosphate

PIP_3 – Phosphatidylinositol (3, 4, 5) - trisphosphate

PKA – Protein kinase A

PSA – Polar surface area

PSF – Prestarvation factor

PstA – Prestalk A

PstAB – Prestalk AB

PstB – Prestalk B

PstO – Prestalk O

REACH – Registration, evaluation, authorisation and restriction of chemicals

REMI – Restriction enzyme-mediated integration

RFP – Red fluorescent protein

VPA – Valproic acid

rWEC – Rodent whole embryo culture assay

UN – United Nations

Acknowledgments

I would like to thank Prof. Chris Thompson for giving me this opportunity and for his help and guidance throughout my PhD. I would also like to thank my industrial supervisors, Ryan Richards-Doran and acknowledge the help of Dr. Kathryn Wolton. I would like to acknowledge the BBSRC and Syngenta for supporting this research project.

Further, I would also like to thank all members of the Thompson lab, past and present, whose help during this work has been invaluable. With special thanks to Dr. Katie Parkinson, Dr. Nicole Gruenheit and Dr. Edward Johnson.

I would especially like to acknowledge the friendship of Dr. Balint Stewart, Dr. Chris Brimson and Dr. William Salvidge.

Finally, I would like to acknowledge the love and support of all my friends and family who have helped me before and during my PhD. Without them I would not have been able to complete this work.

Chapter 1 – Introduction

Before any novel chemical with cosmetic, pharmaceutical or agricultural potential can be employed, it has to be assessed for toxicological safety. Toxicity testing represents a major obstacle for new compounds to reach the market, with an estimated 20% of new compounds lost prior to the final stage of toxicity assessment (1). Toxicity testing covers a wide range of toxicity endpoints. One critical endpoint of toxicity testing is developmental and reproductive toxicity (DART) studies, in which more than 10% of chemicals fail to pass DART regulation (1). Developmental toxicity testing is primarily concerned with the potential of chemicals to adversely affect the normal biological development of an organism. Substances that adversely interfere with embryonic development and cause birth defects are known as teratogens. Classifying a chemical's potential teratogenicity is a key aspect of developmental toxicity compliance. Traditionally, developmental toxicity experimentation has been conducted *in vivo* on mammalian model systems. However, there has been a growing demand for the development of alternative model systems for developmental toxicity evaluation (2). This is due to the drive for the 3R's in toxicity screening. The replacement, reduction and refinement (3R's) of *in vivo* animal testing is sought both for ethical reasons, and due to the financial costs of live animal testing. Simultaneously, to the need for 3R's and a reduction in costs, there is an increasing need for developmental toxicology to be proactive in predicting mammalian teratogenicity. However, only in furthering the current understanding of the underlying mechanisms of developmental toxicity will predicting mammalian teratogenicity improve (3).

In this work we present the evaluation of the amoeba, *Dictyostelium discoideum* (*D. discoideum*), to serve as a non-animal alternative model for the evaluation of teratogenic compounds. We demonstrate *D. discoideum's* propensity for high-throughput (HTP) screening and, by implementing parallel phenotyping screens, highlight the potential to both phenotypically and genetically characterise teratogenicity in a microbial system.

1.1 The history of teratology and the advent of teratogen evaluation

1.1.1 The origin and history of teratology

By the late 19th Century, the disparate fields and theories of early embryology had begun to crystallise into the more recognisable, modern field of developmental biology. The rediscovery of the works of Mendel and early experimental work on the embryogenesis of frogs and sea urchins allowed developmental biology to become an increasingly prominent experimental field by the 1930s (4). The increase in research into developmental processes naturally coincided with an interest in abnormal development and its causes (5). The field of biology concerned with the study of developmental abnormalities, teratology, rose in tandem with developmental biology. However, until the 1930s, teratology was predominantly a descriptive science, with the documentation of birth defects the primary pursuit (6). It has been known and suspected for centuries that certain chemicals can cause birth defects. For example, the drinking of ethanol has, since time immemorial, been a suspected teratogen (7). However, the transition of teratology into a modern experimental science in the 1930s was due to a series of investigative studies into the causes of deformity. The first modern experimental study consisted of feeding pregnant pigs a vitamin A deficient diet and recording the variety of malformations in the piglets (8). Further studies led to the conclusion that environmental factors induce structural birth defects (9). At first, dietary limitations and other environmental factors were the focal point of teratology research. However, by the 1950s, many drugs and chemicals substances had been demonstrated to induce teratogenicity in the mammalian embryo (10–12). Chemicals including hormones, androgens and vitamins were increasingly being screened in model *in vivo* systems to test their exogenous effects on developmental malformations (9).

By the mid-20th century, genetic, nutritional, infectious and chemical factors were established as key teratogenic factors. However, the thalidomide disaster of the 1950's led to an important leap in the awareness of chemically-induced teratogenicity and the screening and study of potential teratogenic compounds. The notoriety of the disaster shifted focus to more stringent drug testing and raised awareness of the possibility of 'non-toxic' teratogenic compounds (13).

1.1.2 The importance of the thalidomide disaster

Thalidomide was first released in 1958, primarily as a sedative. However, its efficacy in treating morning sickness was quickly discovered and promoted. Between its market release and its worldwide ban in 1961, it was one of the highest-selling drugs worldwide (13). A key reason for the rapid adoption of thalidomide was the reported minimal side effects and low toxicity of the drug. The toxicity testing of the time was conducted in rats and reported thalidomide to be safe. Although, the exact nature of the toxicity test conducted remains unknown (14). Almost immediately after thalidomide entered the market, an increase in the global number of birth defects concerning limb abnormalities was reported. Initially, many prominent teratologists were sceptical that thalidomide was the agent behind the increase in reported limb abnormities, as screens conducted on rats resulted in developmental abnormities that were inconsistent with those seen in human patients (15). The prevailing thought at the time was that *in vivo* mammalian testing in a single species was sufficient to predict developmental toxicity in humans. However, basic screening assays in rabbits clearly demonstrated the teratogenic potential of thalidomide (16). The legacy of the disaster is in the lessons learned and the progress made towards modernising teratogen evaluation.

Kim and Scialli (2011) summarise the three key lessons learnt as a result of the thalidomide disaster: firstly, recognition of the difference in the sensitivity and manifestations of different species to the toxicity of compounds; secondly, that seemingly ‘non-toxic’ compounds could cause severe developmental birth defects; and, finally, that all pharmaceutical products should be thoroughly and systematically tested for developmental effects prior to being placed on the market. All of these lessons formed the core thinking behind the subsequent regulation of developmental toxicity screening. In 1966, the U.S Food and Drugs Agency (FDA) formulated regulations for addressing the potential developmental toxic effects of pharmaceutical compounds. The regulations forced developmental toxicity screening towards a bioassay screening basis. All new compounds would have to be stringently evaluated for teratogenicity prior to market release. This attitude and methodology are still relevant and forms the foundation of modern developmental toxicity regulation.

1.1.3. Core principles of teratogenic evaluation

The aims of experimental teratology changed dramatically in the wake of the thalidomide disaster. Increasingly, it was realised that the future of teratogen evaluation was both: effective and universally-applied protocols for compound screening, and furthering the understanding of the underlying mechanisms of action (9,17). It was thought that understanding why certain compounds cause teratogenic effects would positively feedback on the screening process, thus improving accuracy. In 1973, following a decade of increased research into teratogenic compounds, Wilson (1973) collated and published the then current knowledge concerning teratology and formulated the key principles of the field (18). These principles have been continually updated and still form the basis for modern developmental toxicity screening assays (18,19). They can be summarised as follows:

Firstly, susceptibility to teratogenesis depends on both the genotype of the embryo and the developmental stage at which exposure occurs (17). Inter- and intra- species variation is always a consideration in teratogenic screening and continues to be relevant considering the increased use of non-mammalian evaluation models (20). This principle strongly informs the current teratogen safety compliance legislations (Section 1.1.4) as well as the development and usage of modern alternative models (Section 1.2).

Secondly, teratogenic agents act through specific, and sometimes through multiple, mechanisms. This principle has led researchers to recognise the importance of understanding the underlying molecular mechanisms of toxicity. By characterising the mechanism of action of a single teratogenic compound, other drugs known to have therapeutic targets which affect the same molecular mechanisms can be labelled as high risk for teratogenicity. Beedie *et al* (2016) demonstrated the importance of knowing the molecular mechanism of action of teratogenic compounds using thalidomide (21). Research on thalidomide has shown that its teratogenicity is mediated by adversely affecting angiogenesis (22,23) . By screening a cohort of anti-angiogenesis therapeutics, Beedie *et al* (2016) found all the compounds tested caused teratogenicity. Thus, furthering the understanding of the molecular actions of known teratogens will inform both novel compound design and future evaluation protocols.

Thirdly, tissue and cellular access in the developing organism depends on the chemical nature of the teratogenic agent. It has long been known that the developmental toxicity of specific compounds can be affected by factors such as route of absorption, protein binding affinity and maternal/foetal transfer (24) . Whilst these physical factors

are clearly important for higher multicellular organisms, simple parameters such as a compound's solubility can also have implications on alternative evaluation models (25).

Finally, the adverse effect of toxicity on development increases with a compound's dosage, from no-effect to a lethal outcome (17). This principle is important because it underlines two concepts central to teratogen evaluation: firstly, that all chemicals can be considered developmentally toxic if exposure is sufficiently high; and, secondly, for every teratogen there is a dose at which no adverse effect is observable. This principle can be represented in a teratogenic dose response curve (Figure 1.1). At low doses teratogenicity is not observed. However, as the dose increases, a steep dose response curve is observed followed by a long plateau (Figure 1.1). The steep nature of a teratogen's dose-response curve is the sign of a 'true teratogen'(17). A 'true' teratogen exhibits no effect at low doses but rapidly rises to maximum dose response once a threshold for developmental toxicity is reached (26). This pattern is representative of the threshold principle in that many chemical teratogens elicit their developmental toxicity once an exposure 'threshold' is met. The binary nature of the teratogenic threshold has led to the toxicity measurement known as the NOAEL (**N**o **O**bservable **A**dverse **E**ffect **L**evel). Developmental toxicity measurements, using a NOAEL, allow for the teratogenic classification of chemicals. Compounds that require larger doses (than the reasonable expected exposure level) to adversely affect development are non-teratogens and can be classified as such (Figure 1.1). Taken together, Wilson's updated principles of teratology underline the fundamental nature of compound evaluation and teratogenic classification.

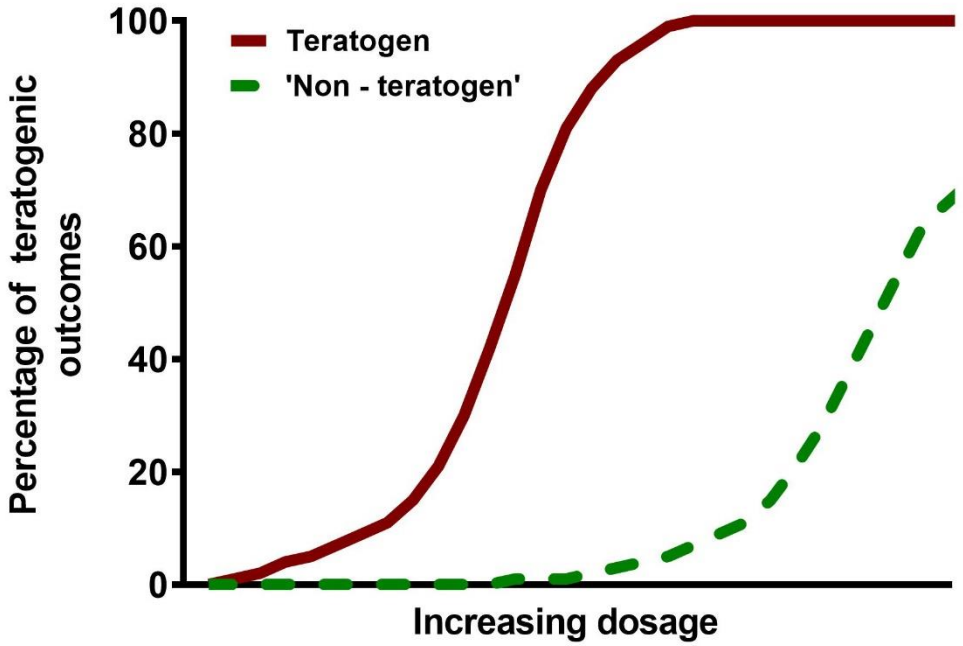

Figure 1.1. A chemical teratogen dose-response curve. A teratogenic compound (red line) requires a lower dose both to reach the minimal and maximum adverse effect response. A compound that requires a dose far greater than the realistic exposure level to exhibit adverse outcomes are classified as non-teratogenic (green line).

1.1.4. Current European Union and international legislation concerning teratogenicity testing and classification

Worldwide, all major legislative bodies currently regulate the evaluation and classification of teratogenic compounds. This regulation is founded on the principles of teratogenicity, stated above, and accounts for both the screening method and biological models needed to legally screen for developmental toxicity. Since the thalidomide disaster, the classification of chemical teratogenicity is primarily used as a safety labelling system. Preventing the human exposure to doses of a chemical that could cause an increased risk of birth defects. Developmental toxicity screening and testing in different political spheres is regulated under different names and laws, however they all share core scientific principles and procedures. The Organisation for Economic Co-operation and Development (OECD), the U.S. Environmental Protection Agency and EU test guidelines for developmental toxicity are the three most implemented testing guidelines (Table 1.1) (27). The guidelines concern *in vivo* toxicity testing and all require dual mammalian testing methodologies with rat and rabbit testing most commonly implemented (28). Ultimately the goal of all developmental toxicity evaluation is ‘safety’, in the form of chemical hazard classification and subsequent labelling.

Table 1.1. Test Guidelines for Reproductive and Developmental Toxicity.

Title	Year
OCED Guidelines	
Prenatal developmental toxicity study	2001
One-generation reproduction toxicity study	1983
Two-generation reproduction toxicity study	2001
Reproduction/developmental toxicity screening test	1995
Combined repeated dose toxicity study with the developmental toxicity screening test	1996
Developmental neurotoxicity study	2003
USA EPA Test Guidelines	
Reproduction/developmental toxicity screening test	1999
Combined repeated dose toxicity study with the development toxicity screening test	1999
Prenatal developmental toxicity study	1998
Reproduction and fertility effects	1998
Developmental neurotoxicity study	1998
EU Annex V Test Methods	
Teratogenicity test – Rodent and non-rodent	2004
One-generation reproduction toxicity test	1988
Two-generation reproduction toxicity test	2004

Adapted from Nielsen *et al*, 2008.

The specific labelling of a compound's teratogenicity differs worldwide, yet generally, the labelling procedure is dependent on the interpretation of the dosing and phenotypic readouts of *in vivo* studies (29). The most widely published classification and labelling system for developmental toxicity is the US FDA pregnancy risk categories (30,31) (Table 1.2). The risk categories range from 'X – Contradicted in pregnancy' to 'A – Controlled studies show no risk' (Table 1.2). Whilst the FDA classification system is concerned with the safe use of medicinal compounds only, other classification systems, including the EU chemical labelling system, concern all chemicals where there is a risk of exposure, including agrochemical applications (32). Although, the developmental toxicity classifications are useful for clinicians and researchers they do not present useful information on the studies and/or data behind the classification (29). This disconnect between the underlying data and the classification itself has, in recent times, led to the US FDA and EU to modifying their approach to teratogenicity testing and classification (29,33). In 2015 the US FDA removed the pregnancy risk categories from packaging; instead increasing the availability of the clinically relevant studies and data (33). However, earlier in 2006 the EU's approach to improving teratogenicity testing and classification was to introduce new thorough guidelines.

Table 1.2. The U.S FDA pregnancy risk categories.

Category	Definition
A	**Controlled Studies show no risk.** Adequate, well-controlled studies in humans have failed to demonstrate risk to the foetus.
B	**No evidence of risk in humans.** Either animal findings show risk, but human findings do not; or, if no adequate human studies have been done, animal findings are negative.
C	**Risk cannot be ruled out.** Human studies are lacking, and animal studies are either positive for foetal risk or lacking as well.
D	**Positive evidence of risk**. Investigations show risk to the foetus.
X	**Contradicted in Pregnancy**. Studies in either human or animals has clearly shown foetus risk which outweighs any medical benefit of the compound.

Current European Union (EU) law concerning the regulation and labelling of reproductively toxic substances falls under the classification, labelling and packaging regulation of chemical substances (CLP regulation). Introduced in 2009, CLP regulation brings EU policy into alignment with the United Nations' (UN) affiliated globally harmonised system (GHS) regarding the control of chemical substances (32). Developmental toxicity is a hazard category under the international GHS. However, before potential teratogenic compounds can be categorised and labelled under CLP regulation in the EU, they must be assessed via EU REACH regulation. Registration, evaluation, authorisation and restriction of chemicals (REACH) is a 2006 EU legislation that as of 2018 concerns any chemical of which 1 tonne per year (or more) is produced or imported into the EU (European Parliament, 2006). REACH requires all new chemicals as well as existing ones to be (re)evaluated for many different toxic effects including reproductive toxicity, the category under which developmental toxicity and teratogenicity is located (European Parliament, 2006). A key criticism of the EU REACH regulation is the perceived overreach of the regulators and the underestimation of the financial costs and numbers of animals required (34). Hartung and Rovida (2009) calculate that REACH will cost € 9.5 billion and require 54 million vertebrate animals between 2009 and 2019 (35). Reproductive and developmental toxicity accounts for the majority of both costs (Figure 1.2).

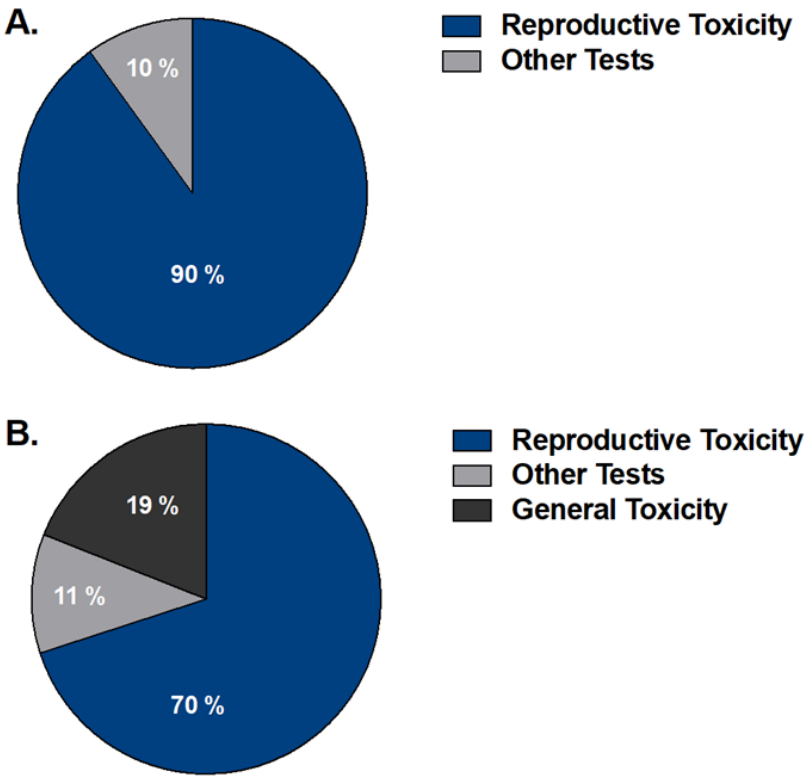

Figure 1.2. EU DART animal and financial costs proportions. Animal and financial costs proportions associated with reproductive and developmental toxicity testing estimated to be required to fulfil REACH legislation within the EU. **A).** Number of animals used. **B)**. Financial costs associated with REACH compliance. Adapted from (34).

The *in vivo* use of mammalian tests is still considered the gold standard of developmental toxicity testing (28). The study design and model mammalian systems used has changed very little in the last 50 years. However, with increased compound demand and development, the implementation of mammalian *in vivo* testing is extremely costly in both financial terms and in terms of the number of animals used (1,28). At present, approximately 90 female animals are estimated to be sacrificed per developmental toxicity study in the EU (2). With the current dual mammalian screening system it is calculated that approximately 5000 animals will be needed per compound evaluated (35). The heavy animal use and financial costs associated with developmental toxicity evaluation has been omnipresent throughout the last 50 years and has led to the research area being a key field in the adoption of the 3Rs (2).

The principles of humane experimental technique concerning live animal experimentation are Replacement, Reduction and Refinement, commonly called the 3Rs (36). All of the 3Rs are critical reasons for the creation of (and continuing development of) alternative developmental toxicity testing models. By their nature, alternative models *replace* traditional *in vivo* testing and *reduce* the consumption of animals. Yet, it is in the *refinement* of animal testing that alternative models cause the greatest effect. As previously discussed, *in vivo* testing is legislated for worldwide. However, this is only relevant for the final safety compliance and registration of a compound. The use of alternative models during the early development stages of new chemicals allows for teratogenic compounds to be identified before the final *in vivo* screening process (20). As new alternative models are developed (and improved) the importance and relevance of *in vivo* screening will diminish. Indeed, currently there are calls to drop all mammalian systems in favour of non-mammalian alternative teratogen evaluation models. Alternative evaluation systems were originally conceived in the 1970s, however in the last decade a variety of systems have been developed and assessed (1).

1.2 Alternative developmental toxicity and teratogen evaluation models

1.2.1. Alternative teratogen evaluation models

Alternative models for teratogen evaluation have been considered since the advent of formalised teratogen evaluation in the 1960s. The increasing need for non- *in vivo* HTP teratogenicity assays has led to a growing need for the development of alternative *in vitro* assays. Originally an *in vitro* teratogen evaluation system was considered to be any cellular, tissue, organ or organism-based methodology other than mammalian embryo *in situ*. *In vitro* systems were typically valued for the ability to control variables in the screening method and to reliably test compounds on a specific aspect of biological development. An early alternative assay that encapsulates this principle is the limb bud assay first used in the 1970s. In the limb bud assay, cells derived from the limb buds of rat embryos are cultured at high density and allowed to differentiate into chondrocytes over a period of 5 days (37). The cells are exposed to compounds during the culture and staining for terminal differentiation is used to quantify teratogenicity. The increasing use of *in vitro* assays, including the limb bud assay, led to the formulation of the ideal characteristics of future *in vitro* models and assays (20). These ideals were first proposed by Wilson in 1978 and are still relevant today for the development of non-mammalian *in vivo* screening alternatives (Table 1.3).

Table 1.3. Key Characteristics of an ideal *in vitro* teratogenicity evaluation system

	Key Features of an ideal in vitro system
I	Simple, easy to perform, yield of interpretable results
II	Rapid, usage of large numbers of samples
III	Giving minimal false negative results
IV	Relevance to mechanisms of teratogenesis
V	Involving some aspects of progressive development
VI	Usable with various types of teratogenic agent
VII	Capability to absorb, circulate and excrete chemicals

Adapted from Schumann (2010).

A variety of different alternative teratogen evaluation models have been developed over the last two decades of research. These are generally categorised as either mammalian models, including: rodent cell assays (ESC), rodent tissue assays (micromass) and whole embryo culture, or non-mammalian models, including: zebrafish, hydra and frog embryo assays (1). These systems differ considerably and therefore a better distinction can be made: whether they are whole organism-based or cellular-based models. Such a distinction allows for the scope and the biological complexity of different alternative assays to be distinguished and therefore effectively critiqued. Ideally, an alternative assay would have sufficient biological complexity to model the full developmental process of an '*in vivo'* development, thereby allowing for the assay to be predictive. However, the assay should also be HTP, and consequently low cost. It is difficult to reconcile these ideals and therefore, generally, whole organism-based assays have biological complexity and predictivity, and cellular-based assays have a propensity for low cost and HTP application (1). Of the current alternative models for teratogen evaluation, the whole rodent embryo culture assay, the zebrafish assay, and human and mouse embryonic stem cell culture assays are the most developed and widely implemented. Together they represent both whole organism and cellular approaches to alternative model systems and therefore will be discussed in greater detail below (Sections 1.2.2 & 1.2.3).

1.2.2 Whole organism-based teratogen evaluation models

The whole organism-based teratogen evaluation models are the closest in biological complexity to an *in vivo* screening system. Mammalian-based models use whole embryo culture *ex utero*. Whilst non-mammalian organisms including: *Hydra*, *Xenopus* and Zebrafish are conducted using full embryonic developments in a laboratory.

1.2.2.1 Rodent whole embryo culture assay

The rodent whole embryo culture assay ($_r$WEC) has been used extensively to assess the potential of small pharmaceutical compounds since it was first developed by D.A. New in 1978 (38). In this method, whole rat embryos are harvested, grown and developed *in vitro*. The embryos exhibit few differences to *in vivo* development and critically can be maintained through many major developmental stages, including organogenesis (38). The $_r$WEC assay is advantageous because a whole embryo is used. Thus, test chemicals can interact with the embryo as if the experiment were conducted

in vivo yet without interference from a maternal component (39). In brief, the assay runs once the preimplantation embryos have been harvested. They can then be cultured for up to 48 hours in a medium primarily constituted of rat serum (39). Compounds of interest are added directly to the serum and a number of toxicity endpoints are examined after the culture period. The toxicity endpoints vary and can include: viability (heat beat, yolk sac circulation), growth (crown to rump length, total protein amount) and developmental morphology (39). Assessment of developmental morphology is critical for teratogenic evaluation and a scoring system is applied to 17 separate developmental endpoints (39). This comprehensive scoring system requires expertise, is time-consuming, and has therefore led to the proposal of simpler methods (40,41). In 2002, the European Centre for the Validation of Alternative Methods (ECVAM) published results on the extensive validation of the $_{r}$WEC assay (42). The ECVAM used a standardised scoring system on a 20-chemical cohort of non-, weakly- and strongly- embryo toxic test compounds. The $_{r}$WEC assay was reported to correctly categorise 14/20 (70%) of the test chemicals. However, the non- and weakly- toxic categories were found to be problematic for the assay (42). At that time the predictive capacity of the assay was regarded as 'good'. However, since then, the incorporation of gene expression profiling and a reduction in the complexity of the readouts, combined with statistical modelling, continues to improve the assay (39,41,43,44). In 2012, Zhang *et al*, tested a refined $_{r}$WEC assay using a cohort of 70 test compounds and reported a predictability score of ~83% (41). The $_{r}$WEC is valued specifically as a mechanistic study platform where known teratogenic agents can be assayed to further understand the mechanism of their teratogenicity (45–47). Using a rWEC assay, Hughes *et al* (2018) were able to demonstrate that the common spina bifida birth defects caused by valproic acid were due to the failure of F-actin to mechanically close a neural fold during the early stages of development (46). However, a key limitation of the $_{r}$WEC assay is the limited developmental period in which experiments can be conducted. The *ex utero* embryo can only be cultured up until the 48-hour period and any teratogenic effects that could occur later during the gestation phase cannot be detected (48). However, the greatest limitation to the $_{r}$WEC is practical. The assay is very labour intensive, requiring considerable expertise in the subjective scoring procedure, thereby increasing both its cost and reliability (39).The potential for adapting the $_{r}$WEC to HTP application is thus also limited. Finally, the $_{r}$WEC requires live rats both as a source of embryos and for the culture media serum. Therefore, whilst the current assay uses 50% fewer animals than in the past, it fails to fully deliver on all the principles of the 3Rs (41).

1.2.2.2 Zebrafish whole embryo culture assay

The zebrafish (*Danio rerio*) is a well-established model organism for toxicology, which, since its first application in 1990, has become a popular model for developmental research (49,50) . Zebrafish developmental processes and pathways are well conserved with humans and Zebrafish embryos are easily grown *ex utero* where their transparency allows for *in vivo* observation of organ and tissue development (50). The practical and biological characteristics of zebrafish have, in the last decade, increasingly seen them implemented in developmental toxicology assays (51). Zebrafish teratogen evaluation assays are conducted in many different laboratories around the world, where overlap in the core procedures can be observed despite each lab implementing its own methodology (52–56). A generalised Zebrafish assay begins a couple of hours after fertilisation when individual embryos are separated into different wells in a multiwell plate and cultured in specialised media (1). Test compounds are simply added to the culture media at the required dose range for between 3 and 6 days, dependent on the period of development being studied. This 6-day maximum assay time frame covers the major aspects of Zebrafish development, including the entirety of organogenesis (52). The assays are scored in a similar manner to the rWEC assay, with viability, growth and morphology assessed throughout development and for different developmental toxicity endpoints. Despite different protocols employed by different laboratories, multiple independent studies have found zebrafish embryo teratogen evaluation assays to correctly predict mammalian teratogens at a rate of ~90% (52,54,57,58). Whilst most of the independent validation studies have been conducted with between 60 to 80 well-defined test compounds, a large cross-model review of 214 test compounds found the Zebrafish assay to be comparable to *in vivo* mammalian screening (59). Sipes *et al* (2011) reported that predictivity between zebrafish and rat or rabbit toxicity was almost as comparable as between the two *in vivo* systems (59). This has led to the increasing demand to change legislation to replace one of the two *in vivo* screens with the zebrafish assay (Section 1.1.4). Current research on zebrafish developmental assays concerns both harmonising existing systems and optimising assays for high throughput, automated systems (60). With the push towards high-throughput automation, limitations in the zebrafish model have been revealed and/or exacerbated due to both temporal requirements and the amount of eggs required. These factors are sufficiently limiting to warrant research into improvements of these practical elements (54). Another limitation of the model system is the aqueous nature of the assay; compounds with low solubility can be difficult to screen which has even been a factor in the selection of test compounds during validation studies (25). Other limitations relate to the current understanding of the pharmacokinetics inherent to the model organism (1). It has been reported that internal

and tissue-specific exposure is sometimes compound specific and therefore further research is required assess the potential effects this could have on assay toxicity predictivity (58,61). Nevertheless, the zebrafish whole embryo culture assay is currently the most well-developed of the alternative teratogen evaluation models.

1.2.3 Cellular-based teratogen evaluation models

Cellular-based teratogen evaluation models represent a further abstraction from *in vivo* testing than whole-organism based models. The potential for cells to differentiate into terminal cell types *in vitro* allows researchers to quantify their behaviour. By challenging the cellular differentiation processes with teratogenic compounds, assays have been developed which, in comparison to whole embryo assays, are more HTP and have lower costs. Whilst a range of different cellular-based teratogen assays have been developed the most advanced and implemented assays are based on embryonic stem cell differentiation (62).

1.2.3.1 Embryonic stem cell assays

The first embryonic stem cell assay based on murine cells was developed in 1998 to screen for embryotoxicity (63). The mouse embryonic stem cell test (mEST) is based on permanent stem cell lines, derived from the inner cell mass of 3.5 day mouse blastocysts (64). Once established, the cells are cultured for up to 10 days in the presence of a test compound in the media. A number of different toxicity endpoints can be assessed, one of which is cytotoxicity. The teratogenicity endpoint is quantified by measuring the effects on cell differentiation into beating myocardiocytes (64). Since the mEST was first constructed, research groups worldwide have reported improvements in the assay. These include allowing the stems cells to form embryoid bodies, thereby increasing the biological complexity of the assay to more closely align it with *in vivo* realities (65–67). Despite the wide use of the mEST, the use of mouse cells still represents a fundamental problem. It is known that a subset of compounds that are highly teratogenic in humans do not correlate to mouse models. Consequently, a human embryonic stem cell test (hEST) has been developed and optimised to improve teratogenic predictivity (64). hEST assays generally operate in a similar way to mEST assays, with the *in vitro* differentiation of myocardiocytes and neuronal cells used as a proxy for *in vivo* developmental processes.

A key benefit of cellular-based teratogen evaluation models is the relative ease in which genetics and molecular biology can be applied. The use of key marker genes that report on the terminal stage of differentiation allows for both the mEST and hEST assays to improve predictivity whilst facilitating the potential for automation. Green fluorescent protein (GFP) ESC lines, where expression is controlled by terminal myocardiocytes differentiation, have allowed the teratogenic assessment to be conducted by FACs. This results in the reduction of both manual observation and the training required for the mEST, increasing HTP (68,69). Simultaneously, the use of cell lineage marker genes as molecular toxicity endpoints has significantly improved the readouts of the assays (70). A modified mEST in which the expression of 12 developmentally regulated genes were measured has been reported to predict ~72 % *in vivo* teratogenicity against a test cohort of 65 compounds (71).

The key advantage of both the mEST and hEST assays relate to the ease at which the cellular models can be used in an HTP manner. Other than the initial isolation (for the mEST) no animals are required for the assays to be operated, decreasing the operational costs. Together these attributes have seen the mEST and hEST used as a tool for rapid teratogenic assessment of novel compounds in the early stages of their development (62). However, the assays are substantially less complex in terms of developmental biology when compared to both whole-embryo assays and *in vivo* screening. Consequently, further research is required to both harmonise the standard procedures regarding lineage markers and to improve the consistency in the formation of more complex embryoid bodies (67,72).

1.2.4 The limitations and future of current alternative teratogen evaluation models

It is widely accepted that non-mammalian alternatives to *in vivo* screening represent the future of DART screening and evaluation. To date, approximately 30 different *in vitro* assays have been reported (1). However, individually, none have both the biological complexity and HTP potential to replace *in vivo* testing. By their nature, *in vitro* assays abstract from *in vivo* testing systems and, therefore, realistically a single *in vitro* assay could never provide the depth or resolution needed for teratogen testing and evaluation (73). However, by implementing a selection of complementary assays in a battery of tests, the biological coverage could match or even surpass *in vivo* animal testing (73). For a future battery of *in vitro* assays to function effectively and in harmony, each component must fulfil a specific role within the battery. Some assays are, for example, designed to act as teratogen screens where others are strongly suited to evaluating the molecular mechanisms associated with known teratogens (74). There is therefore a driving need for new alternative models and assays to address current limitations and gaps in the repertoire of *in vitro* teratogenic evaluation assays. Classic developmental biology model organisms represent a compelling area in which to development new alternative developmental toxicity systems. *Dictyostelium discoideum*, a common model organism in developmental biology, is a microbial system with a complex developmental cycle. Although, mooted as a possible alternative model for the evaluation of teratogenic compounds, the potential of *Dictyostelium discoideum* has never been fully investigated (20).

1.3 *Dictyostelium discoideum*, model organism

Dictyostelium discoideum (*D. discoideum*) is a unicellular eukaryotic soil dwelling amoeba, which feeds via the phagocytosis of bacteria (75). If food is plentiful, *D. discoideum* remains in its unicellular state. However, starvation triggers a comparatively simple multicellular developmental cycle (Section 1.3.2) (76). Since its discovery in 1935, *D. discoideum*'s ease of manipulation and relative simplicity have made it a key model for the study of a range of biological processes (75,77). *D. discoideum* exists as a 'professional' phagocyte and its similarity to mammalian cell types (especially macrophages) has made it a key model organism for conserved biological processes including chemotaxis, endocytosis, micropinocytosis and simple host pathogen interactions (78–81). *D. discoideum* is also recognised as an important non-animal model for biomedical research (75). For example, research on core human diseases including cancers, inheritable diseases and Alzheimer's disease have all been conducted in this ameboid model (82). Finally, *D. discoideum* has a comparative simple developmental cycle compared to higher organisms, and yet it retains many of the major biological processes underlying embryonic development. Many of the pathways and molecular components that regulate development in *D. discoideum* are conserved in higher organisms; therefore, it is widely used as a model organism for the study of developmental processes (75).

1.3.1 *D. discoideum's* advantages as a developmental model

In practical terms, *D. discoideum* cells are easy to grow to high densities in relatively inexpensive facilities. Furthermore, in a laboratory setting, the generation of axenic strains has allowed for experiments to be conducted in the absence of bacteria in homogeneous culture (76). In *D. discoideum*, the growth and developmental phases of the life cycle are strictly separated. This allows for multiple and separate, developmental experiments to be conducted from a single population of cells; greatly reducing experiment setup time and associated costs. The removal of nutrients from a population initiates the developmental cycle and therefore only an inexpensive agar substratum is required to assay *D. discoideum* development. Temporally-speaking, a full developmental cycle only takes 24 hours with easily observable stages and transition in the developmental process. Taken together, these natural attributes in the *D. discoideum* model highlight a system that is both cheap to maintain and operate. *D. discoideum* research is enhanced by its amenability to molecular genetic techniques including: extrachromosomal expression vectors; targeted DNA insertion via homologous

recombination; the generation of REMI (Restriction Enzyme-Mediated Integration) insertional mutant pools and genetic manipulation using Crispr-cas9 (83–87).

Research using *D. discoideum* is supported by the sequencing of its genome in 2005 (88), which revealed that *D. discoideum* diverged from the animal kingdom after the divergence of the plant kingdom, but prior to that of the fungal kingdom (Figure 1.3). However, due to a later fungal gene loss event, *D. discoideum* maintains many more gene similarities to animals than many filamentous and yeast fungal species. *D. discoideum* has an estimated 13,000 genes. *D. discoideum* gene complexity is thus comparable to human gene numbers and substantially more than the 6,000 Saccharomyces cerevisiae genes (Figure 1.4), and is comparable to the common developmental biology research models such as the fruit fly, Drosophila melanogaster (14,000 Genes) and nematode worm, Caenorhabditis elegans (18,000 Genes) (89) (Figure 1.4).

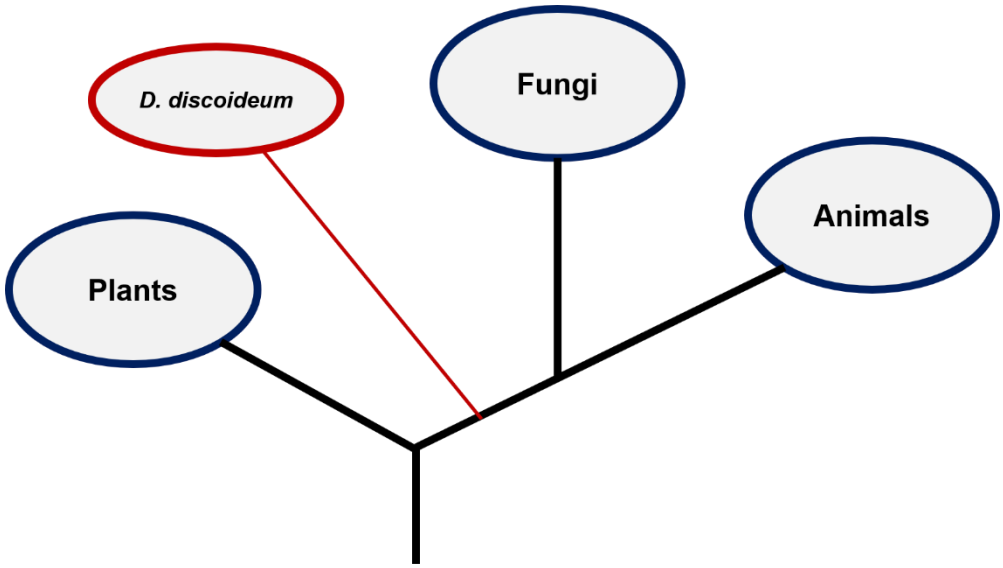

Figure 1.3. *Dictyostelium* evolutionary history. Phylogenetic tree displaying the evolutionary relationship of *D. discoideum* in relation to the Plant, Animal and Fungal kingdoms. Adapted from (75).

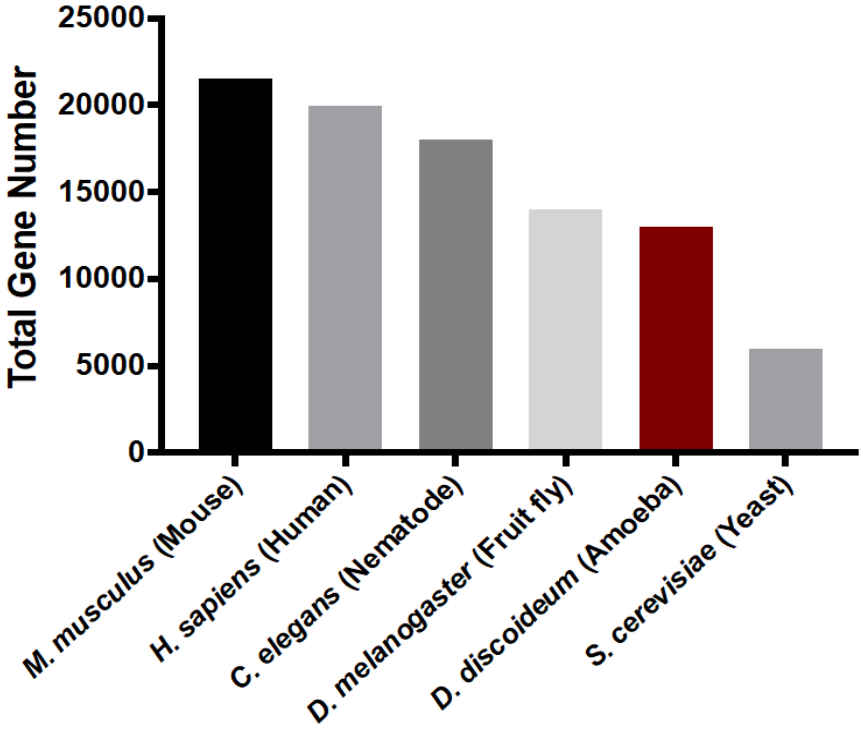

Figure 1.4. Model organism gene numbers. Comparison of the total number of genes for common developmental biology model organisms and humans. *D. discoideum* is highlighted in red and exhibits comparable gene numbers to the others. Adapted from (89).

The consideration of the new roles *D. discoideum* could model (including developmental toxicity testing) are primarily due to its unique developmental cycle which will be discussed in greater detail below (Section 1.3.2).

1.3.2 The *D. discoideum* developmental cycle

1.3.2.1 Development from starvation to aggregation

The *D. discoideum* developmental cycle is initiated by starvation. It is known that only the addition of 7 essential amino acids can delay development, and it is therefore likely that the nitrogen state of the cell is recognised as a proxy for starvation (90). Whilst starvation is the initiation signal that triggers the developmental cascade, vegetatively growing *D. discoideum* cells are already primed for nutrient limitation due to quorum sensing mechanisms (91). During growth, *D. discoideum* cells continually secrete a host of different quorum factors, which accumulate in the environment at a rate proportional to cell density (92). The quorum sensing pathways are critical for development as they act to both prepare cells for starvation and allow individuals in a population to register cell density, which in turn is essential for later developmental processes (91). Prestarvation factor (PSF) is continually secreted by growing cells and reaches a threshold at a cell density of ~10^6/ml. At approximately 10^6/ml, cell density is strongly correlated with a decrease in the availability of nutrients. At this point, cells become receptive to PSF, inducing the expression of the protein kinase YakA (93). An accumulation of YakA initiates an inhibition cascade that culminates in an accumulation of the cAMP receptor (CAR1) and adenylyl cyclase, thereby allowing cells to secrete and respond to cAMP, the key molecule driving aggregation (Section 1.3.2.2) (93).

1.3.2.2 Development from aggregation to the mound stage

As previously discussed, early cell density signal mechanisms act to initiate the production of cAMP. cAMP signalling plays a central role in the aggregation of cells and thus allows *D. discoideum* to undergo multicellular development (94). The cAMP network signals as an oscillator, through a well-characterised circuit. Once cAMP is secreted it binds to the external receptor cAR1, which in turn stimulates an increased production of intracellular cAMP and inhibits internal phosphodiesterase, RegA (95). This double signal results in a rapid increase in cAMP production, the vast majority of which is secreted. This spike in internal cAMP also activates protein kinase A (PKA) which in turn ultimately blocks cAMP production. This feedback regulation, along with an active breakdown of external cAMP, leads to an oscillating signal of cAMP that pulses through the population (95). For the first 4 hours after starvation the cells begin to entrain to the rhythm of cAMP pulses. Between 4 and 8 hours, the cAMP pulses strengthen and the oscillations occur approximately every 6- 8 minutes (96). Cells kinetically respond to the cAMP waves by moving in the direction of an increased gradient; this process

unsurprisingly attracts cells towards a central population forming aggregates. This general process constitutes the aggregation stage of the developmental cycle (Figure 1.5).

During aggregation cells respond to both the cAMP gradient and the direction of the waves to achieve directional sensing. Two key processes that drive directional sensing are receptor activation polarity and entrainment of the signalling mechanism (97). The cells respond to the cAMP signal gradient via the G-protein coupled receptor cAR1 along the leading edge of the cell. The activation of the cAR1 receptors leads to a localised signalling cascade that ultimately results in a localised accumulation of secondary messenger PIP3 (97). PIP3 then activates further downstream signalling which terminally activates actin polymerisation, resulting in pseudopods formation, directing cell migration.

Beyond creating directionality, the cAMP waves also induce the expression of early development genes (98). These pulse-dependant genes are important for priming cells for later differentiation but also include genes needed for aggregation: including a development stage specific adenylyl cyclase and cell adhesion proteins, critical for the streaming stage described below (98). By tying both the migration and changes in specific development gene expression to cAMP waves, the early *D. discoideum* developmental progression is communally controlled. As the pulsatile cAMP waves are generated by the developing cells the pulse induced development genes become synchronised in expression across the whole population. This allows for all of the cells to reach the later mound stage with similar chemotactic and differentiational potential.

As the aggregative cells migrate closer to the mass at the centre of the aggregate, known as the mound, they begin to adhere to each other as they move, forming streams of cells (99). The adherence of cells to one another is a result of multiple cell contact signalling pathways and the increase in cell adhesion is stimulated during early development. After approximately 8 hours after starvation, the majority of cells are moving concertedly in response to the chemotactic signals emanating from central mounds. As cells move together, they deviate towards one another forming streams of cells, constituting the streaming stage of development (Figure 1.5) (99). The majority of cells enter the mound during streaming and therefore the adhesion streaming process plays an essential role in the migration of cells to mounds. When cells enter the mound during streaming, they form large rotating swirls, drawing the streams into the massed centre. This process continues until the formation of the slug, the next phase of development (100).

1.3.2.3 Development from the mound stage to slug migration

During the streaming phase of development, cells begin to diverge into the two main cell type precursors, prespore and prestalk (101). Whilst some cell type specific genes are expressed from the beginning of the developmental cycle, it is not until the mound stage that cells diverge into either prespore or prestalk cells in a position independent, salt and pepper, manner (101–103). However, biases towards fate the choices are already influenced before the development phase has begun. Prestarvation, during the growth phase, cells are primed for the future cell fate choice (102,103). The propensity for cells to ultimately differentiate into different cell types can be affected by various external factors, including: intracellular calcium concentration (104,105), nutrient history (106) and cellular pH. These external factors can disturb the responsiveness and required threshold of developmental signalling pathways and/or the cell cycle, the key regulator of lineage choice bias (103). Thus, whilst the biological mechanics of developmental aggregation are upregulated after starvation, the later cell type differentiational choices are already primed during growth (103). This pre-set bias preceding development allows for the robust proportioning of cells into the two major cell types. Approximately 30% of the developing cells in each slug will become stalk cells with the remainder becoming spores. Elegantly, prestalk bias is linked to the S and start of G2 phase which together encompass 30% of the cell cycle in *D. discoideum* (107). The prespore cells are a homogeneous cell type group, however the prestalk cells can be further subdivided.

Classical molecular characterisation of prestalk cells has allowed researchers to subdivide them into multiple subtypes on the basis of gene expression, positioning and their specific role in later *D. discoideum* development (108). The most prominent and well characterised subtypes are called prestalk-O (PstO), prestalk-A (PstA), prestalk-B (PstB) and prestalk-AB (PstAB) (109). These subtypes were initially deciphered due to expression differences of the *ecmA* and *ecmB* genes in the anterior tip of the slug, with *ecmA* expressed by PstA cell, ecmB expressed by PstB cell and PstO cell expressing neither gene (110). PstAB cells were later found to express both ecmA and ecmB (108). The categorisation of *D. discoideum* prestalk cell types is not fully understood. Whilst stains and markers for the four main cell types above reveal specific developmental positioning and roles, it is uncertain whether further, subtly different prestalk cells exist. However, the comparative transcriptional similarity between differentiating cell types means that, to date, technical limitations permit only the broadest classification of prespore versus prestalks to be distinguished (111).

The two most prominent and well-characterised differentiation signalling factors are cAMP and a chlorinated hexanophenone, DIF-1 (112). cAMP is essential for the differentiation of prespore cells (113). Whilst cAMP is essential for the divergence of prespore cells, it has an equally important inhibitory role in the formation of prestalk cells. The newly differentiated prespore cells quickly begin to synthesise spore coat protein materials and importantly synthesise DIF-1, which in turn is required to induce prestalk cell differentiation. DIF-1 plays an essential role in the differentiation of PstB and plays a partial role in the formation of PstO cells. Once PstB and PstO have differentiated into prestalk cells via the activity of DIF-1, PstA cells in the anterior of the slug begin to produce DIFase, an enzyme that degrades DIF-1 regulating the concentration of DIF-1 (114). Other subtypes of prestalk cells, including PstA and PstAB, diverge independent of DIF-1 (115). Once the mound has fully formed and completely diverged into either prespore or prestalk cells, the different cell types begin sorting within the mound. PstA and PstO cells sort to the top of the mound forming a tip. PstB cells sink to the bottom of the mound forming the base and the prespore cells form the body of the mound where they swirl around. After this primary cell sorting, the tip drives the formation of the slug, the next major phase of *D. discoideum* development. As the prespore cells chemotax towards the tip in a spiral motion, the mound elongates upwards forming a finger, which, after overextension, collapses forming the slug (Figure 1.5) (114).

The slug is enclosed in cellulose fibres and cellulose binding proteins that are secreted during the mound phase, forming a sheath (116). The sheath determines the direction in which the slug migrates, as new sheath is only synthesised at the tip (116). Slugs migrate in response to light and temperature gradient, which is thought to direct the slug to the surface of the soil where spore dispersal is appropriate (117). At the front of the slug PstA cells surround a smaller population of PstAB cells; the PstA in the head of the slug drive its migration (114). The PstA cells in the tip are followed by the PstO cells that form the collar region of the slug. The main body of the slug is made up of the prespore cells that contribute approximately 70-80 % of the total cells in the slug. The prespore region, however, is not homologous and is speckled with anterior-like cells that share a similar molecular expression profile to PstO cells (108). The PstB population is located at the foot of the collar region where the slug first makes contact with the surface (118). The different cell types remain in these locations within the slug as it migrates and only begin to re-sort after the slug halts and the culmination phase of *D. discoideum* begins (Figure 1.5).

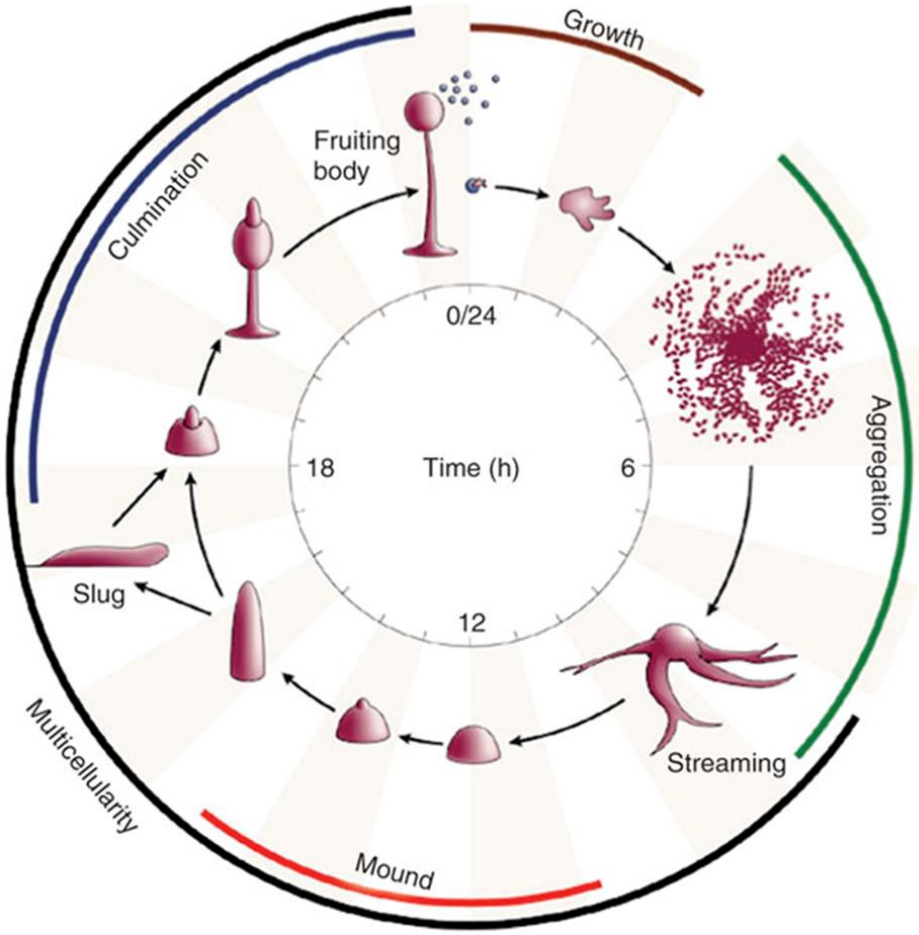

Figure 1.5. *D. discoideum* developmental cycle. Upon starvation vegetative cells aggregate towards central masses via cAMP chemotaxis. Cell adhesion in late stage aggregation causes cells to stream in mass forming a mound. In the mound, cells differentiate into either prestalk or prespore cell types. A sub population of prestalk cells forms a tip on the mound which through further chemotaxis extends the mound into a finger. The finger may then collapse and form a multicellular slug which migrates via phototactic signals. Eventually the slug halts, culminating in a second mound from which the fruiting body develops. During fruiting body formation cells fully develop into either stalk or spore cells. The spores form the head of the body from where they are dispersed completing the development cycle. The whole process takes approximately 24 hours. Figure from (76).

1.3.2.4 Development from slug migration to culmination and spore dispersal

When the slug has migrated to an appropriate position for spore dispersal, terminal differentiation is induced. This process begins with the body of the slug ‘shunting up’ to form a mound structure morphologically similar to the pre-slug mound. The prespore cells continue to move until they sit under the tip in a motion that orientates the tip to point upwards (113). As this early culmination mound forms, both the PstA and PstB cells migrate in an upward direction secreting cellulose fibres throughout the tip (119). The cellulose fibres are subsequently modelled into a stalk tube, which ultimately forms the skeleton of the future fruiting body (119). Once the initial stalk tube has formed, it is pulled downwards through the centre of the culminant via the migration of the PstAB cells (114). When the stalk tube reaches the base of the culminant, the PstAB cells fuse to the outer basel disc, forming the inner basel disk which anchors the fruiting body to the substratum. Approximately one hour after the stalk tube attaches to the base of the culminant, new cellulose fibres are rapidly added to the top, causing the tube to elongate upwards (116). The rise and extension of the stalk tube attracts prestalk cells which terminally differentiate into stalk cells by increasing in volume and secreting thick cellulose walls (120). The stalk cells strongly adhere to one another in a regular order forming a ring around the tube which is eventually compressed via the activity of actomyosin bundles that connect the new cylindrical stalk sheet (121). Once the stalk rises above the substratum, the prespore cells rise off the base and, as a collective, move up the stalk. The prespore cells move away from the PstB cells, which are left behind where they form the outer basel disc. The timing of fruiting body development is orchestrated so that by the time the stalk has fully extended the collective of prespore cells has migrated approximately half way to the apex (113). At this stage the prespore cells begin to terminally differentiate into spores. The production of the spore coat is the most important stage of the differentiation process, allowing for the spores to be robust enough to survive external stresses (122). The spore coat is multi-faceted and is produced in a stepwise manner from 10 specific coat proteins (122).

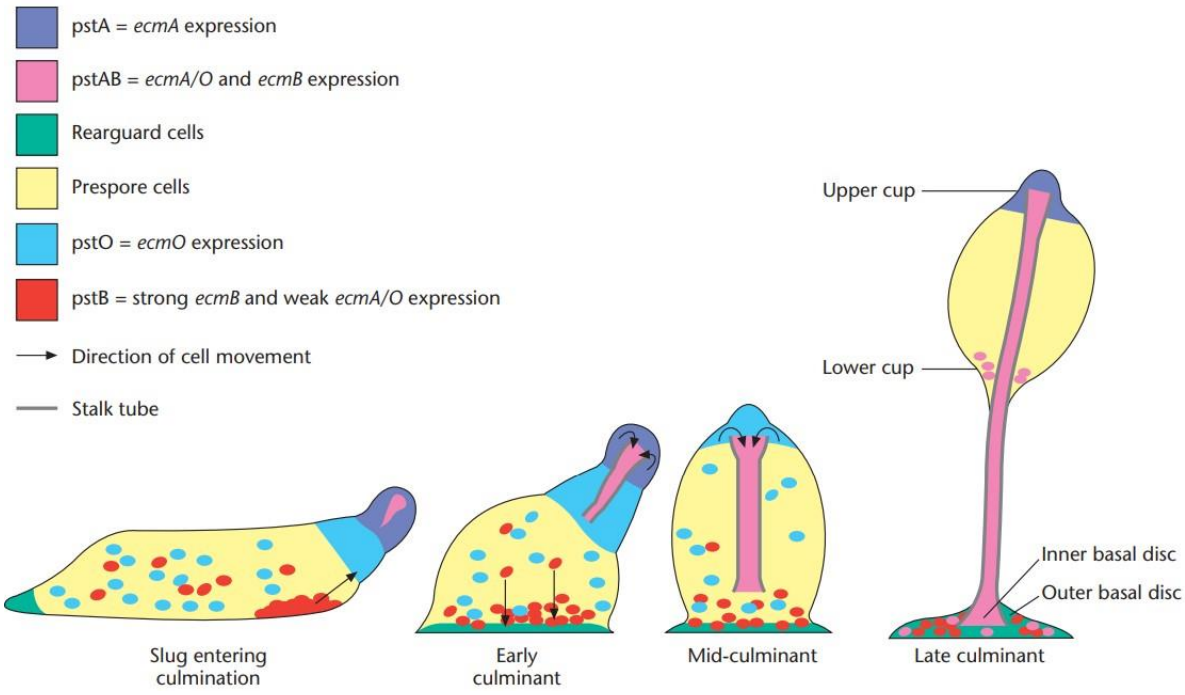

Figure 1.6. Schematic diagram of prestalk and prespore cell locations within the slug and late culminant stages of development. Figure from (114).

The temporal and spatial elements of terminal differentiation during late culmination is orchestrated via the activity of multiple differentiation factor signalling pathways. Cyclic-di-GMP, a common prokaryotic signalling molecule, has been found to be essential for the terminal differentiation of both stalks and spore with cyclic-di-GMP null strains failing to progress pass the slug phase (123). Two peptide signals, SDF-1 and SDF 2, are also essential for terminal differentiation (124). SDF-1 activates a late adenylyl cyclase and SDF-2 converts a protein kinase into a protein phosphatase, which in turn inactivates internal cAMP phosphodiesterase called RegA (124). Together these signals lead to an internal accumulation of cAMP, which in turn activates PKA (124). PKA plays an essential role in the terminal differentiation of spore cells and when PKA is inhibited, fruiting bodies develop normally albeit with a head of undeveloped prespore cells (125).

The developmental process from starvation to mature fruiting body takes approximately 24 hours in a laboratory setting (76). The dispersal of the spores occurs through direct contact with the fruiting body head which subsequently bursts in a mechanism likely to be reliant on small soil invertebrates. Once favourable conditions are met, the spores germinate in an independent manner, releasing vegetative amoebae completing the *D. discoideum* developmental cycle.

1.3.2.5 *D. discoideum* developmental process summary and comparison.

Despite the clear differences between the *D. discoideum* developmental cycle and the developmental biology of higher animal organisms, *D. discoideum* is considered a key developmental model system. This can be primarily attributed to the intersection of the core biological processes behind *D. discoideum* and higher animal development. There is a broad conservation of developmental pathways and where specific mechanisms are divergent the developmental outputs are similar. Briefly, within a 24-hour period, *D. discoideum* exhibits: symmetry breaking and cell type proportioning based on cell cycle position, observable in hESCs during early cell fate choice; self-organisation of cells via cAMP signalling; and, cell to cell adhesion, allowing for populations of cells to chemotax and migrate in order and cooperation (126). Both short- and long-distance migration of divergent cell populations are integral aspects of embryonic development. *D. discoideum* cells show complex gene expression changes as they diverge into pre-terminal cell types which each have positional and functional differences (111). True multicellular structures are formed, and morphogenesis plays a crucial role in the mound, slug and fruiting body structures. During the multicellular structure phase, signalling and morphogenetic gradient boundaries are formed via antagonistic, cell type driven feedback loops (127). *D. discoideum* development climaxes with the terminal differentiation of cells types, including the altruistic cell death of all the stalk cells, analogous to the essential role of apoptosis in higher organismal development (128).

In summary, all of these complex systems and biological processes are regulated and controlled by complex, yet fundamentally conserved, cell signal transduction pathways. *D. discoideum* represents a developmental model system that is both simple and complex, thus comparable to higher organisms, and has therefore become increasingly recognised as a potential system for practical application and pharma-chemical research. This is because *D. discoideum* is microbial and has a quick developmental cycle (~24h), it is a low cost and is a 3R's alternative model for biological research.

1.4 *Dictyostelium discoideum* as a model for the investigation of the molecular basis of drug action and toxicity

1.4.1 Application of *D. discoideum* in environmental toxicity assays

As *D. discoideum* is a soil dwelling organism it has been considered as a test organism for the assessment of environmental quality. Initial studies focused on testing whether *D. discoideum* stress responses could be used as a readout for the assessment of freshwater quality (129). These initial studies found *D. discoideum* to be a responsive model for evaluating soil samples containing a range of different test toxicants. Sforzini *et al* (2008) found *D. discoideum* a highly sensitive model, with quicker readouts, in comparison to other commonly used environmental toxicity bioassay models (129). Sforzini *et al* (2008) found that by measuring sublethal cellular stress responses including: lysosomal membrane stability and endocytotic rate along with tradition chronic toxicity endpoints such as cell viability, *D. discoideum* outperformed other environmental bioassay models (130,131). However, the complex biological processes required for the developmental cycle of *D. discoideum* (Section 1.3.2.5) offered an approach to construct a developmental cycle bioassay for environmental toxicity testing. Rodriguez-Ruiz *et al* (2013) developed the *Dictyostelium discoideum* developmental cycle assay (DDDC), a developmental toxicity assay designed to screen the health of soil samples. The DDDC is based around determining the capacity of *D. discoideum* to undergo development and form normal fruiting bodies as a measure of ecological fitness. Importantly, the DDDC also attempts to identify the toxic mechanisms of action by assessing whether development is arrested at aggregation, migration or culmination (130). Both the quantitative readout and the predictive aspects of the DDDC are characteristics that would feature in Wilson's ideal *in vitro* teratogenicity evaluation system. Whilst the DDDC is an environmental assay, it reinforces the potential applicability of *D. discoideum* to teratogenicity evaluation (Table 1.3). Recent work on the DDDC assay concerns integrating the procedure into a battery of environmental toxicity tests, an important process in the development of both environmental and teratogenicity evaluation systems (74,131). The optimisation and application of *D. discoideum* development bioassays for environmental toxicity assessment is currently more advanced than assays specifically developed for teratogen toxicity evaluation. However, it does expose the potential of using *D. discoideum* as a model for developmental toxicity. Accordingly, some basic proof of principle research has been reported for the application of *D. discoideum* to *in vitro* teratogenicity evaluation assays (20).

1.4.2 Application of *D. discoideum* in teratogenicity evaluation assays

In order to address whether *D. discoideum* could be an applicable model to predict teratogenic toxicity in humans, the effects of four well-annotated human teratogens were tested on *D. discoideum* differentiation (132). In this 2003 study, tretinoin, diethylstilbestrol (DES), phenytoin and thalidomide were screened and their effects on development and differentiation were quantified using LacZ reporter strains for prespore, spore, prestalk and stalk specific genes (132). This simple study revealed mixed results. tretinoin reduced the expression of prestalk and stalk markers until culmination where levels recovered, suggesting a delay in early development. DES completely suppressed development and phenytoin failed even at the highest concentrations to adversely affect development. Thalidomide proved difficult to assay due to its extremely low solubility and therefore four thalidomide derivatives were tested, two of which exhibited developmental toxicity (132). Thalidomide's insolubility and subsequent difficulty in being absorbed by *D. discoideum* cells, reported by Dannat *et al* (2003), demonstrates the importance of the seventh key feature of an ideal teratogenicity evaluation system: the 'capability to absorb and circulate chemicals' (Table 1.3).

Dannat *et al* (2003) concluded that *D. discoideum* could therefore be used as an alternative model in teratogen screening, albeit with a predisposition for false negative results. However, with only four teratogens tested, the true efficacy of *D. discoideum* was hard to discern. By contrast, in the development of a zebrafish developmental toxicology assay, 60 teratogenic compounds were screened to assess the system (58). Alternative teratogenicity evaluation systems by their nature will have a certain percentage of false negative/positive results. However, considerably more compounds need to be tested on *D. discoideum* before a species-specific efficacy can be established. The work by Dannat *et al* (2003), although limited, demonstrates some of both the limitations and advantages associated with establishing an effective *D. discoideum* assay. A critical weakness of this initial study is the low throughput nature of assay. To truly test the capacity for *D. discoideum* to function as a teratogen evaluation model, the toxicity assays developed would need to be higher throughput and quantitative, thereby allowing for a greater number of test compounds to be screened.

1.4.3 Application of *D. discoideum* for the evaluation drug targets

Whilst the use of *D. discoideum* as a practical model system for toxicity assays is limited, increasingly the model has been used in biomedical research to identify the targets of drugs and to understand the molecular mechanism of disease (75,82,133). This is due to the recognition that it contained many orthologs of genes implicated in human disease and biomedical drug treatment (75,88). Furthermore, the genetic potential of *D. discoideum* is paired with a comparative ease for experimental manipulation, including core 'omics approaches. The genetic complexity of the *D. discoideum* genome have seen it become a common model for forward genetic studies (134). The ability to generate pools of random mutants via restriction enzyme mediated integration (REMI) in *D. discoideum* has allowed for the identification of many novel components of biological processes (85). The increased interest in conducting forward genetic studies in *D. discoideum* has led to the recent improvement of REMI, producing a new technology REMI-Seq (86). REMI-Seq, allows for the high-throughput identification of REMI mutants thereby permitting parallel phenotyping studies to be conducted in *D. discoideum.* The development of REMI-Seq highlights the level of interest in using the genetic and HTP potential of *D. discoideum* in the reverse identification of genes associated with traits in higher eukaryotes, including the evaluation of drug targets and associated toxicity.

A key example of drug target evaluation in *D. discoideum* is on the cancer drug, cisplatin. *D. discoideum* has been instrumental in the evaluation of the mechanisms of drug resistance to cisplatin and the identification of new alternative targets in disease treatment (135–137). Whilst, cisplatin is widely used as a chemotherapeutic for a range of cancers, its use is severely limited by the development of drug resistance by populations of tumour cells (137). By selecting for cisplatin growth resistance in a pool of *D. discoideum* REMI mutants, Li *et al* (2000) were able to identify gene loci associated with specific drug resistance mechanisms (135). None of the 5 genes had previously been identified as mediating cisplatin resistance (135). Once identified, the cisplatin resistance genes could be further characterised in biochemical studies in *D. discoideum,* where sphingosine kinase, ablation or overexpression was demonstrated to increase sensitivity or resistance to the drug, respectively (136). In a later *D. discoideum* cisplatin study, Driessche *et al* (2007) demonstrated how transcriptional change analysis could be used to identify new pathways and genes that alter cell responses to cisplatin (137). That changes in the expression of *D. discoideum* genes in response to chemical-mediated toxicity could be used to identify the specific pathways and biological processes affected by the drug typifies why the model system is increasingly used to

study such processes. Beyond cisplatin, *D. discoideum* has been implemented to investigate the biological mechanisms of a wide range of compounds including: botanical components; curcumin (138), fruit and tea derived flavonoids (139,140), caffeine (141) and cannabidiols (142); bisphosphonates used in the treatment of osteoporosis (143) and novel anti-microbials (144). However, *D. discoideum* has been used most extensively in investigating the biological mechanisms of bipolar disorder treatments; a classification of mood stabilising drugs that are also teratogenic (82) .

1.4.4 Teratogenic mood stabilising compounds

Mood stabilising drugs are prescribed for the treatment of bipolar disorders, a spectrum of chronic and recurrent mental disorders. An estimated >1% of the world's population suffers from bipolar disorder, equally affecting all, regardless of gender or ethnic background (145). Generally, symptoms are characterised by a stochastic switch between depressive and manic phases which, without treatment, leads to increased levels of disability and suicide (145). Mood stabilisers are grouped into three clades: lithium, anticonvulsants (valproic acid, lamotrigine, topiramate, carbamazepine, oxcarbazepine) and atypical drugs (olanzapine, risperidone, quetiapine) (146). Lithium and a subset of the anticonvulsant drugs (VPA, lamotrigine, carbamazepine) are known teratogens with US FDA classifications of D, D, C and D respectively (Table 1.2) (147). This group of compounds also has a host of overlapping effects, both on target effects, with mood stabilising and anticonvulsive qualities, and off target effects, mainly, teratogenicity. The mechanism of actions of these related compounds has been of great interest since the discovery of lithium's mood stabilising effects. Bipolar disorders and their treatments are interesting as both the root causes of the disease and why the treatments alleviate the symptoms are not fully understood. Therefore, in characterising the mechanism of action of the treatments, researchers can increase the understanding the disease itself.

The most commonly studied mood stabilising drugs, lithium and VPA, have been reported to inhibit glycogen synthase kinase 3 (GSK-3) (148,149) and cause a depletion in inositol derived signalling compounds, leading to the 'inositol depletion theory' as a bipolar disease cause (150). Inositol is the carbohydrate precursor to all inositol lipids and inositol phosphates in eukaryotes. The use of *D. discoideum* as model for the evaluation of drug targets was instrumental in demonstrating that mood stabilising drugs function via inositol depletion and thus attenuate inositol signalling (151,152). Lithium and VPA block the developmental cycle of *D. discoideum* at the aggregation stage. Because lithium and VPA cause developmental toxicity in *D. discoideum* it suggested

that the drug targets are present in the model system. By screening a pool of REMI mutants for developmental resistance to lithium, Williams *et al* (1999) were able to identify a resistant mutant with loss of the enzyme, Prolyl oligopeptidase (DpoA) (151). In follow up studies conducted in *D. discoideum* the loss of DpoA was demonstrated to cause elevated levels of inositol triphosphate (152). Treatment of lithium and VPA have been shown to cause a significant reduction in inositol triphosphate and thus the loss of DpoA was able to overcome the toxic effects of the drugs (152). These *D. discoideum* studies linked the cellular effects of mood stabilisers with the 'inositol depletion theory' of the cause of bipolar disorder. This mechanism of action was then able to be translated from *D. discoideum* to mammalian neuronal cells, where lithium, VPA and carbamazepine (another mood stabiliser) mediated changes to neuronal cell morphology (152). Interestingly, the mammalian neuronal cell changes induced by the mood stabilising compounds could be reversed with either co-exposure with inositol or by the inhibition of the mammalian Prolyl oligopeptidase (152). These initial discoveries using *D. discoideum* and their translation to mammalian cell biology have subsequently allowed for the mechanism of action of lithium and VPA to be further investigated in the model. King *et al* (2010), working on *D. discoideum* report on how Prolyl oligopeptidase (DpoA) indirectly mediates gene expression changes that regulate inositol metabolism and consequently lithium sensitivity (153). More recently, how VPA functions as a mood stabiliser and epilepsy treatment has been investigated in *D. discoideum* (154). The acute phenotypic effects of VPA exposure were used to explore the role of diacylglycerol kinase (DGKA). Interestingly, different isoforms of DGKA have been linked to epilepsy and bipolar disorders. DGKA functions in the phosphoinositide salvage pathway, where it phosphorylates diacylglycerol (DAG) (producing phosphatidic acid) and is thus directly involved in inositol recycling (154). Ablation of DGKA in *D. discoideum* was found to reduce the rapid acute cellular changes on cell morphology and movement caused by VPA (154). Furthermore, Kelly *et al* (2018) found that the loss of DGKA also mediated resistant to the developmental toxicity of both lithium and VPA treatment. Altogether these studies demonstrate how research in *D. discoideum* on mood stabilising drugs lithium and VPA has allowed for both the targets of the drug and the mechanism of the disease they treat to be investigated. The range of discoveries on the molecular mechanisms of the drugs, initially made in *D. discoideum* have led to further research in mammalian translational studies were the complex biological interactions have been characterised further.

A key biological mechanism attenuated by both lithium and VPA, as indicated by *D. discoideum* research, is inositol-based signalling pathways. Inositol is obtained either by direct uptake, synthesised in a two-step process from glucose-6-phosphate, or

recycled internally from pools of inositol phosphates (149) (Figure 1.7). In the inositol phosphate biosynthetic signalling cycle (Figure 1.7), inositol is first synthesised into phosphatidylinositol (PI) by PI synthase. PI is the basis for the synthesis of up to seven phosphatidylinositol phosphates: PI(3)P, PI(4)P, PI(5)P, $PI(3,4)P_2$, $PI(3,5)P_2$, $PI(4,5)P_2$ and PIP_3 (Figure 1.7). Each of these Phosphoinositides are diverse signalling molecules which mediate a range of cellular processes in eukaryotes. PI is incorporated into the membrane bound PIP_2, via PIP (Figure 1.7). Upon stimulation, PIP_2 is either converted to PIP_3 by PI3 kinase, or cleaved by phospholipase C (PLC), forming inositol-1,4,5-triphosphates (IP_3) and 1,2-diacyl glycerol (DAG) (Figure 1.7). DAG, in an enzymatic two-step process, can be recycled back to PI (Figure 1.7).

Lithium was the first bipolar treatment found to affect the phosphoinoistol cycle as a potent inhibitor of inositol monophosphatase (IMPase) and IPP (155). The enzyme, IMPase, catalyses the conversion of inositol-3-phosphate (IP) into inositol (Figure 1.7) (156). This inhibition leads to a depletion in the quantity of PI produced and a subsequent attenuation in the potential for inositol derived signalling. In *D. Discoideum,* lithium induced IMPase inhibition results in a significant reduction in PIP_3 (156). In *D. Discoideum* and mammalian neutrophils, PIP_3 acts as a secondary messenger coupling actin polymerisation to cellular signals such as chemoattractants. Therefore, PIP_3 plays an essential role in aggregation during development (Section 1.3.2.2) (Figure 1.7). Lithium induced IPP inhibition also causes the depletion of PI by simultaneously diminishing the capacity for inositol stocks to be recovered by the recycling of IP_3 (156) (Figure 1.7). A third enzyme found to be inhibited by lithium, phosphoglucomutase (PGM), converts glucose-1-phosphate into glucose-6-phophate in a reversable reaction (157) (Figure 1.7). In yeast cells, in which this effect was first reported, the inhibition leads to an accumulation of glucose-1-phosphate and therefore, presumably a reduction in cellular inositol synthesis rates (157).

VPA was also found to perturb inositol metabolism, albeit through a different mechanism to lithium (158). In yeast, Veden *et al* reported a decrease in inositol-3-phosphate (IP) and inositol in VPA treated cells, consistent with the inhibition of inositol synthase (Figure 1.7) (159). This hypothesis was confirmed later when VPA *in vivo* (at a therapeutic concentration) in yeast cells resulted in an approximate 35% reduction in inositol synthase enzymatic activity (160). Human inositol synthase was also found to be inhibited by VPA, although, VPA does not directly inhibit the enzyme, unlike the lithium inositol perturbations. *In vitro* enzymatic activity of inositol synthase was not affected by VPA and therefore mediates toxicity indirectly. This indirect inhibition is consistent with VPA functioning as a histone deacetylase inhibitor, affecting cellular metabolism

indirectly through large perturbations of cellular signalling networks. The common effects of inositol depletion for both lithium and VPA highlights the complex and uncertain nature between the two mood stabilisers (Figure 1.7). Whilst the cellular effects on inositol metabolism and signalling are widely held to be on-target effects, mediating treatment of bipolar disorders, the array of biological process affected also presents off target effects, primarily teratogenicity.

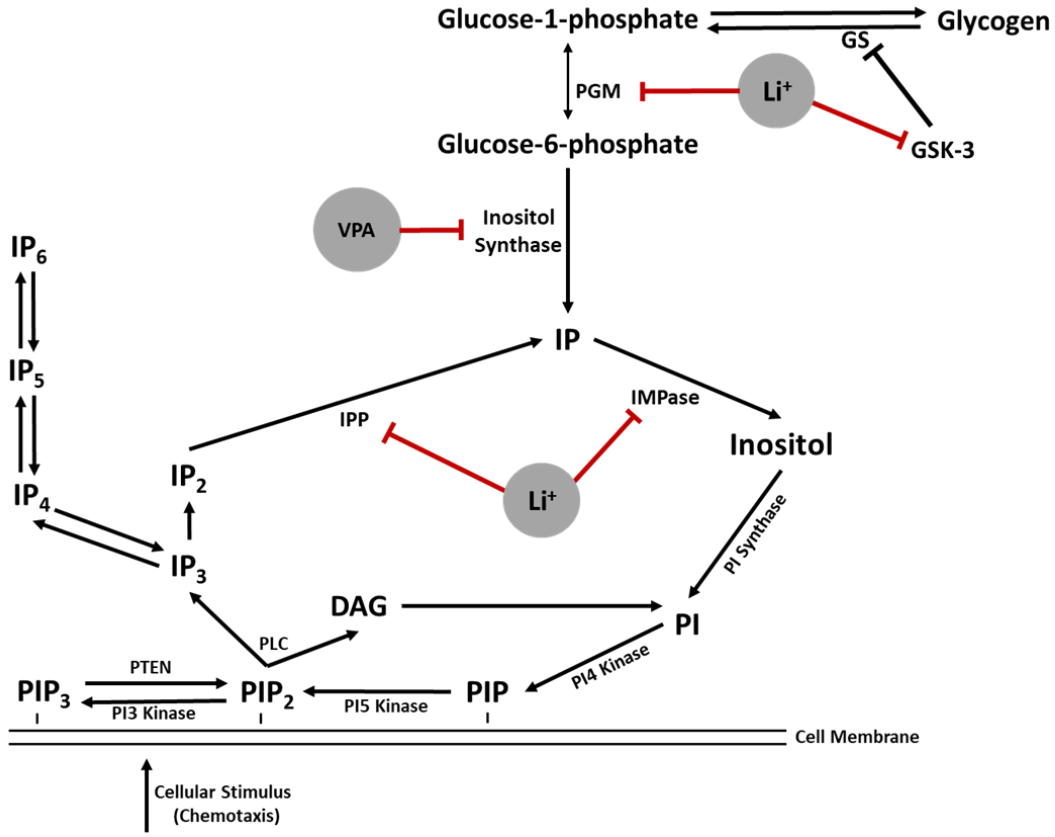

Figure 1.7. Schematic of inositol phosphate biosynthetic cycle with lithium and VPA targets. Inositol can also be synthesised de novo from glucose-1-phospate in a three-step reaction. VPA indirectly inhibits inositol synthase the rate limiting step in de novo inositol synthesis. Inositol is converted into PIP_2 by PI synthase, PI4 kinase and PI5 kinase. Upon cell stimulation PIP_2 is either converted to PIP_3 or hydrolysed by PLC releasing IP_3 and DAG. DAG is recycled back into PI whilst, IP_3 Is either further phosphorylated into secondary messengers $IP_{4\text{-}6}$ or recycled in three enzymatic steps including inositol polyphosphate 1-phosphatase (IPP) and inositol monophosphatase (IMPase), both enzymes are directed inhibited by Lithium. The cellular targets of lithium and VPA reduce cellular levels of inositol and thereby attenuate the phosphoinositide signalling pathways. Figure adapted from (156).

1.4.5 Lithium and VPA, model teratogenic compounds

The developmental toxicity of lithium and VPA in *D. discoideum* was a key characteristic from which the targets of the drugs could be evaluated (151,154). Yet, a complete understanding of how lithium and VPA mediate teratogenicity in mammals is still not fully understood. *D. discoideum,* therefore represents an ideal model for the continued investigation of the developmental toxicity of lithium and VPA. Furthermore, being partially characterised mechanistically, lithium and VPA represent ideal test teratogenic compounds to assess the genetic evaluation potential of new alternative development toxicity models.

Lithium was first reported to inhibit GSK3 in 1996 in *Xenopus* (161). Lithium directly inhibits GSK3 by competing with the magnesium cofactor within the enzyme; this mechanism was discovered in *D. discoideum* and is shown to be conserved in other model systems, including mammals (162). Principally, lithium inhibition of GSK3 is predicted to adversely affect Wnt signalling. Wnt signalling functions centrally in many developmental processes including in early developmental axis formation and cell differentiation and portioning (163). Lithium treatment has be found to induce numerous cell types into differentiation by activating Wnt signalling, including: human kidney, dopaminergic neurons, chondrocytes and osteoblasts (164–166). Furthermore, lithium and other GSK-3 inhibitors result in defects in anteroposterior patterning in Zebrafish, *Xenopus* and sea urchin development (161,163). Interestingly, the addition of inositol to a dominant inhibitory form of GSK-3 reversed the adherent dorsalising axis phenotype in *Xenopus* development, raising the possibility that the teratogenic effects of lithium could be mediated through both mechanisms (167). Recently, the inhibition of phosphoinositide signalling in chick cardiomyocytes with lithium resulted in a reduction in mature cardiomyocytes at therapeutic doses (168). Overall, a unified cause for all of the teratogenic effects of lithium exposure requires further elucidation. The relation and possible indirect molecular link between GSK-3 inhibition and phosphoinositide signalling in the teratogenicity of lithium remains to be fully characterised. Interestingly, lithium mediated teratogenicity in *D. discoideum* affects both cell differentiation and aggregation during development.

The addition of lithium to *D. discoideum* developments results in cell aggregates that do not form fruiting bodies and are comprised of a high proportion of vacuolated stalk cells, arising at the expense of the spore cell population (169). The discovery of GSKA, the *D. discoideum* GSK-3 homolog, and its subsequent ablation, creates a mutant that phenocopies lithium treatment (170). GSKA ablated mutants in development form

very few spore cells, and a large proportion of B type stalk cells (170). Lithium also causes an aggregation defect in the early stage of *D. discoideum* development before cell type differentiation. In a dose-dependent manner, lithium retards the chemotaxis speed and directionality of cells towards cAMP during the aggregation stage of development (156). At lower doses, the cells can take up to twice as long to aggregate into mounds and at higher doses, aggregation is completely abolished. This reduced efficacy in directed cell movement was phenocopied when PI3 kinase inhibitors were added to cells. This indicates that lithium suppression of PIP_3 signalling, as a result of inositol depletion (Figure 1.7), causes the teratogenic aggregation phenotype in *D. discoideum.* Lithium suppression of PIP_3 signalling is conserved in human chemotactic neutrophils (171).

VPA is a potent human teratogenic agent, the comparatively high amount of prescriptions worldwide and its strong teratogenicity has led to the definition of 'foetal valproate syndrome', a host of malformations and traits consistently observed in infants exposed to VPA (172). VPA is an effective histone deacetylase (HDAC) inhibitor at therapeutic conditions; it changes gene expression and indirectly impacts on multiple cellular signalling pathways, including phosphoinoistol signalling. HDAC inhibition caused by VPA was first reported in 2001 by Phiel *et al*, and subsequent research has interestingly revealed that other HDAC inhibitors exhibit antidepressive effects (149,173–175). Histone acetylation levels are one of the many epigenetic modifications that are responsible for the complex gene expression regulation in eukaryotes. Whilst, the precise molecular mechanism of VPA associated teratogenicity (and the broad range of associated malformations caused) is unclear and is likely mediated indirectly via multiple pathways (176). However, structural analogue studies have begun to link known VPA on-target effects to its teratogenicity (177). Recently, the HDAC inhibition directly caused by VPA has been linked to its teratogenicity. Using a twenty-strong collection of structurally diverse VPA derivatives, researchers were able to show that only the compounds that could induce histone acetylation (HDAC inhibition) caused teratogenic malformations in mice (178). Furthermore, Eikel *et al* demonstrated a quantitative correlation between the HDAC inhibitory concentration and teratogenic potential of the VPA derivatives, strongly arguing for HDAC inhibition as the primary cause of VPA teratogenicity (178). Further research has shown that VPA derivatives that do not cause effects on Wnt signalling also do not cause developmental malformations. It is therefore postulated that HDAC inhibition leads to attenuation of Wnt signalling during development and thus teratogenicity (179).

The developmental toxicity effects of VPA on *D. discoideum* at a high dose (0.9 mM) causes cell type specific differentiation effects, with prestalk cell types delayed and reduced in quantity and prespore cells completely abolished (180). VPA in *D. discoideum,* comparative to lithium, also causes dose-dependent reduction in PIP_3 signalling (152). When incubated at lower doses of VPA (0.5 mM), *D. discoideum* developments result in delayed aggregation and mound size abnormalities. With increasing doses (>0.75 mM), *D. discoideum* developments result in complete aggregation abolition, comparable to the teratogenic effects of lithium in *D. discoideum*.

In summary, mood stabilising teratogenic compounds and, more specifically, lithium and VPA, currently occupy a unique position in teratogenic research. The compounds mediate a range of cellular effects which drive their therapeutic use (and potential use) across a broad spectrum of diseases. However, despite the current knowledge of the molecular mechanism of action of both compounds, the complex biology behind both the therapeutic and teratogenic effects of the compounds remain opaque. Furthermore, the mechanistic relation between the compounds is also unclear. Both of the compounds have had their mechanisms of action investigated in *D. discoideum,* yet remain partially characterised in the model. Therefore, lithium and VPA are ideal model compounds to test whether new *D. discoideum* techniques such as REMI-Seq screening could be applied to evaluate teratogenic compounds. They allow for an unbiased genetic phenotyping approach to be assessed; globally investigating the direct and indirect targets of teratogenic compounds. These are critical and under-researched aspects of teratogenic evaluation.

1.5 Project summary and aims

The need to screen novel compounds for toxicity compliance is rapidly increasing as new compounds are produced for medical, environmental or agricultural needs. Developmental toxicity testing, including teratogenicity evaluation, is a critical aspect of toxicity testing compliance. The use of alternative models over *in vivo* testing allows for an increase in HTP screening, whilst simultaneously incorporating the 3Rs into toxicity testing. Thus, the development and use of new alternative models is critical for future screening. This would allow for both HTP screening and the evaluation of the underlying molecular mechanism of actions of (potentially) teratogenic compounds.

In this study, the potential to use the social amoeba *D. discoideum* as an alternative model for teratogenic evaluation will be assessed. As described in section 1.3.1, *D. discoideum* is an excellent model for genetic research and has a unique developmental cycle that possesses many processes which are analogous to mammalian development. Despite these natural advantages, it has received little attention as a possible teratogen evaluation model at present. Therefore, this work has two main aims. Firstly, it aims to evaluate whether *D. discoideum* toxicity endpoints for growth and developmental toxicity can be used to predict known mammalian toxicity values. This critical aspect of the study firstly requires the selection of a cohort of test teratogenic and non-teratogenic compounds, as well as the development of new *D. discoideum* HTP growth and developmental toxicity assays. The primary aim of developing new assays for *D. discoideum* is to facilitate and demonstrate the HTP potential of a *D. discoideum* teratogen evaluation assay. The second key aim of the project is to implement REMI-Seq (Chapter 4) as an unbiased genetic characterisation assay, thereby questioning whether REMI-Seq can be used to describe the relationship between the molecular mechanism of action of related teratogens.

Together the aims of this research are designed to complete the most thorough evaluation of the potential of a *D. discoideum* based teratogen evaluation model known to date.

1.6 Project objectives

To address the aims of this research, the objectives were as follows:

1. Select a cohort of test compounds for comparison to *D. discoideum.* Construct and validate new HTP growth and developmental toxicity assays for *D. discoideum* (Chapter 2).

2. Assess whether *D. discoideum* can provide predictive value for mammalian toxicity values (Chapter 3).

3. Apply new *D. discoideum* forward genetics technology, REMI-Seq, in proof of principle screens to establish whether an unbiased genetic phenotyping assay can be used in developmental toxicity evaluation (Chapter 4).

Chapter 2 – Selection of test compounds and the development of high-throughput *D. discoideum* toxicity assays

2.1 Introductory remarks

Novel pharmaceutical, cosmetic and agrochemical compounds are being synthesised at increasing rates. Consequently, thousands of new compounds require toxicological evaluation annually. Developmental toxicity represents a critical aspect of toxicity evaluation. However, developmental toxicity evaluation is very costly, both financially and in animal lives (34). Therefore, there is a pressing need to identify alternative models for developmental toxicity testing. Microbial model systems provide a new source of models for developmental toxicity testing (20). They offer an increased potential for HTP analysis and genetic tractability. To determine if microbial systems can be used as alternative model it is first important to establish the degree to which toxicity in mammalian systems is reflected in microbial systems. Such studies are also crucial as they will allow us to determine whether the genetic power of the microbial system can be used to characterise the mode of action of teratogenic compounds. Here we test this idea in order to address whether the social amoeba *D. discoideum* represents such a model.

The first consideration of any study evaluating the potential of an alternative developmental toxicity model is to identify a suitable set of compounds for evaluation. To date, only one study has been performed to evaluate the potential of *D. discoideum* as a model for toxicology studies (132). However, this did not implement a HTP assay for the measurement of toxicity, and consequently only four compounds were tested (132). Due to the small number of test compounds, the research failed to clearly establish whether *D. discoideum* could predict mammalian developmental toxicity. We therefore wanted to conduct a more thorough evaluation of *D. discoideum*. Our first objective was to identify a broader range of test compounds. Two criteria were defined to reach this objective: firstly, a sufficiently large number of test compounds should be identified and tested in order to draw significant conclusions (whilst still being experimentally manageable). Secondly, the chosen compounds should also exhibit diversity both in physical structural characteristics as well as known biological MOAs. By basing our research on a wide selection of test compounds chosen in this way we intended to incorporate good aspects of previous studies, such as quantitative measurement of

developmental toxicity, with HTP assessment, in order to ultimately obtain results that can evaluate the potential of the *D. discoideum* system.

The increasing numbers of compounds that require developmental toxicity evaluation means that the evaluation processes must be quick and provide easily interpretable data. Any new *D. discoideum* toxicity assays therefore need to be quantitative, high throughput and have the potential to be scaled up outside of an academic setting. Consequently, the assays need to be both simple in design and demonstrate automatable potential. Furthermore, a major limitation in alternative toxicity models is the expertise and training required to interpret the often-complex developmental toxicity readouts (Section 1.3.2). Therefore, any new *D. discoideum* developmental toxicity assay must have simple toxicity readouts. In the future this would help translate this work into an industrial setting as researchers with relatively little training could employ the developmental assay.

In other models, developmental assays have been adapted to make them HTP (20). For example, fluorescent reporter-based assays, in which a robotic plate reader is used to scan plates automatically, can reportedly process >200,000 samples in a 24-hour period in Zebrafish (181). Whilst this quantity of samples can only be processed with full automation, in an academic environment, a semi-automated system using similar methods could still produce a higher-throughput system (181). In the zebrafish model, the two most common methodologies for increasing sample capacity are time-lapse imaging and automated plate scanners. Both time-lapse imaging and automated scanning have been successfully used with *D. discoideum* in a fully high-throughput manner. For example, Liao et al (2016) were able to screen thousands of novel compounds to identify new chemotaxis inhibitors, using a fluorescence plate scanner and a fluorescent chemotaxis reporter strain (182). Demonstrating the efficacy of HTP *D. discoideum* assays to screen and evaluate libraries of small compounds (182).

In *in vivo* animal developments, the health of the mother can impact on the health of the foetus (183). A chemical that causes maternal toxicity can therefore indirectly cause developmental toxicity and fetal abnormalities. This poses a problem for researchers, because for compounds that cause developmental toxicity at a dose that is maternally toxic, it is impossible to establish whether the developmental toxicity is maternally mediated or directly developmentally toxic (183). Therefore, *in vivo* animal developmental toxicity testing, a distinction is made between the toxic effects on the

mother and the developing embryo(s) (184). In practice this distinction means maternal toxicity is characterised prior to developmental toxicity evaluation *in vivo* (184). However, the distinction between a compound's toxicity at different stages of an organism's life cycle is being questioned. Increasingly, toxicity exposure level testing is being used to validate new alternative toxicological models, such as the zebrafish model (185). This means that developmental toxicity testing is based on dose and exposure effects and not just on a binary classification of developmentally toxicity. These approaches have allowed the relationship between different toxicity endpoints to be compared within and between different species (186). For example, when Ducharme *et al* (2013) conducted a meta-analysis on toxicological data from over 130 compounds in zebrafish, acute toxicity (LC_{50}) significantly correlated with developmental toxicity (187). Strong positive associations were reported between acute toxicity (LC_{50}) and a diverse range of phenotypic defects, including: skeletal defects, cardiovascular defects and neurological impairments (187). Furthermore, in a later study, Ducharme *et al* (2015) demonstrated that zebrafish acute toxicity values (LC_{50}) significantly correlate to *in vivo* rat acute toxicity values (LC_{50}) (188). The significant correlation between a compounds' toxicity values in either acute or developmental endpoints inevitably leads to the suggestion that they are in fact a measurement of the same (or very similar) adverse cellular events. As growth and developmental toxicity endpoint values significantly correlate in complex organism such as zebrafish and rat, we also wanted to test whether they correlate in the microbe, *D. discoideum*. In *D. discoideum* the separation of growth and development allows for this to be accurately tested (Section 1.3.2).

General toxicological information can be condensed to simple readouts such as decreased cell growth rate or death. However, developmental toxicity could lead to a greater range of phenotypes; which could be used to interrogate the mechanistic MOA of developmental toxicity. Therefore, in this study, two new *D. discoideum* growth and developmental toxicity HTP assays were developed. Allowing for the relationship between the two toxicity endpoints to be interrogated in an HTP manner.

This chapter firstly focuses on the selection of the test compounds, subsequently characterised in the study, and the development and validation of new toxicity assays.

2.2 Aim

Select a cohort of test compounds and construct new HTP growth and developmental toxicity assays by which to screen them.

2.3 Objectives

- Select a cohort of well characterised and annotated mammalian teratogenic and non-teratogenic compounds.

- Construct, optimise and validate a time-lapse microscopy based HTP growth toxicity assay.

- Construct, optimise and validate a fluorescent reporter based HTP and quantitative developmental toxicity assay.

2.4 Results

2.4.1 Test compound selection

The first phase of test compound selection involved compiling a list of well-annotated mammalian teratogens. However, the degree to which each teratogen has been annotated and classified varies widely. Whilst some compounds have been classified as human teratogens, others have only been characterised in animal models and many are only suspected to be teratogens due to case study-based research (189). Given that the majority of annotated teratogenic compounds are medicines, the US FDA classifications of teratogens was used to assess teratogenic capacity. Only compounds from the C, D and X categories of the US FDA classifications were included for further analysis. Categories C, D and X are defined as, 'risk cannot be ruled out', 'positive evidence for risk' and 'contradicted in pregnancy' respectively (Table 1.2) (30). Well-annotated teratogens that were not medicines were only considered if they had a 1A or 1B reproductive toxicity classification from the EU chemical agency, an equivalent to a C, D or X FDA classification (190). The first stage of selection, resulted in a list of 107 compounds that could be defined as mammalian teratogens (Figure 2.1).

In the second phase of the compound selection process, teratogens were sub-classified by their known mammalian mode of action (MOA). This allowed the final selection of teratogenic compounds to represent the broadest possible teratogenic MOAs, and thus allows an unbiased appraisal of *D. discoideum.* In the most comprehensive attempt to categorize the teratogenic mechanisms of medical drugs, Van Gelder *et al* (2010) report that teratogenic medicines could be categorized into at least one of six primary MOA categories: folate antagonism, neural crest cell disruption, endocrine disruption, oxidative stress, vascular disruption and specific enzyme/receptor mediated. The final category, 'specific enzyme/receptor mediated', can be considered an umbrella heading under which many more specific categories of MOA can be grouped. The first five categories are the most concise classifications into which Van Gelder *et al* (2010) could assign teratogens and therefore represent the foundation from which an equal number of final test compounds were selected. Multiple reviews, which independently proposed the different MOA classifications, were consulted in the categorisation process (189,191–193) (Figure 2.1).

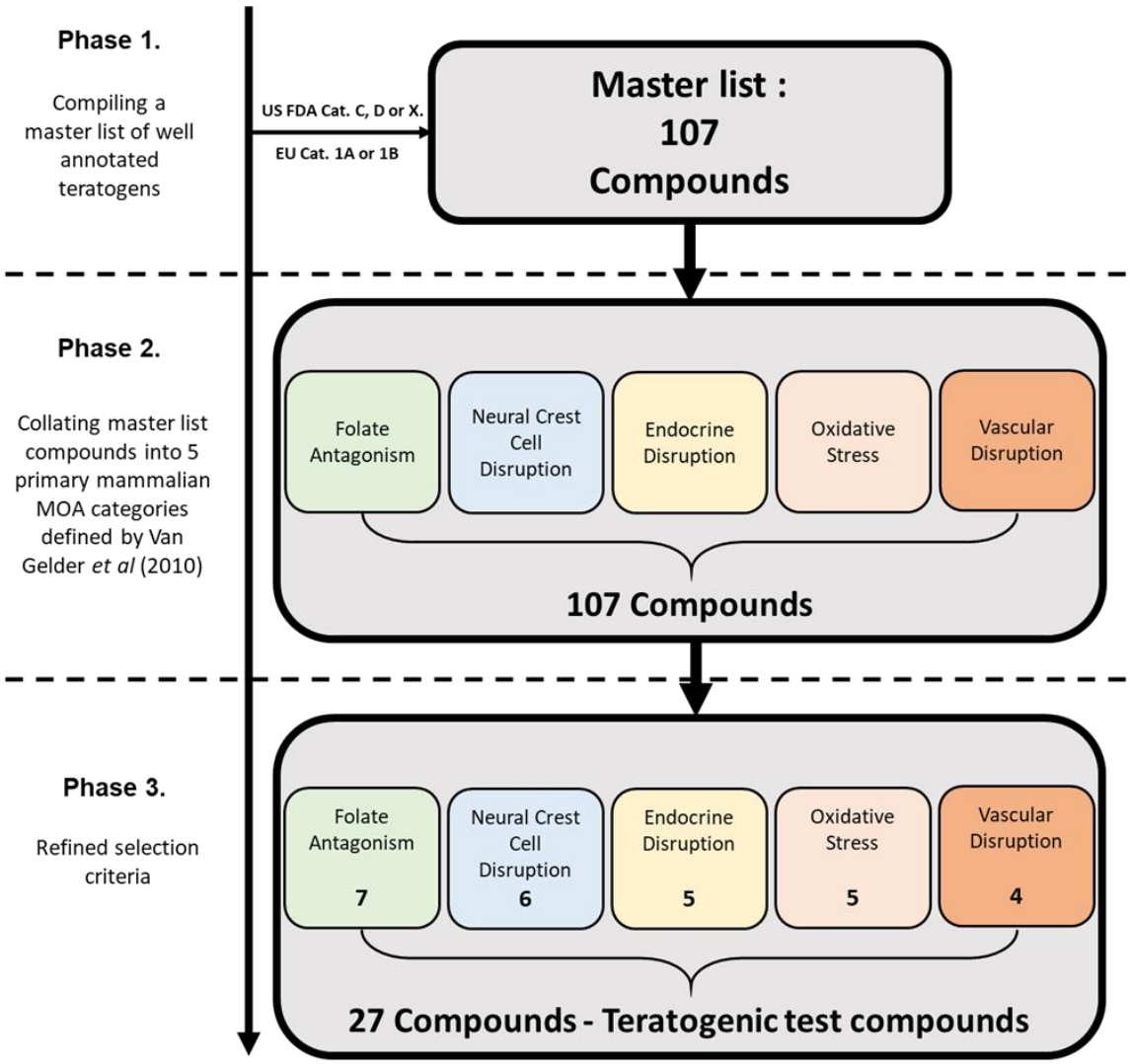

Figure 2.1. Schematic flow diagram of the three phases of compounds selection and categorisation. From top to bottom, phase one compiled annotated teratogens into a master list using the US FDA and EU teratogen classification systems. Phase two collated compounds from the master list into categories defined by van Gelder *et al* (2010). The final phase refined the compounds leaving only well-annotated and well-characterised compounds in the 1st cohort of teratogenic test compounds.

Finally, the list was refined so that approximately 5 well-characterised and -annotated teratogens were selected for each key group. The refined selection criteria were predominately based upon the depth of characterisation of specific teratogens, with practical considerations of cost and suitability for laboratory use (including excessive toxicity) also taken into consideration (Figure 2.1). As a result, 27 teratogenic compounds were selected to be screened in this study (Table 2.1).

Table 2.1. All teratogenic and non-teratogenic test compounds

Number	Compound Name	General Usage	Classification	US FDA	Primary Solvent
1	**Methotrexate** hydrate	Anti-cancer	Teratogen	X	DMSO
2	**Pemetrexed**	Anti-cancer	Teratogen	D	H_2O
3	**Lamotrigine**	Bi-polar, Epilepsy	Teratogen	C	DMSO
4	**Carbamazepine**	Bi-polar, Epilepsy	Teratogen	D	DMSO
5	**Phenytoin** sodium	Epilepsy	Teratogen	D	DMSO
6	**Primidone**	Epilepsy	Teratogen	D	DMSO
7	**Valproic Acid** sodium	Bi-polar, Epilepsy	Teratogen	X	H_2O
8	**Lithium** chloride	Bi-polar disorder	Teratogen	D	H_2O
9	**Acitretin**	Auto-Immune	Teratogen	X	DMSO
10	**13-*cis*-Retinoic Acid**	Acne	Teratogen	X	DMSO
11	**Retinoic Acid**	Acne	Teratogen	D	DMSO
12	**Bosentan** hydrate	Hypertension	Teratogen	X	DMSO
13	**Sitaxentan** sodium	Hypertension	Teratogen	D	H_2O
14	**Bexarotene**	Anti-cancer	Teratogen	X	DMSO
15	**Cadmium Sulphate** monohydrate	Industrial Electrical Component	Teratogen	-	H_2O
16	**Hydroxyurea**	Antineoplastic	Teratogen	D	H_2O
17	**Cyclophosphamide** monohydrate	Anti-cancer	Teratogen	D	H_2O
18	**Cisplatin**	Anti-cancer	Teratogen	D	H_2O
19	**Lead (II) Acetate** trihydrate	Heavy Metal	Teratogen	-	Glycerol
20	**Clomifene** citrate salt	Estrogen Receptor Modulator	Teratogen	X	DMSO
21	**Raloxifene** hydrochloride	Estrogen Receptor Modulator	Teratogen	X	DMSO
22	**Finasteride**	Male Baldness Treatment	Teratogen	X	DMSO
23	**Vinclozolin**	Fungicide	Teratogen	-	DMSO
24	**Diethylstilbestrol (DES)**	Synthetic estrogen	Teratogen	X	DMSO
25	**Salicylic Acid**	Pain, Inflammation	Teratogen	C	H_2O
26	**Nifedipine**	Anti-Angina, Anti-hypertensive	Teratogen	C	DMSO
27	**Warfarin** sodium	Anticoagulant	Teratogen	D	DMSO
28	**Metoclopramide** hydrochloride	Stomach medication	Non-teratogen	B	H_2O
29	**Cefotaxime** sodium	Antibiotic	Non-teratogen	B	H_2O
30	**Sulfasalazine**	Rheumatoid arthritis	Non-teratogen	B	DMSO
31	**Ascorbic acid**	Dietary vitamin	Non-teratogen	A	H_2O
32	**Acebutolol** hydrochloride	Anti-Angina, Anti-hypertensive	Non-teratogen	B	H_2O
33	**Camphor**	Multipurpose compound	Non-teratogen	B	Ethanol
34	**Citric acid**	Acidifier	Non-teratogen	-	H_2O
35	**Penicillin G** sodium	Antibiotic	Non-teratogen	B	H_2O
36	**Saccharin** sodium hydrate	Sweetener	Non-teratogen	-	H_2O
37	**Metformin** hydrochloride	Diabetes treatment	Non-teratogen	B	H_2O

Finally, a group of well-defined non-teratogenic controls were selected to complement the teratogenic test compounds. Once again, the US FDA teratogen classification system was used; with only compounds with an A or B, defined as ‘controlled studies show no risk’ and ‘no evidence of risk in humans’ respectively, selected (Table 2.1). A master list of 30 non-teratogenic compounds was compiled from which 10 compounds were selected for the test cohort (Table 2.1). Again, practical considerations contributed to the refinement of the list. In addition, the use of specific compounds as non-teratogenic controls in the recent research effort to establish a zebrafish developmental toxicity model was taken into account in the selection of test compounds (52,57).

The final 37 test compounds were selected primarily on the basis of their classification and characterisation of (non-) teratogenicity. However, we also ensured that the list also represents compounds with diverse structural and physical properties (Appendix table A7.1). The compounds are equally split between H_2O and Dimethyl sulfoxide (DMSO) as primary solvents with 17/37 (45%) and 18/37 (48%) respectively. Furthermore, the compounds are also structurally diverse with a molecular weight range between 42.39 and 598.08 g/mol, which corresponds to a range in calculated structural complexity (2 – 839) (Appendix table A7.1). The polar surface area (PSA) of the compounds ranges between 0 and 230 with a median of 71.6. Compounds with a PSA greater than 140 are generally less capable of permeating eukaryotic cell membranes (194). Conversely, compounds with a PSA score below 60 are well absorbed. The test compounds selected have diverse PSA scores across the cohort, in order to represent the different natural propensities for cellular absorption (Appendix table A7.1). The final physical characteristic assessed, the partition coefficient, is a measure of a compound's hydrophobic or hydrophilic nature. Similar to the PSA, the partition coefficient relates to cellular uptake efficiency, by influencing whether compounds require a transporter or efflux channel to enter the cell and influencing the ability for cells to remove chemicals from the cytosol. Once again, the test compounds exhibit a range of values across the partition coefficient (-2 – 8.19 CLogP) (Appendix table A7.1). These properties were also compared between the non-teratogenic and teratogenic compounds (Figure 2.2). No significant difference was observed between the two groups, with the exception of the partition coefficient (Figure 2.2 D). However, there is no difference in PSA values (Figure 2.2 C) and the CLogP values strongly overlap, therefore we consider the lists to represent a diverse range of compounds without any major differences between the teratogenic or non-teratogenic compounds. Thus, the 37 chosen test compounds were subsequently used in the remainder of this research (Table 2.1).

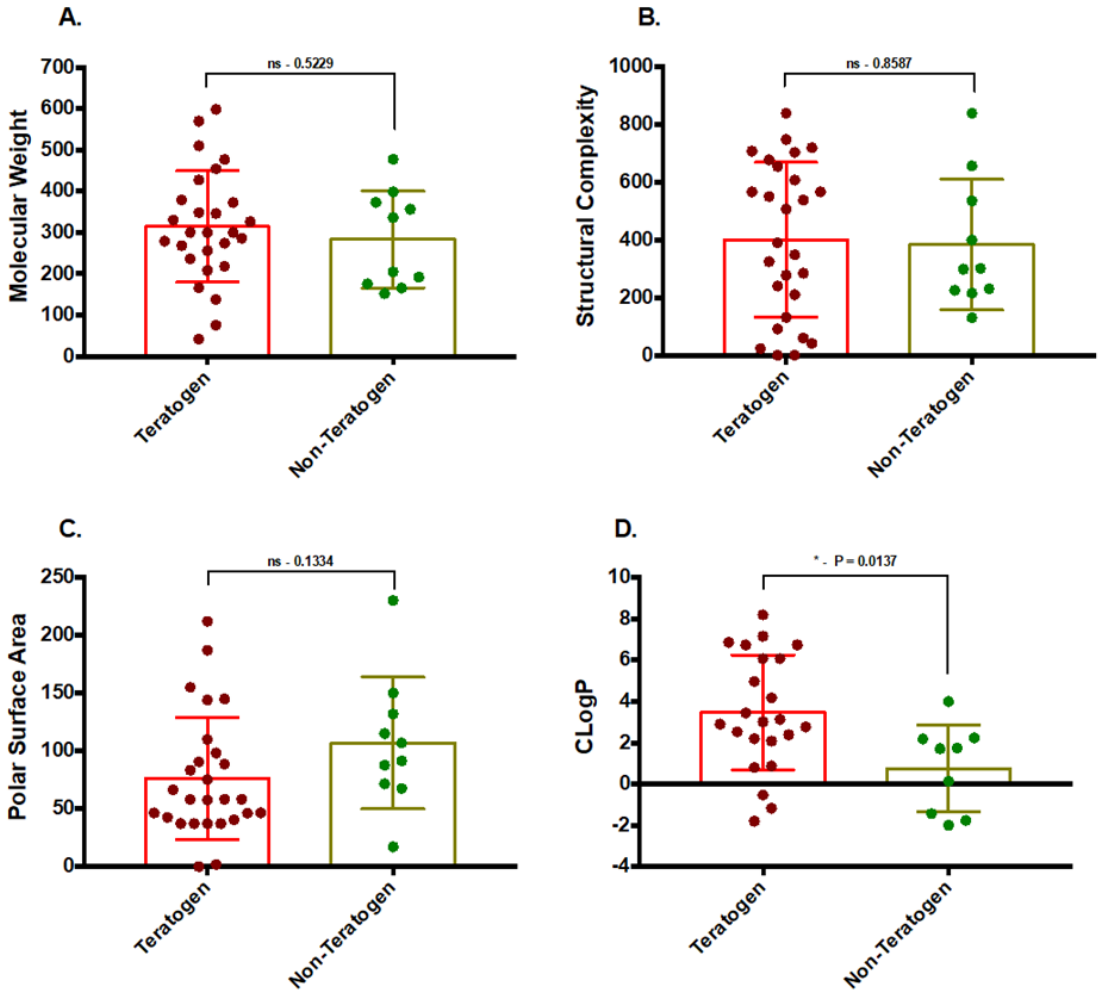

Figure 2.2. Comparison of the physical characteristics of the selected teratogenic and non-teratogenic compounds. The molecular weight **(A)** and the calculated structural complexity **(B)** between the teratogenic and non-teratogenic test compounds are not significant. **C.** A comparison of the polar surface area of the teratogenic and non-teratogenic compounds is not significant. **D.** A significant difference is found between the teratogenic and non-teratogenic compounds partition coefficient (CLogP) (P = 0.013) (Determined by unpaired T-test $p<0.05$).

2.4.2 Development, optimisation and validation of a novel time-lapse microscopy-based growth toxicity assay for *D. discoideum*

In conventional *in vivo* toxicity testing, compounds are generally only considered teratogenic when the developmentally toxic dose results in minimal or no maternal toxicity (52). Therefore, before developmental toxicity can be assessed in any model system, the general toxicity of the test compound must be determined. This principle is also applied to cell based alternative assays, such as the mouse or human embryonic stem cell assays (Section 1.2.3). In these assays both cytotoxicity and developmental toxicity endpoints are measured (64). There is also increasing evidence that cytotoxic and developmental toxicity are comparable. We therefore also sought to investigate the relationship between these toxicity endpoints in *D. discoideum.* Furthermore, by defining toxicity values using different endpoints more comparisons to mammalian data will be possible. This should allow us to better evaluate whether *D. discoideum* can be used to predict mammalian endpoints. Therefore, it is important to measure toxicity effects on growth as well as development.

In order to measure toxicity, we sought to establish a method to measure the growth rate of *D. discoideum* cells in the presence of each compound. The use of a haemocytometer is the primary method to measure cell number in *D. discoideum* (76). This is because *D. discoideum* cells are irregularly sized and settle rapidly, and thus are unsuited to measurement by optical density (195). Alternatives, such as coulter or growth counter machines, allow for more accurate measurement of cell number, but still require individual samples to be processed for counting and are low throughput. Manual cell counts require a considerable amount of a researcher's time, with measurements repeatedly made over several days to produce a growth curve, ultimately reducing the capacity to screen a high number of compounds (196). Consequently, applying these methods to toxicity analysis would require multiple sampling over time making HTP analysis difficult. In fact, ideally, a cell growth toxicity assay would not require manual input during the compound dosing period; allowing for the assay to be automated in the future.

D. discoideum cells can be grown vegetatively attached to a substratum and thus a whole population can be imaged using a single focal plane. We therefore investigated the possibility of developing an alternative assay (multi-well plate based) that would allow *D. discoideum* growth to be measured in an HTP manner by time-lapse microscopy. In this, cells were filmed over a period of time and the number of cells per frame plotted to

generate a growth curve. The automation of the filming process using a programmable automated stage and multi-well plates allows for the development of a semi-automated HTP growth assay. The first requirement of this type of automated system is the recognition of individual cells. The TrackMate plug-in for Image J software was tested to count cells, frame to frame (197). This was found to work well when the image was inverted, giving a stronger contrast between background and cells (Figure 2.3 A).

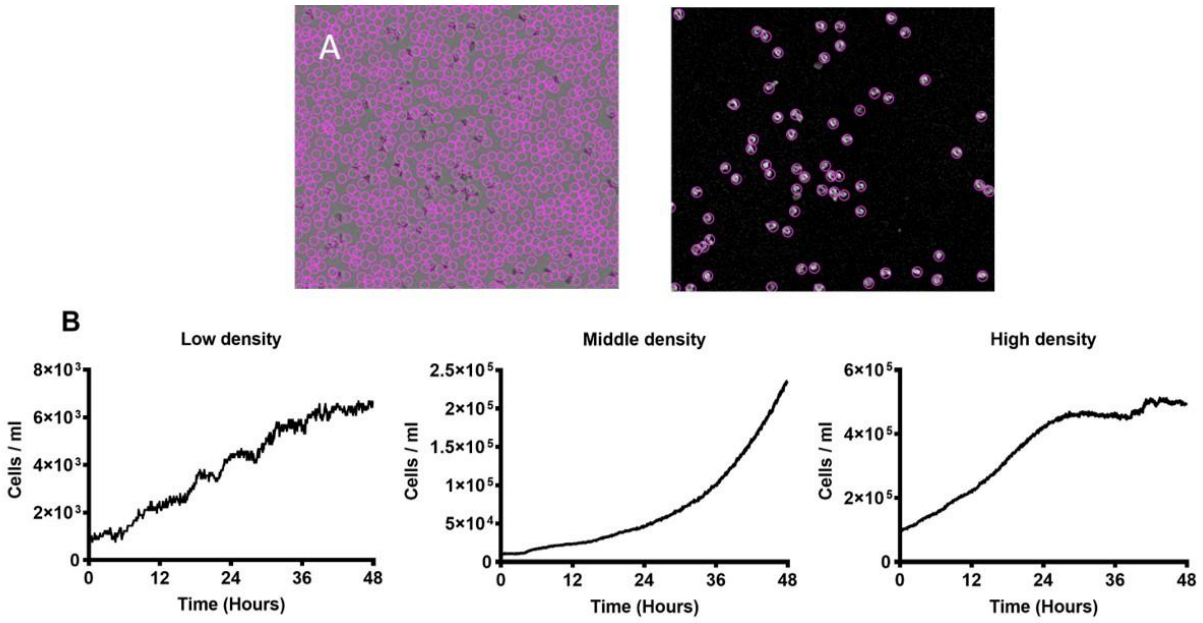

Figure 2.3. Automated cell recognition and reconstructed growth curves from differing seeding densities. A. Automated cell recognition cannot differentiate between individual cells (Left Panel) unless the image is inverted causing a greater contrast between cell and background (Right Panel). **B.** 48h growth curves constructed with initial seeding densities of $1x10^3$, $1x10^4$ and $1x10^5$ / ml (Left, middle and right graphs respectively). Data represents mean cell density of 8 technical replicates.

Cell density affects the growth rate of axenically grown *D. discoideum* cells, with lag, log and stationary growth phases (data not shown). We wanted to compare growth rates during the log phase of growth. Therefore, growth conditions that minimised the lag and stationary phase and thus maximised the log phase were desired. To determine the density that produced a smooth, accurate growth curve whilst maintaining individual cell recognition, multiple wells were filmed for 48 hours with starting densities ranging between $1x10^3$/ml to $1x10^5$/ml, with a framerate of 7.5 minutes (Figure 2.3 B). At the lower cell densities, the number of cells that migrate in and out of frame accounted for a large percentage of overall cells filmed, ultimately resulting in a noisy growth curve (Figure 2.3 B). In contrast, at the highest seeding density, a smooth growth curve was seen although cells appeared to reach stationary phase after only 24 hours of growth.

Inspection of the data revealed this is due to problems with cell detection and not a halt in cell growth. Cells begin to overlap one another at higher cell densities and single cells cannot be distinguished (Figure 2.3 B) (Data not shown). Consequently, the middle density of $1x10^4$/ml was found to produce the most reproducible growth curves (Figure 2.3 B).

A major obstacle to creating an assay that is HTP is large amounts of data slowing down processing time. Therefore, we wanted to minimise the image file size created during each assay. By reducing the number of images taken, the time need to process the images is also reduced. In order to determine the lowest possible frame rate without increasing error, frames were sequentially removed from data extracted from three wells originally filmed at 7.5-minute frames (Figure 2.4 A). The error of the growth rate is unaffected with frame rates between 7.5 minutes and 1 hour. However, with lower frame rates of 2, 4, 8 and 16 hours, the error between the three wells increased (Figure 2.4 A). Therefore, all subsequent growth assays were conducted with a one-hour frame rate.

In order to further increase the throughput of the growth assay we wanted to film cell growth in multiwell plates. Filming cells in a multi-well format reduces manual input and facilitates HTP. This also allowed the inter- and intra-well growth rate reproducibility to be compared. We first tested whether cells in different parts of the same well grew at a different rate. This allowed us to determine whether replicate films within a single well were required. Using 24 well plates, growth variance within and between wells was simultaneously assessed (Figure 2.4 B). Cells were filmed in 9 wells, with five growth films equally spaced within each well (Figure 2.4 B). There was no significant difference in growth rates between any of the five positions within a well (Figure 2.4 C). There was also no significant difference in growth rates between the 9 different wells (data not shown). Therefore, cell growth rate and its measurement are consistent both within and between separate wells. Finally, we tested whether the assay could be scaled up to allow more compounds and/or concentrations to be tested simultaneously. The above assays were performed in 24 well dishes, so we next tested the growth rate in 96 well dishes. (Figure 2.4 D). The average doubling rate is slightly faster in a 24 well plate, although not significantly different, with the error between wells similar in both formats (Figure 2.4 D). With a greater capacity for HTP and lower associated costs, the 96-well format (in triplicate) was selected for use in all subsequent growth assays.

Finally, once the time-lapse microscopy growth assay had been optimised, the assay was validated by testing the effects of lithium, a known cytotoxic and teratogenic

agent characterised in multiple model systems (168,198). Growth rates in lithium chloride (LiCl) were compared to an untreated control between an incubation period of 8 and 48 hours (Figure 2.4 E). The growth rate of cells treated with 5 mM LiCl is unaffected, but higher concentrations of 10- and 20 mM reduced growth rates to ~77 and ~30 %, respectively (Figure 2.4 E). The toxicity threshold of LiCl has been is reported to occur at dosages >6mM, with concentrations above 10 mM reported to be cytotoxic in both *D. discoideum* and different mammalian cell types (198,199). The comparable results to previous studies validate the efficacy of the growth assay. This assay therefore provides a HTP method to assess toxicity during the growth phase in *D. discoideum*, as defined as a significant reduction in cell population doubling rates.

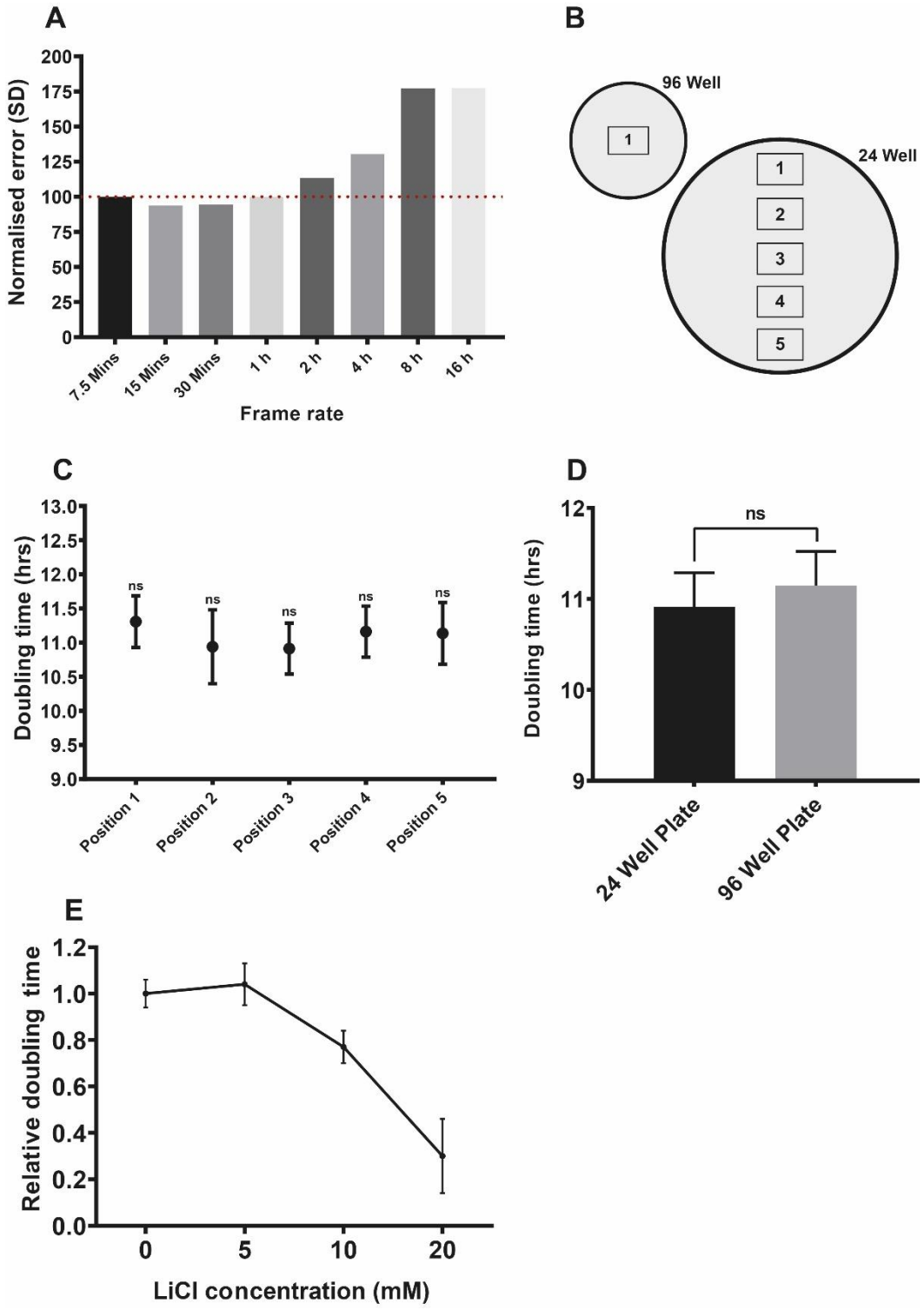

Figure 2.4. Optimisation of a time-lapse microscopy-based growth assay.
A. Sequentially removing frames from a triplicate set of films shot with 7.5-minute frames results in an increase in error with a frame rate ≥2 hours. **B.** Schematic representing the position of frames within a 24 and 96 well. **C.** Doubling rates associated with five separate locations within a 24 well exhibit no significant difference P= 0.78 (Determined by ANOVA $p<0.05$) (Mean and S.D., n=45). **D.** Doubling rates between 24 and 96 well plates are not significantly different with similar error between wells P=0.21 (Determined by unpaired T-test $p<0.05$) (Mean and S.D, n=9). **E.** Relative growth rates of Ax4 (8-48 hour) when treated with 5, 10 and 20 mM LiCl (Mean and S.D., 3 technical replicates).

2.4.3 Construction, optimisation and validation of a novel quantitative developmental toxicity assay for *D. discoideum*

A developmental assay for screening the teratogenic effects of compounds needs to provide robust and reproducible read outs of the key processes and transitions throughout the *D. discoideum* developmental cycle. Previous attempts to quantify the effects of teratogens on the development of *D. discoideum* have used reporter strains in which LacZ was placed under the control of cell type specific promoters. These reporters are induced at the mound stage of development. Thus, they only provide a coarse readout of developmental progression. This method is also labour-intensive and requires destructive sampling, meaning that replicates are required at every time-point (132). It therefore is unsuitable for HTP analyses. However, we reasoned that a variation on this approach using a wider variety of promoters to control expression of GFP or RFP at different developmental stages might provide a suitable alternative (84). This would allow real time measurements of promoter activity throughout development. Moreover, although expression can be quantified by microscopy, the use of a fluorescence multiwell plate reader (FPR) greatly increases the potential for HTP analysis. An FPR-based assay for *D. discoideum* would allow different developmental reporter strains to be quantitatively measured over developmental time, reporting on the advancement through key developmental stages. Furthermore, the assay would be automatable, quantitative and HTP. Indeed FPRs form the basis of HTP methods in a wide range of bioassays across a number of model organisms and is commonly adapted for automation (181).

2.4.3.1 Optimisation of *D. discoideum* development to a 96 well format

In the laboratory, *D. discoideum* development is initiated by removing cells from growth media and plating cells onto nutrient-free agar (76). It is critical in a FPR-based assay that the timing of development and therefore fluorescent marker expression is uniform within the same population of developing cells. Many factors can affect the uniformity of development, which in extreme cases can result in heterogeneous development on the same plate. Standard methods have been optimised for uniform development, and typically employ 6 cm or 10 cm diameter plates (76). Therefore, we next tested whether homogeneous development could also be obtained in a 96 well format.

The effects of buffer volume, total cell number plated and whether cells were spotted or spread on the agar were all tested in a 96 well plate format. Major developmental transitions of streaming to mound, mound to slug and culmination were observed to assess development quality and uniformity. The optimisation of development began firstly by defining the amount of buffer to be plated on the agar; with 5 µl found to be optimal (Data not shown). Once the quantity of buffer had been defined the effects of cell number were assessed with $2x10^5$ ($4x10^7$ / ml), $5x10^5$ ($1x10^8$ / ml) and $1x10^6$ ($2x10^8$ / ml) spotted onto plates and the homogeneity of development observed at key transitional stages (streaming, mound, slug and terminal culmination) (Figure 2.5) At $1x10^6$ ($2x10^8$ / ml), the highest cell number tested, individual streams of cells could not be observed after 6 hours of development. Many large irregular shaped mounds were formed, and later development was heterogeneous, with slugs and fruiting bodies both seen at 21.5 hours (Figure 2.5). At an intermediate cell number of $5x10^5$ ($1x10^8$/ml), a similar messy streaming phase was observed, again resulting in oversized, irregular mounds. The lower cell number of $2x10^5$ ($4x10^7$ / ml) formed well defined streams when spotted into the agar, resulting in round mounds and uniform slug formation, which resulted in a complete synchronous development (Figure 2.5). However, whilst with a spotted delivery of cells development is synchronous the size of individual structures are not uniform (Figure 2.5). Therefore, to test whether a different plating method resulted in better structure size uniformity, cells at a concentration of $4x10^7$/ml ($2x10^5$ / development) were spread rather than spotted onto the plate. The spread developments were found to transition better between stages in unison, with mounds, slugs and the resulting fruiting bodies of a similar size (Figure 2.5). Therefore, spreading $2x10^5$ cells at a concentration of $4x10^7$/ml was used in all subsequent 96 well developments.

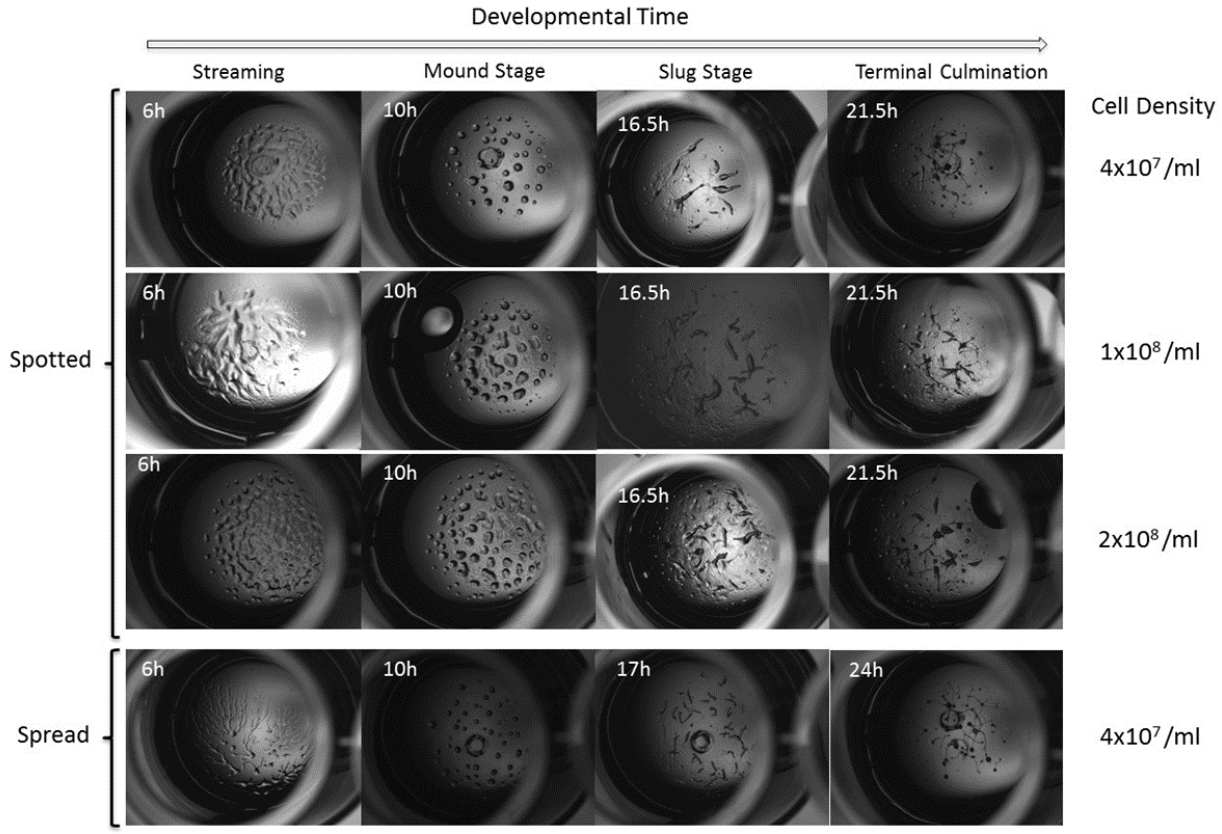

Figure 2.5. Optimisation of *D. discoideum* development to a 96 well format. Starved *D. discoideum* cells were spotted into 96 wells at concentrations of either $4x10^7$, $1x10^8$ or $2x10^8$ cells per ml. Development was observed at four key transitional stages of development, using even homogenous development as an indicator to optimal conditions. Spreading cells at from the density of $4x10^7$ / ml produces the most uniform development.

2.4.3.2 Fluorescence plate reader assay proof of principle and optimisation

FPR based assays in other model systems have been conducted in aqueous media (181). However, an agar substratum is required for *D. discoideum* to develop. Therefore, plates were scanned at both GFP and RFP wavelengths with varying quantities of agar to determine whether the agar was auto fluorescent and whether the signal was dependant on the amount of agar (Figure 2.6 A, 2.6B). Both clear and opaque black 96 well plates were tested as background signal has previously reported to be reduced using black plates (181). For both the RFP and GFP excitation and emission wavelengths, the quantity of agar within the well had no effect on the background signal (Figure 2.6 A, 2.6 B). In all conditions tested, the black opaque plates reduced the background signal for both GFP and RFP wavelengths (Figure 2.6 A, 2.6 B).

We next tested whether we could detect the fluorescence of known markers above background throughout development. For this, a PspA-GFP / EcmAO-RFP dual reporter strain was used. PspA is a prespore marker, which is expressed after cell type differentiation and is most highly expressed after ~16 hours during the slug stage (Figure 2.6C, 2.6E). EcmAO is a prestalk marker that exhibits a similar expression profile, with a peak of expression during the slug stage (Figure 2.6D, 2.6E). Three other *D. discoideum* strains were also used to optimise the system, an unlabelled parental laboratory strain Ax4, and strains constitutively expressing actin-GFP and actin-RFP. The four experimental strains were developed in a 96 well plate and after 16 hours the plate was measured at both GFP and RFP excitation/emission wavelengths (Figure 2.6F, 2.6G). At both wavelengths the negative control Ax4 strain exhibited a small but detectable signal above background, and is likely due to auto-fluorescence as previously reported (200). A much stronger signal could be detected from the actin-RFP and actin-GFP strains which, as expected, is reciprocal, dependant on whether GFP or RFP wavelengths are used (Figure 2.6F, 2.6G).

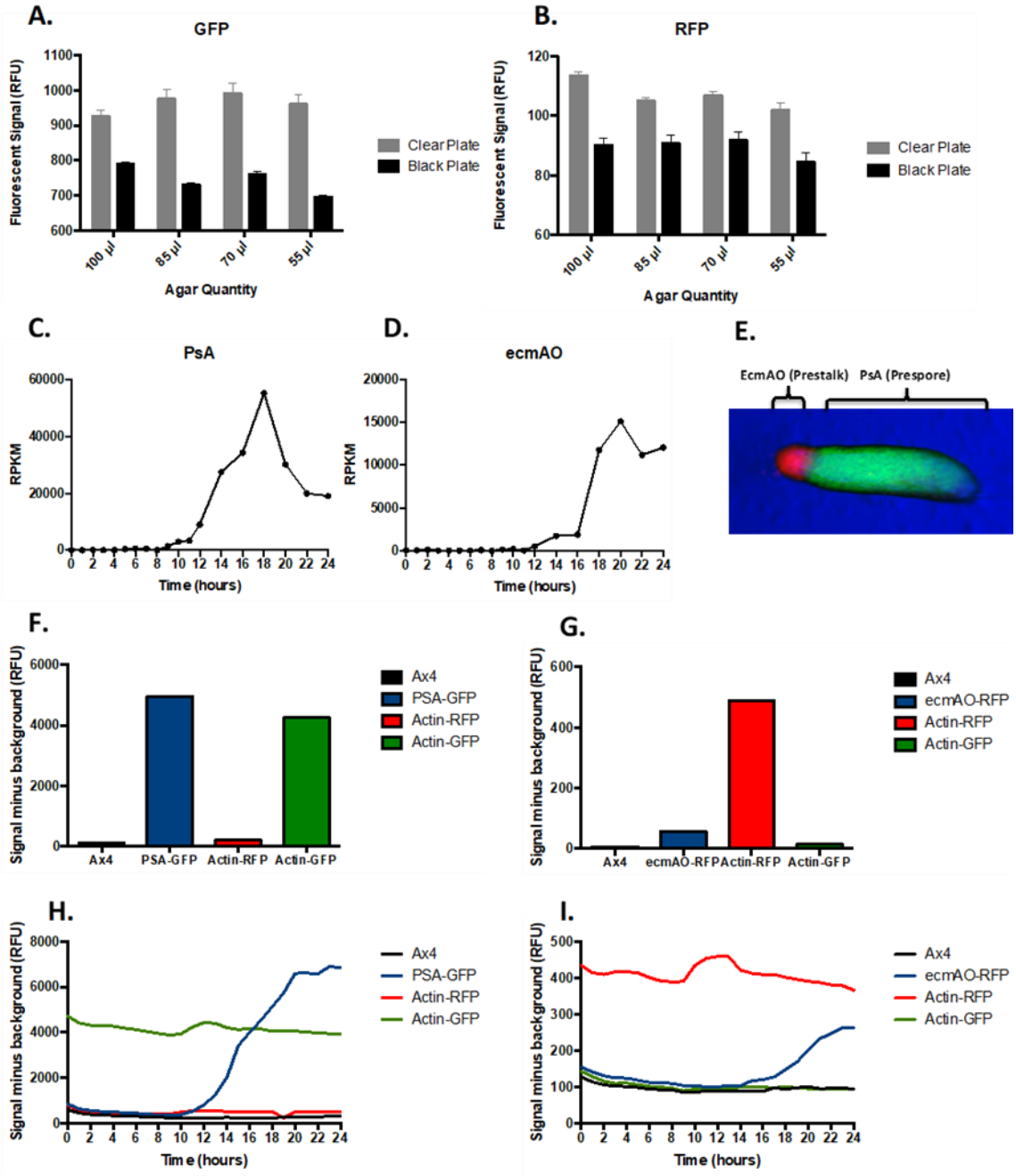

Figure 2.6. Plate reader-based *D. discoideum* quantitative development assay proof of principle. A and B Black 96 well plates reduce background GFP (A) and RFP (B) fluorescent compared to clear plates. Amount of agar used in either plate had no effect on background fluorescence. **C and D**. Cell type specific genes, PsA (C) and EcmAO (D) are most highly expressed from 12 hours of development (Data from (201)). **E**. Fluorescent image of 16h developed cells co-expressing Psa-GFP and EcmAO-RFP. ~75% of the slug expresses Psa-GFP and ~25% EcmAO-RFP. **F and G.** Non fluorescent Ax4, Psa-gfp/EcmAO-rfp and actin-gfp/rpf strains were development for 16h before GFP (F) and RFP (G) fluorescence was measured using a plate reader. A signal was detected in wells containing PsA-GFP/EcmAO-RFP for both RFP and GFP channels. A high signal from Actin-GFP and RFP strains could only be detected with the appropriate channel. Minimal fluorescent was detected for Ax4 in both channels. **H and I.** When same 4 strains were developed in the plate reader and fluorescent measure for 24h the developmental expression of PsA- GFP (H) and EcmAO-RFP (I) could be detected.

Fluorescent signals from developmentally and constitutively expressed genes could be detected at a single time point above background signals. We next tested whether the FPR could be used to provide automated and HTP measurements of expression over a full 24-hour developmental cycle. All strains were developed within the plate reader and measurements taken every 2 hours for 24 hours. It was expected that these measurements should mirror gene expression profiles seen in RNA sequencing data (201). The developments progressed normally and uniformly throughout all stages within the FPR (data not shown). GFP and RFP readings for the actin-GFP/RFP lines was constant (Figure 2.6H, 2.6I). The signal from the PspA and EcmAO reporters is slightly higher than background until 10 and 12 hours respectively, when the signal for each rapidly increases (Figure 2.6H, 2.6I). The rapid increase in signal for both reporters mirrors the expected RNA expression profile of the two genes. The RNA expression data suggests that the signal should decrease after approximately 18h of development (Figure 2.6H, 2.6I). However, a plateau in signal for both reporters is present at 24 hours (Figure 2.6H, 2.6I). The delay in signal decrease is likely due to the natural delay caused by fluorescent protein maturation, well documented in different model systems (202).

The signal strength of PspA compared to EcmAO is also consistent with the relative expression levels and proportions of prespore and prestalk cells in the slug. (Figure 2.6C, 2.6D, 2.6E). PsA is more highly expressed than EcmAO, and also marks prespore cells which form the majority of the slug (Figure 2.6C, 2.6D, 2.6E). Together, these data vindicate our approach for constructing an HTP *D. discoideum* developmental assay.

2.4.3.3 Selection of developmental reporter promoters, construction of reporter strains and validation of the assay

The FPR assay can be used to quantify gene expression during development. However, the ecmA and psA cell type reporters only allow development to be crudely analysed. We therefore wanted to design reporters that allow all major stages and transitions during *D. discoideum* development to be precisely defined. Published high resolution RNA sequencing data throughout development allows genes to be identified that are expressed at specific stages (201). Genes were chosen for candidate developmental reporter genes based on two criteria. Firstly, only genes with a comparatively high expression were selected; secondly only genes which had a sharp peak of expression representing >30% of total expression in a single time point were selected. From this initial selection, genes with the highest expression were plotted together and manually curated until 10 genes remained that covered different stages of development (Figure 2.7 A). The promoters for these 10 genes were cloned into RFP expression vectors and transformed in *D. discoideum* cells. The developmental reporter strains constructed are numbered one to ten, with one at the start of development, reporting on the growth to development transition and ten concluding with the culmination of the fruiting body (Figure 2.7 A). Because, a delay in fluorescence is expected due to mRNA translation and fluorescent protein maturation, we sought to define which stage of development our candidate genes reported on (202). Both fluorescence microscopy and a fluorescence plate reader were used to characterise each of the 10 developmental reporter strains.

Four of the reporter strains were unsuccessful. Strain two, which was designed to act as early aggregation marker, was fluorescent throughout development without any detectable peaks and was discarded (data not shown). Strain four was designed to report on the early streaming stage however, plate reader measurements and observation found the strain to fluoresce later at the mound stage and surplus to requirements (data not shown). Fluorescence could not be detected or observed in strains six or seven possibly due to low expression of the gene (data not shown).

Strain one was designed to act as a growth marker which then turns off after starvation. Indeed, peak fluorescence was observed at the start of development and decreases as development proceeds (Figure 2.7 B). Normal progression through aggregation would therefore be expected to result in a gradual reduction in florescence. Strain three is expected to begin expression after around 3h and peak at 5h. Fluorescence can be detected from ~4h, but the signal continues to rise throughout development (Figure 2.7 C). Indeed, when observed by microscopy, fluorescence can

be seen to begin during streaming and therefore strain three was classified as a streaming reporter (data not Shown). Strain five was designed to report on the mid stage of development around the mound formation stage (Figure 2.7 D). Indeed, the signal begins at approximately 11h and continues to increase to a peak around 20h. Observation of development shows these measurements correspond to the late mound stage, with fluorescence increasing through the slug stage and decreasing in later stages (data not shown). Strain five therefore, as designed, reports on development from the mound to slug stage. Strain eight was designed to be a specific slug reporter. The signal rises sharply during the slug stage, which allows the strain to be a developmental reporter of this stage. However, unlike other reporters constructed, a strong fluorescent signal is observed throughout development (Figure 2.7 E). Both strains nine and ten exhibit a sharp increase in fluorescence towards the end of development (Figure 2.7 F, 2.7 G). Strain nine reports on the transition of the culmination mound to fruiting body at approximately 20h and therefore is considered a developmental marker for early culmination. Strain ten reports on the successful completion of development and therefore the construction of a mature fruiting body (Figure 2.7 G). Consequently, although not always faithfully mirroring transcription profiles, these developmental markers cover the key developmental stages from aggregation to fruiting body formation. When previously constructed reporters for prespore and prestalk cell types are also considered, the major stages and cell types of *D. discoideum* development are covered.

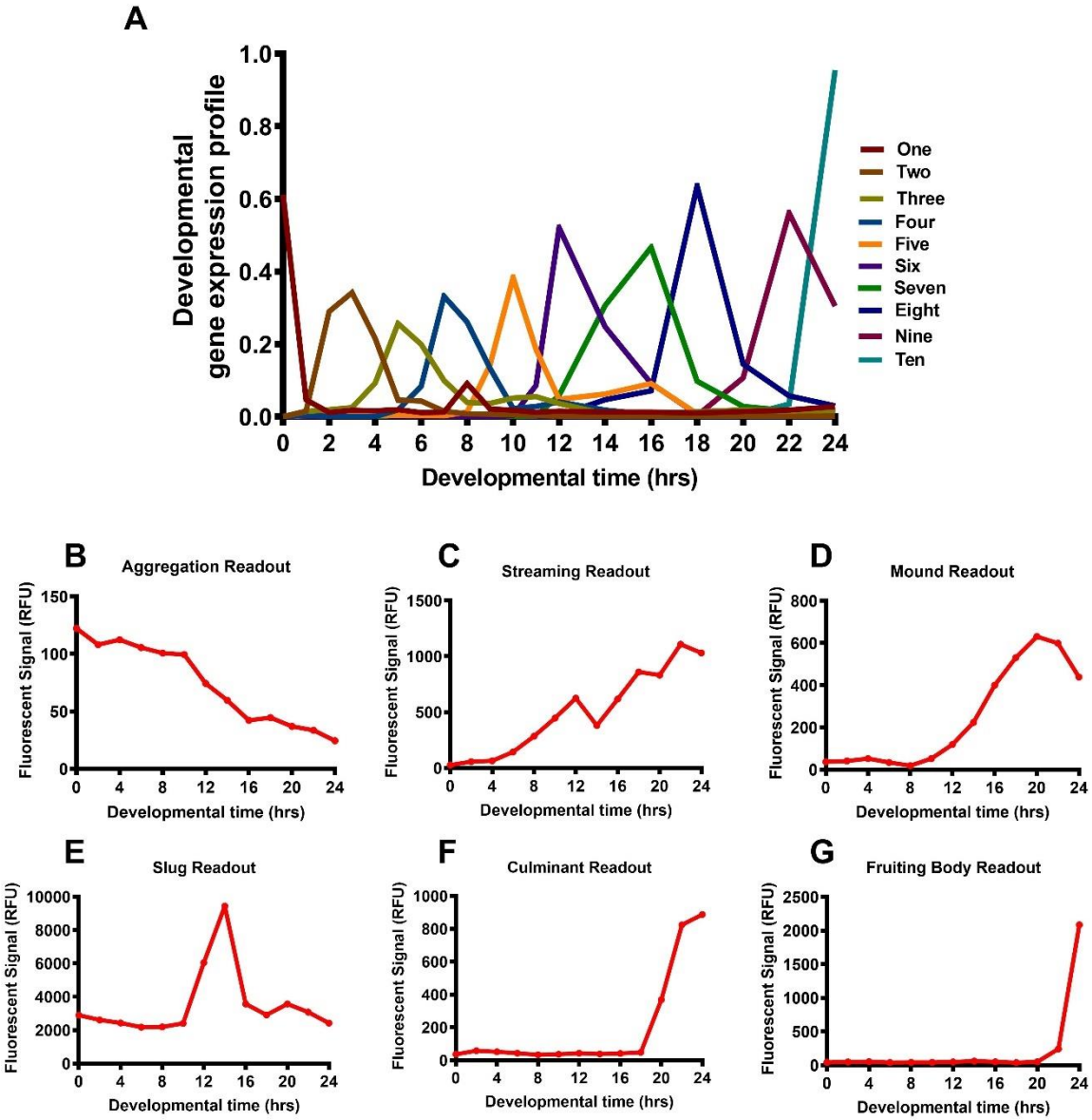

Figure 2.7. Selection of developmental reporter strains and reporter strain fluorescent profile. A. Developmental expression profile of ten genes which together report on all stages of development beginning with gene one reporting of growth to development transition and ending with gene ten that reports on fruiting body maturation. RNA expression data from (201). **B, C, D, E, F and G.** Fluorescence signal profile of successful developmental reporter strains when fluorescence signal is measured in a plate reader over a 24-hour development.

We next validated how the reporter strains responded to the effects of a known developmentally toxic compound *in D. discoideum*. Lithium chloride (LiCl) was chosen because it causes a dose dependant attenuation of cAMP chemotaxis and is thus delays or blocks aggregation (171). Aggregation is severely disrupted by acute treatment of 10 mM or a prolonged treatment at > 1mM (data not shown). In order to assess the effects of LiCl on the fluorescent reporter strains, they were developed on agar at either 5 or 10 mM LiCl. The experiment was conducted using a 96 well plate in a plate reader with fluorescence readings taken over a 24 h development period. At the LiCl concentrations assayed (5 mM, 10 mM), the aggregation block was expected to prevent any major developmental structures forming over the 24h period. Indeed, the aggregation reporter remains at high levels throughout the developmental period at both doses of LiCl when compared to the control (Figure 2.8 A). This is supported by the other major developmental reporters, which never turn on, suggesting that no multicellular development structures formed (Figure 2.8). The FPR result therefore mirrors the observed block in *D. discoideum* aggregation. Whilst this result validates the assay, we also sought to investigate whether it could be used to detect more subtle developmental phenotypes, such as an aggregation delay. Therefore, the experiment was repeated using a lower dose of LiCl (Figure 2.8 E, 2.8 F). At a dose of 2.5 mM LiCl, aggregation is severely delayed with partial, localised streaming of cells after 24h (with many cells also seen in loose aggregates) (data not shown). Again, as expected, the aggregation reporter remains on throughout the developmental period at the lower LiCl dose. However, the degree to which the reporter florescence remains is lessened in comparison to the 5 mM dose (Figure 2.8 E). This suggests a partial progression through aggregation, which should be detected in the streaming reporter. At the lower dose the streaming reporter readout does activate (Figure 2.8 F). However, the strength of the signal in comparison to the control is lessened (Figure 2.8 F), presumably because only a few structures progress to this stage of development. Therefore, both the timing and strength of signal from the reporters can be used to characterise the more phenotypically subtle aggregation delay. The FPR assay can therefore be used to define common *D. discoideum* developmental toxic phenotypes, such as developmental delays or blocks a key development stage. Furthermore, the assay is HTP, provides a quantitative readout and critically does not require any expertise on observing *D. discoideum* development.

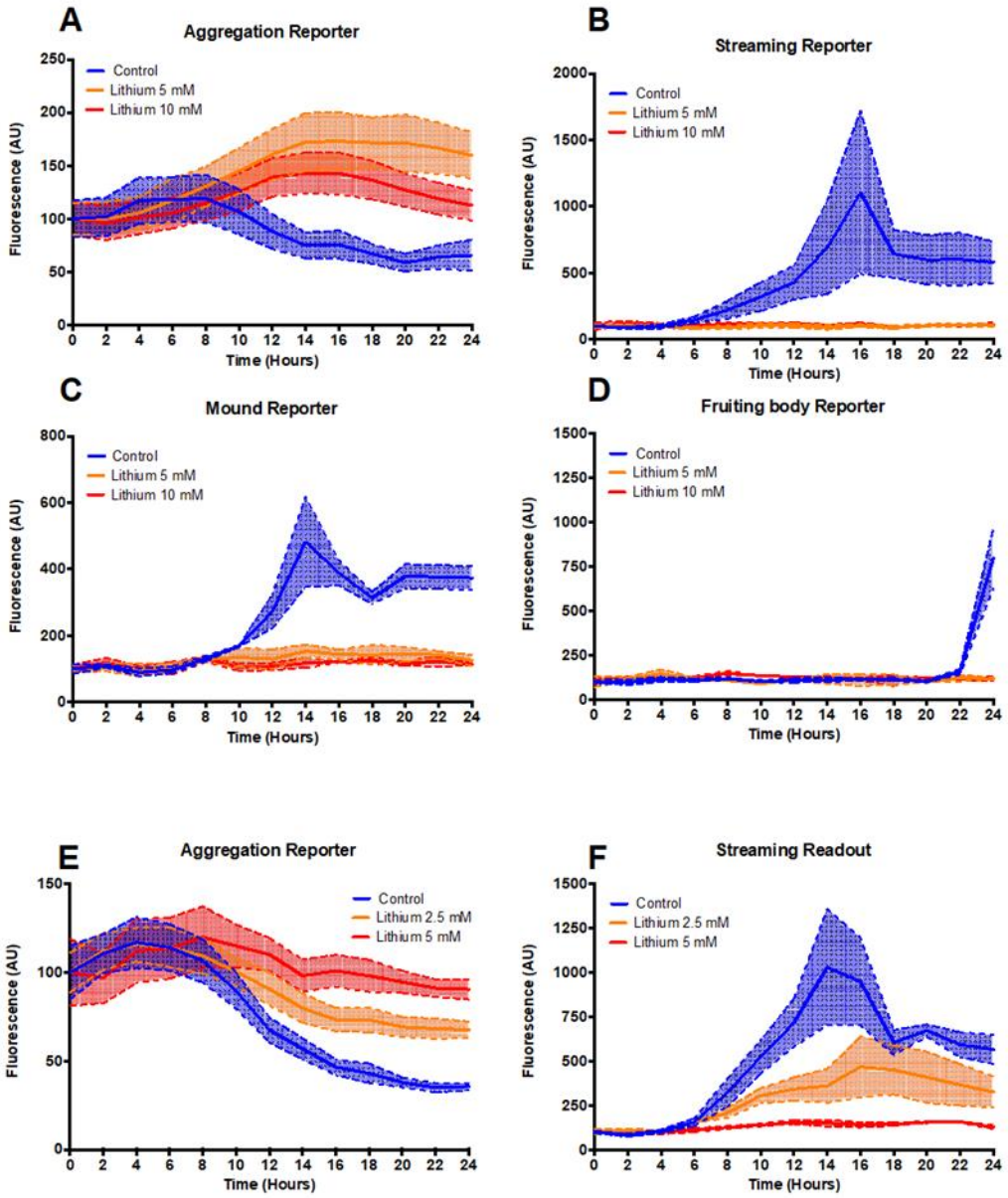

Figure 2.8. Validation of the fluorescence plater reader assay. A, B, C and D. Fluorescent reporter readout assay results for aggregation, streaming, mound and fruiting body at 5 or 10 mM LiCl. Normalised to the mean value of timepoint 0h. (Mean ± SD, 3 technical replicates). **E and F**. Fluorescent reporter readout assay results for aggregation and streaming at 2.5 mM LiCl. Normalised to the mean value of timepoint 0h. (Mean ± SD, 3 technical replicates).

2.5 Chapter discussion

This chapter details the selection of test compounds and the development of new assays which could be used to characterise the compounds' toxicity profiles. The test compounds were selected as well-characterised and classified (non-) teratogens thereby allowing accurate comparisons to be made to mammalian *in vivo* data.

To date, only one study has attempted to address the efficacy of *D. discoideum* as a teratogenic evaluation model (132). In this study, four well-characterised human teratogens –tretinoin, diethylstilbestrol, phenytoin and thalidomide – were selected for screening (132). Four test compounds is a small sample size, and thus it was difficult to draw general conclusions. Whilst there are no centralised guidelines or core sets of test teratogens from which to select test compounds, the initial phase of assessing assay efficacy in zebrafish and *Xenopus laevis* consisted of approximately 10 teratogens (61,203). Whilst these first proof of principle screens can provide some indication about the suitability of alternative models, further assessments with more compounds are required before conclusions about the predictive value of a system can be drawn (52). In the second phase of screening the number of test compounds is generally between 20 and 60, depending on the ease with which larger numbers of test compounds can be screened in different models (25,52). In contrast to preliminary efficacy screening in vertebrate model systems, our approach of designing and constructing new higher-throughput *D. discoideum* assays allowed for the initial cohort of test compounds to contain 37 compounds (Table 2.1). The initial assessment of 37 compounds (27 teratogenic and 10 non-teratogenic) allows for the overall predictive value of *D. discoideum* to be assessed. Our approach in this initial 'phase one' stage of assessment can therefore be considered analogous to later-stage studies in other alternative teratogen models.

Biasing the set of test compounds in alternative developmental toxicity model evaluation is a cause of concern (48). Augustine-Rauch *et al* (2016), suggest that because test sets of compounds are largely based on pharmaceuticals, they are biased towards containing potent biological agents (48). This, in turn, does not reflect the range of compounds that will be ultimately screened in developmental toxicity assays. Such biases could mean that the efficacy of individual model systems is overestimated (48). The simplest method to reduce the effect of biased test compound sets is to increase the number of chemicals tested. However, as well as increasing the number of

compounds tested, we also took into account the teratogenic MOA during test compound selection. This differs from other methods in which a distinction is only made between strong and weak teratogenicity, or other arbitrary groupings, such as general structure and compound class prior to testing (52,204) (Figure 2.1). Furthermore, by initially using the broadest MOA categories possible, as defined by van Gelder *et al* (2014), the predictive correlation between *D. discoideum* and *in vivo* teratogen evaluation can be conducted without extensive MOA bias. By taking this approach we are minimising the risk of only testing compounds that will inherently (not-) have toxicity outcomes.

We have designed assays that allow toxicity to be assessed through two endpoints, growth and development. Yet, as *D. discoideum* is a relatively untested model for screening chemical toxicity, which endpoints are the most applicable to mammalian *in vivo* endpoints is unknown. Furthermore, which endpoints in *D. discoideum* are the best readouts for chemical toxicity are also unknown. For example, *D. discoideum* cells change morphology in response to structurally diverse bitter-tasting chemicals (205). As a bitter taste is considered an evolved response to recognise toxic substances, the *D. discoideum* morphology change could be a readout for chemical toxicity (205). Interestingly, Cocorocchio *et al* (2015) found a significant correlation between *D. discoideum* morphology response and rat taste aversion values, for a broad range of bitter tasting chemicals (205). The study demonstrates that responses to potentially toxic chemicals significantly correlates between *D. discoideum* and animal models and that many different endpoints may be a viable measure of toxicity in *D. discoideum.* However, as our study is in an initial stage assessment of *D. discoideum* as a model for teratogenic evaluation the appropriate endpoint measures are developmental toxicity and cell population doubling rate evaluation. The growth toxicity assay fulfils two roles. Firstly, it provides a simple measure of 'general' toxicity for compounds never tested in *D. discoideum* before. Secondly, it provides a measure of toxicity to which the developmental endpoint values can be compared. A comparison between growth and developmental toxicity is important for two reasons. Firstly, as introduced in section 2.1, a significant relationship between acute and developmental toxicity have been reported both within, and between, zebrafish and rat models (187,188). Thus, by assessing both endpoints*,* their potential relationship can be established in *D. discoideum*. Secondly, it allows for compound doses to be defined as non-toxic during growth, prior to testing on development. A process analogous to untangling the potentially misleading adverse effects of maternally mediated toxicity in animal testing (Section 1.1.3). In the EU, teratogen evaluation *in vivo* is conducted after single dose and repeat dose toxicity testing, allowing compounds to be tested at doses that are negative or minimally

maternally toxic (190). With the exception of embryonic stem cell assays where cell viability and differentiation are measured simultaneously, alternative whole embryo-based assays in accordance with *in vivo* testing generally define a dose range after general toxicity testing (64). Whilst some research groups have reported testing compounds in zebrafish by using doses calculated from two mammalian species, the difference in toxicity sensitivity between species and between compound classes makes it preferable to characterise a dose range using the test model itself (52). This is made easy in *D. discoideum* because growth and development can be separated. Vertebrate embryonic development is intrinsically linked to cell proliferation. However, there is no cell proliferation during development in *D. discoideum* (76).

To our knowledge there have been no recent reported attempts to construct a HTP or semi-automated growth assay in *D. discoideum.* This is because the quantification of media turbidity with an automated plate reader, a widely developed (and commercialised) HTP technique, is not possible. This is due to the irregular size and shape of *D. discoideum* cells, which if measured by optical density produce inaccurate growth curves (76,206). However, despite this efforts have been made to develop *D. discoideum* specific growth and viability assays that are quantitative and higher throughput (207,208). However, these assays require a substantial setup time (207) or multiple destructive sampling in order to generate a growth curve (208). Consequently, it is difficult to measure the effects of large numbers of compounds on growth rate and scale up the assays for future industrial use. Other *D. discoideum* toxicity studies have avoided manually counting cells in viability assessments by using membrane impermeable dyes (130,209). Cells are incubated with the dye during treatment with toxicants and with the population observed using fluorescence microscopy at the end of the assay. Dead cells are brightly fluorescent, and thus distinguishable from alive cells. Such assays avoid an excessive need for manual input during the procedure, yet, although potentially adaptable to HTP are not currently. Moreover, they require additional reagents to function, increasing financial costs. The construction of a time-lapse microscopy-based growth assay (Section 2.4.2) allows *D. discoideum* cell population doubling rates to be assayed in a multiwell format, which in an academic laboratory substantially increases assay capacity. Other than a microscope, multiwell automated stage and growth media, the assay requires no addition reagents to function. Furthermore, a key advantage of basing an assay on the imaging of cell populations is its adaptability. In this research the growth assay is used to assess the population growth rate of compound treated cells, establishing an accurate *D. discoideum* toxicity endpoint. However, in future toxicological evaluation studies new *D. discoideum* toxicity endpoints

maybe required. For example, measurements of changes in cell morphology or cell motility, which have been used to assess chemical-mediated changes in *D. discoideum*, could easily be conducted in a modified version of the growth assay (152,205). The adaptability of our growth assay has also made it beneficial to *D. discoideum* research outside of toxicological study. The live cell tracking and HTP aspects form the basis of a new method devised to track cells during growth and differentiation (103). The adapted assay was able to investigate cell-cycle position dependency in *D. discoideum* cell type differentiation (103). The growth assay developed in this research has also, independently, been adapted for the measurement of non-axenic, wild-type strains (Data not shown). The effects on growth rate by growing different WT *D. discoideum* strains on different bacterial food sources has been investigated using the HTP assay (Dr. Balint Stewart 2019, Pers. Comm.). Beyond *D. discoideum* research, the growth assay described in this study could, with full automation, provide a methodology for increasing assay capacity for cellular systems that, like *D. discoideum,* attach to a substratum and are irregularly sized.

Manual observation of developmental progression is the simplest method by which developmental toxicity can be assessed. It is the primary method by which teratogenicity is evaluated in *in vivo* animal testing. However, *in vivo* animal testing is low through-put and the developmental toxicity phenotypes are generally gross morphological changes, making manual observation pertinent (17). Manual observation is also the core method for evaluating developmental toxicity in new alternative model systems, including zebrafish (25,52,186,210). The key limitation of manual observational, subjectivity, has led to the formation of unified scoring systems for zebrafish assays (57). However, despite unified scoring systems, only 71% teratogen classification concordance was found between two separate zebrafish laboratories working on the same set of 37 compounds (52). Beyond, causing inaccuracy due to subjectivity, manual observations are low through-put and thus expensive. Researchers need to be trained to accurately diagnosis developmental toxicity. Furthermore, as many toxicity phenotypes are subtle the training must be thorough, further increasing costs. Altogether, the expense and inaccuracies associated with manual observation in zebrafish assays have recently led to the development of automated morphological assessment of embryos (210). However, from the outset, we wanted to demonstrate HTP, quantitative, assessment of developmental toxicity in *D. discoideum* with readouts that do not require observation nor expertise.

The construction of a new *D. discoideum* assay which could be HTP, and not require observation or expertise, is challenging. Information on developmental

progression needs to clear, allowing for all stages of a *D. discoideum* development to be analysed. Furthermore, the differentiation of the different cell types also needs to be assessed (Figure 1.6). The data from the assay needs to be fine grained enough to detect a wide range of potential toxicity phenotypes, including subtle changes in either morphology, temporal progression or cell type differentiation. Yet, developmental readouts also need to be streamlined making the assay HTP. The use of fluorescent reporter strains has facilitated the rapid collection of quantitative *in vivo* data across different model organisms (181). Fluorescent reporter strains allow for measurements on live samples, preventing destructive sampling, a key limitation in previous attempts at creating a *D. discoideum* developmental toxicity assay (132). In fact, recently, fluorescent reporters have been used to screen for chemical-mediated developmental toxicity in *D. discoideum* (182). Liao et al (2017) used fluorescence aggregation reporters to screen for chemotactic inhibitory drugs in an HTP manner. The use of a fluorescence plate reader in tandem with fluorescent reporter strains facilitated the rapid collection of quantitative *in vivo* data (181,182). However, Liao et al's *D. discoideum* HTP assay does not require a full *D. discoideum* development to proceed uninhibited. To our knowledge there have been no reported attempts to use a fluorescence plate reader to quantitively measure progression through a complete *D. discoideum* development. In a zebrafish embryo model, Walker *et al*, (2012) report a method for an automated *in vivo* reporter quantification assay (181). Critically they paired a multiwell fluorescence plate reader with whole embryo developments *in vivo*. Demonstrating a HTP platform that was also flexible for a wide range of biological assays. Interestingly, Walker *et al*, (2012) used different reporter lines to quantify changes in differentiating cell types, *in vivo* (181). However, we had to assess the viability of using a similar approach for a HTP *D. discoideum* developmental toxicity assay. We were able to demonstrate that a complete *D. discoideum* development could be conducted within a multiwell fluorescence plate reader and that the effects of agar and other parameters had no effect on fluorescence measurement (Section 2.6). Initial attempts to detect a signal were unsuccessful. However, after using a plate reader with a definable Z-focus and option of top-down read, strong but sensitive signals could be detected. Both a definable Z-focus and top-down read were also critical parameters to detect fluorescence in zebrafish embryos and are therefore likely a critical feature required for a plate reader to assay fluorescence *in vivo* (181).

A key advantage of using a fluorescence plate reader in creating a HTP assay over alternative methods, including time-lapse microscopy, is the sensitivity gained with the measurements. As discussed earlier, without human observation the measurements of an automated development assay need to be able to detect subtle changes. Previously,

FPR assays have been shown to detect changes in very small subpopulations of zebrafish cell types, such as rod eye cells (181). However, *D. discoideum* developments are considerably smaller and formed of many separate structures. To demonstrate the measurement sensitivity in our developmental toxicity assay, fluorescence from a PsA-GFP / EcmAO-RFP duel reporter strain was assessed. The data showed that the signal from a PspA – GFP strain was ~49x greater than Ax4 control, whilst the signal from an EcmAO-RFP strain was only 11x stronger than the control (Figure 2.6). As PspA is both more highly expressed and also marks for prespore cells which form the majority of the slug, the result demonstrates the sensitivity of our method.

As with our HTP growth assay, a key advantage of the development assay is its adaptability. The number and makeup of the individual reporter strains can be changed to suit the parameters of different studies. For example, if a large library of chemicals needs to be screened for the inhibition of a specific biological process, such as chemotaxis, only the aggregation or slug reporters may be necessary (211). *D. discoideum*, has been successfully used in environmental and soil toxicity evaluation where the capacity to form fruiting bodies is measured observationally (130). The DDDC assay developed by Rodriguez-Ruiz *et al* (2013), would be greatly improved as a HTP assay using a modified version of our developmental toxicity assay. Using only the fruiting body marker, the assay would provide a HTP, binary readout of soil health assessment. Furthermore, as fluorescence is measured with a top-down read in the multiwell plate reader it is likely that *D. discoideum* developments using a soil substratum would be achievable. Albeit, the possibility and optimisation required for soil developments has currently not been tested.

The developmental toxicity assay we have developed is HTP, allows quantitative measurement throughout a whole *D. discoideum* development, does not require manual observation and is flexible; amenable to modification, allowing it to function across a range of different *D. discoideum* studies. Critically it does not require novel hardware to function, using only ‘off-the-shelve’ scientific instrumentation, increasing accessibility and reducing operational costs. However, whilst the method developed in this study can collect data in a HTP manner the time taken to process the data can reduce throughput. Automating data processing would further improve the HTP potential of the assay as well as reducing the need for expertise in analysing the results. Automation and machine learning are increasing being used in developmental toxicity evaluation (212). Machine learning is process that has been extensively used to improve the automation of data processing (212). For example, we could feed a machine learning algorithm fluorescence reporter data from our assay after a treatment known to cause a specific developmental

toxicity phenotype. The algorithm would then identify recurrent patterns from the reporter strains that match specific adverse phenotypes. In turn redundant measurements for each reporter throughout development can be identified, reducing the quantity of data collected, further increasing HTP potential. In a preliminary exercise, we fed a machine learning algorithm data from the aggregation reporter after lithium treatment, a compound that causes an aggregation minus phenotype (Figure 2.8). The algorithm found that of the 13 measurements taken every 2 hours across the 24-hour assay, only the final one was crucial for finding a significant difference between the control and compound treatment data (data not shown). Whilst such refinements to the data processing procedure of our FPR developmental toxicity assay are in their infancy, they highlight the potential for all aspects of the assay to be automated in the future.

Overall, the development of two new toxicity assays presented in this chapter allows for the growth and developmental toxicity profiles of our test compounds to be characterised. The large cohort of test compounds will allow for a greater appraisal of *D. discoideum*'s potential to predict mammalian toxicity values.

Chapter 3 – Evaluating the potential of *D. discoideum* to function as an alternative model for toxicity testing

3.1 Introductory remarks

If *D. discoideum* is to be used as a model for developmental toxicity testing, it is critical that it provides predictive value for mammalian toxicity. The obvious phenotypic differences between *D. discoideum* and mammalian systems make the toxicological comparison both critically important and difficult. For example, it is impossible to compare the systems based on morphology. Consequently, a simple toxicological comparison was made: is toxicity observed in either model system, and if so at what dose?

One problem with this approach, however, is that the appropriate toxicity endpoints need to be compared. This presents a challenge, as *in vivo* toxicity studies often cite different endpoints and dose descriptors (LD_{50}, $LC_{50,}$ NOAEL, LOAEL etc.) (213). Single dose acute toxicity studies generally use a small number of dose concentrations and measure mortality rates (such as LD_{50}) (Figure 3.1) (213). Longer-term chronic toxicity studies and developmental toxicity studies generally use a range of doses to establish a dose-response curve (Figure 3.1). In developmental toxicity studies, the chief motivation is safety evaluation. Consequently, they investigate doses that result in toxicity, yet reflect expected exposure levels. Therefore, the readouts are commonly the **N**o **O**bservable **A**dverse **E**ffect **L**evel (NOAEL) or **L**owest **O**bservable **A**dverse **E**ffect **L**evel (LOAEL). The NOAEL and LOAEL are the doses of a study which exhibit the highest non-toxic and lowest toxic dose respectively (Figure 3.1). Despite being widely used, NOAEL/LOAEL readouts have several limitations (214). Firstly, the use of the NOAEL focuses on a single dose and does not incorporate information on the slope of the dose-response curve (Figure 3.1). Secondly, the NOAEL is limited to an experimental dose; thus, the number and spacing of doses in a study influence its value. Finally, as variability in the data is not taken into account when defining a NOAEL, a NOAEL is likely to be higher with decreasing sample sizes. One way to avoid these limitations is to simultaneously define a LOAEL dose. By defining a LOAEL and a NOAEL dose, confidence in the value of both is increased. When only a NOAEL is defined, the toxicity threshold is assumed but not characterised to an accurate value. It is this toxicity threshold that provides a value by which to compare toxic predictivity across endpoints or species. Therefore, despite not incorporating information on a dose response curve,

the NOAEL/LOAEL threshold represents a value that can be used to compare growth toxicity and developmental toxicity between *D. discoideum* and mammalian *in vivo* data.

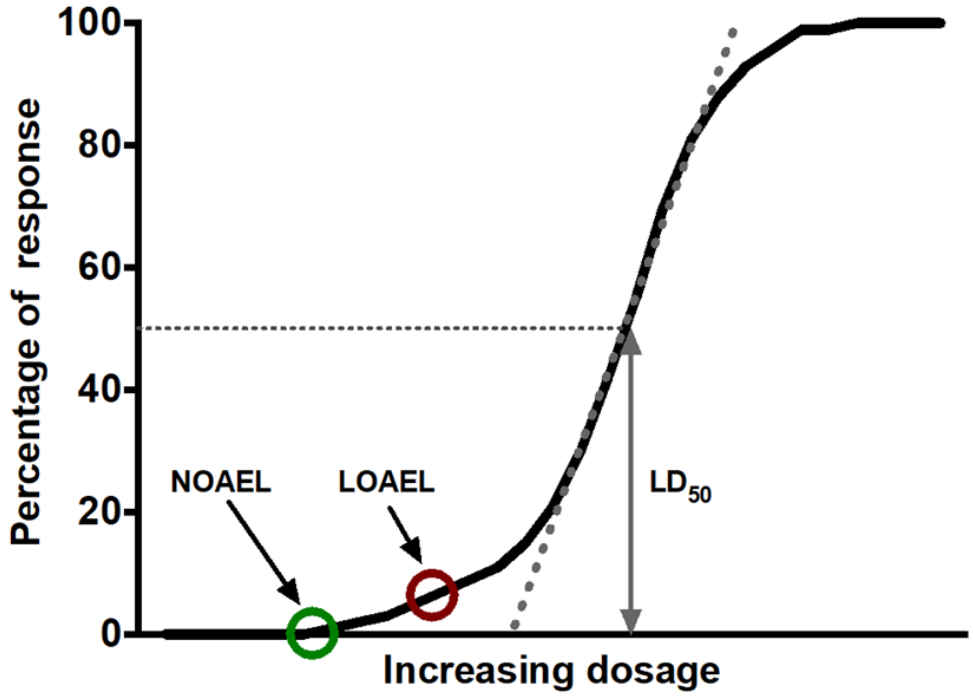

Figure 3.1. An example toxicity dose curve. An increasing dose of toxic agent causes an increase in percentage response. The slope of the dose curve is used to calculate toxicity dose indicators including LD_{50}. The No Observable Adverse Effect Level (NOAEL) is the highest dose of the study to exhibit no biologically significant changes. The Lowest Observable Adverse Effect Level (LOAEL) is conversely the lowest dose to detect a significant change.

The NOAEL/LOAEL toxicity threshold is not only a good foundation from which to compare toxicity values across species, but between different endpoints within a species (214). Recent studies have reported that toxicity values at growth and development endpoints are correlated in zebrafish toxicity studies (187,188). This indicates that the cytotoxic mechanism of a compound's toxicity is the same, independent on whether the readout for a compounds' toxicity is death (acute toxicity, LD_{50}) or a developmental defect (teratogenicity). Furthermore, recent studies have reported that zebrafish acute toxicity values significantly correlated with *in vivo* rat acute toxicity values. Consequently, one predicts that mammalian acute and developmental toxicity endpoint values may also correlate with each other. Theoretically this would make sense, assuming the molecular target(s) of a toxic compound are present in both species, in both growth and developmental stages. Moreover, if the *in vivo* toxicological values from the acute and development endpoints of complex animals are the same, our expectation is that they will agree in the simpler microbial *D. discoideum* model.

To test these ideas, we first sought to establish whether there was a significant relationship between mammalian acute and developmental toxicity endpoints. Next, we sought to characterise the toxicity profiles of our test compounds using the HTP growth and developmental assay reported in chapter 2. Using the *D. discoideum* toxicity data, we then tested whether there is a relationship between the growth and developmental toxicity endpoints in this system. Finally, the *D. discoideum* toxicity data was compared to mammalian *in vivo* data, allowing us to evaluate the potential of *D. discoideum* to function as an alternative model for toxicity testing.

3.2 Aim

Establish whether *Dictyostelium* can provide predictive value for mammalian developmental toxicity.

3.3 Objectives

- Collect mammalian *in vivo* acute, repeat dose and developmental toxicity data and establish whether the toxicity endpoints correlate.
- Apply the time-lapse microscopy growth assay to the characterisation of the test compound's growth toxicity profiles.
- Characterise the phenotypic and developmental toxicity profiles of the test compounds.
- Apply the fluorescent reporter assay to validate the developmental toxicity profiles of the test compounds.
- Compare *Dictyostelium* toxicity values to mammalian *in vivo* data.
- Compare *Dictyostelium* growth and developmental toxicity values.

3.4 Results

3.4.1 Collection of *in vivo* mammalian toxicological values

In vivo mammalian toxicity characterisation is multifaceted with a multitude of toxic endpoints, drug administrative routes, model animals and lengths of dosing regime (213). In order to evaluate mammalian toxicology data, data sets need to be collected with uniformly administered procedures and consistent toxicity measurement in a single species. This also allows the relationship between mammalian toxicity endpoints to be assessed. Therefore, firstly, only data collected from rat *in vivo* studies were selected. This is because rats are the most commonly used model organism in toxicology studies and therefore more data is available with a wider range of endpoints for each of the test compounds (188). Secondly, where possible, the same administrative route (Oral administration) was used for all compounds. For oral administration route 100% bioavailability was assumed for the dosing concentration. Finally, the *in vivo* dosing data in mg per kg per day was converted to a molarity concentration, allowing comparisons to *D. discoideum* data*,* as described in recent zebrafish research (188).

Data was collected for three rat *in vivo* endpoints, acute toxicity (represented by the LD_{50}), repeat dose toxicity (split into subacute and subchronic data sets) and developmental toxicity as (represented by the rat foetal teratogenicity endpoint) (Appendix table A7.2). Acute toxicity relates to adverse events that arise after a single exposure (215). Acute toxicity assessment *in vivo* is tested after exposure to a large single dose. Usually acute toxicity testing is the first to be conducted to give new compounds a toxicity profile, with the LD_{50} dose a universal used toxicity measurement (215). However, an animal LD_{50} is an experimental readout for organismal death and thus very different to a cellular growth endpoint that we will define in *D. discoideum.* Therefore, in order further test the predictive relationship, another rat endpoint, repeat dose toxicity was collected. *In vivo* repeat dose toxicity assessments are conducted for variable lengths of time, most commonly 2 weeks, 4 weeks, 3 months and 6 months with 2 years as the maximum length of time. Repeat dosing studies are generally conducted using a single daily dose over the experimental period. The length of a repeat dose toxicity study can have a large impact on the results of the study. This is because, generally, toxicity will be observed at lower doses when the length of exposure is greater and vice versa. In light of this we split the repeat dose endpoint into two datasets dependent on the length of the study. The ‘subacute’ and ‘subchronic’ data sets correspond to a dosing length of ≥ 7 - ≤ 28 days or 3 – 6 months, respectively. Where

possible, NOAEL and LOAEL doses were collected for each test compound at the repeat dose endpoints (subacute and subchronic). Only LOAEL doses were collected for the developmental toxicity endpoint as not all studies achieve a NOAEL.

3.4.2 Different Mammalian *In vivo* toxicity endpoint values significantly correlate

Recent toxicology studies in zebrafish have reported that acute toxicity (~ equivalent to *D. discoideum* growth toxicity) and developmental toxicity values significantly correlate (186). We therefore wanted to test whether this was true for the mammalian data sets we collected. To test the relationship between the endpoints the rat acute, repeat dose (subacute and subchronic) and fetal teratogenic toxicity values were compared using Pearson's correlation tests. Thus, in total between the 6 data sets, 15 comparisons were made (Figure 3.2). All comparisons were found to be positively correlated and, with only one exception, the correlations were found to significantly correlate (Figure 3.2). These results indicate that all the endpoints provide data sets to which *D. discoideum* toxicological predictivity can be assessed. Moreover, the fact that a significant relationship between different endpoints can be seen in a mammalian model is revealing. It raises the possibility that the underlying mode of action that results in a phenotype of animal death or embryonic development could be related.

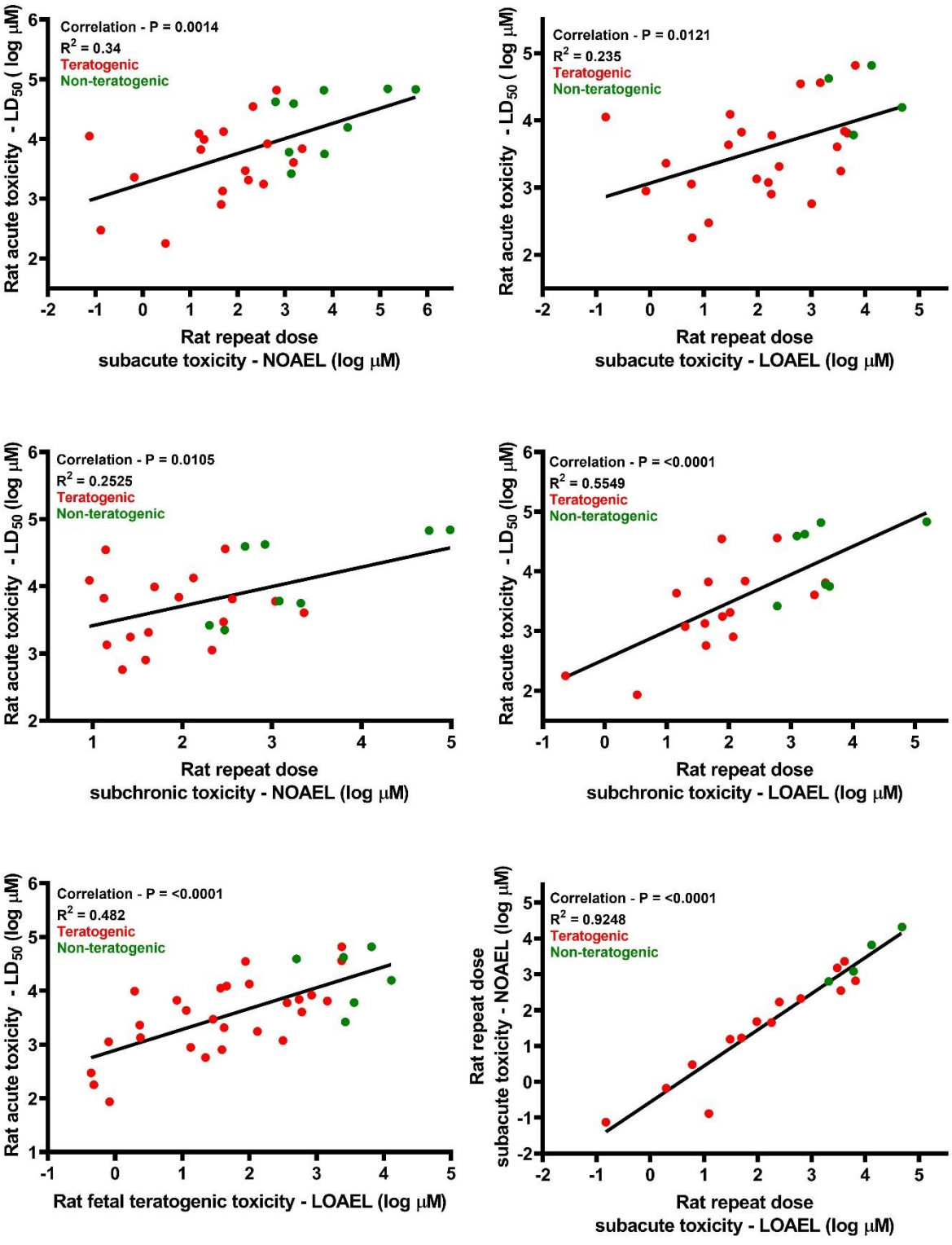

Figure continues on next page.

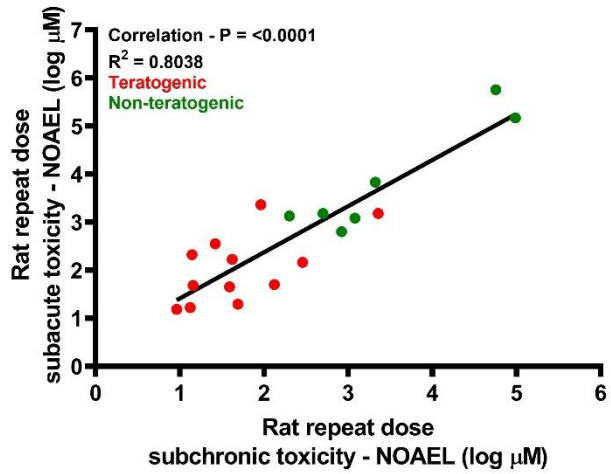

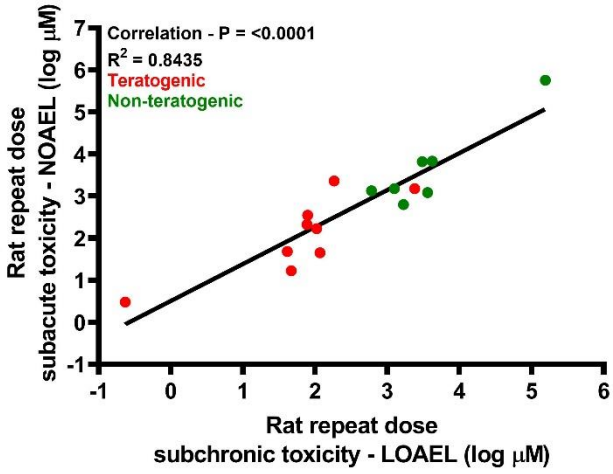

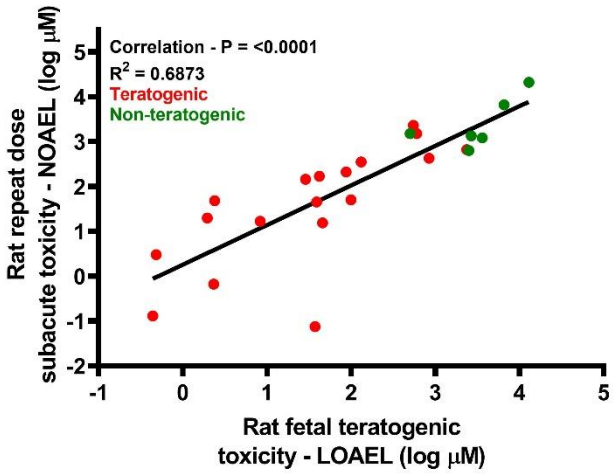

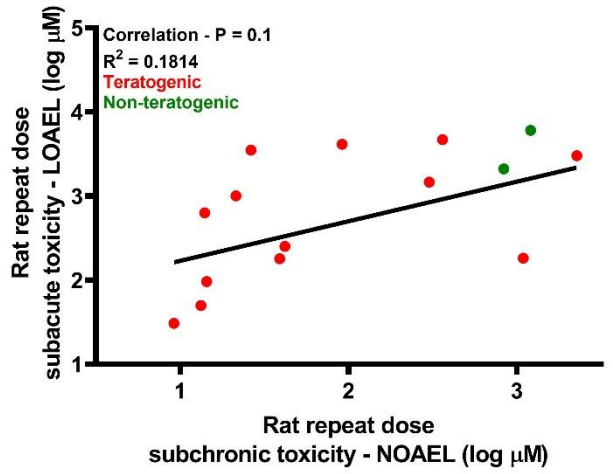

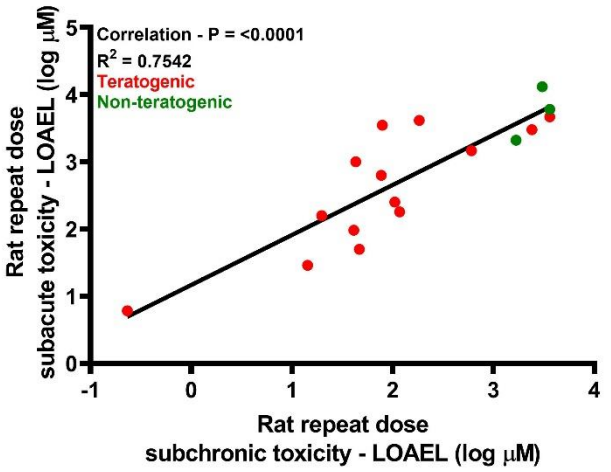

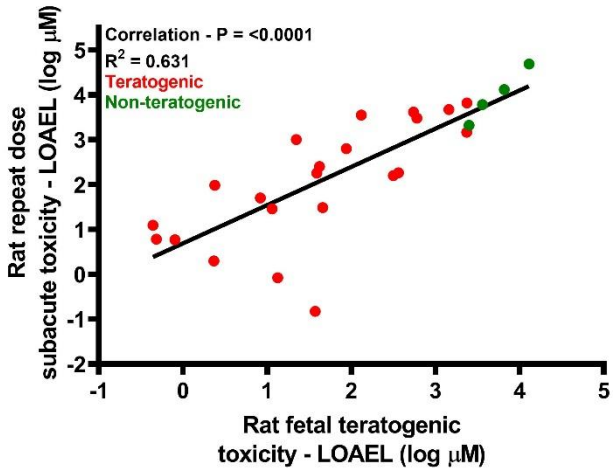

Figure continues on next page.

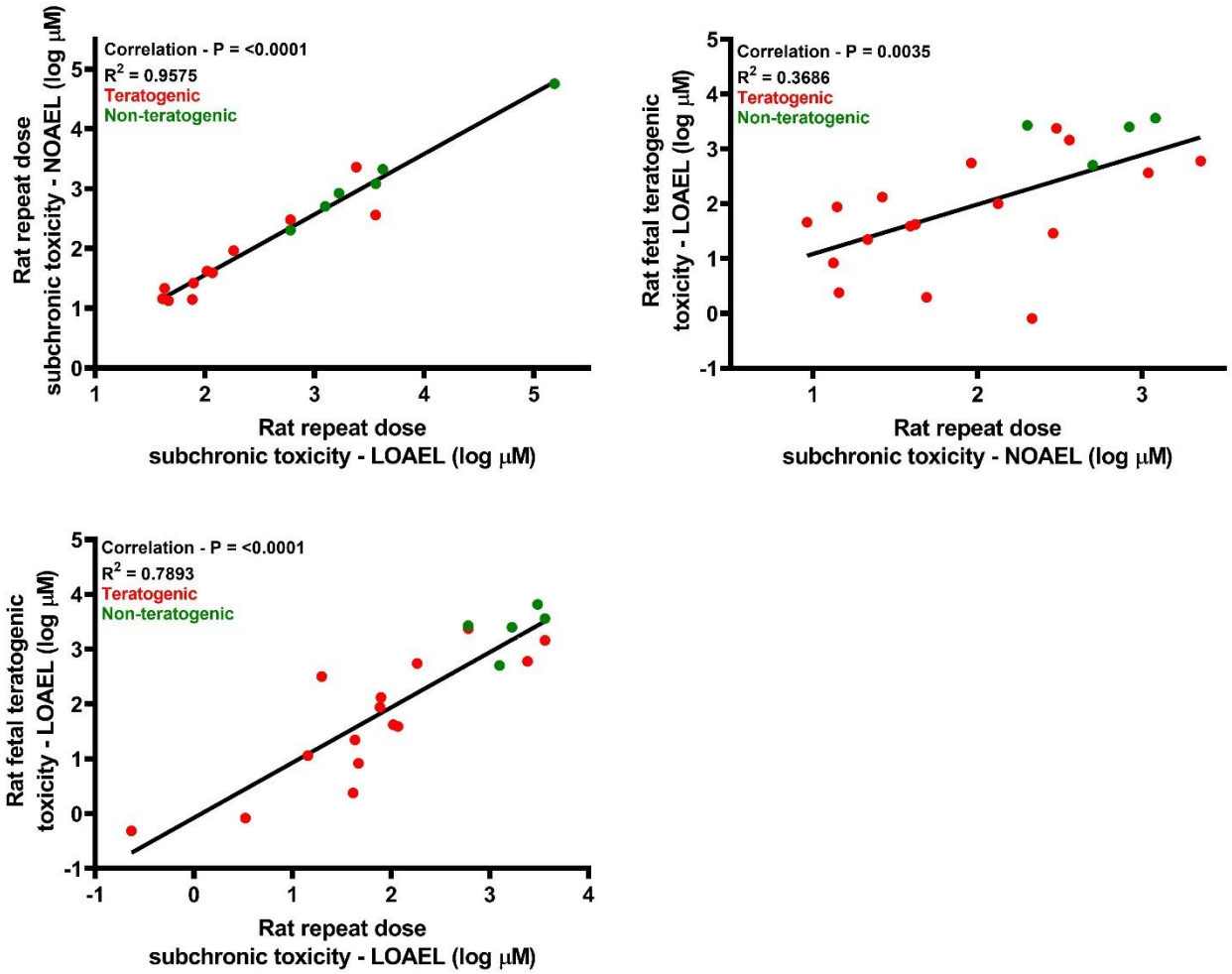

Figure 3.2. Across multiple endpoints *in vivo* rat toxicity values significantly correlate. In vivo rat toxicity values for 6 datasets: acute toxicity (LD50), repeat dose – subacute (NOAEL & LOAEL), repeat dose – subchronic (NOAEL & LOAEL) and developmental toxicity (LOAEL) correlated to each other. All comparisons conducted by Pearson's correlation test. The log of the toxicity values in micromoles are presented. The animal toxicity values were converted to a molarity concentration as described in section 6.3. Teratogenic compounds are coloured red and non-teratogenic compounds are coloured green. Figure over pages 93 - 95.

3.4.3 Characterisation of growth toxicity values in *D. discoideum*

In the previous section rat acute, repeat dose and developmental toxicity values were found to significantly correlate (Figure 3.2). This raised the possibility that in *D. discoideum*, the different stages at which toxicity can be assessed may result in different phenotypic outcomes, but at potentially similar values. To test this idea, we profiled the toxicity of our test compounds at the growth and developmental stages. As many of our test compounds have not been assessed in *D. discoideum,* we first used our newly developed HTP growth assay to test the compounds.

Before measuring the effects of each compound, we first defined the effects of common solvents for our test compounds on growth, to determine the highest non-toxic carrier concentration. The solvents were assayed at concentrations ranging from 0.25 to 5 %, in triplicate wells, for 48 h (Figure 3.3). DMSO and ethanol were found to kills cells at the highest concentration (5%), but growth rates were unaffected at 2 % or lower (Figure 3.3). Further experiments revealed a significant reduction in growth rate at a concentration of 2.5 % for both DMSO and ethanol (Data not shown). A carrier concentration of 1 % was therefore used for all further growth experiments in this research, to ensure no toxicity affects from the solvent.

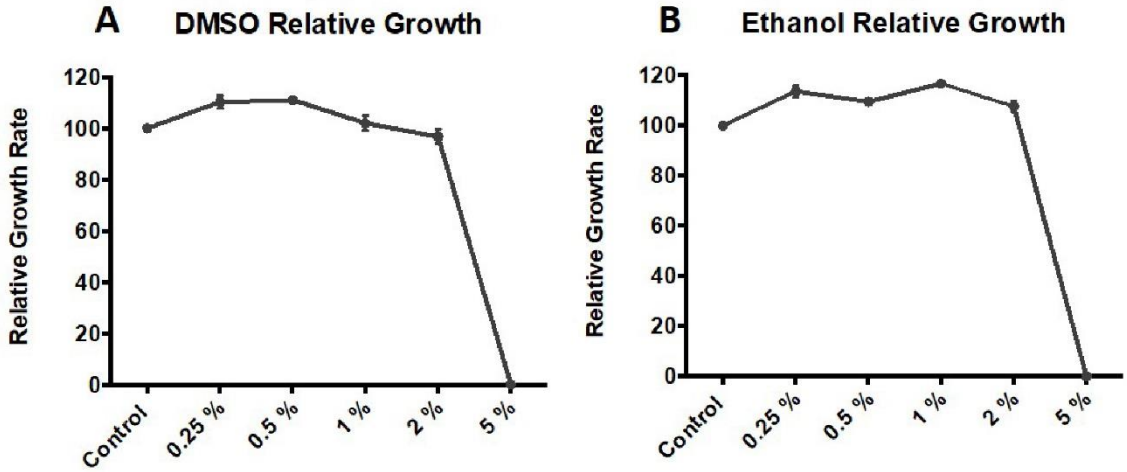

Figure 3.3. Growth toxicity of common solvents. The relative population doubling rate of Ax4 measured between 8 – 48h when incubated with increasing percentage of DMSO **(A)** or ethanol **(B)**. Mean ± SD. Data represents 3 triplicate wells.

The vast majority of the test compounds have never been tested in *D. discoideum*. In order to define NOAEL and LOAEL doses we first choose a starting dose which could be refined further. This anchor dose was selected by converting the rat LD_{50} mg/kg for each compound to a molar concentration. The rat LD_{50} was selected from either intravenous (IV) or intraperitoneal (IP) administered treatment. Data from these administrative routes were used as the absorption of chemicals into the bloodstream is intuitively most similar to adding compounds directly to *D. discoideum* growth media (185). Once this dose was identified, a dose range spanning higher and lower than the anchor dose was defined (Figure 3.4 A). The initial ranges ranged from a 4x to 1000x fold depending on the variability of the published initial anchor dose (data not shown). All growth toxicity was assayed using the microscope-based growth assay (Section 2.4.2) over a 48h period using triplicate wells per concentration. Cell numbers were quantified every hour with the doubling rate calculated during the exponential phase as described in section 2.4.2. This approach allowed the NOAEL/LOAEL toxicity threshold (where possible) to be flanked during the first experimental dose range (Figure 3.4 B). This allowed subsequent experiments to focus around the toxicity threshold narrowing the dose range further (Figure 3.4 C, 3.4 D). This process was repeated three times, establishing a NOAEL and if possible, LOAEL for all of the test compounds. The experiments from which the NOAEL or LOAEL were extracted are presented in figure 3.5 and summarised in table 3.1.

Due to the maximum solvent concentration every compound tested had a maximal dose up to which we could assay toxicity (Table 3.1). Furthermore, because growth medium is an aqueous solution some compounds precipitated at higher doses. After testing the 37 compounds, 24 could be assigned both a NOAEL and LOAEL values (Table 3.1). Therefore, 13 compounds remained in which a LOAEL could not be defined. Of these, 8 did not exhibit growth toxicity at the highest assayable dose (Primidone, cyclophosphamide, cisplatin, cefotaxime, ascorbic acid, acebutolol, penicillin G, metformin) (Figure 3.4 E, 3.4 F). Thus, these compounds only have an assigned NOAEL value, which is an underestimation (Table 3.1). The maximum dose for a further five compounds was limited by precipitation (phenytoin, 13-cis-retinoic acid, retinoic acid, bosentan, bexarotene). Despite the use of alternative solvents, the compounds consistently crystallised in the aqueous media, limiting the dose at which growth toxicity could be assayed (data not shown). Due to the limited exposure to the compounds these NOAELs are possibly an overestimation. Therefore, in both cases a NOAEL is recorded with a solubility caveat (Table 3.1).

To summarise, the HTP growth assay developed in section 2.4.2 was used to characterise the growth toxicity profile of the test compounds. Many of the test compounds had never been tested in *D. discoideum* before and whilst the solubility of a subset of the compounds limited the dosing potential; a toxicity endpoint was identified for all compounds. With the growth toxicity of the test compounds characterised we could proceed to characterise developmental toxicity.

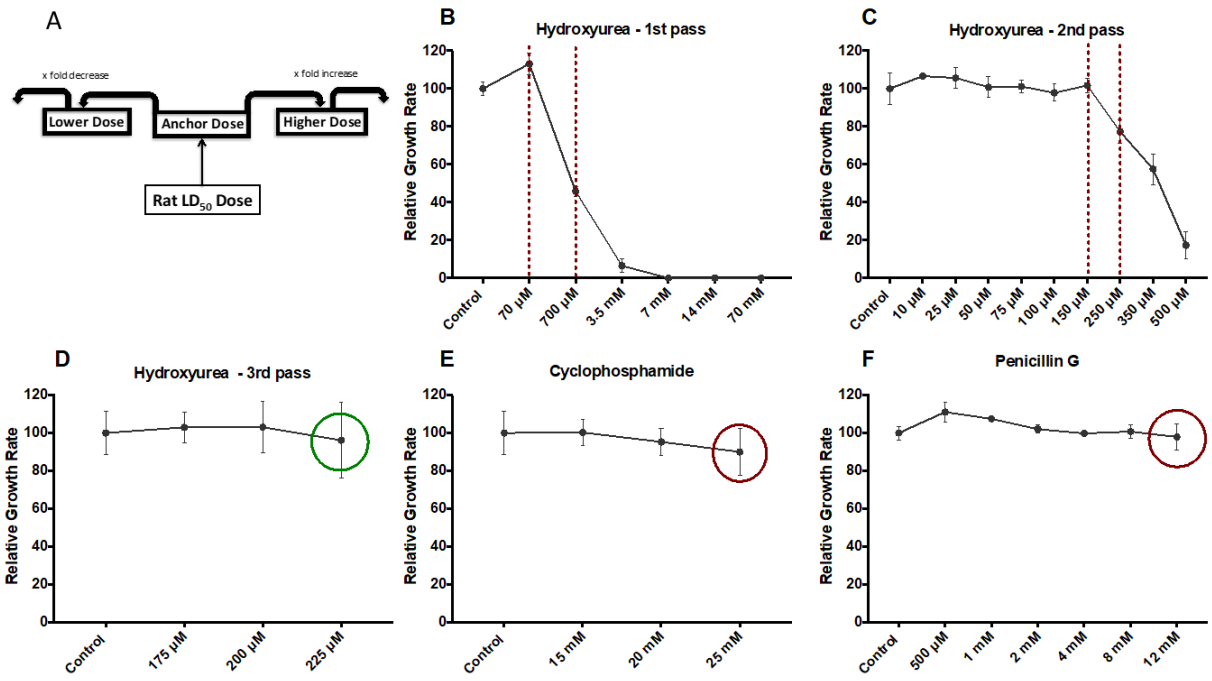

Figure 3.4. Examples from the growth toxicity characterisation procedure.
A. Schematic of the dosing procedure for establishing the toxicity threshold. **B.C.D.** Examples of the first and second pass allowing for a reduction in the dosing range and the establishment of an accurate NOAEL in the third pass. Red lines indicate the dose range for the subsequent pass. The relative population doubling rates of Ax4 (8-48 hour) when treated with varying doses of hydroxyurea (Mean ± S.D., 3 triplicate wells). **E. & F.** The relative growth rates of Ax4 (8-48 hour) when treated with cyclophosphamide or Penicillin G. Examples of compounds found to have no effect on growth at the maximal dose assayable. (Mean ± S.D., 3 triplicate wells).

Table 3.1. Summary of growth toxicity values.

	Compound Name	Primary Solvent	~ Max. Assayable concentration	Highest tested NOAEL	NOAEL	LOAEL
1	**Methotrexate** hydrate	DMSO	1 mM	-	15 µM	30 µM
2	**Pemetrexed**	H_2O	-	-	20 µM	40 µM
3	**Lamotrigine**	DMSO	1 mM	-	200 µM	300 µM
4	**Carbamazepine**	DMSO	1 mM	-	300 µM	500 µM
5	**Phenytoin** sodium	DMSO	1 mM (Crystals >300 µM)	300 µM (HDA)	300 µM *	-
6	**Primidone**	DMSO	2 mM	2 mM (HDA)	2 mM *	-
7	**Valproic Acid** sodium	H_2O	-	-	250 µM	500 µM
8	**Lithium** chloride	H_2O	-	-	5 mM	7.5 mM
9	**Acitretin**	DMSO	500 µM	-	27.5 µM	30 µM
10	**13-*cis*-Retinoic Acid**	DMSO	1 mM (Crystals >17.5 µM)	17.5 µM (HDA)	17.5 µM *	-
11	**Retinoic Acid**	DMSO	1 mM (Crystals >10 µM)	10 µM (HDA)	10 µM *	-
12	**Bosentan** hydrate	DMSO	2 mM (Crystals >120 µM)	120 µM (HDA)	120 µM *	-
13	**Sitaxentan** sodium	H_2O	-	-	400 µM	500 µM
14	**Bexarotene**	DMSO	500 µM (Crystals >5 µM)	5 µM (HDA)	5 µM *	-
15	**Cadmium Sulphate** monohydrate	H_2O	-	-	15 µM	25 µM
16	**Hydroxyurea**	H_2O	-	-	225 µM	250 µM
17	**Cyclophosphamide** monohydrate	H_2O	25 mM	25 mM (HDA)	25 mM *	-
18	**Cisplatin**	H_2O	30 µM	30 µM (HDA)	30 µM *	-
19	**Lead (II) Acetate** trihydrate	Glycerol	-	-	250 µM	300 µM
20	**Clomifene** citrate salt	DMSO	-	-	250 nM	500 nM
21	**Raloxifene** hydrochloride	DMSO	500 µM	-	20 µM	25 µM
22	**Finasteride**	DMSO	1 mM	-	75 µM	100 µM
23	**Vinclozolin**	DMSO	2 mM	-	10 µM	15 µM
24	**Diethylstilbestrol (DES)**	DMSO	-	-	2.5 µM	5 µM
25	**Salicylic Acid**	H_2O	14 mM	-	2.5 mM	3 mM
26	**Nifedipine**	DMSO	1 mM	-	50 µM	75 µM
27	**Warfarin** sodium	DMSO	5 mM	-	450 µM	500 µM
28	**Metoclopramide** hydrochloride	H_2O	-	-	1.5 mM	2.5 mM
29	**Cefotaxime** sodium	H_2O	10 mM	10 mM (HDA)	10 mM *	-
30	**Sulfasalazine**	DMSO	-	-	750 µM	1 mM
31	**Ascorbic acid**	H_2O	5 mM	5 mM (HDA)	5 mM *	-
32	**Acebutolol** hydrochloride	H_2O	1.2 mM	1.2 mM (HDA)	1.2 mM *	-
33	**Camphor**	Ethanol	5 mM	-	3.5 mM	4 mM
34	**Citric acid**	H_2O	-	-	3.5 mM	4 mM
35	**Penicillin G** sodium	H_2O	12 mM	12 mM (HDA)	12 mM *	-
36	**Saccharin** sodium hydrate	H_2O	100 mM	-	35 mM	70 mM
37	**Metformin** hydrochloride	H_2O	5 mM	5 mM (HDA)	5 mM *	-
	*** Highest dose assayable (HDA)**					

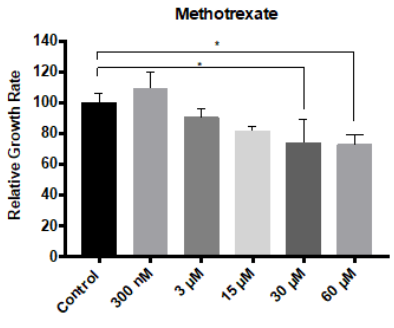
Methotrexate
Relative Growth Rate
Control
300 nM
3 µM
15 µM
30 µM
60 µM

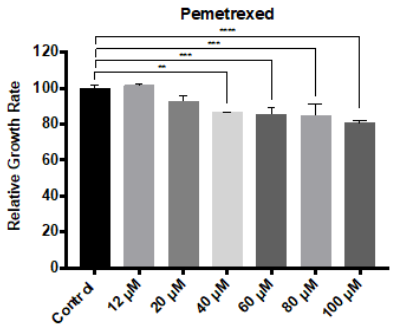
Pemetrexed
Relative Growth Rate
Contrd
12 µM
20 µM
40 µM
60 µM
80 µM
100 µM

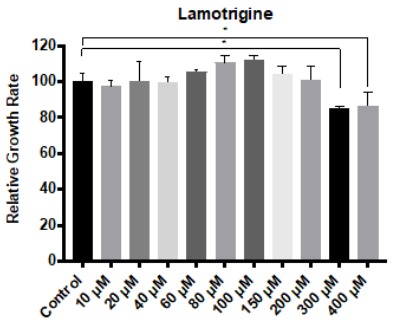
Lamotrigine
Relative Growth Rate
Control
10 µM
20 µM
40 µM
60 µM
80 µM
100 µM
150 µM
200 µM
300 µM
400 µM

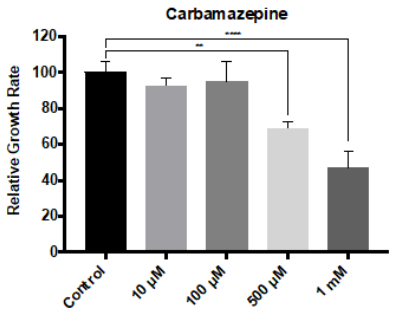
Carbamazepine
Relative Growth Rate
Control
10 µM
100 µM
500 µM
1 mM

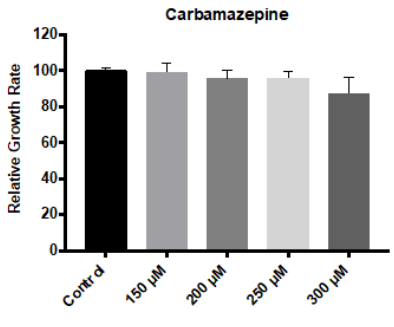
Carbamazepine
Relative Growth Rate
Contrd
150 µM
200 µM
250 µM
300 µM

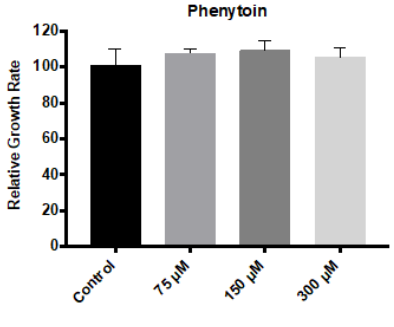
Phenytoin
Relative Growth Rate
Control
75 µM
150 µM
300 µM

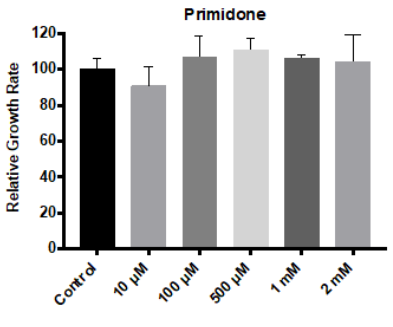
Primidone
Relative Growth Rate
Contrd
10 µM
100 µM
500 µM
1 mM
2 mM

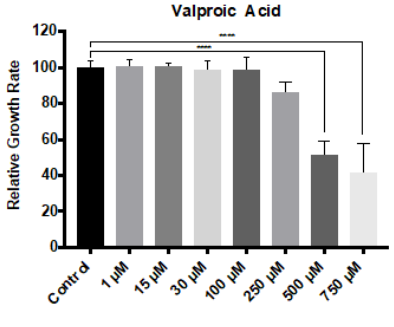
Valproic Acid
Relative Growth Rate
Contrd
1 µM
15 µM
30 µM
100 µM
250 µM
500 µM
750 µM

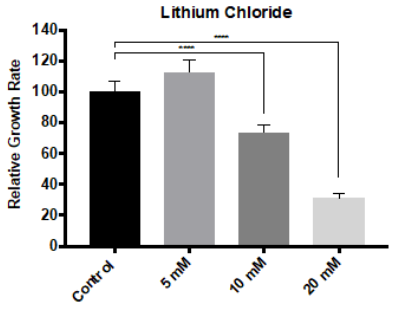
Lithium Chloride
Relative Growth Rate
Control
5 mM
10 mM
20 mM

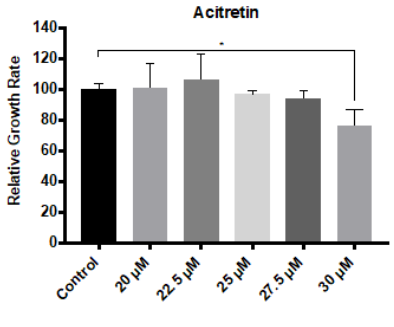
Acitretin
Relative Growth Rate
Control
20 µM
22.5 µM
25 µM
27.5 µM
30 µM

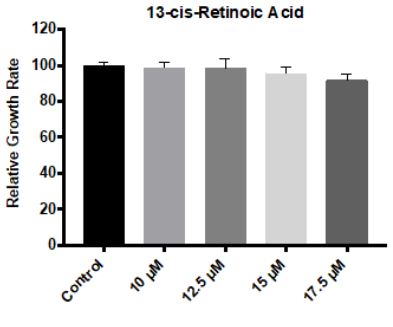
13-cis-Retinoic Acid
Relative Growth Rate
Control
10 µM
12.5 µM
15 µM
17.5 µM

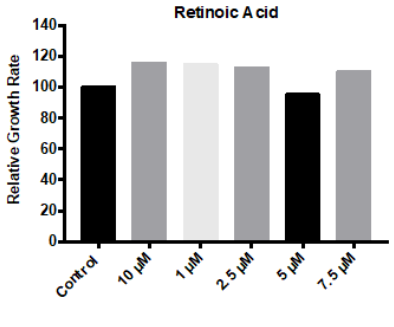
Retinoic Acid
Relative Growth Rate
Control
10 µM
1 µM
2.5 µM
5 µM
7.5 µM

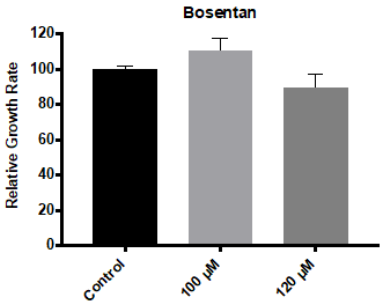
Bosentan
Relative Growth Rate
120
100
80
60
40
20
0
Control
100 µM
120 µM

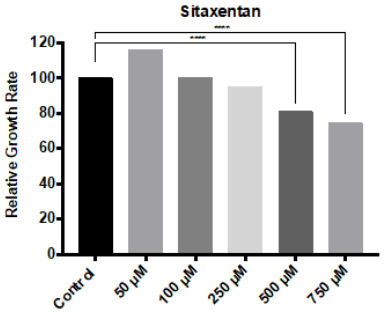
Sitaxentan
Relative Growth Rate
120
100
80
60
40
20
0
Contrd
50 µM
100 µM
250 µM
500 µM
750 µM

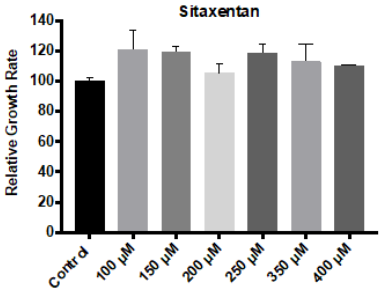
Sitaxentan
Relative Growth Rate
140
120
100
80
60
40
20
0
Contrd
100 µM
150 µM
200 µM
250 µM
350 µM
400 µM

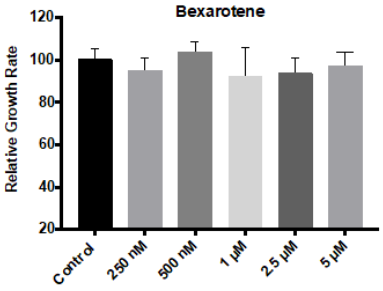
Bexarotene
Relative Growth Rate
120
100
80
60
40
20
Contrd
250 nM
500 nM
1 µM
2.5 µM
5 µM

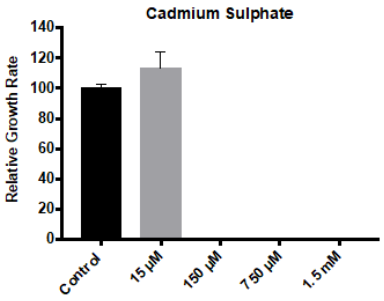
Cadmium Sulphate
Relative Growth Rate
140
120
100
80
60
40
20
0
Contrd
15 µM
150 µM
750 µM
1.5 mM

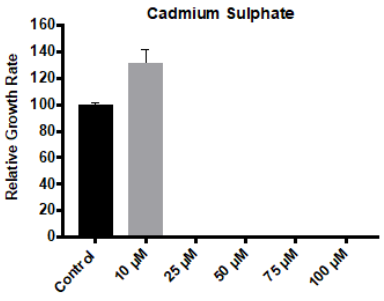
Cadmium Sulphate
Relative Growth Rate
160
140
120
100
80
60
40
20
0
Contrd
10 µM
25 µM
50 µM
75 µM
100 µM

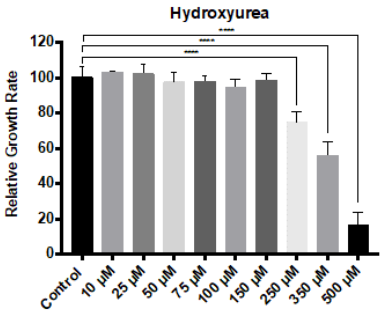
Hydroxyurea
Relative Growth Rate
120
100
80
60
40
20
0
Control
10 µM
25 µM
50 µM
75 µM
100 µM
150 µM
250 µM
350 µM
500 µM

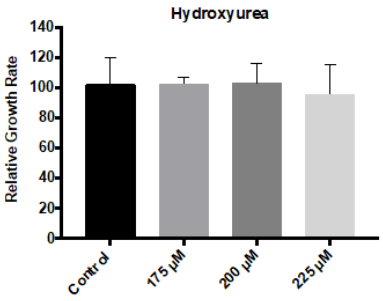
Hydroxyurea
Relative Growth Rate
140
120
100
80
60
40
20
0
Contrd
175 µM
200 µM
225 µM

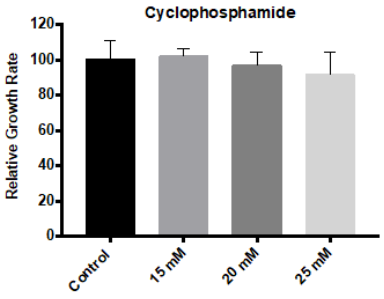
Cyclophosphamide
Relative Growth Rate
120
100
80
60
40
20
0
Control
15 mM
20 mM
25 mM

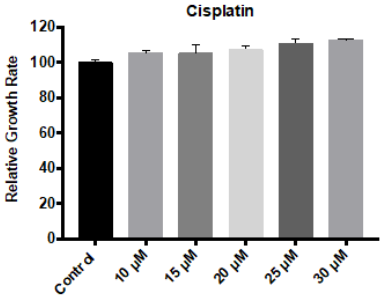
Cisplatin
Relative Growth Rate
120
100
80
60
40
20
0
Contrd
10 µM
15 µM
20 µM
25 µM
30 µM

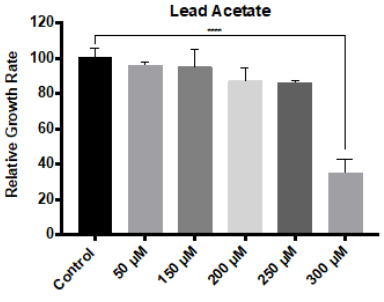
Lead Acetate
Relative Growth Rate
120
100
80
60
40
20
0
Control
50 µM
150 µM
200 µM
250 µM
300 µM

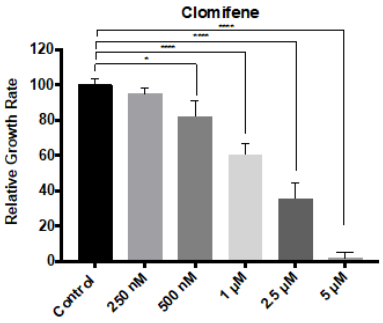
Clomifene
Relative Growth Rate
120
100
80
60
40
20
0
Contrd
250 nM
500 nM
1 µM
2.5 µM
5 µM

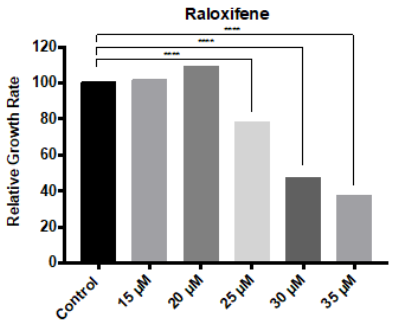
Raloxifene
Relative Growth Rate
Control
15 µM
20 µM
25 µM
30 µM
35 µM

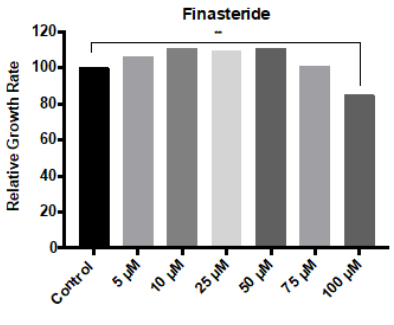
Finasteride
Relative Growth Rate
Control
5 µM
10 µM
25 µM
50 µM
75 µM
100 µM

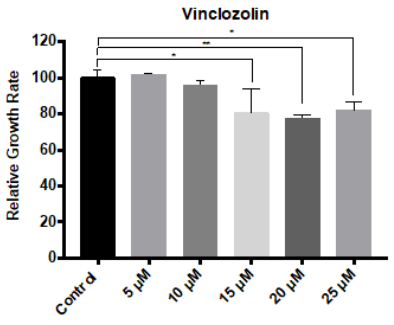
Vinclozolin
Relative Growth Rate
Control
5 µM
10 µM
15 µM
20 µM
25 µM

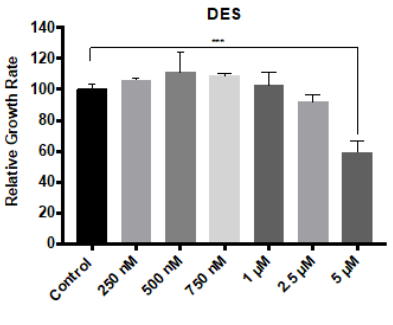
DES
Relative Growth Rate
Control
250 nM
500 nM
750 nM
1 µM
2.5 µM
5 µM

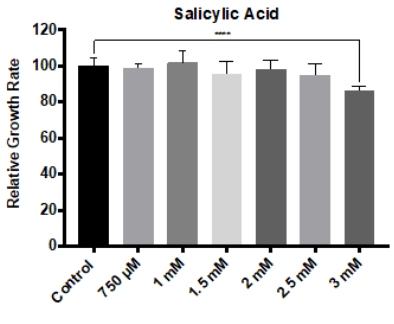
Salicylic Acid
Relative Growth Rate
Control
750 µM
1 mM
1.5 mM
2 mM
2.5 mM
3 mM

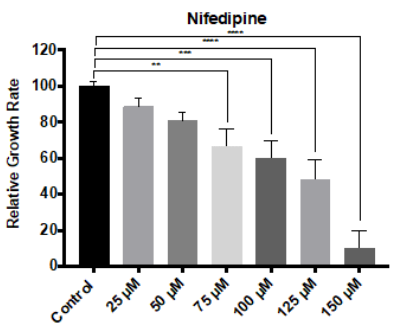
Nifedipine
Relative Growth Rate
Control
25 µM
50 µM
75 µM
100 µM
125 µM
150 µM

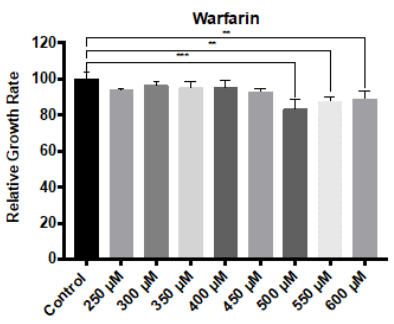
Warfarin
Relative Growth Rate
Control
250 µM
300 µM
350 µM
400 µM
450 µM
500 µM
550 µM
600 µM

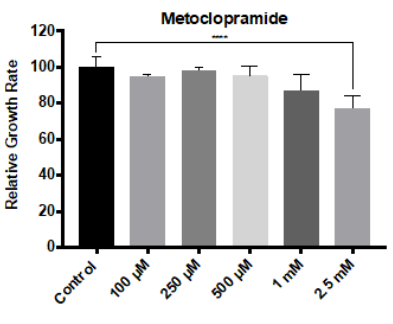
Metoclopramide
Relative Growth Rate
Control
100 µM
250 µM
500 µM
1 mM
2.5 mM

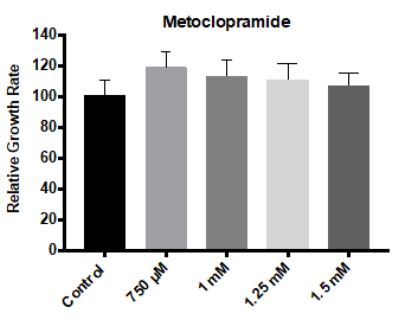
Metoclopramide
Relative Growth Rate
Control
750 µM
1 mM
1.25 mM
1.5 mM

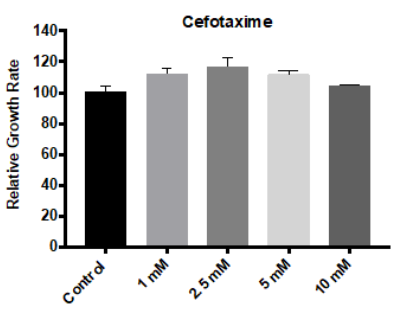
Cefotaxime
Relative Growth Rate
Control
1 mM
2.5 mM
5 mM
10 mM

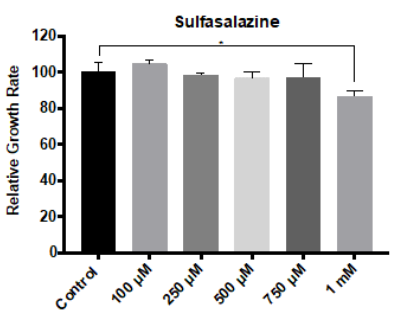
Sulfasalazine
Relative Growth Rate
Control
100 µM
250 µM
500 µM
750 µM
1 mM

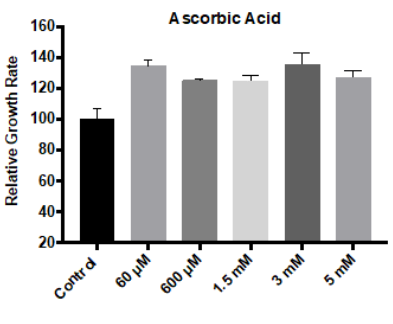
Ascorbic Acid
Relative Growth Rate
Control
60 µM
600 µM
1.5 mM
3 mM
5 mM

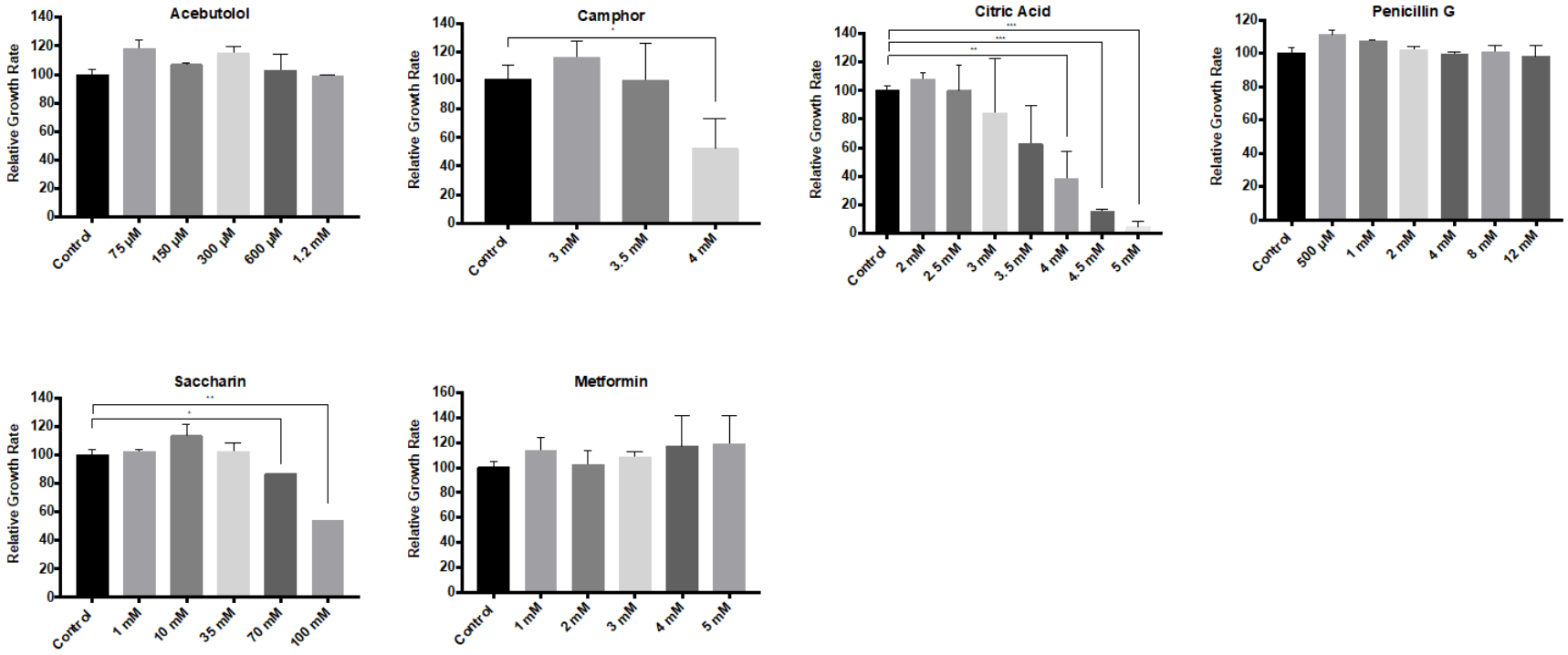

Figure 3.5. Relative growth rates for test compounds toxicity profiles. Ax4 cells were assayed in a 96 well format for 48h through the application of the assay described in section 2.4.2. All data is normalised to the doubling rates of the internal standard of the relevant solvent. All graphs presented are where the NOAEL and LOAEL endpoints were finally identified after 3 passes. Data represents the mean ± SEM for three replicate wells. * indicates significant difference where *=p<0.05, **=p<0.01, ***=p<0.001 and ****=p<0.0001. Figure over pages 100 - 103.

3.4.4 Qualitative characterisation of developmental toxicity in *D. discoideum*

D. discoideum development can be divided into discrete morphological stages, with clear transitions between them (Section 1.3.2). These stages are marked by a multitude of complex, choreographed gene expression changes throughout development (201). Therefore, our test compounds could adversely affect a broad range of developmental processes. Because of the potential for a variety of different developmental toxicity phenotypes, two methods were used to test our compounds. Firstly, we performed a manual 'qualitative' assessment of developmental toxicity by visualising *D. discoideum* developments at different stages. This relied upon *D. discoideum* expertise, but allowed a detailed description of toxicity phenotypes. Secondly, we wanted to demonstrate that the FPR assay (Section 2.4.3) could provide a quantitative measurement of developmental toxicity. Therefore, we sought to integrate the qualitative developmental toxicity assessment with targeted use of the quantitative FPR assay. By taking this dual approach we were also able to validate the subjective nature of our manual qualitative assessment using the FPR. This, in turn, further validated our HTP FPR assay (Section 2.4.3).

The goal of our developmental toxicity profiling was to define the NOAEL/LOAEL threshold for each compound. We therefore attempted to define the dose at which an adverse developmental phenotype was seen at any stage of development. Furthermore, as mammalian *in vivo* developmental toxicity is defined only at doses which have no or a minimal impact on maternal toxicity we took a similar approach. We used the NOAEL, defined during the growth toxicity testing, to anchor the doses tested during the developmental toxicity. This allowed any association between the two endpoints to be disentangled. In addition to the growth NOAEL dose, three lower doses (5-, 25- and 125-fold) were assayed; along with two higher doses (5- and 25-fold) (Figure 3.7). This approach allows for a broad overview of the teratogenic dose range; with the 5-fold spacing significantly closer than the 10-fold interspecies uncertainly factor currently used in UK developmental toxicity legislation (216).

Prior to the experiment a range of solvent concentrations were assessed for effects on *D. discoideum* development. Concentrations greater than 1% for both DMSO and ethanol were found to disrupt normal developmental progression, in agreement with previously published data (Data not shown) (132). Therefore, a carrier concentration of 0.5% was used in all subsequent development assays. Due to the maximum solvent concentration of 0.5%, maximal solubility concentrations limited our ability to test some

compounds at the dose 25-fold higher than the growth NOAEL (Figure 3.7). However, all compounds could be assayed at the growth NOAEL dose and the majority (22 out of 37) at the 5-fold higher dose (Figure 3.7). Observations of developments were taken at the timings of the major stages of development: Aggregation (~4h), streaming (~8h), mound (~12h), slug (~16h), culminant mound (~20h) and fruiting body (24h). A further observation was also taken at 48h in order identify compounds/doses that resulted in severe developmental delay. In parallel, images were recorded for all of the test compounds; generally, at the mound, slug and/or fruiting body stages where abnormal developmental phenotypes are more apparent. Full phenotypic descriptions for all test compounds (with corresponding images) are in appendix figure A7.1. Figure 3.6 shows representative data for the teratogenic compound acitretin and non-teratogenic compound sulfasalazine. Both compounds have no effect on early development, with normal timing and morphology of aggregation, streaming and mound formation. However, 1.1 µM acitretin induces a delay in slug formation; causing heterogenous developmental progression; including, stalled mounds and smaller fruiting bodies (Figure 3.6). Likewise, sulfasalazine induces a broad range of post mound defects, although a much higher dose of 200 µM is required (Figure 3.6). These examples typify the trends seen for many test compounds. Developmental phenotypes can be induced in a dose dependent manner and non-teratogenic compounds generally require a higher dose to elicit a teratogenic effect.

The qualitative characterisation of developmental toxicity for the test compounds is summarised in figure 3.7. Doses which exhibit a discernible developmental difference, at any stage of development, compared to internal controls are coloured maroon (Figure 3.7). Doses which do not adversely affect *D. discoideum* development are coloured in green (Figure 3.7).

A

9. Acitretin					
Dose	220 nM	1.1 µM	5.5 µM	*27.5 µM*	137.5 µM
Aggregation 4h	Normal	Normal	Normal	Normal	Normal
Streaming 8h	Normal	Normal	Normal	Normal	Normal
Mound 15h	Normal	Normal	Normal	Normal	Normal
Slug 18h	Normal	Delayed slug formation ~ 2h	Delayed slug formation ~ 2h	Delayed slug formation ~ 2h	Delayed slug formation ~ 2h
Culminate mound 20h	Normal	Hetrogenous development progression | Emerging slugs | Some Small culminates mounds	Hetrogenous development progression | Emerging slugs | Some Small culminates mounds	Hetrogenous development progression | Emerging slugs | Some Small culminates mounds	Hetrogenous development progression | Emerging slugs | Some Small culminates mounds
Fruiting body 24h	Normal	Some stalled mounds | Smaller and normal fruiting bodies	Loose mounds | Some stalled mounds | Some micro fruiting bodies	Loose mounds | Some stalled mounds | Some micro fruiting bodies	Loose mounds | Some stalled mounds | Some micro fruiting bodies
48 h	Normal	Normal	Normal	Normal	Normal

B

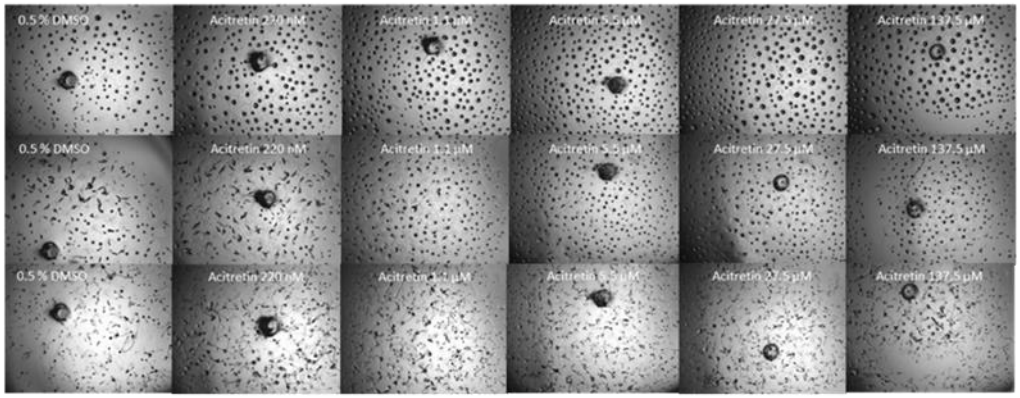

C

30. Sulfasalazine				
Dose	8 µM	40 µM	200 µM	*1 mM*
Aggregation 4h	Normal	Normal	Normal	Normal
Streaming 8h	Normal	Normal	Normal	Aggregation minus lawn | Micro streams forming
Mound 14h	Normal	Normal	Larger mounds | Irregular shaped mound | Lawn of early aggregation minus	Larger mounds | Irregular shaped mound | Lawn of early aggregation minus
Slug 19h	Normal	Normal	Hetrogenous development progression | Streaming | loose mounds | slugs | culminant mounds	Extremely hetrogenous development progression | Streaming | loose mounds | slugs | culminant mounds
Culminate mound 20h	Normal	Normal	Hetrogenous development progression | Streaming | loose mounds | slugs | culminant mounds	Extremely hetrogenous development progression | Streaming | loose mounds | slugs | culminant mounds
Fruiting body 24h	Normal	Normal	Hetrogenous development progression | Many stalled mounds and fruiting bodies	Large loose mounds
48 h	Normal	Normal	Hetrogenous development progression | Stalled mounds | collapsed fruiting bodies	Many large loose mounds | Few fruiting bodies

D

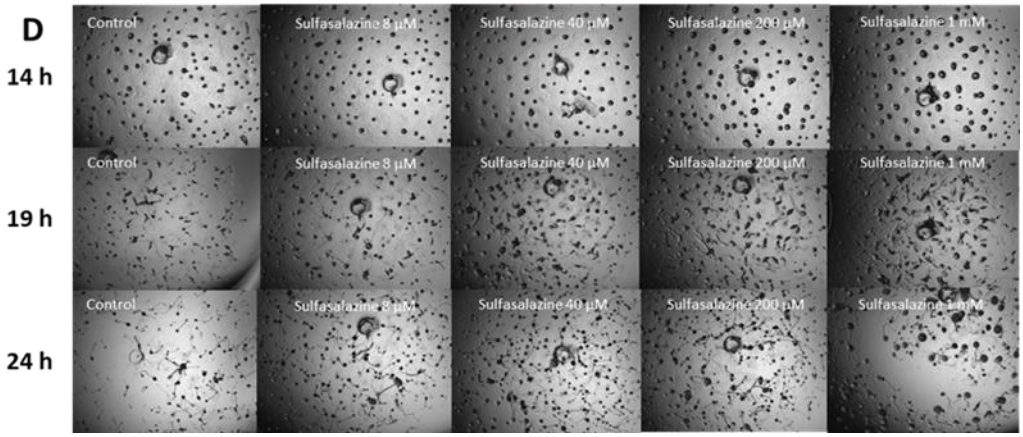

Figure 3.6. Examples of test compound developmental toxicity phenotypes. Descriptions and representative images of the development toxicity profiles for test compounds: acitretin and sulfasalazine.

Developmental Toxicity Summary						
Compound	**25 Fold higher**	**5 Fold higher**	**NOAEL Dose**	**5 Fold lower**	**25 Fold lower**	**125 Fold lower**
Methotrexate	125 µM	25 µM	**5 µM**	1 µM	200 nM	40 nM
Pemetrexed	-	60 µM	**12 µM**	2.4 µM	480 nM	96 nM
Lamotrigine	-	-	**200 µM**	40 µM	8 µM	1.6 µM
Carbamazepine	-	1.5 mM	**300 µM**	60 µM	12 µM	2.4 µM
Phenytoin	-	-	**300 µM**	60 µM	12 µM	2.4 µM
Primidone	-	-	**2 mM**	400 µM	80 µM	16 µM
Valproic Acid	2.5 mM	500 µM	**100 µM**	20 µM	4 µM	800 nM
Lithium	-	25 mM *	**5 mM**	1 mM	200 µM	40 µM
Acitretin	-	137.5 µM	**27.5 µM**	5.5 µM	1.1 µM	220 nM
13-*cis*-Retinoic Acid	-	87.5 µM	**17.5 µM**	3.5 µM	700 nM	140 nM
Retinoic Acid	250 µM	50 µM	**10 µM**	2 µM	400 nM	80 nM
Bosentan	-	600 µM	**120 µM**	24 µM	4.8 µM	960 nM
Sitaxentan	-	-	**400 µM**	80 µM	16 µM	3.2 µM
Bexarotene	-	25 µM	**5 µM**	1 µM	200 nM	40 nM
Cadmium Sulphate	-	75 µM *	**15 µM**	3 µM	600 nM	120 nM
Hydroxyurea	**5 mM**	1 mM	**200 µM**	40 µM	8 µM	1.6 µM
Cyclophosphamide	-	-	**25 mM**	5 mM	1 mM	200 µM
Cisplatin	-	-	**30 µM**	6 µM	1.2 µM	240 nM
Lead (II) Acetate	5 mM *	1 mM	**200 µM**	40 µM	8 µM	1.6 µM
Clomifene	6.25 µM	1.25 µM	**250 nM**	50 nM	10 nM	2 nM
Raloxifene	500 µM	100 µM	**20 µM**	4 µM	800 nM	160 nM
Finasteride	1.875 mM *	375 µM	**75 µM**	15 µM	3 µM	600 nM
Vinclozolin	250 µM	50 µM	**10 µM**	2 µM	400 nM	80 nM
Diethylstilbestrol (DES)	25 µM	5 µM	**1 µM**	200 nM	40 nM	8 nM
Salicylic Acid	-	-	**3 mM**	600 µM	120 µM	24 µM
Nifedipine	625 µM *	125 µM	**25 µM**	5 µM	1 µM	200 nM
Warfarin	-	2 mM *	**400 µM**	80 µM	16 µM	3.2 µM
Metoclopramide	-	-	**1.5 mM**	300 µM	60 µM	12 µM
Cefotaxime	-	-	**10 mM**	2 mM	400 µM	80 µM
Sulfasalazine	-	-	**1 mM**	200 µM	40 µM	8 µM
Ascorbic acid	-	-	**5 mM**	1 mM	200 µM	40 µM
Acebutolol	-	6 mM	**1.2 mM**	240 µM	48 µM	9.6 µM
Camphor	-	-	**3 mM**	600 µM	120 µM	24 µM
Citric acid	50 mM *	10 mM *	**2 mM**	400 µM	80 µM	16 µM
Penicillin G	-	-	**12 mM**	2.4 mM	480 µM	96 µM
Saccharin	-	-	**35 mM**	7 mM	1.4 mM	280 µM
Metformin	-	-	**5 mM**	1 mM	200 µM	40 µM

Teratogenic
Non-teratogenic
* = Cells are Dead
Dose not possible

Figure 3.7. Summary of the qualitative developmental toxicity test testing. A dose corresponding to the growth toxicity NOAEL was used as an anchor for a five-fold increment dose range across all the test compounds. The *D. discoideum* developments were repeated in multiple independent experiments. Doses which exhibited any defects (at any developmental stage) are coloured red. Normal developments are coloured green. Cells marked with an Asterix indicate concentrations where cells have clearly died. Concentrations which could not be assayed due to maximal solubilities are coloured in cream. The highest non-toxic dose is the experiment NOAEL and the lowest toxic dose the assigned LOAEL.

After the developmental toxicity profiling, a NOAEL and LOAEL value could be assigned to 31 of the 37 test compounds (Figure 3.7). The remaining six compounds (lamotrigine, phenytoin, primidone, camphor, penicillin G, metformin) did not exhibit developmental toxicity at the highest dose testable and therefore could only be assigned a NOAEL value (Figure 3.7). The NOAEL value for these compounds is thus likely an underestimation of the true toxicity threshold. Three of these compounds are non-teratogenic control compounds (camphor, penicillin G, metformin). Of the 3 teratogenic compounds (lamotrigine, phenytoin, primidone), phenytoin and primidone also did not produce any adverse effects on *D. discoideum* growth up to the highest dose tested.

We noted that 21 out of the 27 teratogenic compounds affected development at the growth toxicity NOAEL dose or lower (Figure 3.7). Only lamotrigine, phenytoin, primidone, bosentan, hydroxyurea and clomifene do not affect development at the growth toxicity NOAEL dose (Figure 3.7). Although, lamotrigine, hydroxyurea and clomifene, do exhibit developmental toxicity at a five-fold higher dose (Figure 3.7). Phenytoin and primidone have never been found to be toxic and bosentan was found to crystallise in the aqueous growth assay at concentrations greater than 120 µM (Table 3.1). Consequently, solubility at the same concentration in the aqueous agar for the development assay may limit bosentan uptake, possibility explaining the lack of toxicity at the developmental endpoint. At the growth NOAEL dose, 27 out of the 37 compounds did cause developmental toxicity (Figure 3.7). This suggests that the development endpoint is more sensitive in comparison to the growth rate endpoint. This observation can be seen at the dose fivefold lower than the growth NOAEL, where 17 out of 37 compounds also exhibit developmental toxicity. Interestingly, a difference in the toxicity values for the (non-) teratogenic compounds could be observed (Figure 3.7). At the fivefold lower dose, 15 out of 27 (55%) of the teratogenic compounds exhibit developmental toxicity in *D. discoideum*, with only 2 out of 10 (20%) of the non-teratogenic compounds affecting development (Figure 3.7).

With accurate LOAEL and/ or NOAEL developmental toxicity values recorded, we sought to next validate these potentially subjective values by implementing the quantitative FPR assay on each test compound.

3.4.5 Quantitative validation of developmental toxicity profiles

By observing the phenotypic effects caused by the test compounds on development, we were able to assign NOAEL and LOAEL values for most compounds. However, this approach requires training, experience and is labour intensive. Therefore, in order to simultaneously validate the developmental toxicity data and to test the efficacy of the FPR assay, a single dose for all 37 test compounds was tested using the FPR assay (Section 3.7). Previously, we have shown that the FPR assay could be used to determine the teratogenic effect of lithium (Figure 2.8). However, the wide range of different developmental phenotypes seen with the test compounds represents a more stringent test (Appendix figure A7.1).

The fluorescent reporter strains (Figure 2.7) for the major stages of *D. discoideum* development were used to qualitatively measure developmental phenotypes. The reporter strains were assayed in triplicate wells in a 96 well format and incubated in a temperature controlled FPR with fluorescent readings taken every 2 hours (0h to 24h), as described in section 6.6. For each compound the highest developmental toxic dose which did not exceed the growth toxicity NOAEL was selected (Figure 3.7). Where this was not possible the highest assayable dose was selected. Thus, 7 of the 37 doses tested were not expected to result in developmental toxicity. Quantitative toxicity profiling resulted in the generation of a large dataset (Appendix figure A7.2) which could be compared to the qualitative observations (Appendix figure A7.1). In the FPR assay the timing and strength of expression of the fluorescence reporters (individually and taken together) provide a picture of developmental progression (Section 2.4.3). Moreover, they should allow developmental toxicity to be determined without direct observation or *D. discoideum* expertise. To test this idea, the profile of each reporter strain was processed, quantitatively, in several different ways. Firstly, we determined whether each marker exhibited a significant peak of expression (Figure 3.8 A) and secondly, if they did, when the peak level of expression occurred in comparison to the control untreated developments (Figure 3.8 B). Thus, together, these measurements allowed for a complete block or delay in timing of developmental stages to be defined. Next, in order to compare the FPR data results to the qualitative observations we scored the developmental stages as either ‘normal’, ‘delayed’ or ‘not reached’ across the qualitative dataset (Figure 3.9 A). When we compared the quantitative and qualitative datasets identical observations were found in 128/167 (77%) cases. The results increased to 135/167 (81%) when defects in timing and lack of expression were pooled together (Figure 3.9 C). Next, we assessed the quantitative FPR dataset by determining the level

of expression of each marker at its peak between the control and treated developments (Figure 3.8 C). This allowed us to also quantitatively determine if development was asynchronous, or partially blocked. The qualitative dataset was rescored adding whether heterogenous developmental stage progression was seen. Thus, categories 'heterogenous' and 'delay and heterogenous' were added to 'normal', 'delay' and 'stage not reached' (Figure 3.9 B). With this additional phenotypic data combined with the timing data, 136/167 (82%) of the observations were found to be in agreement between the qualitative and quantitative datasets (Figure 3.9 C).

The qualitative observational data and FPR assay results for all of the test compounds can be found in figures A7.1 and A7.2, respectively. All comparative validations of the qualitative (and quantitative) toxicity profiles are summarised in figure 3.9. In summary, the FPR assay correctly classified whether 35 of the 37 compounds (95%) exhibited developmental toxicity (Figure 3.9 C). Of the seven compounds not expected to cause developmental toxicity by qualitative observations (Lamotrigine, phenytoin, primidone, acebutolol, camphor, penicillin G, metformin), only one exhibited any defects in reporter gene activity (Figure 3.9). Similarly, of the 30 compounds which were scored as developmentally toxic all but one (Vinclozolin) showed no effects with one or more developmental reporter (29 / 30) (Figure 3.9). To conclude, the qualitative developmental toxicity profiles can be validated by FPR assay reporters. Beyond validating our developmental toxicity values, the success of the FPR assay demonstrates the potential of our *D. discoideum* HTP, quantitative developmental toxicity assay.

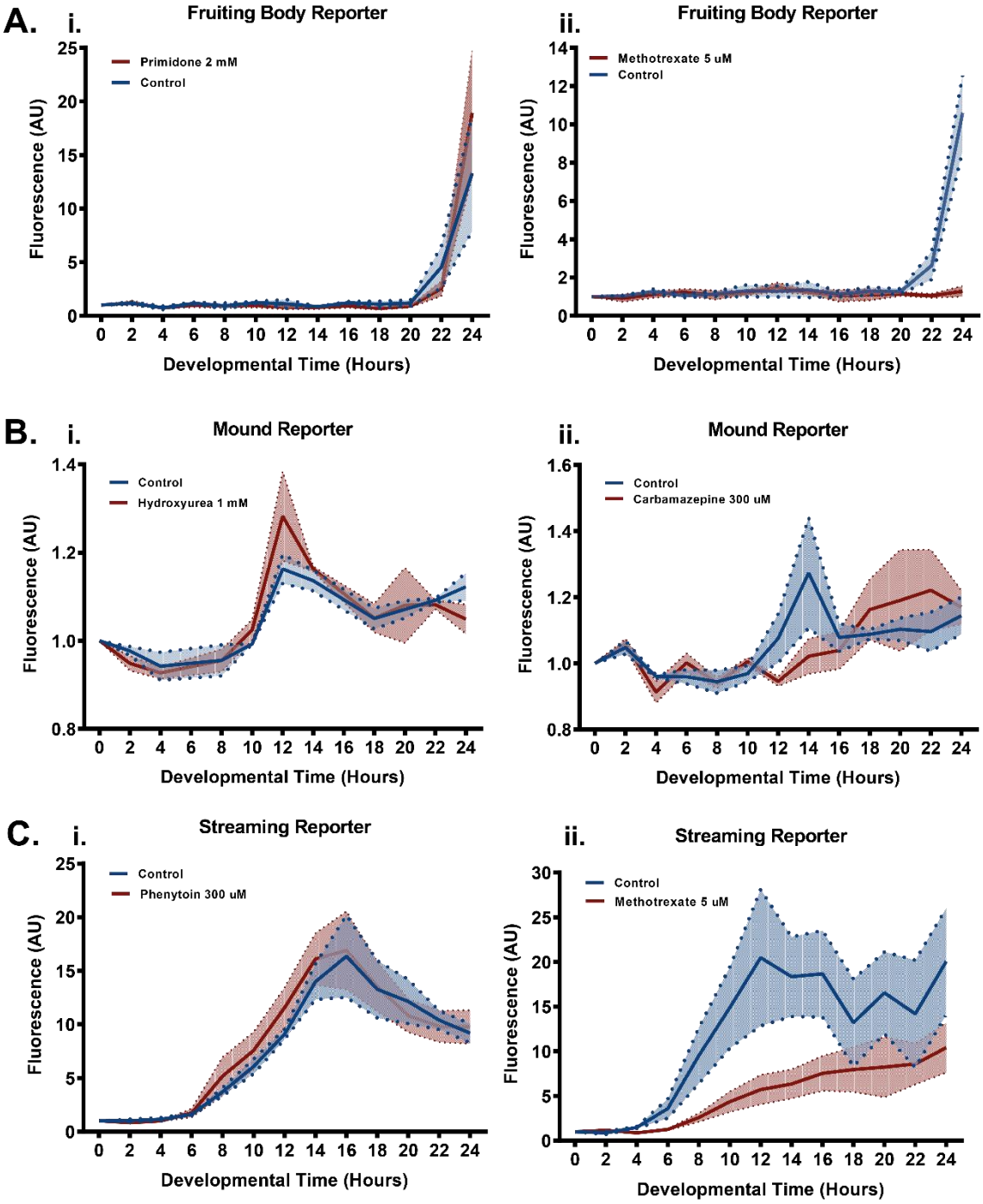

Figure 3.8. Examples of the three quantitative measures by which the FPR data was processed. Examples of FPR results that demonstrate the three measures by which the dataset was quantitively processed: the existence of a profile (A), the timing of the profile (B) and strength of the fluorescent signal (C). Ax4 cell lines expressing RFP at the fruiting body, mound and streaming stage of development were developed under standard 96 wells conditions (Section 6.6) on KK2 agar. Data is normalised to each replicates value at time point 0h. Data represents the mean ± SEM of three well replicates. In the **(i)** panel of each example the control and compound treatment show similar fluorescent profiles.

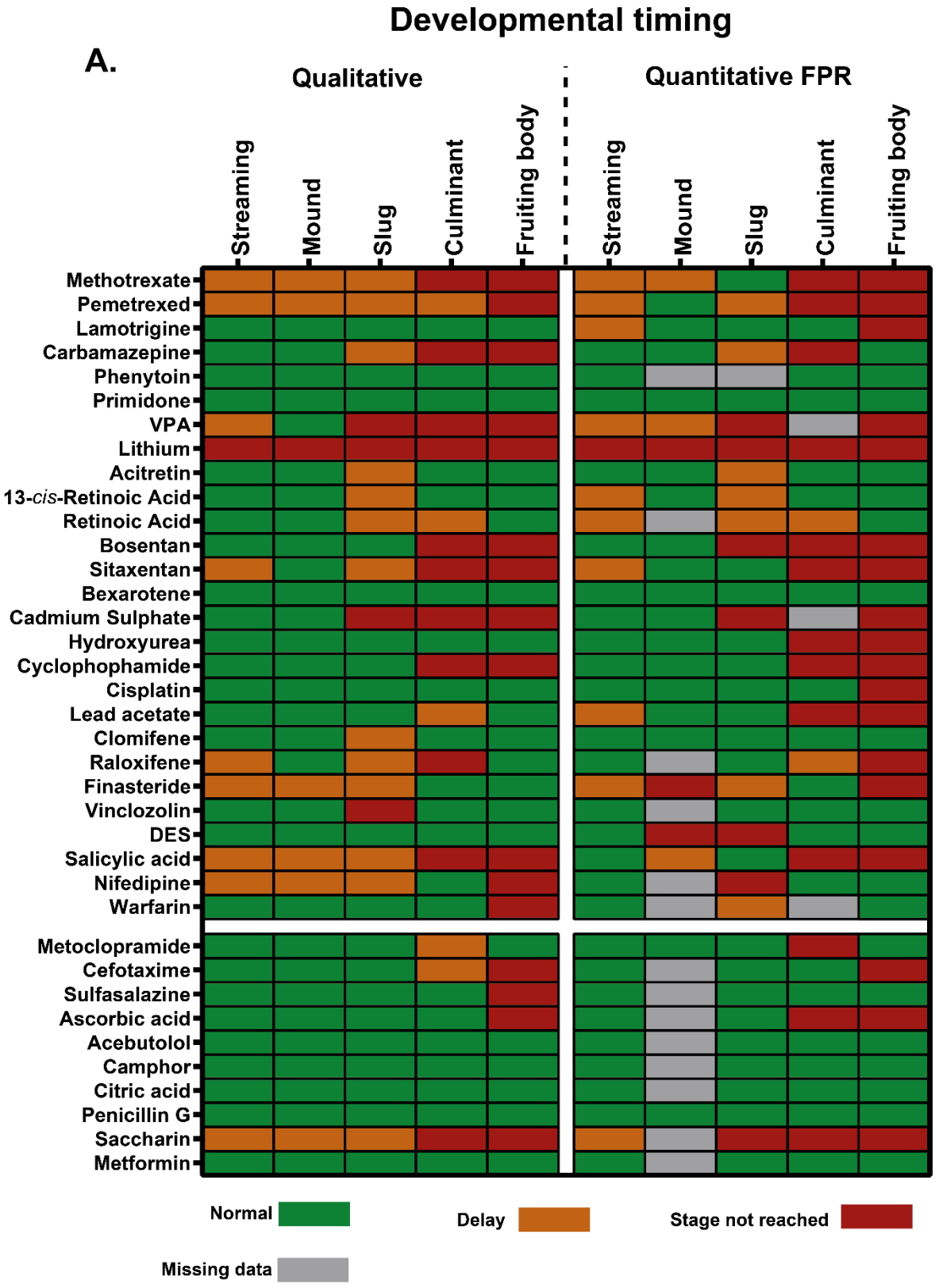

Figure continues on next page.

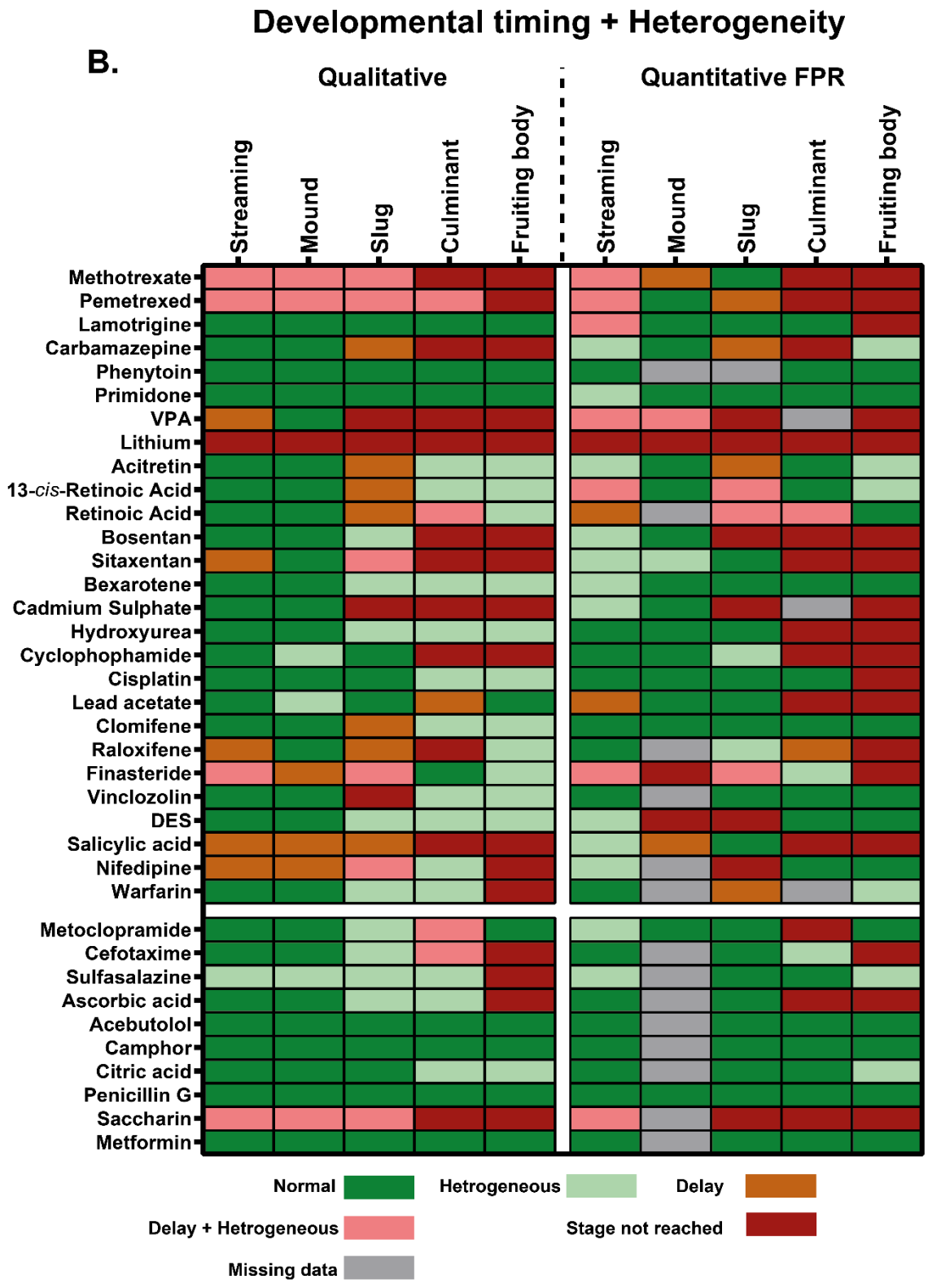

Figure continues on next page

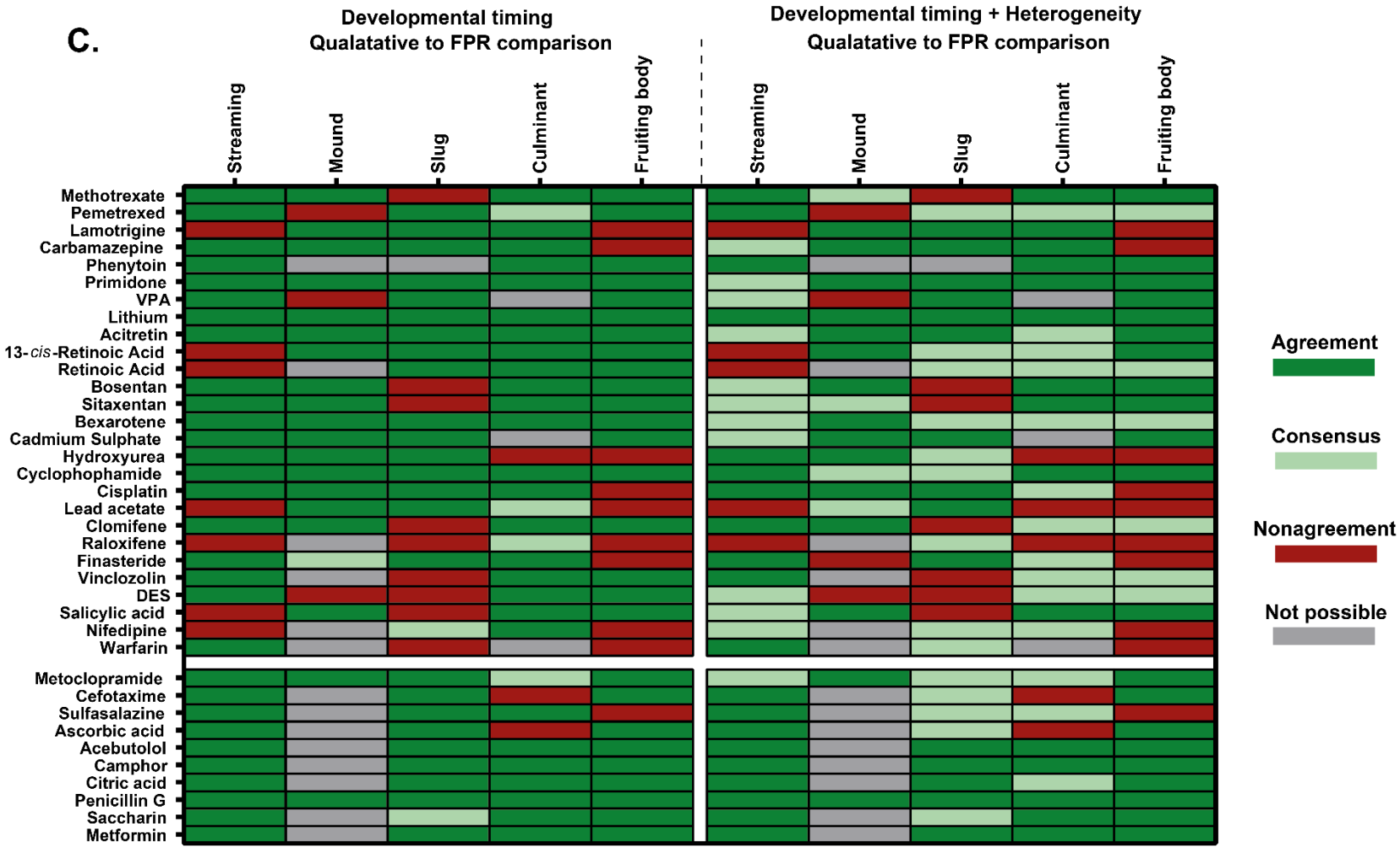

Figure legend on next page.

Figure 3.9. The qualitative and quantitative *D. discoideum* developmental toxicity datasets are similar. Heatmaps depicting the effects of the test compounds on the timing of the stages of development **(A)** and heterogenous developmental progression along with the timing **(B)**. The streaming, mound, slug, culminate and fruiting body stages of development are scored for the qualitative (left maps) and quantitative FPR data (right maps). **(C)** Heatmaps that depict the comparisons between the qualitative and quantitative scoring of toxicity for developmental timing (left) and developmental timing and heterogeneity (right). Figure over pages 112 – 114.

3.4.6 *D. discoideum* growth and developmental toxicity values significantly correlate

A relationship between acute and developmental toxicity endpoint values has been reported in zebrafish (187,188). Furthermore, we found a significant relationship between acute, repeat dose and developmental toxicity values in the *in vivo* rat data sets we collated (Section 3.4.2). This suggests that the underlying toxic mode of action of a compound is the same, regardless of where in an organism's life cycle it is measured. As cell proliferation is broadly separated from development in *D. discoideum* it represents an ideal model in which to test this hypothesis. We compared the NOAEL *D. discoideum* dose values for growth and development (Figure 3.10). Growth and developmental toxicity values in *D. discoideum* were found to significantly correlate (Figure 3.10). Thus, toxicity profiling does not reveal large differences in dosing values at different stages. However, measuring toxicity at different endpoints does result in different phenotypes, which can have advantages or disadvantages depending on the aims of the study. For example, because the growth endpoint readout is simpler, it can be measured more easily. In contrast, profiling toxicity during development allows a wider range of different phenotypes to be characterised, which may be important to understand and evaluate the MOA of teratogenic compounds.

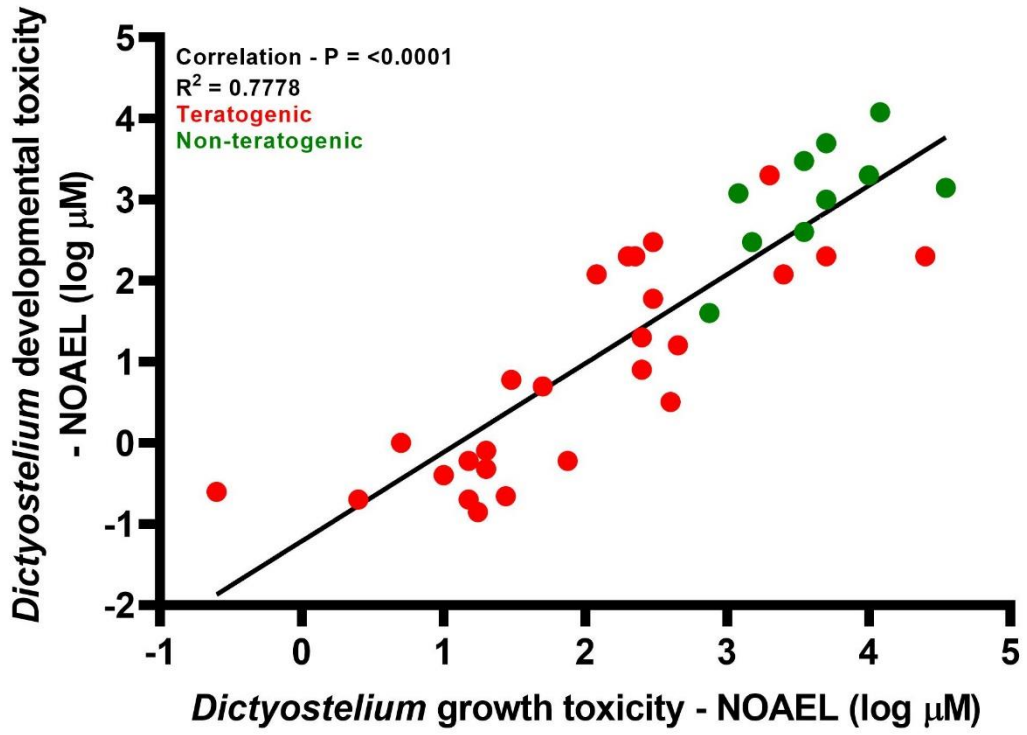

Figure 3.10. *D. discoideum* growth and developmental toxicity values significantly correlate. Correlation of the NOAEL doses for growth and developmental toxicity in *D. discoideum* characterised in sections 3.4.3 and 3.4.4, respectively.

3.4.7 Mammalian classified (non-) teratogenic compounds require significantly different doses to mediate toxicity in *D. discoideum*.

During the characterisation of growth and developmental toxicity in *D. discoideum,* a difference in the behaviour of the (non-) teratogenic compounds was observed. During growth toxicity testing, 5 out of 10 (50%) non-teratogenic compounds did not exhibit growth toxicity at the highest dose assayable (Table 3.1). In contrast (excluding the compounds limited by crystallisation) only 3 out of 27 (11%) of the teratogenic compounds were non-growth toxic at the highest concentrations assayable. Furthermore, during the qualitative developmental toxicity profiling, only 2 out of 10 (20%) of the non-teratogenic compounds affected development (at a dose fivefold lower than the growth NOAEL) (Figure 3.7). In contrast, 15 out of 27 (55%) of the teratogenic compounds exhibit developmental toxicity in *D. discoideum* at the same dose level (Figure 3.7). These observations highlight a difference between the compound classes, and suggest that *D. discoideum* can distinguish between the teratogenic and non-teratogenic compounds. We next assess this relationship further, by comparing the average growth and developmental toxicity NOAEL values between the teratogenic and non-teratogenic compounds (Figure 3.11). The average growth NOAEL for the non-teratogenic compound is significantly higher than the average NOAEL of the teratogenic compounds (Figure 3.11 A). A similar result was found for the mean developmental toxicity NOAELs (Figure 3.11 B).

These results illustrate the teratogenicity threshold principle discussed in section 1.1.3 , which states that teratogenic compounds may be safe to pregnant women at low doses (Figure 1.1) (217). Conversely, significantly higher doses of non-teratogens have the potential to become toxic (Figure 1.1). It is therefore unsurprising that compounds classified as non-teratogenic tend to exhibit a higher toxicity threshold. However, it was encouraging to find that this relationship still holds in the *D. discoideum* toxicity data, as it provides the first indication that it could provide toxicity values that are predictive of mammalian toxicity outcomes.

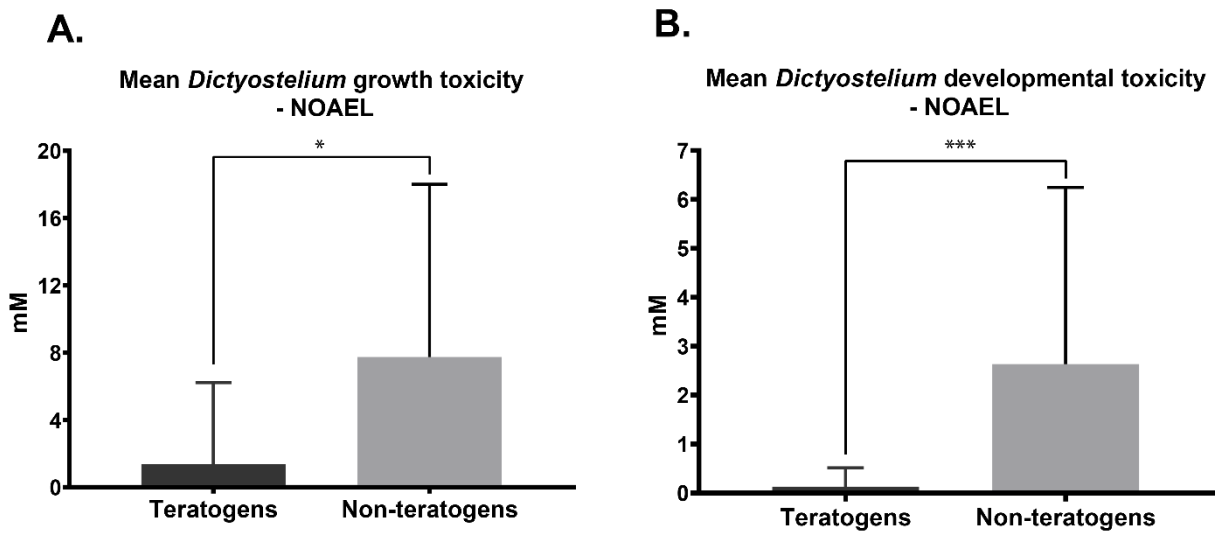

Figure 3.11. Comparison of the mean growth and developmental toxicity NOAELs for teratogenic and non-teratogenic test compounds. A. The mean growth toxicity NOAEL for the test compounds. * represents statistical analysis t-test P=0.0047. **B.** The mean developmental toxicity NOAEL for the test compounds. *** represents statistical analysis t-test P=0.0014. Data represents the mean ± SD.

3.4.8 Growth and developmental toxicity values correlate between *Dictyostelium* and rat model systems.

If *D. discoideum* is going to be used as an alternative model for developmental toxicity testing it must be predictive of mammalian toxicity values for a broad range of chemicals. We therefore compared the *D. discoideum* toxicity data to our collected rat toxicity data sets (Figure 3.12). Firstly, both the *D. discoideum* growth and developmental toxicity values were found to positively correlate to the rat acute toxicity (LD_{50}) data (Figure 3.12). The rat LD_{50} values are larger; this is likely due to a multitude of factors as discussed by Erhirhie *et al* (2018), including the experimental design of acute toxicity studies, where fewer but larger doses are usually tested (215). Nevertheless, the predictive nature of the *D. discoideum* toxicity values is remarkable given the differences between the experimental methods and biology of each system. Next, in order to further probe the predictive relationship between the systems, a second comparison was made to rat repeat dose toxicity (Figure 3.12). Again, both the *discoideum* growth and developmental toxicity values were found to positively correlate to the rat data but with a high degree of significance (Figure 3.12). The numerical value of the rat repeat dose toxicity data is closer to the *D. discoideum* values than the acute toxicity values, revealing a stratification of the teratogenic and non-teratogenic compound (Figure 3.12). Predictably, the compounds classified as non-teratogenic require the highest doses to elicit toxic effects in both model systems. In the final comparison the *D. discoideum* toxicity datasets were found to significantly correlate to the rat fetal teratogenic LOAEL values (Figure 3.12). Moreover, the relationships between the two sets of developmental data are some of the strongest in the 24 correlation analyses (Figure 3.12). Again, as expected, the non-teratogenic compounds generally require a higher concentration to reach the toxic threshold in both systems (Figure 3.12). Taken together, these results present strong evidence of the efficacy of *D. discoideum* to predict toxicity in mammalian systems using multiple endpoint measures.

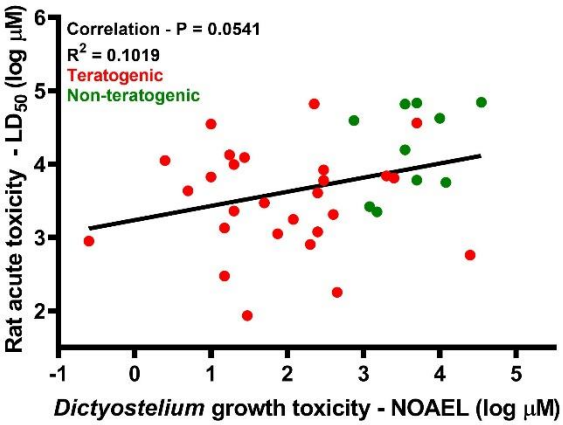

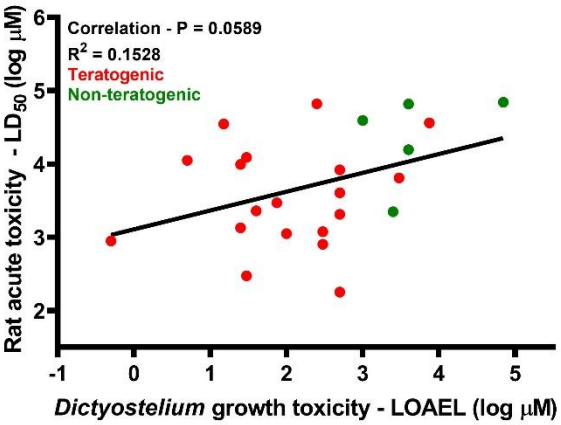

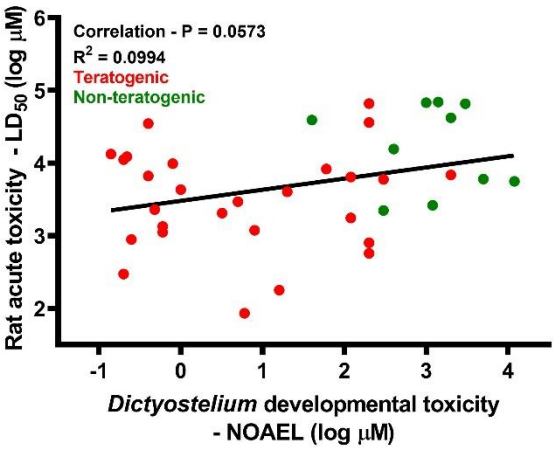

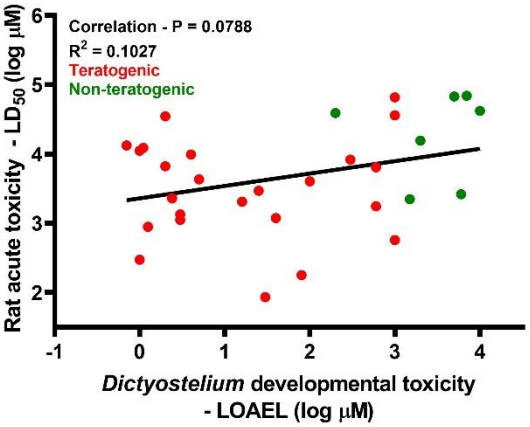

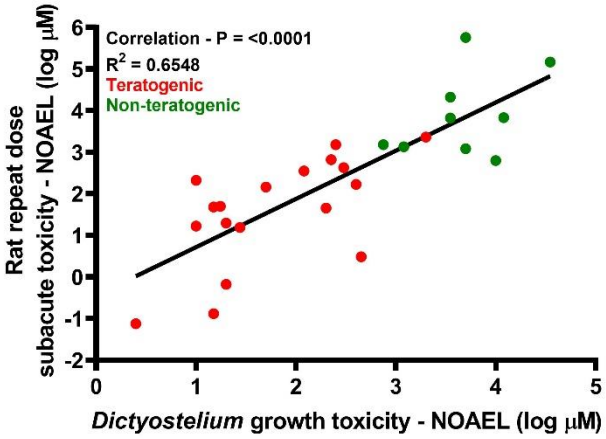

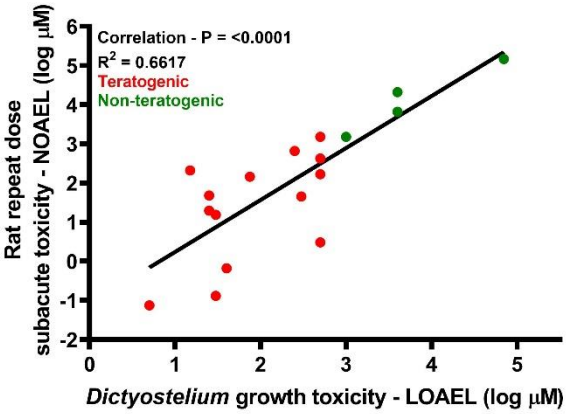

Figure legend on next page.

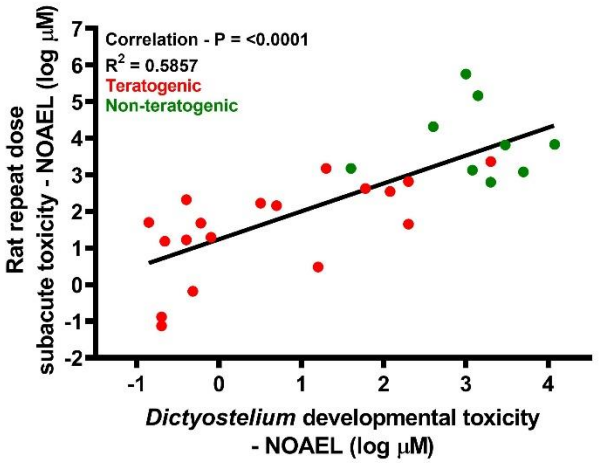

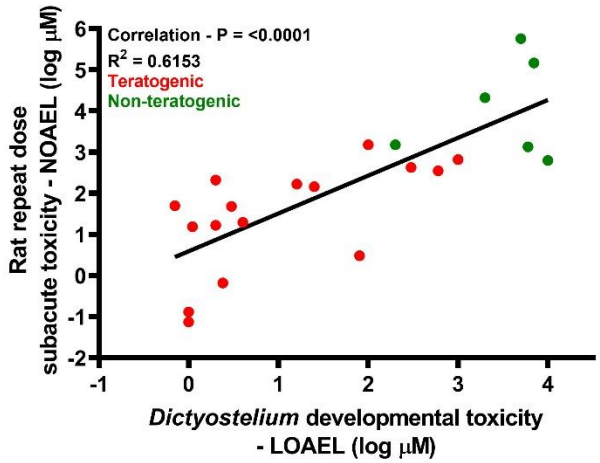

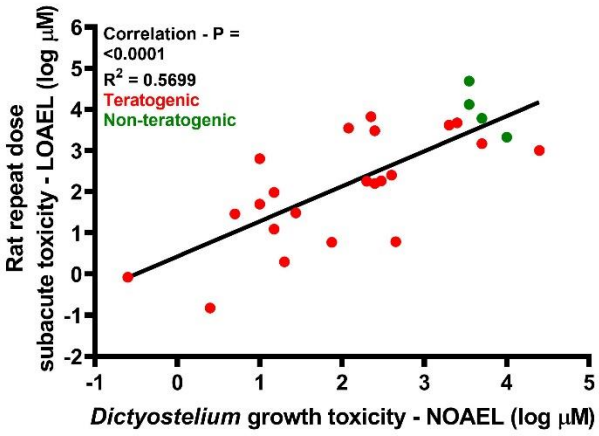

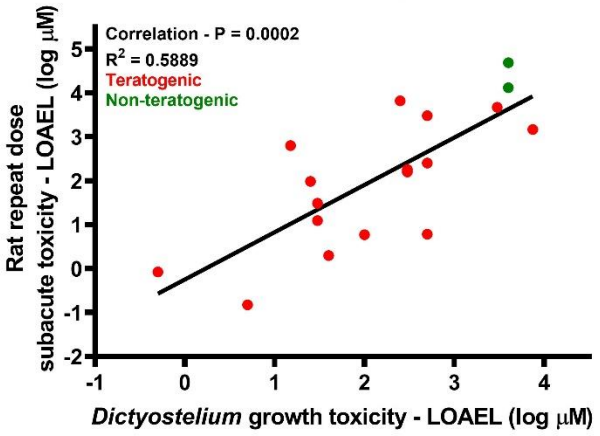

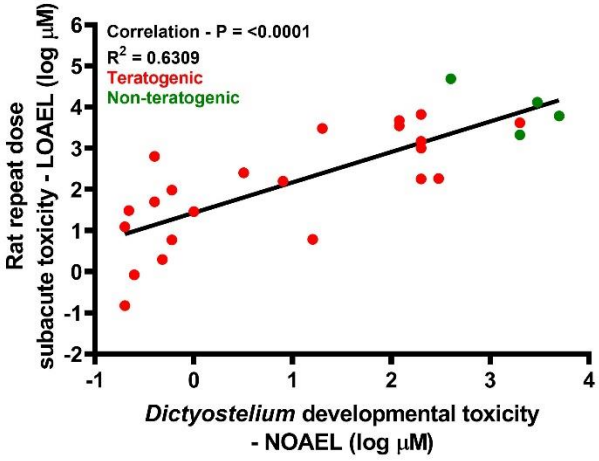

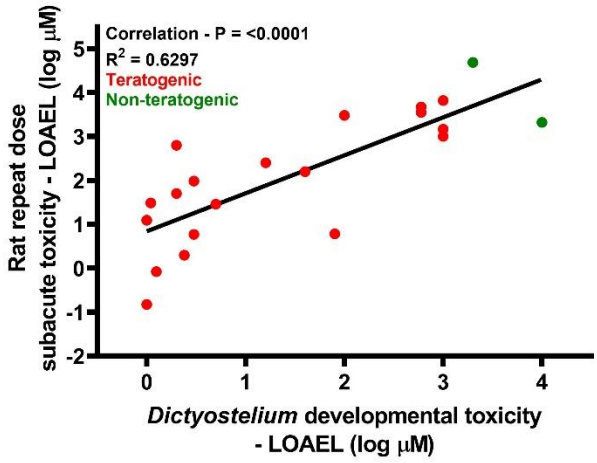

Figure legend on next page.

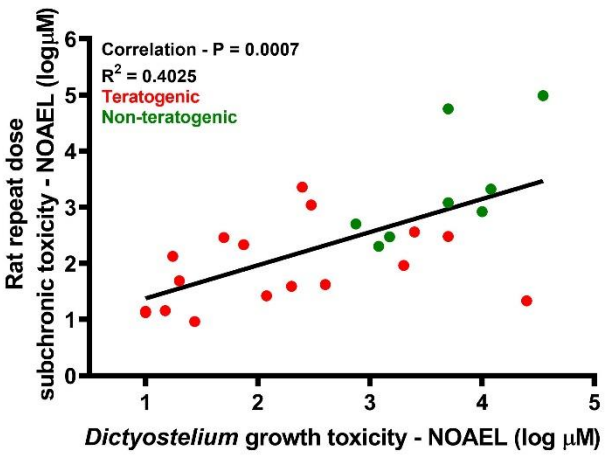

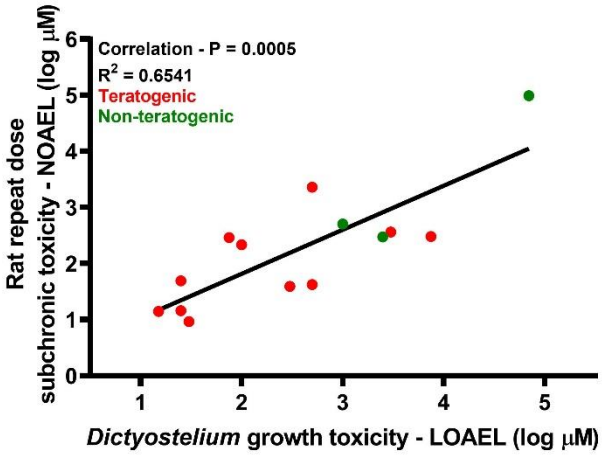

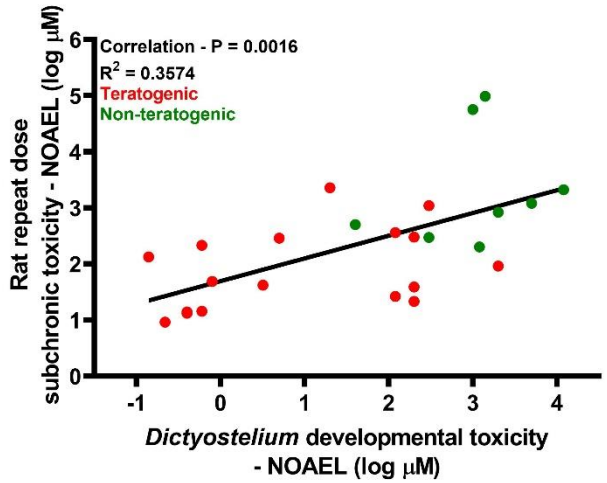

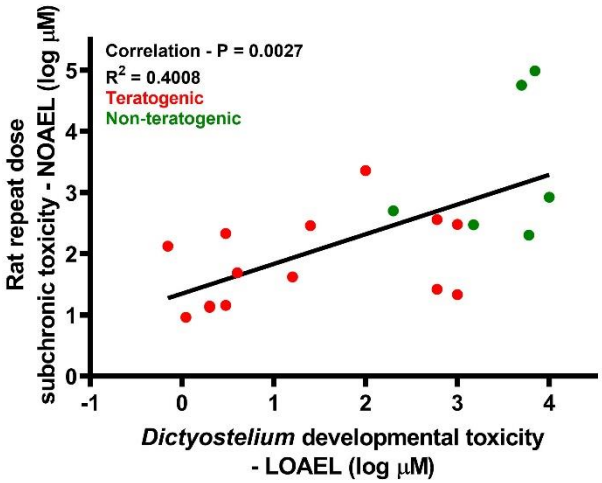

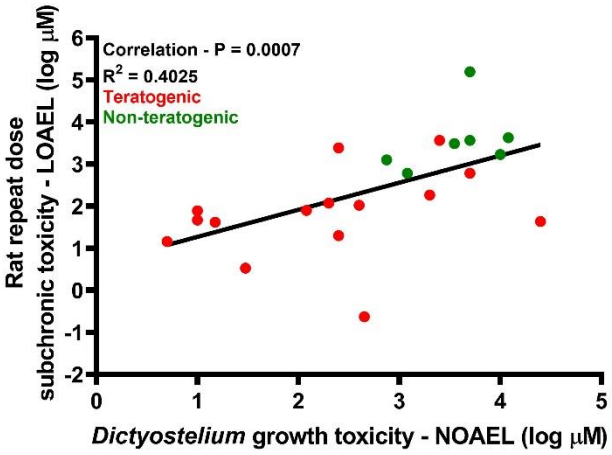

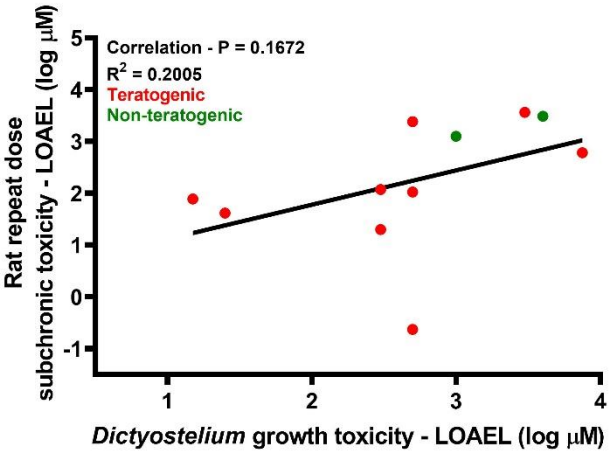

Figure legend on next page.

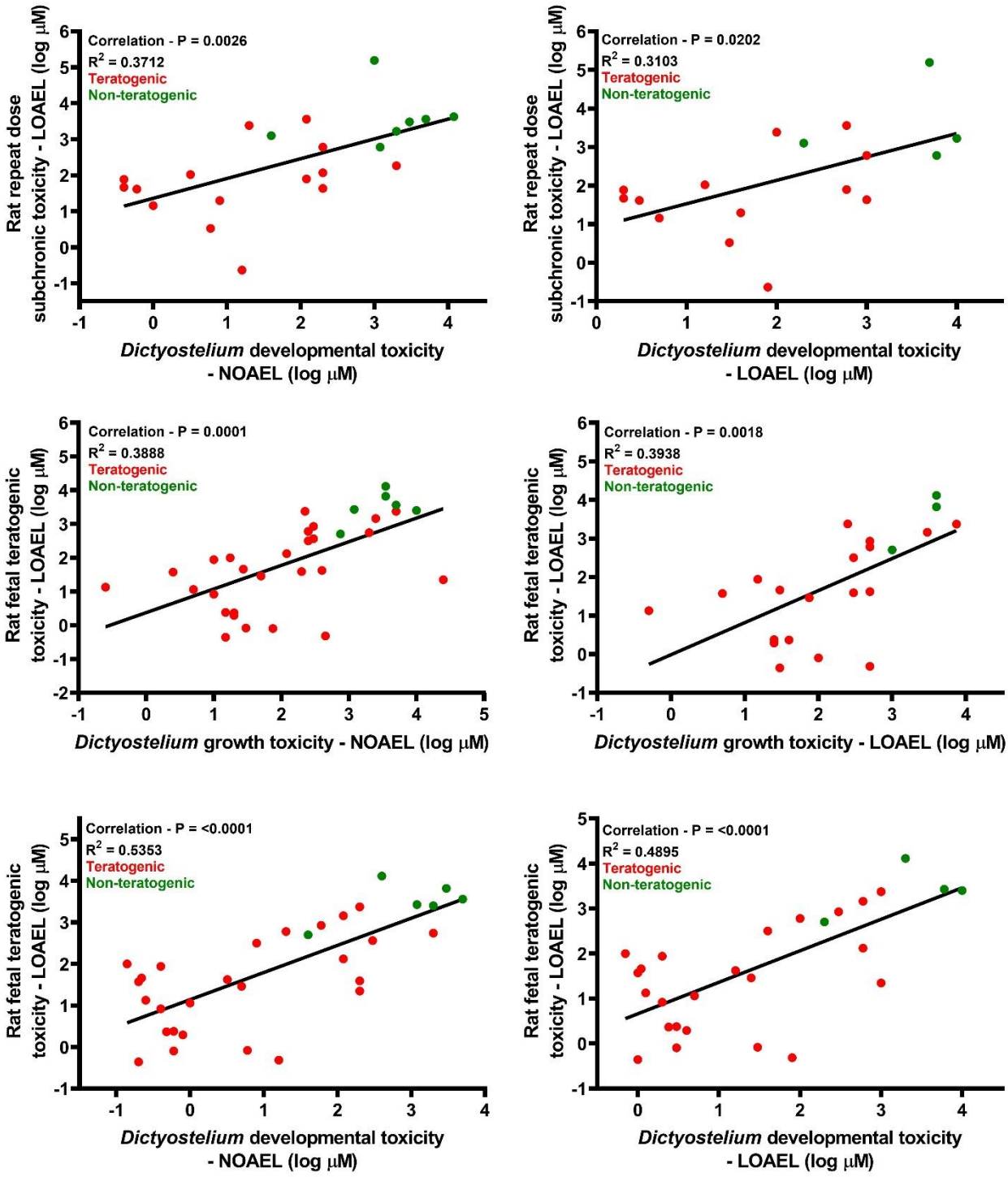

Figure 3.12. Growth and developmental toxicity values correlate between *D. discoideum* and mammalian systems. *In vivo* rat toxicity values for 6 datasets: acute toxicity (LD_{50}), repeat dose – subacute (NOAEL & LOAEL), repeat dose – subchronic (NOAEL & LOAEL) and developmental toxicity (LOAEL) correlated to 4 *D. discoideum* datasets: growth toxicity (NOAEL & LOAEL) and developmental toxicity (NOAEL & LOAEL). All comparisons conducted by Pearson's correlation test. The log of the toxicity values in micromoles are presented. The animal toxicity values were converted to a molarity concentration as described in section 6.3. Teratogenic compounds are coloured red and non-teratogenic compounds are coloured green. Figure over pages 120 - 123.

2.5 Chapter discussion

The aim of this chapter was to determine the suitability of *D. discoideum* to function as an alternative teratogenic evaluation model. The objective was to compare the toxic dose of different compounds and experimental endpoints between *D. discoideum* and a mammalian *in vivo* testing system. Through the use of new *D. discoideum* toxicity assays we have been able to characterise the toxicity profiles of 37 test compounds. The test compounds were selected as well-characterised and classified (non-) teratogens thereby allowing extensive comparisons to be made to *in vivo* mammalian data.

A key result in this chapter was the significant correlation between the rat acute, repeat dose and developmental toxicity values for our test compounds (Figure 3.2). Furthermore, a significant relationship was established between the growth and developmental endpoint toxicity values in *D. discoideum*. This data builds upon similar results reported for zebrafish (187). These observations suggest that the molecular mechanism underlying toxicity is the same, regardless of when in an organism's life cycle, they initiate toxicity. The significant relationship between the different rat endpoints is interesting. Firstly, the results suggest that measuring toxicity at different endpoints only provides different toxicological phenotypic information. This is especially important for early stage general toxicity testing where only simple measures of toxicity are necessary (218). By using the most relevant *in vivo* tests the number of animals used will decrease, fulfilling the need for 3Rs in toxicity evaluation (2). Furthermore, the results suggest that interspecies profiling provides a better measure of toxicity variance than intraspecies endpoint experiments. The results also have implications for *D. discoideum* as an alternative evaluation model. The results suggest that in the future, compounds could be tested at either the vegetative or developmental stage of *D. discoideum*, depending on the question being addressed. For example, in the early stage of compound discovery vast libraries of novel compounds initially only require toxicity dosing to be assessed. Allowing for both excessively toxic and biological inert compounds, to be disposed before further resources are wasted on their development. In *D. discoideum,* such analysis would preferentially be conducted during the vegetative stage were simple readouts allow for HTP analysis of toxicity. However, toxicological evaluation in the *D. discoideum* development stage is more appropriate for later stage toxicity assessments, where more complex phenotypic readouts maybe required. For example, once a novel class of biologically active compounds is identified, characterising the on- and/or off targets and their relations to compound structure requires greater phenotypic toxicity information. Understanding what specific endpoints within a model readout for and which toxicological information is most comparable to animals is an

overlooked aspect of evaluating new models (219). In the future *D. discoideum* test procedures may be streamlined as specific readouts are found to correlate to animal phenotypes. Examples of what this process may look like can be found in recent zebrafish research (187,188). Interestingly, Ducharme *et al* (2015) report that zebrafish behavioural endpoints such as spontaneous movement and touch response significantly correlate to multiple rat and rabbit acute toxicity endpoints (188). Finally, the relation between the growth and development endpoints has implications for the genetic and mechanistic evaluations of teratogenic compounds. The targets of developmental toxins do not have to be screened and evaluated within a developmental context, thus making their evaluation simpler. This greatly increases the potential for the genetic power of *D. discoideum* to be used in developmental toxicity evaluation.

Initial studies assessing a new organism for use as an alternative developmental toxicity model generally present evidence to demonstrate that they can predict mammalian toxicity (1). These are followed up by phase two studies which evaluate methods, protocols and compare results generated by independent laboratories (52,61). If teratogenic classification is not concordant between different research groups (regardless of a harmonised protocol) the new organism may not be a good model for industrial use (52). Although, our research can be considered an initial phase study, a small subset of the test compounds have previously been screened in *D. discoideum* by another group, using a related but different assay. This therefore allows an initial comparison of inter-laboratory results in *D. discoideum.* 3 of the 4 compounds tested by Dannat *et al* (2003) by lacZ staining were also in our cohort of test compounds (Retinoic acid, DES and phenytoin). At 10 µM, Dannat *et al* (2003) report that retinoic acid delayed early development, specifically inhibiting the expression of an *ecmA* reporter with the eventual formation of fruiting bodies (132). The same dose was assayed through our FPR assay, with an identical developmental toxic phenotype (Appendix figure A7.2). Exposure to 1 µM of DES was reported to exhibit a sharp reduction in ecmA-LacZ expression with no effect on the PspA reporter (132). Again, the same phenotype was replicated in our FPR assay results (Appendix figure A7.2). Interestingly, the third shared test compound, phenytoin, did not affect *D. discoideum* at the highest assayable dose, in both our and Dannat *et al*'s study (132). Despite, being a small sample of compounds, assessed using different methods, the concordance of results between our study and Dannat et als' suggests a robustness in the toxicity data generated from *D. discoideum.* This reliability of toxicity measure in *D. discoideum* may be a feature that will allow it to be used widely in the future, by multiple industrial toxicity evaluation laboratories.

Despite the increase in the development of new alternative models for developmental toxicity testing (Section 1.2) there is no universal consensus on how to validate the efficacy of the new models (220,221). A major limitation in previous validative approaches was to only consider test compounds as 'positive' or 'negative', teratogenic or non-teratogenic (220). However, a binary approach completely misconstrues the threshold principle toxicology were any chemical is toxic at a high enough dose (185). Recent research on the validation of new alternate developmental toxicity models, zebrafish and *Xenopus,* have attempted to improve on the binary approach (61,222). The improved method uses a ratio between the growth and developmental values to calculate a teratogenicity score for a set of test compounds (220). A threshold is then set on the teratogenicity score so the compounds can be labelled at teratogenic or not; the compound classifications are then compared to the mammalian classification. Using this validative method recent research on an alternative zebrafish system, report that 87% of 34 test compounds were successfully classified (57). Although, the zebrafish system reported both false positive and false negative results (57). The alternative frog embryo teratogenesis assay (FETAX) was developed earlier than other systems and has therefore been assessed with a larger quantity and range of test compounds (203,222). The performance of FETAX over 400 compounds resulted in an 81% predictivity to mammalian developmental toxicity using a similar validative approach. Whilst, the teratogenicity ratio score approach does provide easy to sell percentage metrics it also has limitations. The imprecise definition of maternal or general toxic effects, lack of teratogen ratio concordance across species and the arbitrary nature of the threshold has led to the proposal of a better exposure based validative approach (221). Daston *et al* (2014) propose testing a series of well characterised test compounds at both a positive and negative exposure dose. They collated a test set of 20 compounds, of which 5 (hydroxyurea, retinoic acid, salicylic acid, saccharin, valproic acid) were used in our study (Table 2.1). Interestingly, 5 out of 6 (83%) exposure level classifications were correctly labelled using our *D. discoideum* values (data not shown). Despite the low number of comparisons, these results align with our correlation data suggesting that our quantitative FPR assay has the potential to be used to characterise a novel compound's toxicity profile.

One limitation associated with toxicity measurements in our *D. discoideum* assays is the requirement for growth and development to take place in aqueous media. The aqueous nature of the toxicity assays leads to solubility and crystallisation problems, ultimately limiting the maximal dose at which low solubility compounds could be tested. Five of the teratogenic compounds (phenytoin, 13-cis-retinoic acid, retinoic acid, bosentan, bexarotene) precipitated out of solution at high concentrations, limiting the

ability to completely profile their toxic effects. Recently developed zebrafish assays are also wholly conducted in an aqueous environment (25,52,58,61). In a large 60 compound study in zebrafish, in order to avoid solubility complications, all test compounds selected were water soluble (25). However, we incorporated test compounds with a broad range of structural polarity and solubility (Section 2.4.1). Assessing the relationship between compound solubility, cellular uptake and growth toxicity in *D. discoideum* is not an objective of this research. However, perhaps unsurprisingly a negative correlation between the partition coefficient (cLogP) and the growth toxicity NOAEL was observed in the test compounds (Data not shown). The partition coefficient is a measure of a compound's solubility preference in either a water or lipid solute (223). The lower the cLogP score the more hydrophilic a compound is. Lower cLogP scores (>1) are associated with poor membrane permeability which has an impact on toxicological endpoints (224). The negative correlation between the cLogP and the growth toxicity NOAEL suggests that the aqueous nature of the assay requires the more membrane impermeable compounds to need a greater toxic dose. Media grown *D. discoideum* cells uptake nutrients via the process of macropinocytosis, whereby whole vesicles of extracellular fluid are incorporated into the cell (80). However, how this specialised method of fluid uptake impacts on the intracellular concentrations of potentially toxic compounds (of varying solubility and polarity) is unknown. In both our qualitative toxicity assessments and the FPR based toxicity assay compounds are delivered to cells by dissolving them in the development agar. Cells are not exposed until plated onto the agar, the point of development initiation. Poor compound solubility may affect uptake into the cell which is further temporally limited by the quick 24-hour development period. Dannat *et al* (2003) suggest that compounds with poor solubility and cellular uptake could be preincubated before being plated onto the agar substratum (132). They additionally report that the intracellular concentration of compounds is higher after growth culture exposure rather than agar exposure at the same dosage (132). This leads them to conclude that exhibited developmental toxicity may be the cause of phenotypes, rather than cytotoxicity, even when greater doses are applied than the calculated growth NOAEL. Interestingly, when we compared the growth and developmental toxicity NOAELs of the test compounds, a higher dose was generally required in the growth phase (Figure 3.10). This trend suggests that either compound exposure via an agar substratum does not limit intracellular concentrations, or that development cells uptake more and/or are more sensitive to toxicants. During growth phase, toxic stress has been reported to induce a reversible cell type which is resistant to a range of toxins, including heavy metal and antibiotics (225). Since such a highly programmed toxin resistant technique exists and presumably protects wild cells from sudden environmental toxins, it is likely (together with other cellular physiological properties) to make *D. discoideum*

more resistant to toxic stress during growth rather than development (225). Despite the minor solubility and crystallisation limitations, as well as the complex nature of cellular compound uptake, the growth and developmental toxicity characterisation was a success. The measurements from our assays are meaningfully validated by significant correlations to rat *in vivo* data. Furthermore, it is likely that the toxicological relationship between the *D. discoideum* and mammalian data would improve had we chosen only soluble compounds. The current significant correlations between the two models is thus limited by noise, strengthening the conclusion that the *D. discoideum* data is predictive.

The final objective of this chapter was to assess how predictive *D. discoideum* is of mammalian developmental toxicity. We were able to demonstrate that our data significantly correlates to *in vivo* rat data (Figure 3.12). We find that both the growth and developmental toxicity data separately correlate to rat toxicity endpoints. The strong correlations suggest that our growth inhibition and developmental toxicity endpoints in *D. discoideum* are excellent metrics from which to accurately predict mammalian toxicity. This contrasts to the more complex zebrafish where research was conducted to find which endpoints are best for mammalian comparison (188). Furthermore, if the correlation between *D. discoideum* and mammalian toxicity is supported with further analysis on a greater number of compounds a future challenge will be to determine a *D. discoideum* conversion factor (226). The conversion factor could be applied to *D. discoideum* toxicity values in order to obtain a mammalian equivalency factor. Although, in turn this would require an interspecies uncertainty factor, which can only be accurately calculated by comparing large data sets between species. The robustness of both the *D. discoideum* endpoints, suggests that the comparatively simpler, yet genetically complex, *D. discoideum* is a reliable system for mammalian toxicity prediction. Our comparisons are, to our knowledge, the strongest evidence for the application of *D. discoideum* as a new alternative model in toxicity characterisation to date.

In conclusion, the toxicological data presented in this chapter validates the phenotypic potential for *D. discoideum* to function as an alternative teratogen evaluation model. Our results, thus, allow us to assess the potential of the model to genetically evaluate teratogenic compounds.

Chapter 4 – A parallel phenotype approach to classify and characterise the targets of teratogenic compounds

4.1 Introductory remarks

A recent developmental toxicity testing consortium concluded that the use of human cells (or tissues) and toxicity simulation was the future of the field (227). By using only human cell studies, in tandem with *in silico* simulation, the need for *in vivo* animal testing (and the significant associated costs) would be limited. However, if toxicity modelling and simulations are to become an effective alternative to animal testing, greater knowledge of key toxic events at the cell and molecular level is required (228). Furthermore, by understanding the underlying causes of toxicity, compound safety evaluation and exposure guidelines will be enhanced (227). Finally, knowledge of whether toxicity is due to on- or off- target effects can affect the decision to continue the development of new chemicals (229). Consequently, in the last decade, characterising the developmental toxicity mechanisms for a broad range of chemical classes and structures has increasingly become a goal of safety testing (230).

The standard approach to understanding teratogenic mechanisms is to assume a simple direct connection between the molecular initiating event and phenotypic outcome (Figure 4.1 A). However, in biological systems, the molecular interactions that mediate cellular toxicity are likely to be more complex (Figure 4.1 B). Furthermore, even though different compounds may affect different molecular pathways, they may result is similar phenotypic outcomes (Figure 4.1 B). Thus, whilst measuring the phenotypic response to a toxic compound can provide dose response information, interpreting phenotypes to predict the underlying mechanism of toxicity is problematic. It is therefore very difficult to define a framework to characterise the cell- and molecular-level toxicity information (for many toxic compounds) needed for effective *in silico* development toxicity simulation and modelling. One way the complex biological mechanisms behind developmental toxicity can be characterised is to simplify the link between chemically-induced toxic events and adverse outcomes. Developmental toxicological pathway networks (dTPNs) are an attempt to shift the focus of understanding teratogenic mechanisms from evaluating phenotypic outcomes to characterising the key molecular and cellular toxic steps that mediate developmental toxicity (Figure 4.2) (227,231,232).

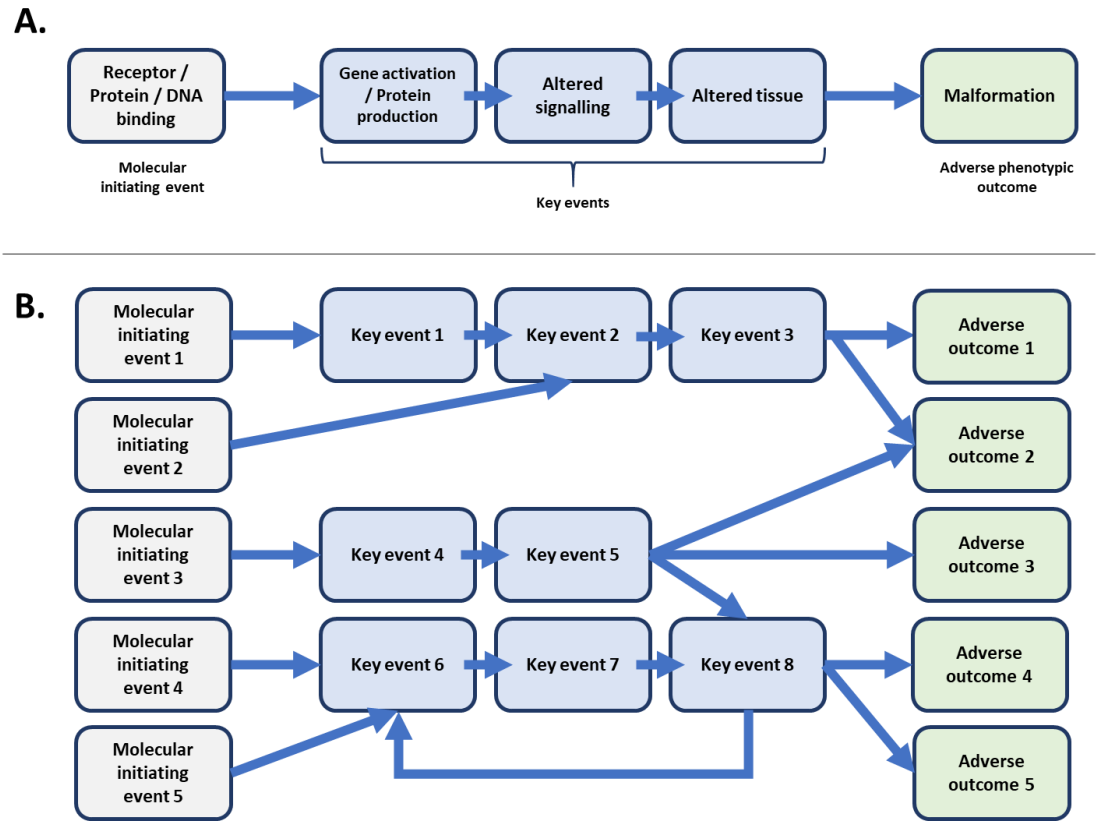

Figure 4.1. Schematic of a standard linear toxicity event and complex interconnected outcome pathways. A. In a linear model of a teratogenic compound's adverse effects, a molecular initiating event triggers a cascade of key toxicity events which results in an adverse phenotypic outcome. **B.** A more biologically representative model demonstrates the complex interconnected pathways associated with developmental toxicity. Figure adapted from (227).

The key to understanding how development toxicity leads to adverse phenotypes is to identify the gene networks affected by different chemicals. 'Genetic phenotyping' approaches would allow teratogenic compounds to be characterised by their mechanisms of action as opposed to the adverse phenotypes they cause. The challenge, however, is that few methods exist to interrogate the gene networks responsible for phenotypic change in response to chemical perturbation (233). For example, if sufficient genetic and phenotypic information is available, variance in drug response can used to identify loci that affect toxicity (233). However, genome wide association studies of this kind require a huge investment to acquire large genetic and phenotypic datasets (and thus are very low throughput). Gene expression changes induced by chemical-mediated teratogenicity can also be used to assess gene network change (234). However, such RNA-sequencing studies also have limitations for genetically phenotyping responses to

toxic compounds. Critically, some toxic compounds have been reported to minimally affect transcriptional change making the approach problematic (234). Parallel phenotyping provides an alternative approach. In this, a population of thousands of genetic variants are screened simultaneously to identify mutants that exhibit a desired phenotypic outcome (for example, resistance or hypersensitivity to chemical toxicity). When coupled with next generation sequencing, parallel phenotyping can provide a powerful tool to identify genes associated with developmental toxicity. However, developing such a method in a mammalian or higher animal model would be unfeasible. Parallel phenotyping requires a simpler model system, with a smaller compact genome that can be genetically manipulated. Consequently, the ease with which microbial systems (including *D. discoideum*) can be genetically manipulated means they can be powerful systems for genome-wide functional analysis. We have already demonstrated *D. discoideum* can be used to predict toxicity in higher organisms (Chapter 3). We, therefore, sought to establish whether it could also be used in a parallel phenotype approach to comprehensively characterise genes associated with developmental toxicity.

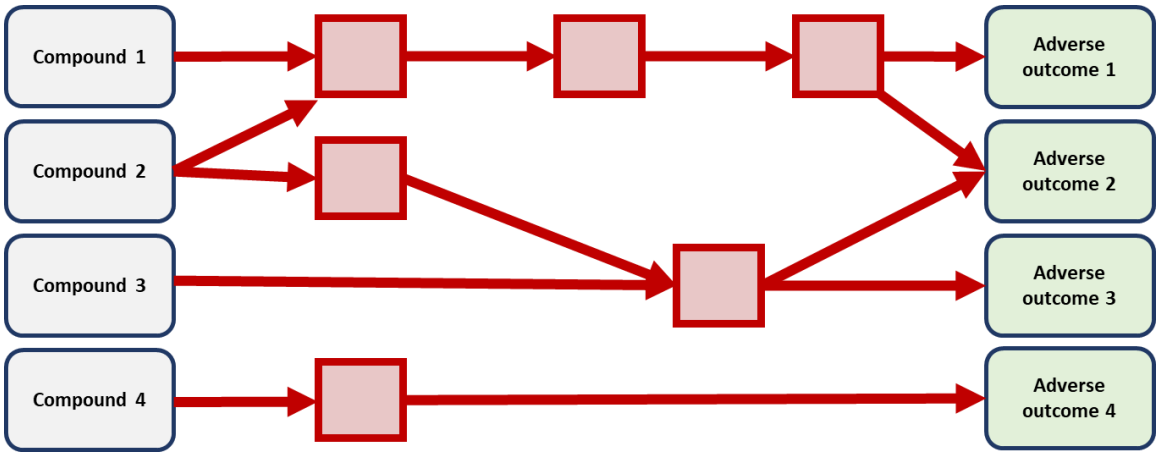

Figure 4.2. A schematic of a developmental toxicity pathway network. Four different compounds cause different adverse phenotypic outcomes dependent on modelled key events (red squares). Figure adapted from (227).

In *D. discoideum,* libraries of mutants can be generated by restriction enzyme mediated integration (REMI). REMI works by the random integration of a linear piece of DNA into *D. discoideum* cells. Cells are electroporated with a mixture that includes both the linear DNA (including a selective resistance gene) and a restriction enzyme. The restriction enzyme is chosen to generate double strand breaks in the genome with complementary ends to facilitate integration of the DNA fragment which can generate

single gene deletion strains. REMI has allowed forward genetic analysis and the identification of novel components of many biological processes, including susceptibility to toxicity (Section 1.4.3) (151). However, REMI is limited by the need to identify each individual mutant. Recently, a new method, (REMI-Seq) has been developed in *D. discoideum* which allows the insertion sites of complex pools of REMI mutants to be identified simultaneously (86). Moreover, because this method, is quantitative, it allows the relative abundance of each mutant to be determined. Therefore, if the mutant pool is sequenced before and after a selection, mutants that increase or decrease in abundance can be identified. REMI-Seq thus represents a new method by which genes that underlie developmental toxicity can be identified. Knowledge of these genes allows a 'genetic phenotype' to be ascribed to developmentally toxic compounds, and thus different compounds can be compared and classified based on this phenotype. Furthermore, REMI-Seq technology allows the toxic mode of action of a group of (suspected) teratogens to be assessed, without any visual phenotypic characterisation.

In order to assess the utility of REMI-Seq as a 'genetic phenotyping' tool for teratogen evaluation and categorisation, we performed proof of principle screens with lithium and valproic acid (VPA). This is because studies in *D. discoideum* over the last 20 years have allowed aspects of the mode of action and teratogenic effects of these mood stabilising compounds to be determined. We find that REMI-Seq can be used to identify novel genes that affect the susceptibility of *D. discoideum* cells to the toxic effects of lithium and VPA. These mutants can be experimentally validated, illustrating the quantitative reproducibility of REMI-seq. Finally, by studying the gene networks associated with VPA and lithium toxicity, the mechanistic relationship between the two compounds and specific biological processes disrupted could be assessed. This revealed a significant relationship between the toxicological mechanisms of lithium and VPA. Together, our proof of principle screens highlights the potential of the *D. discoideum* REMI-Seq assay to characterise the targets and relationships between teratogenic compounds.

4.2 Aims

Establish whether *Dictyostelium* forward genetics can distinguish the mechanistic relationship between compounds with similar phenotypes, using a genetic phenotyping approach.

Identify genetically the specific targets of teratogenic compounds and thereby the biological processes disrupted.

4.3 Objectives

- Select conditions, conduct and validate the success of lithium and VPA REMI-Seq screens.
- Identify significantly enriched (advantaged) and depleted (disadvantaged) mutants from the sequencing results of the lithium and VPA screens.
- Validate the expected phenotypes of the putative lithium and VPA advantage and disadvantage mutants.
- Assess the potential toxicological relationship, genetically, between lithium and VPA.
- Implement gene ontology analysis to identify the potentially shared biological process and pathways mediating lithium and VPA toxicity.

4.4 Results

4.4.1 Defining REMI-Seq screen conditions

We found significant correlations between growth and developmental toxicity endpoints in the rat model and *D. discoideum* (Figure 3.2, 3.10). Furthermore, lithium and VPA affect both growth and developmental toxicity in *D. discoideum* (Figure 3.12). This suggests that the molecular mechanisms of action of compounds in either growth or development are likely to be related. Therefore, we reasoned that vegetative growth, rather than development, could be used in REMI-Seq screens to identify mutants with altered responses to lithium or VPA. We therefore first set out to identify a dose that provides a moderate selective pressure for each compound. This is because at a high selective pressure, only the most resistant or sensitive mutants can be identified, thus reducing the number of mutants that can be identified. The relative population doubling rate of Ax4 cells was tested over 48h in different doses of lithium and VPA. From this, a dose of 7.5 mM for lithium and 1 mM for VPA was selected for REMI-Seq screening (Figure 4.3 A, 4.3 B).

Next, we sought to establish whether these doses would allow a known, developmentally resistant mutant to be identified. REMI screens have previously been conducted in *D. discoideum* to decipher the mode of action of lithium (151,235). Williams *et al* (1999) described a mutant from a lithium developmental toxicity resistance screen with an insertion in the *dpoA* gene (151). However, its resistance to the effects of lithium treatment during growth have not been reported (153). Therefore, we assayed its growth rate in 10- , 15- and 20 mM lithium over a 48h period (Figure 4.3 C). At all three concentrations, the *dpoA* mutant exhibited resistance to the effects of lithium on growth compared to the parental Ax2 control (Figure 4.3 C). The *dpoA* mutant could grow at 15- and 20 mM, doses which completely prevent cell growth in the control (Figure 4.3C). These results suggest that by conducting a REMI-Seq screen during growth (at a dose causing a 50% reduction in growth rate) should enable mutants that affect the sensitivity of cells to lithium (and VPA) during growth and development to be identified.

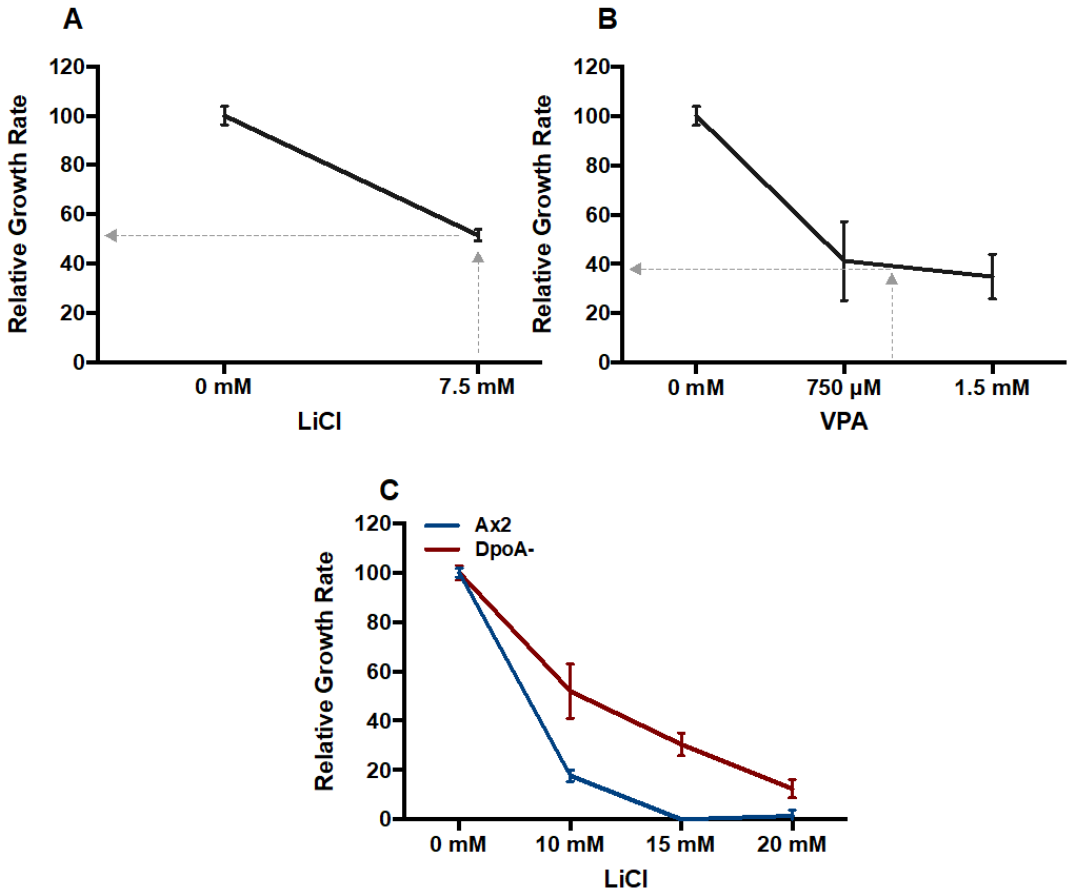

Figure 4.3. Growth resistance of a developmental toxicity resistant mutant and REMI screen test compound concentration analysis. Relative population doubling rates of Ax4 (8-48 hour) when treated with LiCl **(A)** or VPA **(B).** A dose that elicits an ~50% relative growth rate was selected for both lithium and VPA (Grey arrows). Data represents three well replicates (Mean ± SD). **C**. Relative growth rates of a parental Ax2 and *dpoA* KO mutant (8-48 hour) when treated with 10, 15 and 20 mM of LiCl (Mean ± S.D., 3 well replicates).

4.4.2 The REMI-Seq Screen

A REMI-Seq mutant pool containing ~ 21,000 mutants (86) was grown up in tissue culture. The mutant pool was split into separate plates for screening in the presence of either 1 mM VPA or 7.5 mM lithium. In addition, a 1% DMSO screen was conducted as this does not affect cell growth rate (Figure 3.3). The DMSO screen therefore serves as a control to identify mutants that purely grow faster or slower in tissue culture. Each screen was conducted in duplicate (Figure 4.4).

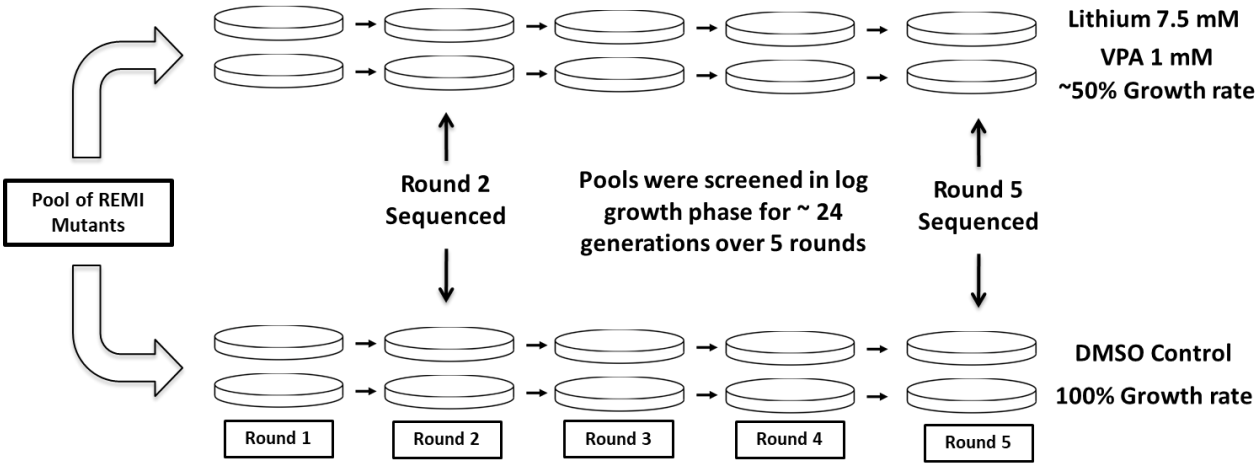

Figure 4.4. A schematic of the REMI-Seq screening methodology. A pool of ~21,000 REMI-Seq mutants were treated with either lithium 7.5 mM, VPA 1 mM or DMSO 1% in duplicate screens. The screens were conducted at log growth phase over 5 rounds after which approximately 24 cell generations had transpired. DNA was extracted from rounds 2 and 5 for sequencing.

Mutant cells were initially seeded at 2 x10^5 cells / ml and grown until confluent (approximately 1.5 – 3 x10^6 cells / ml or 3 - 4 generations) before being counted and re-seeded in new plates at 2 x10^5 cells / ml. This constitutes one round of selection (Figure 4.4). After each round, cells were frozen for storage. The screens were stopped after 5 rounds (approximately 15 - 24 generations) as the time taken for the lithium and VPA plates to reach confluence had dramatically decreased (Data not shown).

Before the samples were processed for sequencing, we tested whether the growth rate of each pool had actually changed. This would be consistent with the composition of each pool changing, as resistant (advantaged) mutants increase in frequency. A competition assay was performed where a wildtype GFP fluorescent strain was mixed 50/50 with cells from round 4 of the lithium, VPA or DMSO screens (Figure 4.5). The competition mixtures were grown in identical conditions to the screens, with or without the corresponding compound. The relative proportion of labelled to unlabelled cells was scored by flow cytometry before the competition, and after each round of the competition (Figure 4.5). If growth advantaged mutants had been enriched then they should outcompete the labelled wildtype cells in the presence of each compound. Both the lithium and VPA round 4 pools increased in proportion to wild type cells in the presence of the compounds (Figure 4.5 B, 4.5C). This did not occur if the absence of the test compounds (Figure 4.5 B, 4.5 C). Furthermore, round 4 of the DMSO screen did not increase or decrease in relative frequency, suggesting there has not been extensive

selection for mutants that are simply growth advantaged in standard tissue culture conditions (Figure 4.5 B, 4.5 C). These results suggest that the later rounds of the lithium and VPA screens are enriched for resistant mutants. Cells from round 5 were therefore grown up for gDNA extraction and sequencing.

The presence of enriched ‘advantaged’ mutants at round 5 will also impact our ability to detect hypersensitive or ‘disadvantaged’ mutants. This is because advantaged mutants that increase in frequency will take up more of the finite sequencing reads at the expensive of neutral and disadvantaged mutants. In practice this means that as a selection progresses neutral mutants decrease in frequency. Therefore, in the later rounds, the enrichment of strong resistant mutants means that ‘neutral mutants’ drop out of the population. At this stage, neutral and disadvantaged mutants cannot be distinguished, thereby masking the truly disadvantaged mutants. However, we reasoned that disadvantaged mutants should be easier to detect at earlier rounds (as they are first to dropout) before the advantaged mutants have overtaken the pool. Consequently, we also sequenced DNA from round 2 cells, which allowed us to preferentially identify disadvantaged mutants (Figure 4.4).

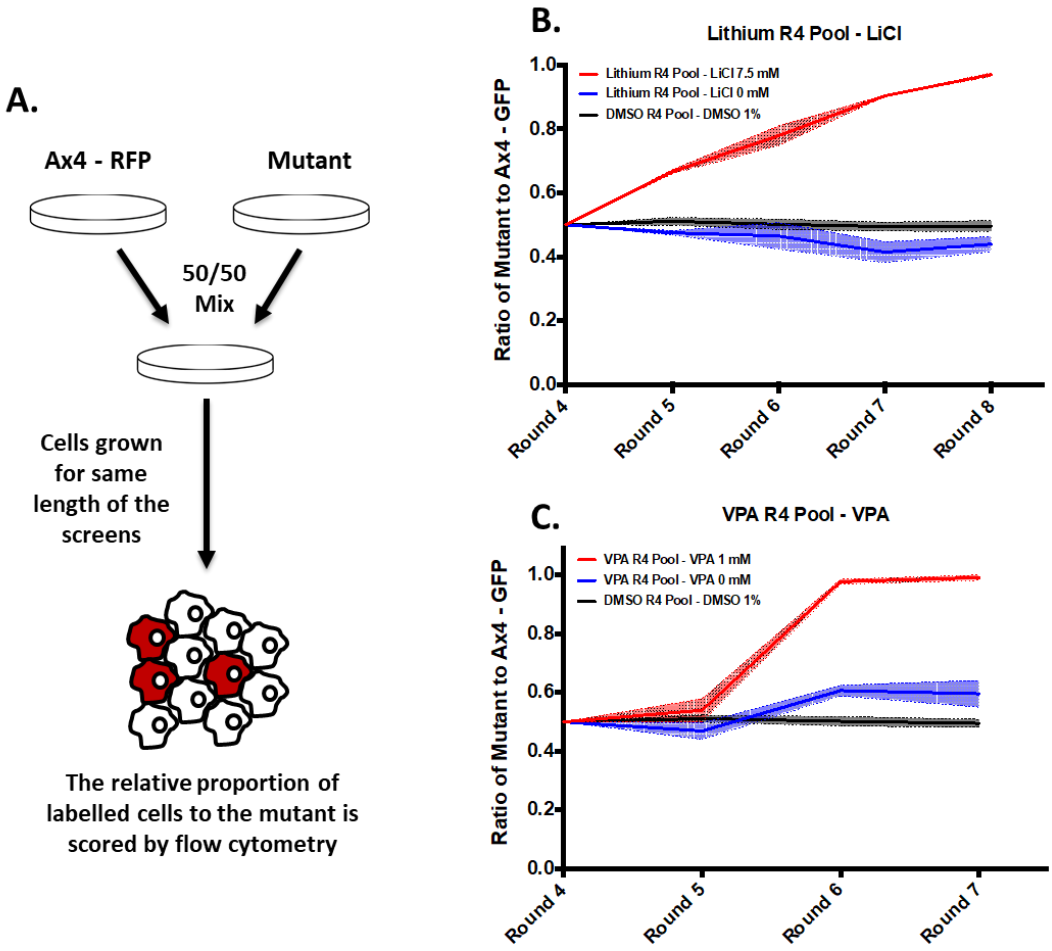

Figure 4.5. Schematic for competition assays and validation of screen selections. **A.** A schematic for a competition assay where fluorescently labelled wildtype cells are mixed equally with unlabelled cells. After a period of growth, with or without compound treatment, the relative proportion of labelled cells to mutant cell is scored by flow cytometry. **B.C.** Normalised ratio of lithium and VPA round 4 mutants to Ax4-GFP. The REMI mutant pools increase in frequency only with the compound treatment (Red). Without the selective pressure the lithium and VPA pools (Blue) behave similarity to the DMSO control screen (Black). (Mean ± SD., data representative of 2 biological replicates).

4.4.3 REMI-Seq sequencing data and quality assessment

DNA was extracted from both biological replicates of rounds 2 and 5 for the DMSO, lithium and VPA selections, and prepared for REMI-Seq analysis (Methods section 6.8.2) (86). Samples from round 2 were pooled and sequenced. In addition, samples from round 5 were pooled and sequenced separately. This yielding ~450- and ~490 million reads, respectively. Approximately 60 % of the reads could be mapped to a genomic REMI insert location as described by Gruenheit *et al* (2019) (86). Finally, to allow comparisons across the different samples, the raw read count data for each insertion point was normalised, to take into account the total number of reads per sample (86). From the round 2 samples, we could detect in total 8531 unique barcoded mutants (Table 4.1). Due to a higher sequencing depth, 12,743 unique barcoded mutants could be detected in the round 5 screens (Table 4.1).

Table 4.1. Number of unique mutants and gene insertions in the REMI screen rounds.

Unique Mutants	Round 2	Round 5
Bin 10000	113	72
Bin 1000	2536	2729
Bin 100	5882	9942
Total Mutants	**8531**	**12743**

The normalised read counts of the biological replicates were compared to assess the quality and reproducibility of the data (Figure 4.6). Biological replicates were highly correlated for all three screens for both rounds 2 and 5 ($P = <0.0001$) (Figure 4.6). Technical reproducibility was, however, dependent on read count abundance (Figure 4.6). At around approximately 100 read counts, technical dropouts increase in frequency (Figure 4.6). This has previously been reported during the development of the REMI-Seq method and is thus accounted for in later analyses (86). It is noteworthy that the lithium and VPA screens contain fewer mutants in both biological replicates at round 5 than round 2, or either rounds of the DMSO control (Figure 4.6). This suggests advantaged mutants have been enriched at the expense of other mutants. The apparent success and biological reproducibility of the screens allowed us to next identify significantly advantaged and disadvantaged mutants.

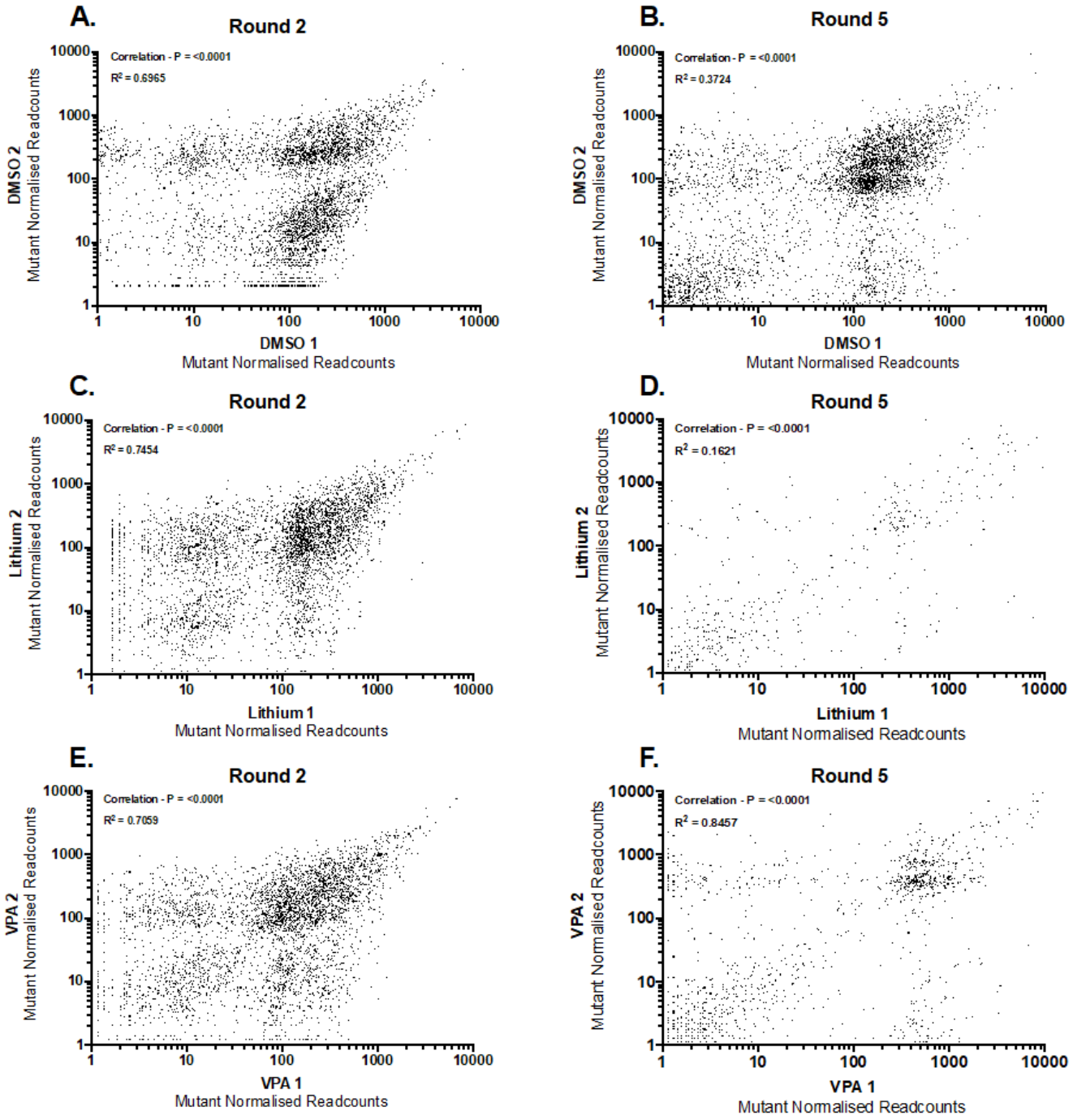

Figure 4.6. The biological replicates for REMI-Seq screens significantly correlate. A.B.C.D.E.F. Correlations of the normalised data for the two biological replicates for the lithium, VPA and DMSO screens, rounds 2 and 5. All of the biological replicates significantly correlate (P= <0.0001) (Pearson's Correlation).

4.4.4 Identification of putative advantaged and disadvantaged mutants

In any growth selection, mutants with inherent growth advantages or disadvantages will increase or decrease in frequency, respectively (85,86). In order to distinguish these from those that had become significantly enriched or depleted in the presence of lithium or VPA, we compared the relative abundance of every mutant to the abundance in the DMSO screen (Figure 4.7 A). The DMSO screen has been through the same number of generations as the compound screens, and therefore provides an internal control for inherent growth mutants. However, before this analysis was performed, the mutants were divided into three bins depending on their mean normalised readouts in the DMSO screen. The three bins are termed bin 100, 1000 and 10,000 and correspond to normalised reads of 1-100, 100-1000 and >1000, respectively. The relative fold change of each mutant was calculated separately for each bin in comparison to the mean DMSO readcount, for each replicate of the lithium and VPA screens (rounds 2 & 5) (Figure 4.8). This allowed the average change in behaviour for all mutants in each bin to be determined. To allow comparisons between bins, replicates and rounds, the foldchange data was next represented as a Z score (Figure 4.7 B). This process allows for thresholds to be set for mutants that deviate significantly from the mean using the Z score values. (Figure 4.8). For example, mutants with a Z-score > 1.5 are > 1.5 standard deviations from the mean and mutants with a Z-score < -1.5 are < -1.5 standard deviations from the mean (Figure 4.8).

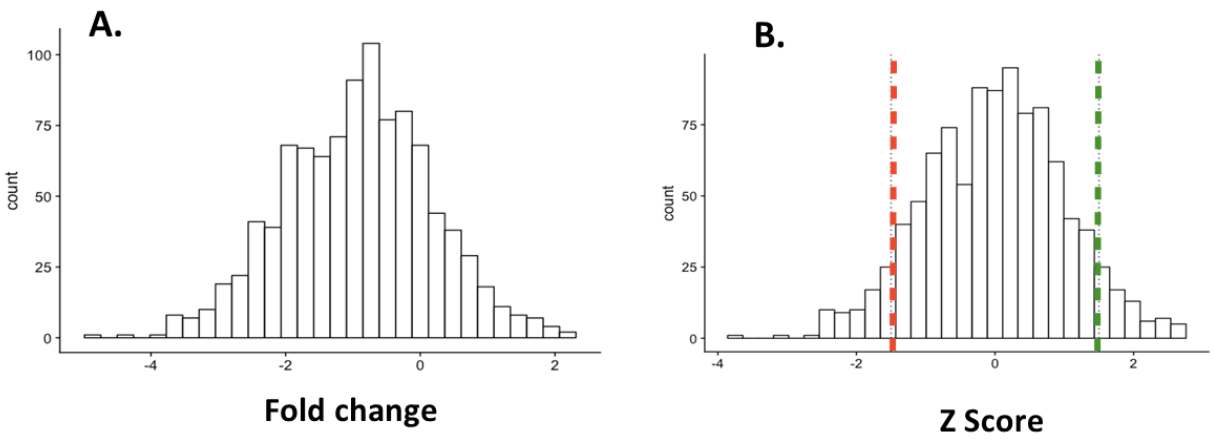

Figure 4.7. A schematic diagram of the REMI-Seq mutant fold change analysis. A. An example of when the log foldchange of every mutants' reads are compared to a non-selective control. **B.** The representation of the foldchange data as a Z score centres data around zero, allowing for thresholds to be set.

By comparing the Z scores for each biological replicate, the change in mutant abundance for each bin across both rounds can be visualised (Figures 4.9, 4.10). Next, we used the Z-score thresholds to identify significantly advantaged and disadvantaged mutants (Figure 4.8). Both replicates were required to exhibit a Z score above the chosen threshold (Figure 4.8). This represents a stringent selection criterion by which we sought to reduce the number of false positive and negative mutants. We compared the number of mutants identified at different Z-score thresholds, at rounds 2 and 5 for the lithium and VPA screens (Figure 4.11).

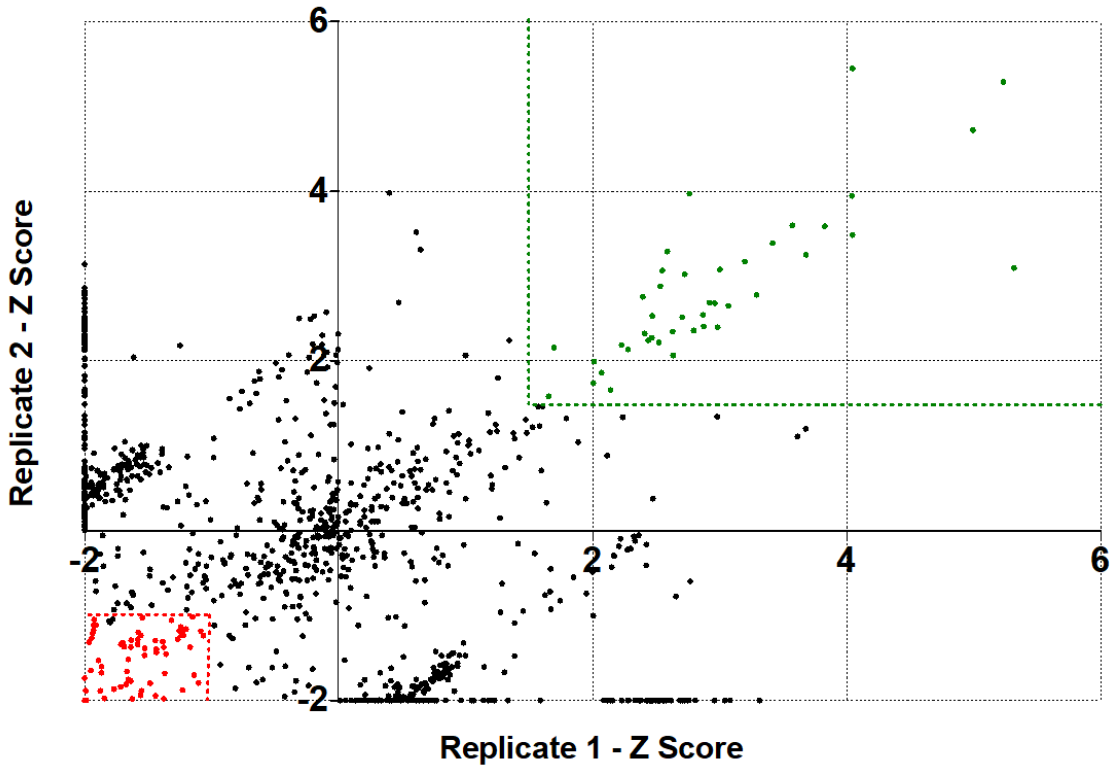

Figure 4.8. An example of Z score threshold analysis for the selection of advantage and disadvantage mutants. Thresholds applied to both of the biological replicate Z scores allows for the selection of significantly outlying mutants. Green dotted line indicates a dual 1.5 advantage cut-off. Red dotted line indicates a -1 disadvantage mutant cut-off.

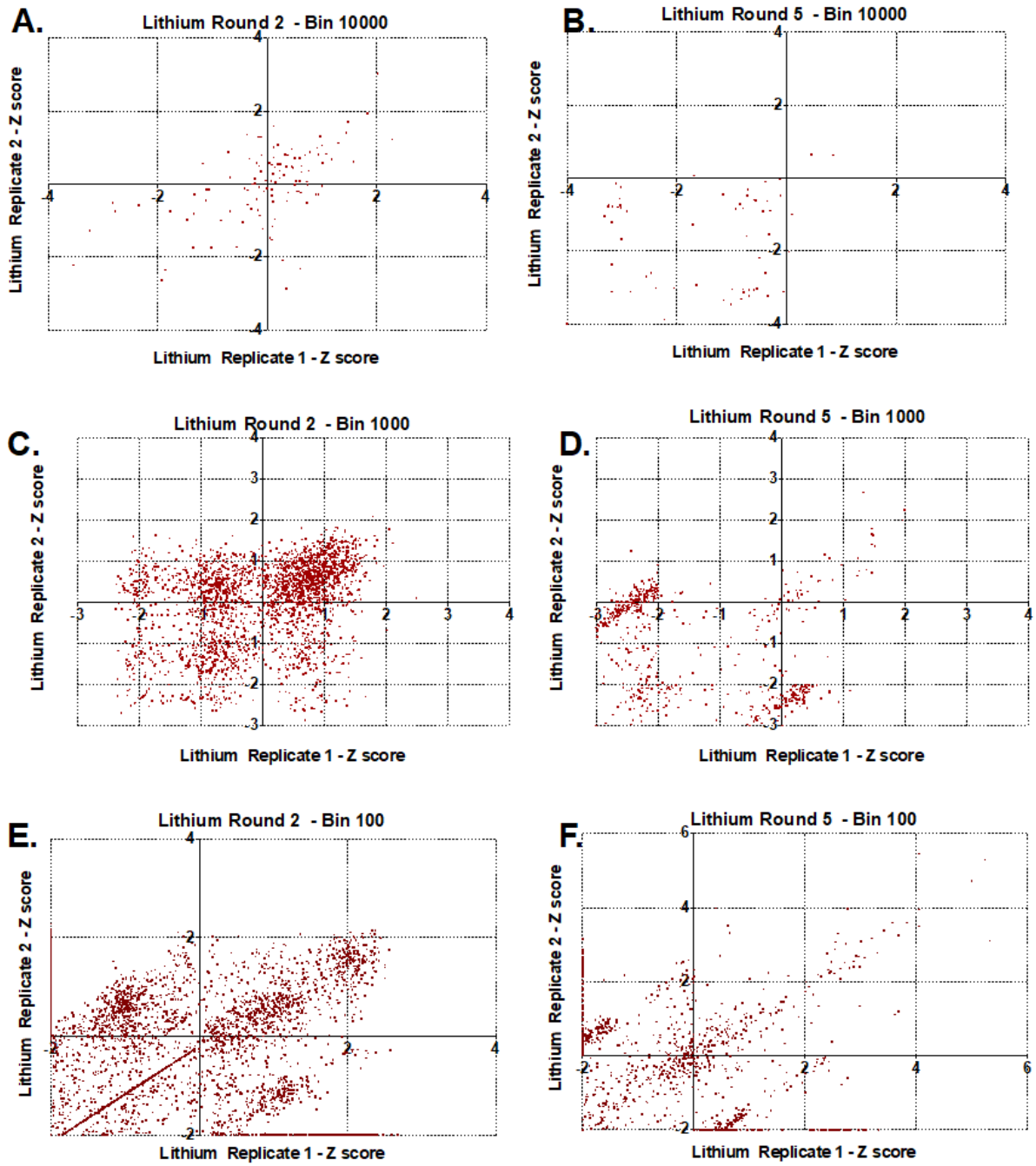

Figure 4.9. Z - Score analysis of binned lithium biological replicates. The log foldchange of every mutants' reads in the lithium screen in comparison to mean DMSO readcount, as a Z score. A correlation of the biological replicates Z scores allows for the relative changes in mutant abundance to be observed. **A.B.** Mutants in bin 10,000. **C.D.** Mutants in bin 1000. **E.F.** Mutants in bin 100. Across all bins significantly fewer mutants remain in the later round 5 in comparison to round 2 due to the advanced selection.

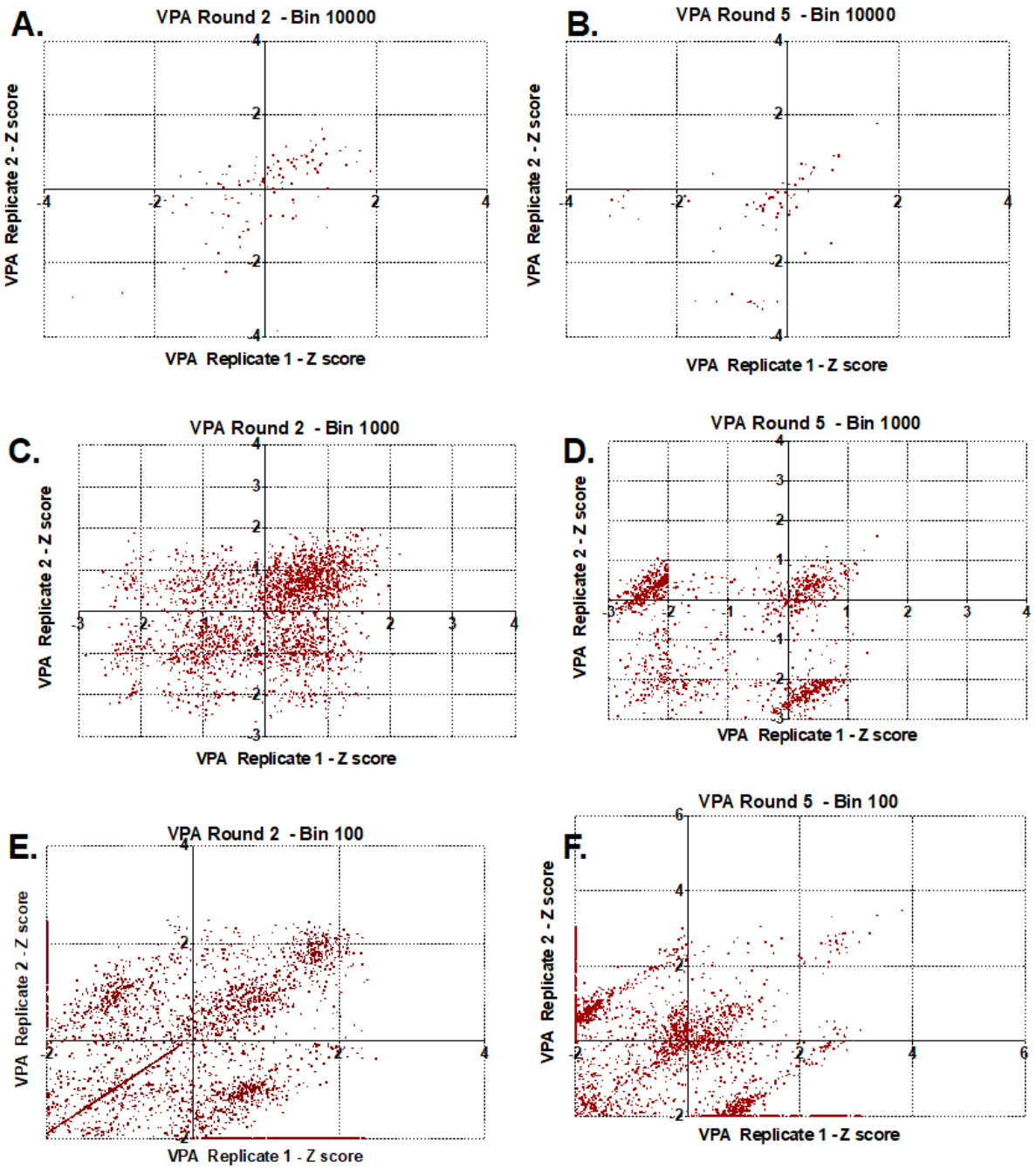

Figure 4.10. Z-score analysis of binned VPA biological replicates. The log foldchange of every mutants' reads in the VPA screen in comparison to mean DMSO readcount, as a Z score. A correlation of the biological replicates Z scores allows for the relative changes in mutant abundance to be observed. **A.B.** Mutants in bin 10,000. **C.D.** Mutants in bin 1000. **E.F.** Mutants in bin 100. Across all bins significantly fewer mutants remain in the later round 5 in comparison to round 2 due to the advanced selection.

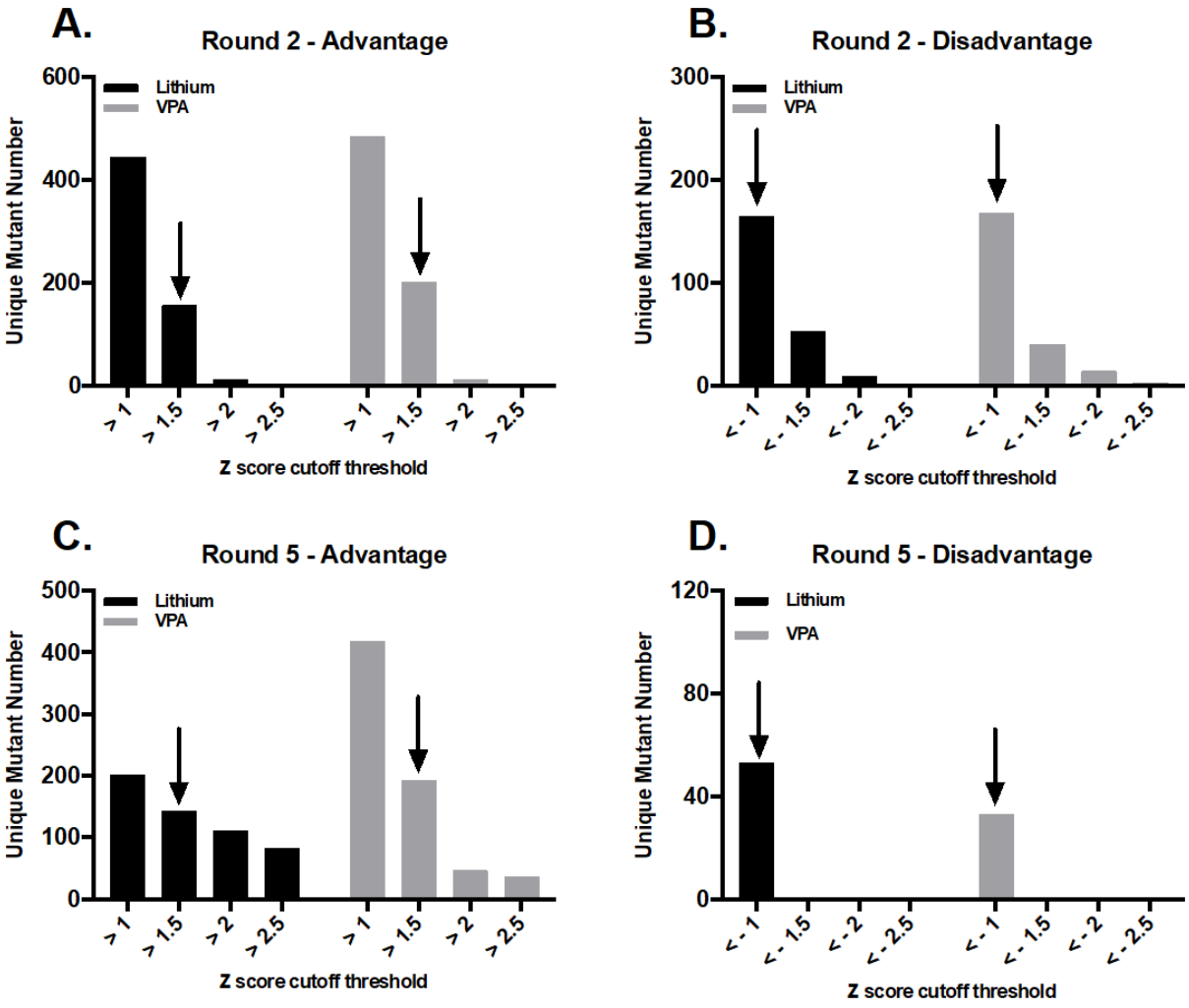

Figure 4.11. Varying cut-off thresholds for Z scores results in a range of putative advantage or disadvantage mutants. Z score cutoffs of 1, 1.5, 2 and 2.5 were applied to both biological replicates to select for varying amounts of lithium and VPA advantage mutants. Varying amounts of disadvantage mutants were selecting by applying Z score cutoffs of -1, -1.5, -2 and -2.5 to both biological replicates of the lithium and VPA screens. Round 2 advantage (A) and round 5 disadvantage (D) exhibit few mutants with stringent cutoffs thresholds. Black arrows indicate the intermediate threshold ultimately used to select the mutant lists.

Based on these observations, a threshold of > 1.5 (Z score) was used to define advantaged mutants for both screens (Figure 4.11). We hypothesised that this is strict enough to provide confidence in the makeup of the lists without overly reducing the number of significant mutants. This threshold resulted in the identification of 155 and 142 unique insertions for round 2 and round 5 lithium, and 201 and 193 for rounds 2 and 5 VPA respectively (Table 4.2). For the disadvantaged selection, a less stringent threshold of -1 (Z score) was used (Figure 4.11). This is because only mutants from the bins 1000

and 10,000 could be defined as disadvantaged. Since the technical dropout rate for mutants with reads of less than 100 is very high, this means that the number of mutants that could be identified was lower (86). At this threshold, 164 and 53 unique disadvantaged insertions could be identified for round 2 and round 5 of the lithium selections, and 168 and 33 for rounds 2 and 5 of the VPA selection (Table 4.2).

Table 4.2 The number of putative advantage and disadvantage mutants initially selected

All Putative Mutants	Lithium				VPA			
	Round 2		Round 5		Round 2		Round 5	
	Advantage	Disadvantage	Advantage	Disadvantage	Advantage	Disadvantage	Advantage	Disadvantage
Bin 10000	2	6	2	4	-	5	1	1
Bin 1000	7	158	62	49	9	163	136	32
Bin 100	146	-	78	-	192	-	56	-
Total	155	**164**	**142**	53	201	**168**	**193**	33

After defining advantaged and disadvantaged mutants, we attempted to assign each mutant to a disrupted gene. In addition to intragenic insertions, promoter insertions were assigned to the most likely gene. In *D. discoideum,* promoters are typically located within 1000 bp upstream their gene. Therefore, mutants with a REMI insertion <500 bp upstream of the start codon were assigned to the corresponding gene. Mutants with an intergenic insertion > 500 bp upstream of a gene were removed (Tables 4.3, 4.4). The lists were also further refined by removing mutants with insertional sites in 'uncharacterisable' loci. This included insertions in pseudogenes, tRNA genes and transposable elements (Tables 4.3, 4.4). Finally, a small number of advantaged mutants were removed because they had less than 100 readcounts in rounds 2 and 5 of the lithium or VPA treated pool (Tables 4.3, 4.4). Again, the high technical dropout rate for mutants with less than 100 reads means that mutants could have 0 reads in the DMSO screen and 100 reads at the lithium or VPA endpoints, which could appear as an enrichment, but is actually technical noise. Finally, we further ensured that all inherent growth mutants were removed. For this, we compared our mutant lists to previously reported axenic growth mutants (86). No previously characterised axenic advantaged mutants were found in our lists, but a small number of axenic growth disadvantaged mutants were removed from the round 2 disadvantaged lists (Tables 4.3, 4.4). This suggests that our approach to identifying only lithium and VPA dependent mutants was largely successful.

Table 4.3. Round 2 lithium and VPA dis-/ advantage mutant list refinement.

	Lithium R2 Advantage	Lithium R2 Disadvantage	VPA R2 Advantage	VPA R2 Disadvantage
Total	**155**	**164**	**201**	**168**
Intragenic	110	117	141	121
Intergenic	45	47	60	47
Intragenic Total	45	117	141	121
Intragenic unique mutants	106	115	139	119
Intergenic Total	45	47	60	47
Intergenic 500bp upstream (Not duel)	12	16	21	15
Total	**122**	**133**	**162**	**136**
Pseudogenes	9	4	10	7
tRNA	1	2	2	3
Transposable element	1	5	4	2
< 100 Mean read count	10	-	33	-
<100 in one rep & <150 in the other	8	-	12	-
Known growth disadvantage	-	8	-	7
Both read counts > -1.5 SD	-	10	-	6
Final total	**93**	**104**	**101**	**111**

Table 4.4. Round 5 lithium and VPA dis-/ advantage mutant list refinement.

	Lithium R5 Advantage	Lithium R5 Disadvantage	VPA R5 Advantage	VPA R5 Disadvantage
Total	**142**	**53**	**193**	**33**
Intragenic	93	34	138	17
Intergenic	49	19	55	16
Intragenic Total	93	34	138	17
Intragenic unique mutants	91	34	128	17
Intergenic Total	49	19	55	16
Intergenic 500bp upstream (Not duel)	13	12	17	7
Total	**106**	**46**	**155**	**24**
Pseudogenes	3	2	5	1
tRNA	3	-	4	-
Transposable element	18	2	4	1
< 100 Mean read count	6	-	2	-
<100 in one rep & <150 in the other	-	-	-	-
Known growth disadvantage	-	-	-	-
Both read counts > -1.5 SD	-	-	-	-
Final total	**76**	**42**	**140**	**22**

4.4.5 Validation of the putative lithium and VPA advantage and disadvantage mutants

Before using the gene lists to investigate the mechanistic relationship between lithium and VPA, we validated our approach of identifying mutants. Firstly, we determined whether independent insertions in the same gene were seen. As multiple copies of genes in the lists is the first indication that they are valid. Independent copies of gene insertions were found in all four finalised lists (Table 4.5).

Table 4.5. Mutant and gene numbers in the final screen lists.

Final Mutant / Gene lists	Lithium		VPA	
	Round 2 Disadvantage	**Round 5** Advantage	**Round 2** Disadvantage	**Round 5** Advantage
Mutants	104	76	111	140
Genes	**101**	**74**	**109**	**130**
	2 copies of DDB_G0269270 2 copies of DDB_G0276829 2 copies of DDB_G0288919	3 copies of DDB_G0284721	2 copies of DDB_G0269270 2 copies of DDB_G0276829	4 copies of DDB_G0274577 2 copies of DDB_G0277245 3 copies of DDB_G0281103 2 copies of DDB_G0283289 2 copies of DDB_G0284295 3 copies of DDB_G0288121

Next, we experimentally assessed the relative fitness of a selection of individual mutants in comparison to wildtype cells, both with and without lithium or VPA. The competition assay described in section 4.4.2 was used because it allows mutants to be tested under identical conditions to the screen (Figure 4.4). Individual mutants were obtained from the REMI-Seq-Bank, a collection of over 12,000 individual insertional mutants in over 5500 *D. discoideum* genes (86). The REMI-Seq-Bank was created in parallel to the REMI-Seq screen pools and thus contains many mutants with identical insertional sites to the putative mutants on the lithium and VPA lists (or alternative alleles of the same mutants) (86). In order to assess whether mutant behaviour recapitulated their expected lithium or VPA phenotype from the screen, we compared the mean replicate Z score for each mutant, to a competition fitness score. The competition fitness score was calculated as the relative difference between a mutant's performance with and without the drug at round 3 and the final round of the competition (as described in methods section 6.9) (Figure 4.12 A, 4.12 B). The competition fitness score accounts for mutants that have a growth defect without the addition of a drug (Figure 4.12 A).

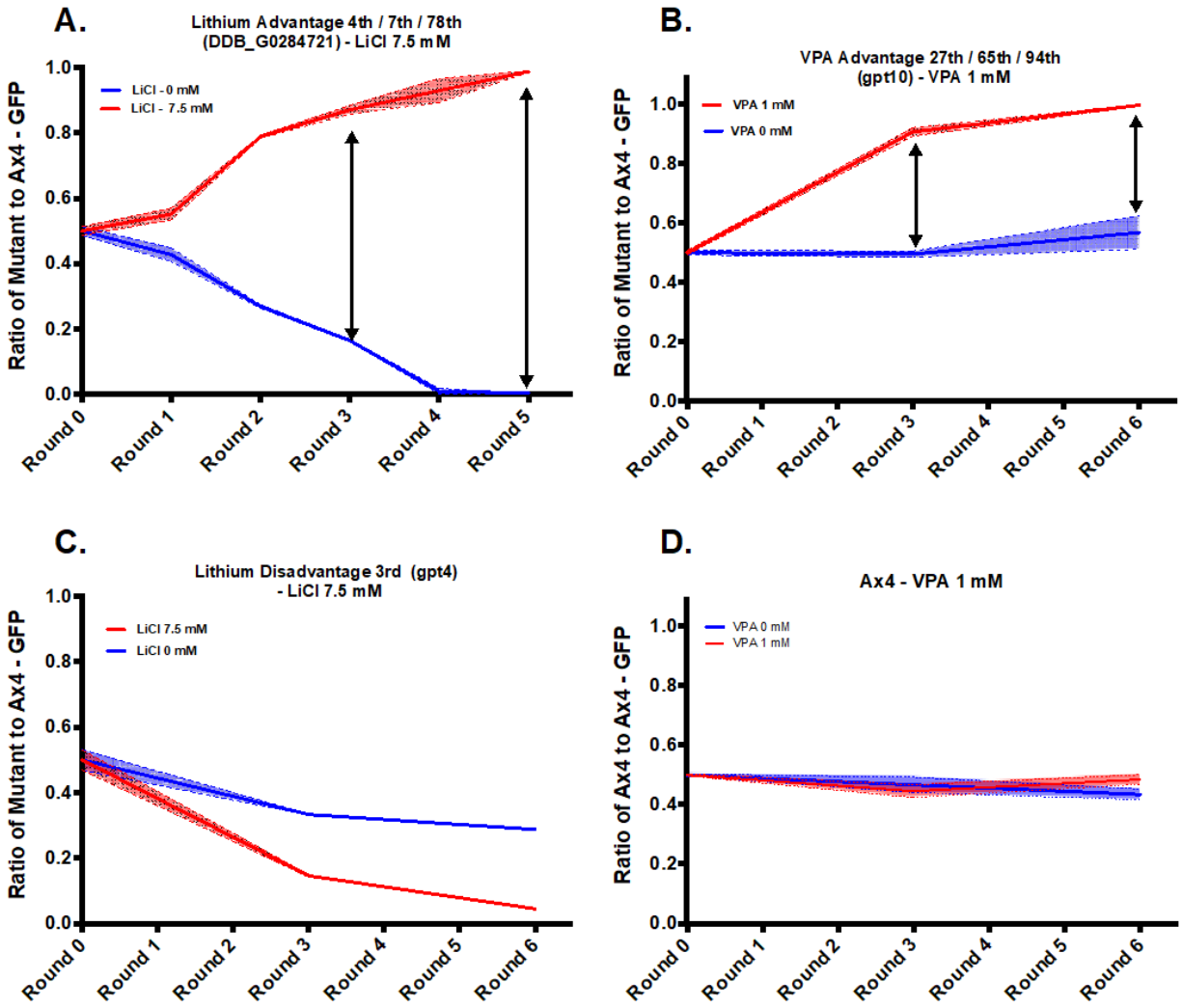

Figure 4.12. Growth competition fitness assay examples. A.B. Lithium advantage mutant *DDB_G0284721* and VPA advantage mutant gpt10 both out compete the labelled control, but only when treated with LiCl or VPA respectively. Black arrows indicate the rounds at which the competition fitness score is calculated for every competition**. C.** Lithium disadvantage mutant gpt4 is out competed by the wild type in the presence of lithium. **D.** A control Ax4 strain grows at the same rate as the labelled WT cells in and without the presence of the 1 mM VPA. All data representative of mean ± SEM of 2 biological replicates.

In total we selected 44 mutants for validation from the round 2 and 5 mutant lists (Appendix figure A7.3). Both advantage and disadvantage mutants (19 and 25, respectively) were selected for validation with an equal split between the lithium and VPA screens (21 and 23, respectively) (Appendix figure A7.3). Illustrative data for three mutants and an Ax4 control are shown in (Figure 4.12). We found that 34 out of the 44 (77 %) mutants exhibited the expected behaviour and recapitulated the advantaged or disadvantaged phenotype (Figure 4.13). However, as previously discussed, the abundance of advantage mutants within a REMI-Seq pool will reduce the relative

abundance of neutral mutants. This suggests that round 2 should be better for the identification of disadvantaged mutants and that round 5 should be better for identifying advantaged mutants. Therefore, we compared the validation results across rounds of the selection.

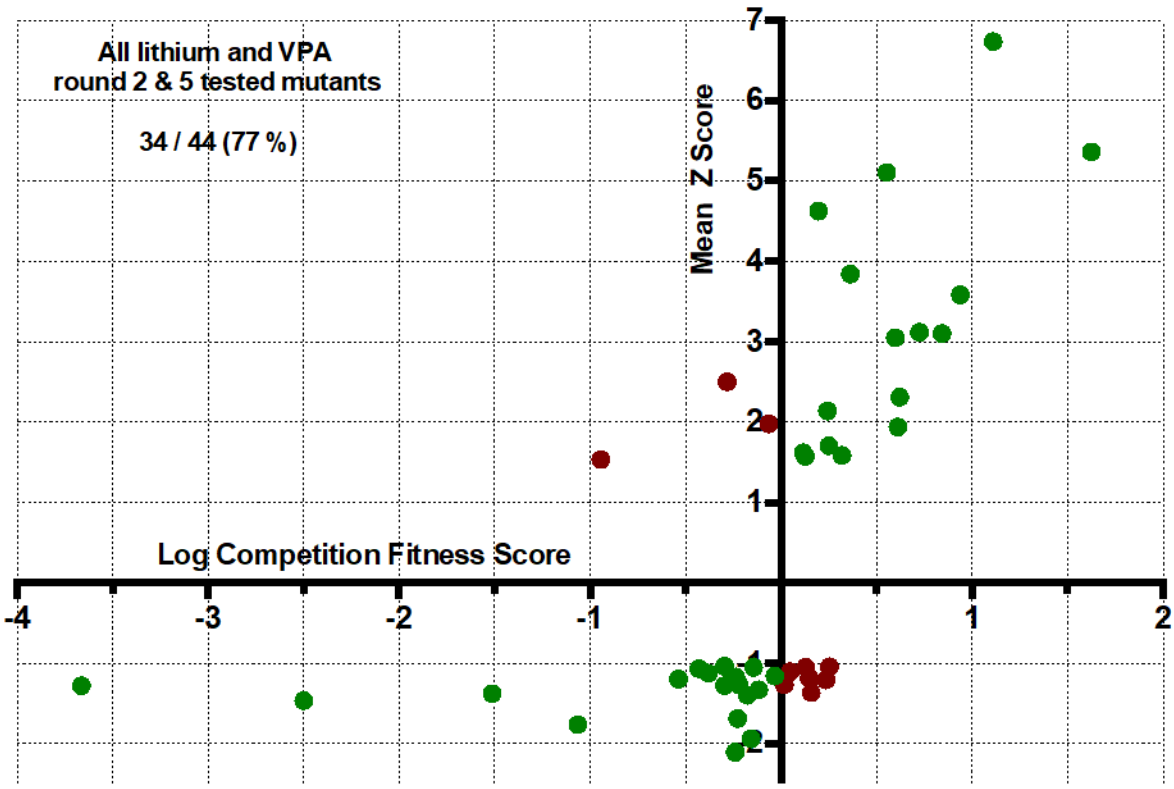

Figure 4.13. Correlation of mean screen Z score to competition fitness score. The mean Z score of the screen's biological replicates is used as a measure of each mutants' expected resistance or sensitivity phenotype. The log competition fitness score calculated from the relative performance of the individual mutants in and not in the presence of the relevant compound (See Methods 6.9). 34 out of the 44 tested mutants validate the expected phenotype (Green). Red dots indicate mutants that did not validate.

15 mutants from the round 2 disadvantaged mutant lists were assessed. Of these 7 mutants were from the lithium screen and 8 mutants from the VPA screen. All 7 of the lithium round 2 disadvantage mutants validated (Appendix figure A7.3). Of the 8 VPA mutants tested, 6 recapitulated the expected phenotype (Appendix figure A7.3). Next, we examined data from the round 5 advantage mutants. In total 15 mutants from the round 5 advantaged lists were assessed; 6 mutants from the lithium and 9 mutants from the VPA screen. All 6 of the lithium mutants exhibited a positive competition score, validating their expected phenotype (Appendix figure A7.3). Similarly, 8 of the 9 VPA

advantage mutants tested were resistant (Appendix figure A7.3) (Figure 4.14). Therefore, in total, 27 out of 30 (90 %) round 2 disadvantage and round 5 advantage validated (Figure 4.14 B).

Mutants from the (potentially noisy) round 2 advantaged and round 5 disadvantage lists were also assessed (Figure 4.14). 2 mutants from both the lithium and VPA round 2 advantaged lists were assessed, along with 10 mutants from the round 5 disadvantage lists (6 from the lithium screen and 4 from the VPA screen). In total, only 7 out of 14 (50%) mutants validated (Figure 4.14 A). This finding mirrors our expectation on the lack of reliability of the round 2 advantage and round 5 disadvantage lists. Therefore, in further studies, only the genes the round 2 disadvantage and round 5 advantage lists were used to assess the genetic targets and relation between lithium and VPA. The full gene lists can be found in appendix tables A7.3 & A7.4.

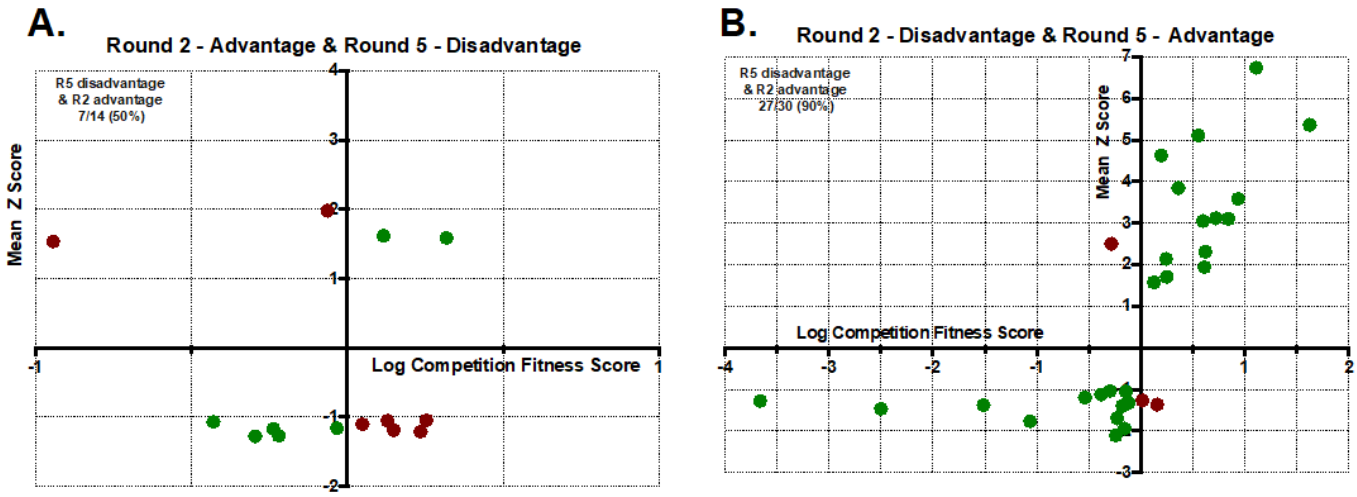

Figure 4.14. Separated mutant validation analysis. A. From the potentially unreliable mutant lists, round 2 advantage and round 5 disadvantage, only 7 out of the 14 mutants tested recapitulate expected phenotypes. **B.** In combination, 27 out of 30 lithium and VPA mutants validate from the round 2 disadvantage and round 5 advantage list. Green dots indicate an expected phenotype score. Red dots indicate mutants that did not validate.

4.4.5.1 lsrA is developmentally resistant to lithium

The screens were conducted in order to identify genes that affect developmental toxicity. However, because the screens were performed during vegetative growth, we tested whether the identified mutants were also developmentally resistant. For this, we chose the lsrA mutant as it was one of the most significantly advantaged mutants from either the lithium and VPA screen (Appendix table A7.3). After 3 days of developmental exposure, lsrA was found to be developmental resistant to lithium (Figure 4.15). lsrA produced normal fruiting bodies at 2.5 mM lithium and small fruiting bodies at 5 mM, doses which caused tiny and no fruiting bodies respectively in the control (Figure 4.15). This result suggests that our vegetative growth screens have also identified developmentally resistant mutants.

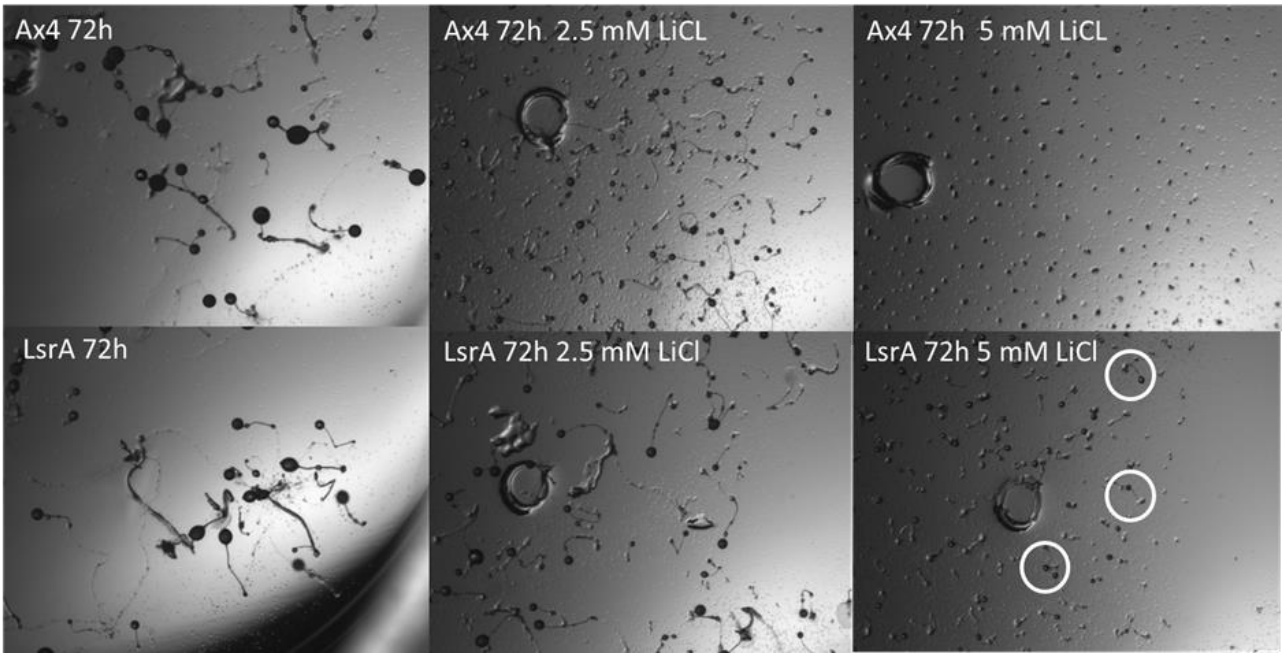

Figure 4.15. lsrA is developmentally resistant to lithium. After 72 hours of exposure to 2.5- or 5 mM lithium, growth resistant mutant lsrA is able to form fruiting bodies. The tiny fruiting bodies produced in 5 mM lithium are highlighted and phenocopy the fruiting bodies formed by Ax4 in the lower 2.5 mM drug exposure.

4.4.6 Many genes identified in the lithium and VPA screens are common

REMI-Seq has the potential to provide an unbiased genetic phenotype for developmentally toxic compounds. We chose lithium and VPA for this proof of principle study because both compounds are therapeutic mood stabilisers and known mammalian teratogens (Section 1.4.5). Yet, it is unknown to what extent the genetic targets are shared. However, lithium and VPA are known to share biological processes (i.e., phosphoinoistol signalling) and thus can be used to assess whether this relationship can be seen in a genetic phenotype (as defined by REMI-Seq). To test this idea, firstly we simply compared the lithium and VPA gene lists (Appendix tables A7.3, A7.4). For the round 5 advantage comparison, 7 genes were present in both of the lithium (74 genes) and VPA (130 genes) lists (Figure 4.16 A). Although the number of genes is small, the overlap is highly statistically significant (P= 0.0008) (Figure 4.16 A). Similarly, we found a significant overlap of 24 genes between the round 2 disadvantage lists (P=<0.00001) (Figure 4.16 B).

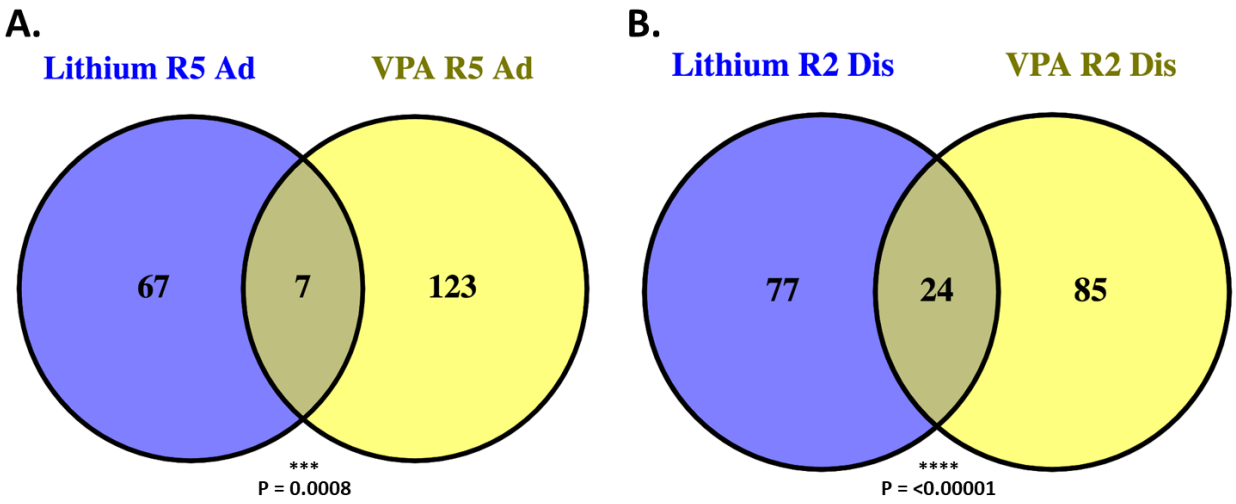

Figure 4.16. Ablated lithium and VPA resistance and sensitivity genes significantly overlap. To determine whether the number of genes that overlapped between lithium and VPA was significantly larger than would be expected by chance, hyper-geometric testing was conducted. **A.** 7 genes are shared between the lithium and VPA advantage list (p=0.0008). **B.** 24 genes are shared between the lithium and VPA disadvantage lists (p=<0.00001) (236).

The gene list overlaps suggest that the gene networks lithium and VPA adversely affect are significantly shared. However, we reasoned that this might actually be an underestimation of the genetic relationship between lithium and VPA. This is because the gene lists were created using strict cut-offs, with both biological replicates required to reach a Z score threshold before a mutant was considered significantly over- or under-enriched (Figure 4.11). For a mutant to be found significantly enriched in both the lithium and VPA screens, the strict cut-off must of be reached four times, creating a statistical 'double discovery' problem. In order to test this idea, we compared the mean Z scores of the significant advantaged or disadvantaged, lithium or VPA mutants, in the other screen (Figure 4.17). For the lithium or VPA disadvantaged mutants their average Z score is significantly lower than a random sample of the same number of mutants (Figure 4.17 A, 4.17 B). The same result was found for the advantaged mutant lists where their average Z score is significantly higher than a random sample of the same number of mutants (Figure 4.17 C, 4.17 D). Most importantly, for both the lithium and VPA disadvantage mutants lists their average Z score in the other screen was significantly lower than the random samples of mutants (Figure 4.17 A, 4.17 B). Similarly, the average Z scores of the advantaged lithium and VPA mutants is significantly higher in the other screen than expected by random sampling (Figure 4.17 C, 4.17 D). These results suggest that our initial strict thresholds underestimate the relationship between lithium and VPA screens.

To further test this idea, we reassessed the relationship between the lithium and VPA, advantage and disadvantage lists, using relaxed criteria. For both the advantaged and disadvantaged lists, the mean replicate Z score was used to assign the mutants into three categories (for both compounds): advantage (>0.5 Z score), neutral (-0.5 - 0.5 Z score) and disadvantaged (< 0.5 Z score). When the mutants were clustered by category on a heatmap, the similarity between the screens is evident (Figure 4.18). Under the relaxed analysis using Z score comparisons, 35% of the significant advantaged mutants and 58% of the significant disadvantage were common between lithium and VPA (Figure 4.18 A, 4.18 B).

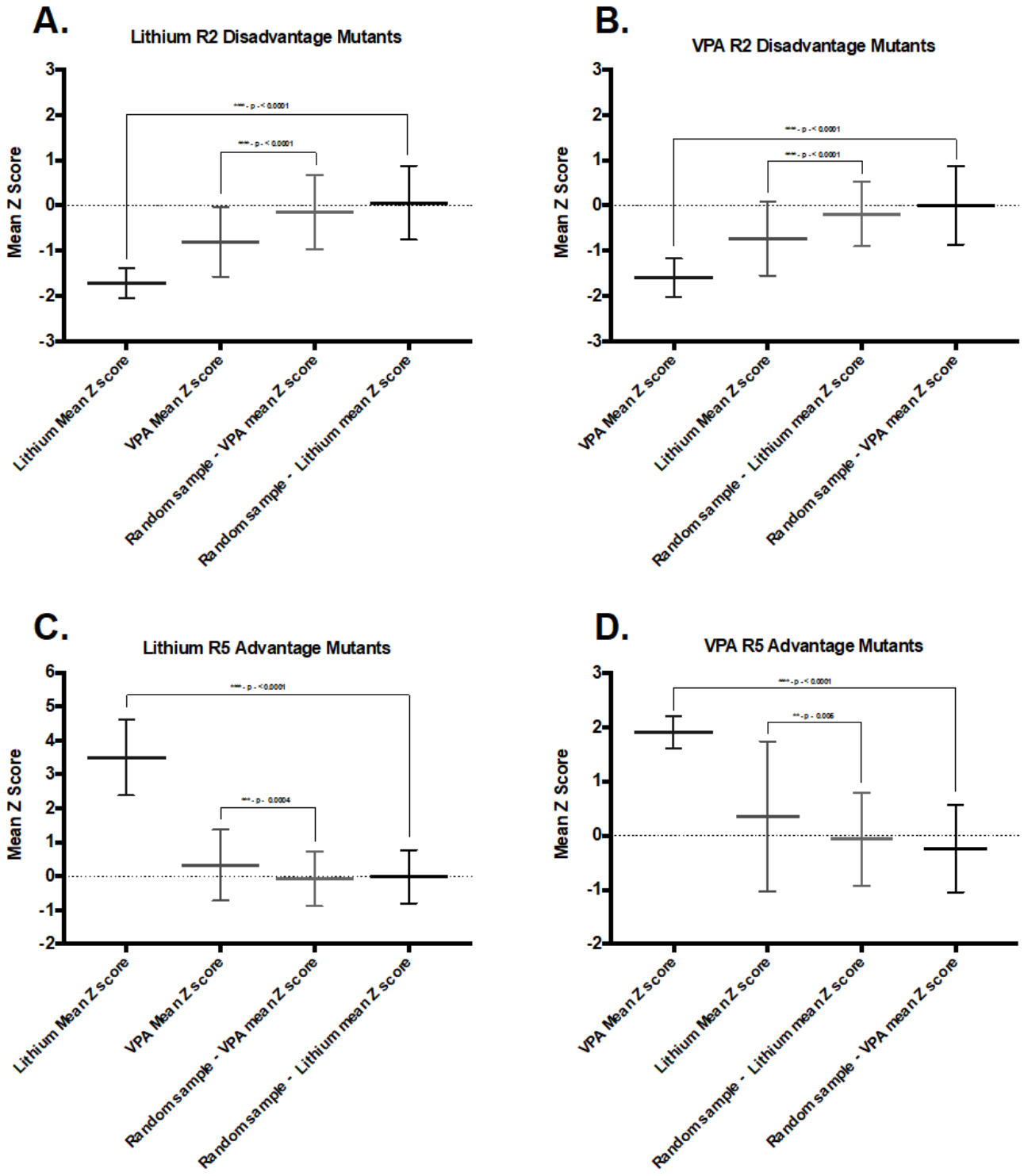

Figure 4.17. Lithium and VPA advantaged and disadvantaged mutants behave significantly similarly the other drug. The mean Z score of the lithium and VPA advantaged (Round 5) and disadvantaged (Round 2) mutants is significantly different to when the same number of mutants are randomly sampled from the Round 2 or Round 5 screens. **A & B.** The round 2 lithium and VPA disadvantage mutants have a significantly lower mean Z score in the other compound than when a similar number of mutants are randomly sampled. **C & D.** The round 5 lithium and VPA advantage mutants have a significantly higher mean Z score in the other compound than when a similar number of mutants are randomly sampled. Mutants were randomly sampled 10x. Mean ± SD. Significance was tested using a T-test.

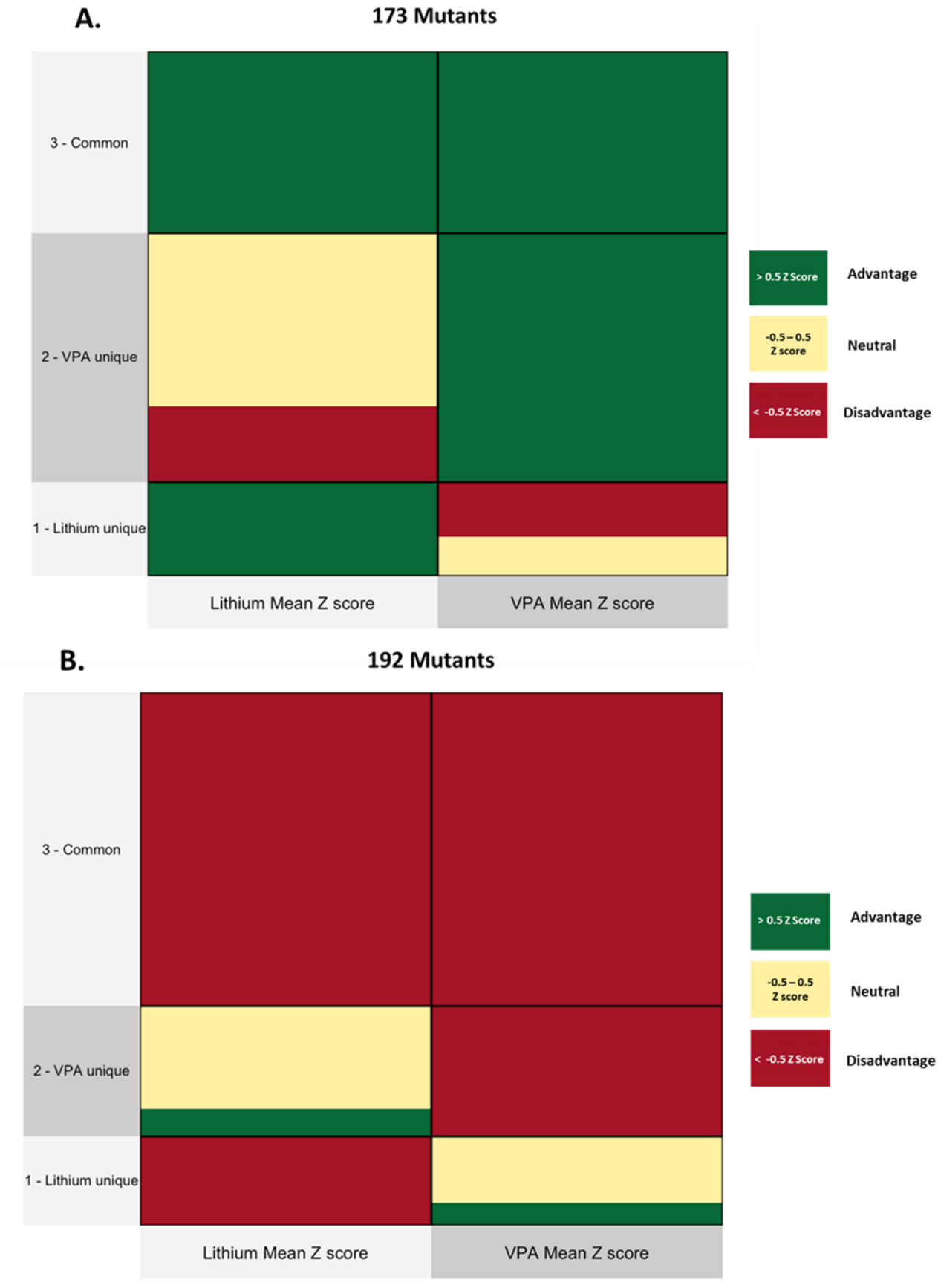

Figure legend on next page.

Figure 4.18. Heatmaps of significant lithium and VPA advantage and disadvantage mutant's Z scores. A. 173 (removing NAs) significant advantage mutants for lithium and VPA R5 cluster into three groups when the mean replicate Z score for each mutant is compared: common, uniquely lithium and uniquely VPA advantaged. **B.** 192 (removing NAs) significantly disadvantage mutants for both lithium and VPA R2 clustered into three groups when the mean replicate Z score for each mutant is compared. Figure on page 156.

Finally, to compare the performance of advantaged and disadvantaged mutants from one screen to their behaviour in the other screen, we ranked all mutants from lowest to the highest mean Z score, for each screen. The ranked mutants were split into quartiles, with Q1 containing the mutants with the greatest fold decrease and Q4 containing mutants which increased the most. If the behaviour of mutants in the two screens is unrelated then the significant outliers from one screen would be expected to be evenly distributed across the rankings in the other. In contrast, disadvantaged and advantaged lithium mutants were significantly enriched in the first and fourth quartile of the VPA screen, respectively (P=<0.0001) (P=0.0235) (Figure 4.19 A, 4.19 B). A similar pattern was found for the significant VPA advantaged and disadvantaged mutants (P=<0.0001) (P= 0.0013) (Figure 4.19 C, 4.19 D) when compared to their rank in the lithium screen.

Together these data suggest there is a strong mechanistic link between each compounds' toxic effects. A significant proportion of mutants behave similarly in both drugs, although mutants tend to have a stronger phenotype in the compound that they were selected in. To directly test this idea, we selected 3 VPA and 2 lithium advantaged mutants that had previously been experimentally validated, but were initially only identified in either the VPA or lithium screen. The mutants were reassessed in the competition assay (as described in section 4.4.2) in both lithium and VPA (Figure 4.20). All 3 of the 'VPA specific' mutants (DDB_G0274825, DDB_G0277245, gpt10) exhibited a growth advantage in the presence of 7.5 mM LiCl (Figure 4.20 A B C). However, the lithium resistance was weaker in comparison to their VPA growth resistance (Figure 4.20 A B C). Similarly, the lithium resistant mutant DDB_G0274981, was also resistant to 1 mM VPA (Figure 4.20 E). Only the unique lithium resistance mutant (fslE) failed to display a phenotype (Figure 4.20 D) in VPA. These results, validate the Z score analyses, revealing that even though weaker non-significant z scores are often phenotypically relevant. Furthermore, this shows that our initial gene lists underestimate the mechanistic similarity of lithium and VPA.

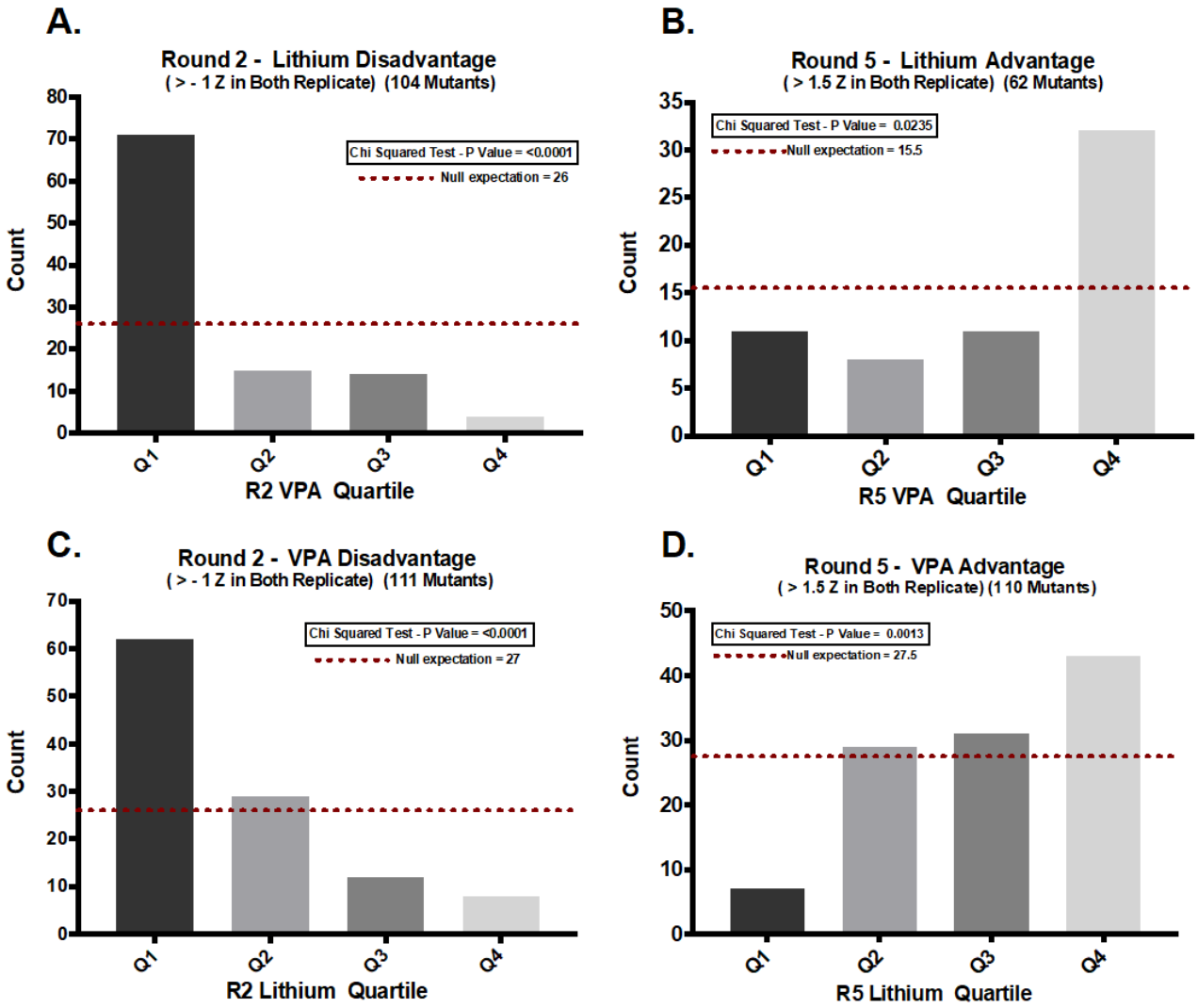

Figure 4.19. Rank testing reveals a strong bias for mutants to have similar phenotypes in both screens. Every mutant with a valid Z score (removed NAs) in both the lithium and VPA screens were ranked in each screen according to their biological replicate mean Z score. The ranked mutants were split into quartiles with Q1 being the greatest decreased mutants and Q4 being the greatest increased. Mutants from the previously generated advantage and disadvantage, lithium and VPA, lists were assessed as to where they ranked in the opposite screen. Significant enrichment in any of the quartiles was assessed using a Chi squared test. **A.** Lithium disadvantage mutants are significantly enriched in the VPA Q1 rank. **B.** Lithium advantage mutants are significantly enriched in the VPA Q4 rank. **C.** VPA disadvantage mutants are significantly enriched in the lithium Q1 rank. **D.** VPA advantage mutants are significantly enriched in the lithium Q4 rank. These mutants are only coming from the Q1 quartile.

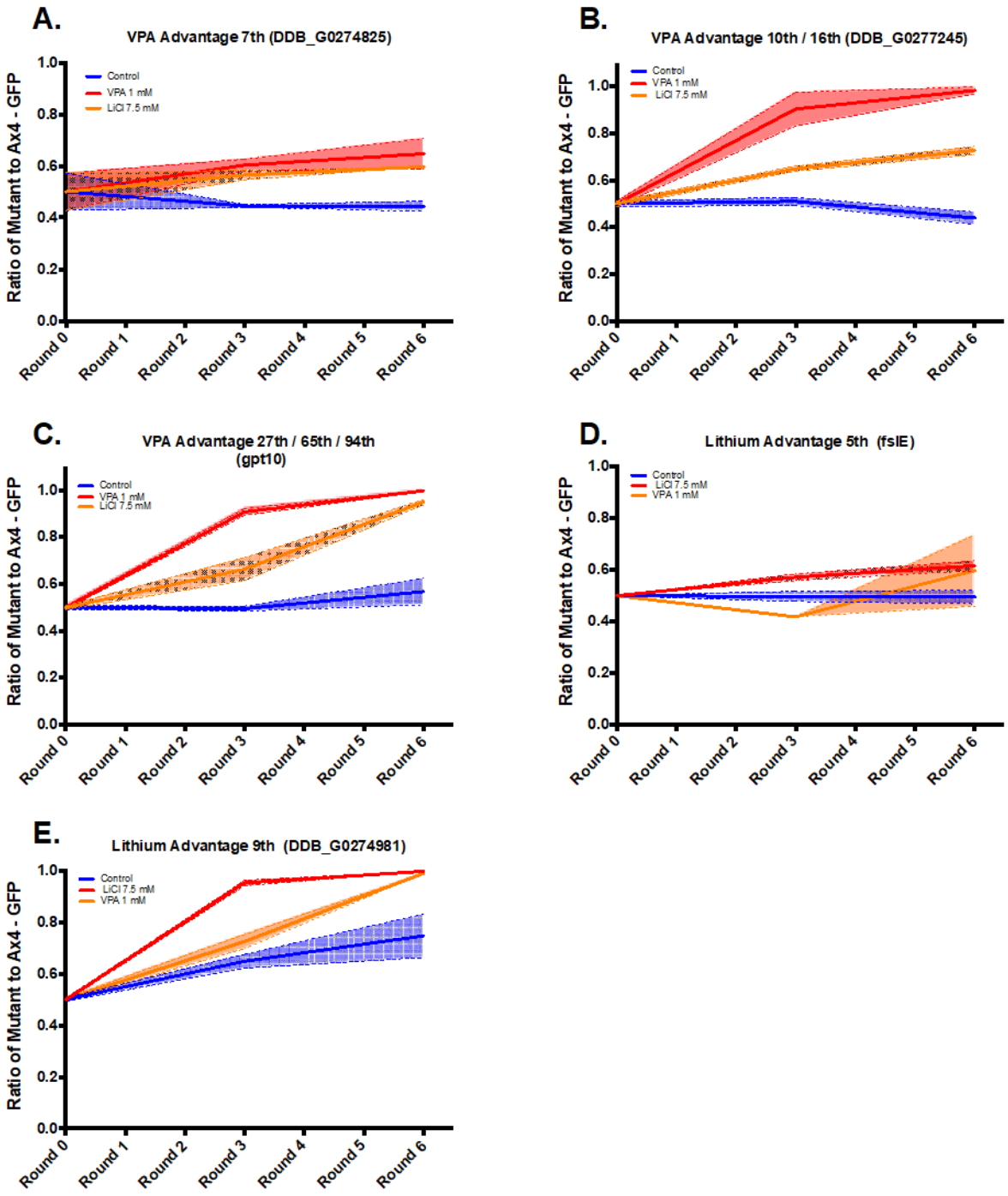

Figure 4.20. A subset of previously classified unique lithium or VPA advantage mutants are also weakly advantaged in the other compound. Individual REMI mutants were mixed in equal proportions with GPF label wildtype cells and growth in the presence or absence of 7.5 mM LiCl or 1 mM VPA, for a number of generations corresponding to one round of our screen conditions. The relative proportion of the REMI mutant to labelled control was assessed by flow cytometry after every round. **A.B.C.** Previously validated VPA advantage mutants out compete wild type cells to a lesser extent in 7.5 mM LiCl. **D.** Validated Lithium advantage mutant, *FslE*-, grows at the same rate as the labelled WT cells in 1 mM VPA. **E.** Lithium advantage mutant DDB_G0274981 out competes wild type cells to a lesser extent in 1 mM VPA than in LiCL.

4.4.7 Understanding the relationship between lithium and VPA through gene ontology (GO) analysis

The overlap between the gene lists identified by REMI-Seq and their Z-score trends suggests that the mechanism by which lithium and VPA exert their toxic effects on cells is similar. To further test this idea, and to better understand the mode of action of these compounds, we analysed the gene lists to identify the pathways and biological processes affected by the compounds. Gene ontology (GO term) analysis was performed on the lithium and VPA gene lists using the GSEAbase R package with a significance cut-off of p=0.05 for overrepresented terms (237). To maximise the number of potential significant terms, we conducted the analysis on three separate gene lists: a lithium list containing the 173 advantaged and disadvantaged genes, a VPA list contain 235 advantaged and disadvantaged genes, and a third list combining the previous two lists, containing all 376 genes. In order to identify overrepresented terms, lists were compared to a gene universe based on all detectable mutants in either round 2 or 5 of the screen (86). In addition, categories of genes which had previously been removed from the analysis (tRNAs, pseudogenes, transposable genetic elements) were removed from the universe (Tables 4.3, 4.4). This resulted in a universe containing 6161 genes. Analyses were conducted to identify over-enrichment in both the Molecular Function and Biological Process GO term categories. After the analyses were conducted on the three gene lists, the significant GO terms were combined. 70 and 46 GO terms were found for the Biological Process and Molecular function categories respectively (data not shown). However, when genes driving the GO terms were examined, many similar terms were found to be represented by the same genes (Data not shown). Therefore, redundant terms were removed using the REVIGO tool (238). The new simplified lists contained 34 and 23 GO terms for the Biological Process (BP) and Molecular function (MF) categories respectively (Tables 4.6, 4.7).

Table 4.6. Refined Biological Process GO terms.

GO BP ID	Term	P value	Expected count	Count	Genes
GO:0006012	**Galactose metabolic process**	0.000311	0.20	3	galE uppA galK
GO:0042738	**Exogenous drug catabolic process**	0.001689	0.95	5	cyp508A2-1 cyp508A2-2 cyp519B1 cyp519E1 cyp519D1
GO:0007041	**Lysosomal transport**	0.002813	0.34	3	lvsA lvsB vamp7B
GO:0005996	**Monosaccharide metabolic process**	0.004409	1.15	5	pckA galE ugt52 uppA galK
GO:0046579	**Positive regulation of Ras protein signal transduction**	0.004617	0.13	2	gbpC ric8
GO:0009410	**Response to xenobiotic stimulus**	0.005771	1.22	5	cyp508A2-1 cyp508A2-2 cyp519B1 cyp519E1 cyp519D1
GO:0016601	**Rac protein signal transduction**	0.010317	7.82	15	mgp3 zizA gacI gxcN gefJ gxcS gefC gacK DDB_G0288811 gacL gefK gbpC ric8 kxcB roco5
GO:0051336	**Regulation of hydrolase activity**	0.011329	8.64	16	mgp3 ctnA zizA gacI gxcN gefJ gxcS gefC gacK DDB_G0288811 gacL gefK gbpC ric8 kxcB roco5
GO:0019318	**Hexose metabolic process**	0.012181	0.95	4	pckA galE uppA galK
GO:0005991	**Trehalose metabolic process**	0.013227	0.20	2	treh tpsB
GO:0009812	**Flavonoid metabolic process**	0.013227	0.20	2	ugt52 stlB
GO:0009813	**Flavonoid biosynthetic process**	0.013227	0.20	2	ugt52 stlB
GO:0005975	**Carbohydrate metabolic process**	0.015917	9.73	17	fut11 pckA ctnA galE DDB_G0276439 DDB_G0278171 DDB_G0278551 DDB_G0282715 treh iliG fut2 tpsB nagC dgtA ugt52 uppA galK
GO:0010646	**Regulation of cell communication**	0.020500	11.5	19	mgp3 NA adcB ctnA zizA gacI gxcN gefJ pldB gxcS gefC gacK DDB_G0288811 gacL gefK gbpC ric8 kxcB roco5
GO:0051272	**Positive regulation of cellular component movement**	0.025270	0.27	2	myoK gbpC
GO:0051050	**Positive regulation of transport**	0.026150	0.68	3	myoK pldB rpkA
GO:0009966	**Regulation of signal transduction**	0.036145	10.68	17	mgp3 NA adcB zizA gacI gxcN gefJ gxcS gefC gacK DDB_G0288811 gacL gefK gbpC ric8 kxcB roco5
GO:0006281	**DNA repair**	0.042388	4.69	9	rev3 abcH3 mus81 DDB_G0278869 msh3 nhej1 rad54b DDB_G0287149 arpE
GO:0034976	**Response to endoplasmic reticulum stress**	0.019507	0.22	2	DDB_G0280773 npl4
GO:0036065	**Fucosylation**	0.019507	0.22	2	fut11 fut2
GO:0042180	**Cellular ketone metabolic process**	0.025466	0.25	2	gloB1 stlB
GO:0050766	**Positive regulation of phagocytosis**	0.025466	0.25	2	myoK rpkA
GO:0006995	**Cellular response to nitrogen starvation**	0.039241	0.32	2	atg6A DDB_G0283753
GO:0044550	**Secondary metabolite biosynthetic process**	0.039241	0.32	2	DDB_G0286363 stlB
GO:0043562	**Cellular response to nitrogen levels**	0.039241	0.32	2	atg6A DDB_G0283753
GO:0031288	**Sorocarp morphogenesis**	0.041681	1.32	4	atg6A psaA abcG18 stlB
GO:0019222	**Regulation of metabolic process**	0.043994	11.81	18	mgp3 nosip lsrA DDB_G0275159 NA ifkB gxcN gefJ gxcS DDB_G0280133 gefC gacK DDB_G0288811 gefK warA gbpC arpE DDB_G0295785
GO:1901617	**Organic hydroxy compound biosynthetic process**	0.022079	0.62	3	pdx2 ugt52 stlB
GO:0007032	**Endosome organization**	0.022989	0.24	2	lvsA abcG18
GO:0061077	**Chaperone-mediated protein folding**	0.022989	0.24	2	DDB_G0278455 ric8
GO:0007034	**Vacuolar transport**	0.026364	0.66	3	lvsA lvsB vamp7B
GO:0016197	**Endosomal transport**	0.026364	0.66	3	lvsA lvsB vamp7B
GO:0043326	**Chemotaxis to folate**	0.040635	0.33	2	pldB ric8
GO:0072524	**Pyridine-containing compound metabolic process**	0.047581	0.82	3	tkt-1 ctnA pdx2

Table 4.7. Refined Molecular Function GO terms.

GO BP ID	Term	P value	Expected count	Count	Genes
GO:0016712	**Oxidoreductase activity**	0.0019	0.98	5	cyp508A2-1 cyp508A2-2 cyp519B1 cyp519E1 cyp519D1
GO:0035251	**UDP-glucosyltransferase activity**	0.0031	0.35	3	tpsB dgtA ugt52
GO:0019825	**Oxygen binding**	0.0038	1.12	5	cyp508A2-1 cyp508A2-2 cyp519B1 cyp519E1 cyp519D1
GO:0004497	**Monooxygenase activity**	0.0173	3.38	8	nosip cyp508A2-1 cyp508A2-2 cyp519B1 DDB_G0286363 cyp519E1 cyp519D1 redA
GO:0005085	**Guanyl-nucleotide exchange factor activity**	0.0232	4.93	10	zizA gxcN gefJ gxcS gefC gefK gbpC ric8 kxcB roco5
GO:0008144	**Drug binding**	0.0290	37.90	49	dhx57 tbck abcG11 act26 mkcF gdt8 uduC abcA7 DDB_G0271550 pckA DDB_G0272384 cyp508A2-1 DDB_G0273573 cyp508A2-2 abcA5 myoK fncM DDB_G0275535 abcG18 abcH3 ifkB glnA1 DDB_G0277245 DDB_G0278455 DDB_G0278909 roco6 DDB_G0280133 fhkB msh3 helE dhkM cyp519B1 sgkB oplah rad54b mrkB cyp519E1 DDB_G0287001 gbpC abcC7 rrpB cyp519D1 dnaja1 abcB3 galK DDB_G0292550 kxcB DDB_G0293678 roco5
GO:0004177	**Aminopeptidase activity**	0.0373	0.77	3	psaB psaA dpp3-2
GO:0043169	**Cation binding**	0.0171	27.37	38	mkcF psaB nosip DDB_G0272434 tkt-1 DDB_G0272965 DDB_G0273077 dpp3-2 cyp508A2-2 DDB_G0274153 DDB_G0275097 DDB_G0275535 mus81 DDB_G0277245 DDB_G0277763 pldB DDB_G0279681 hdaC DDB_G0281217 DDB_G0282715 zntA DDB_G0283819 cyp519B1 DDB_G0286459 DDB_G0287001 ugt52 DDB_G0288683 DDB_G0289637 adhfe1 DDB_G0290527 stlB DDB_G0291348 cyp519D1 dnaja1 DDB_G0291694 kxcB DDB_G0293682 redA
GO:0046872	**Metal ion binding**	0.0229	27.03	37	mkcF psaB nosip DDB_G0272434 tkt-1 DDB_G0272965 DDB_G0273077 dpp3-2 cyp508A2-2 DDB_G0274153 DDB_G0275097 DDB_G0275535 mus81 DDB_G0277245 DDB_G0277763 pldB DDB_G0279681 hdaC DDB_G0281217 zntA DDB_G0283819 cyp519B1 DDB_G0286459 DDB_G0287001 ugt52 DDB_G0288683 DDB_G0289637 adhfe1 DDB_G0290527 stlB DDB_G0291348 cyp519D1 dnaja1 DDB_G0291694 kxcB DDB_G0293682 redA
GO:0003887	**DNA-directed DNA polymerase activity**	0.0337	0.30	2	rev3 DDB_G0287149
GO:0016840	**Carbon-nitrogen lyase activity**	0.0337	0.30	2	DDB_G0277245 pdx2
GO:0016811	**Hydrolase activity, acting on carbon-nitrogen (but not peptide) bonds, in linear amides**	0.0343	0.73	3	hdaC pdx2 dcd3A
GO:0016810	**Hydrolase activity, acting on carbon-nitrogen (but not peptide) bonds**	0.0469	1.38	4	hdaC oplah pdx2 dcd3A
GO:0004693	**Cyclin-dependent protein serine/threonine kinase activity**	0.0199	0.22	2	DDB_G0292550 DDB_G0295785
GO:0097472	**Cyclin-dependent protein kinase activity**	0.0199	0.22	2	DDB_G0292550 DDB_G0295785
GO:0036094	**Small molecule binding**	0.0272	27.63	37	tbck abcG11 act26 d2hgdh gdt8 uduC abcA7 pckA DDB_G0272384 cyp508A2-1 cyp508A2-2 myoK fncM abcG18 abcH3 ifkB gxcN gefJ DDB_G0278909 gxcS DDB_G0280133 fhkB gnbp helE gefC rpkA sgkB rad54b DDB_G0286297 cyp519E1 gefK gbpC ranA abcB3 galK DDB_G0292550 DDB_G0293678
GO:0017111	**Nucleoside-triphosphatase activity**	0.0314	11.36	18	abcG11 mgp3 abcA7 DDB_G0272384 myoK abcG18 abcH3 gxcN gefJ gxcS gnbp gefC gacK DDB_G0288811 gefK gbpC ranA abcB3
GO:0003924	**GTPase activity**	0.0314	5.88	11	mgp3 gxcN gefJ gxcS gnbp gefC gacK DDB_G0288811 gefK gbpC ranA
GO:0000149	**SNARE binding**	0.0327	0.29	2	vamp7B DDB_G0290231
GO:0005524	**ATP binding**	0.0330	15.61	23	tbck abcG11 act26 gdt8 abcA7 pckA DDB_G0272384 myoK fncM abcG18 abcH3 ifkB DDB_G0278909 DDB_G0280133 fhkB helE sgkB rad54b gbpC abcB3 galK DDB_G0292550 DDB_G0293678
GO:0098772	**Molecular function regulator**	0.0334	4.47	9	mgp3 gxcN gefJ gxcS gefC gacK DDB_G0288811 gefK gbpC
GO:0097367	**Carbohydrate derivative binding**	0.0383	22.86	31	tbck abcG11 act26 gdt8 abcA7 pckA DDB_G0272384 myoK fncM abcG18 abcH3 ifkB gxcN gefJ DDB_G0278909 gxcS DDB_G0280133 fhkB gnbp helE gefC rpkA sgkB rad54b gefK gbpC ranA abcB3 galK DDB_G0292550 DDB_G0293678
GO:0019901	**Protein kinase binding**	0.0401	0.32	2	psaA DDB_G0295785

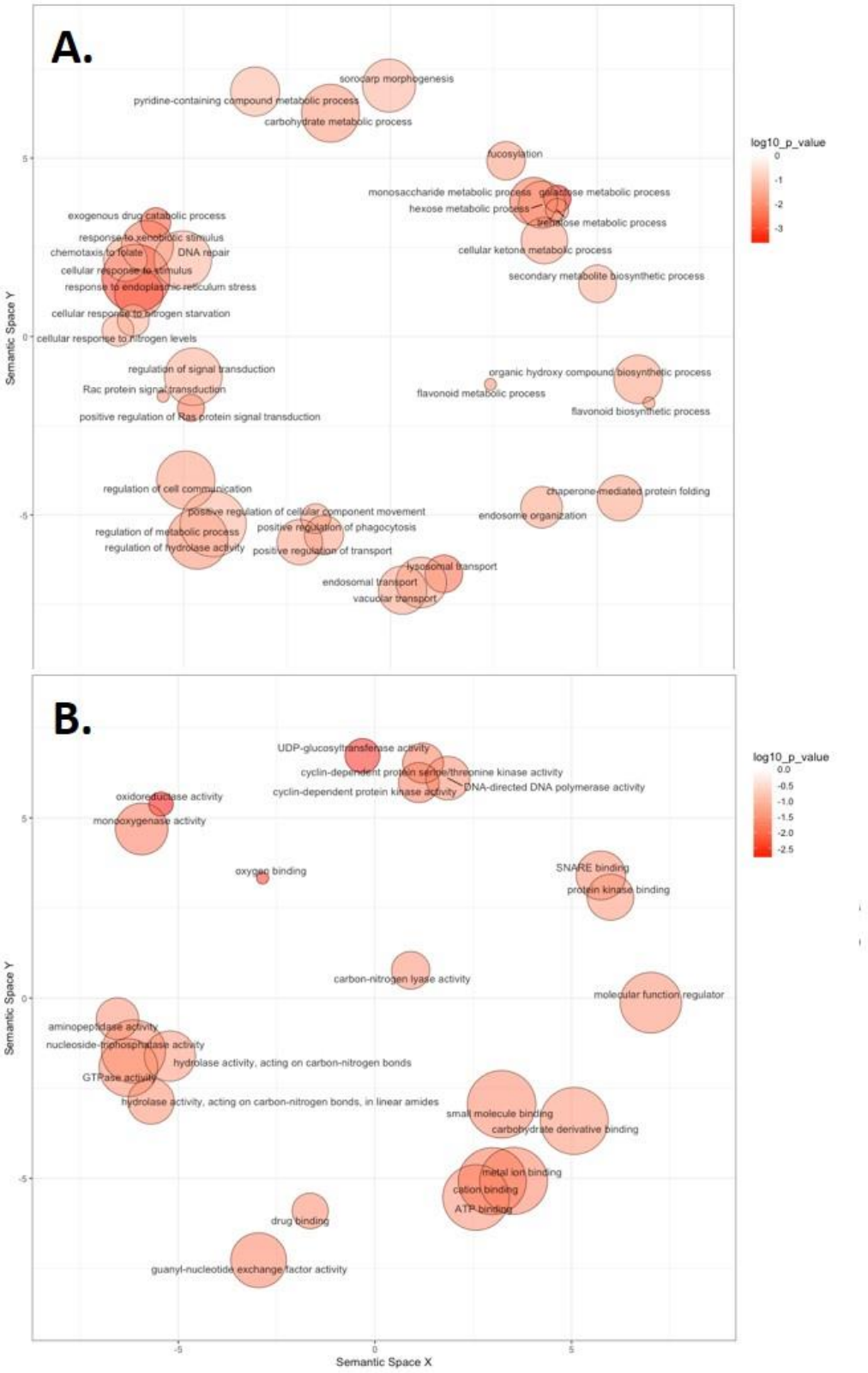

Figure 4.21. Scatterplots of the significantly over-enriched biological process and molecular function GO terms. The refined, combined GO terms from the lithium, VPA and 'combined' GO term analysis were plotted on semantic space using the REVIGO tool (238). GO terms with biological similarities are plotted closer together. The size of each plot represents the biological complexity of the term, with larger plots representing 'broader' terms. Plots are coloured on a white-red scale for each GO terms' p-value. **A.** Scatterplot for the Biological Process category. **B.** Scatterplot for the Molecular Function category.

The GO terms for BP and MF over-enrichment were plotted using the REVIGO tool, onto an arbitrary, semantic X / Y axis (238). The GO terms are plotted in clusters with the space between them representative of the biological difference between them. Furthermore, the size of each individual circle is indicative of the specificity of the term, with larger circles for broader terms. When plotted with the p-value of each term, both the BP and MF plots show clear clusters (Figure 4.21 A, 4.21 B). However, the different clusters are separated, suggesting that the over-enriched BP and MF GO terms are labels for different pathways and processes (Figure 4.21 A, 4.21 B). Whilst plotting GO terms in this way allows clear visualisation, it does not distinguish whether individual GO terms are specific to lithium or VPA, or common between the two. We therefore next assessed the genes underlying the GO terms, which allowed us to determine which screen the genes came from. This allowed every BP and MF GO term to be classified as either unique to lithium or VPA, or common between the two (Figures 4.22, 4.23). When we plotted the BP and MF GO terms, but false coloured as either lithium, VPA or common (Figure 4.24). The majority of the BP and MF GO terms for were common to both compounds (Figure 4.24 A, 4.24 B). 86 % and 78 % of the BP and MF GO terms were common to both lithium and VPA, respectively (Figure 4.24 A, 4.24 B). These data builds upon our gene list overlap and Z-score trend analysis (Section 4.4.6), strongly suggesting a close toxicological mechanistic link between the lithium and VPA. In summary, using our lithium and VPA gene lists, we have been able to identify biological processes and mechanisms underlying the compounds' toxicity using GO term enrichment analysis.

Molecular Function

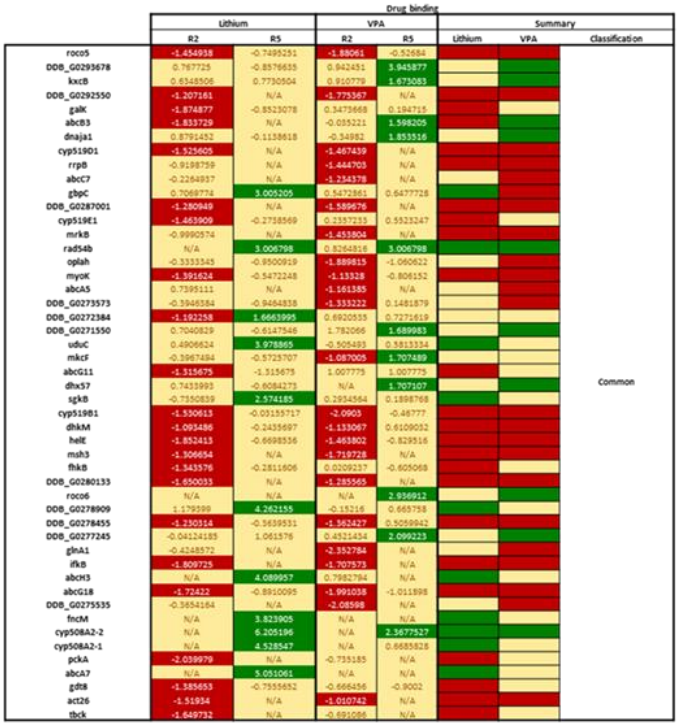

Drug binding

	Lithium		VPA		Summary		
	R2	R5	R2	R5	Lithium	VPA	Classification
roc05	-1.454938	-0.7495251	-1.88061	-0.52684			
DDB_G0293678	0.767725	-0.8576635	0.942451	3.945877			
kxcB	0.6348506	0.7730504	0.910779	1.675083			
DDB_G0292550	-1.207161	N/A	-1.775367	N/A			
galK	-1.874877	-0.8523078	0.3473668	0.194715			
abcB3	-1.833729	N/A	-0.035221	1.598205			
dnaja1	0.8791452	-0.1138618	-0.34982	1.853516			
cyp519D1	-1.525605	N/A	-1.467439	N/A			
rrpB	-0.9198759	N/A	-1.444703	N/A			
abcC7	-0.2264937	N/A	-1.234378	N/A			
gbpC	0.7069774	3.005205	0.5472861	0.6477728			
DDB_G0287001	-1.280949	N/A	-1.589676	N/A			
cyp519E1	-1.463909	-0.2738569	0.2357233	0.5523247			
mrkB	-0.9990574	N/A	-1.453804	N/A			
rad54b	N/A	3.006798	0.8264816	3.006798			
oplah	-0.3333345	-0.9500919	-1.889815	-1.060622			
myoK	-1.391624	-0.5472248	-1.13328	-0.806152			
abcA5	0.7395111	N/A	-1.161385	N/A			
DDB_G0273573	-0.3946384	-0.9464838	-1.333222	0.1481879			
DDB_G0272384	-1.192258	1.6663995	0.6920535	0.7271619			
DDB_G0271550	0.7040829	-0.6147546	1.782066	1.689983			
uduC	0.4906624	3.978865	-0.505493	0.5813334			
mkcF	-0.3967494	-0.5725707	-1.087005	1.707489			
abcG11	-1.315675	-1.315675	1.007775	1.007775			
dhx57	0.7433993	-0.6084273	N/A	1.707107			Common
sgkB	-0.7350839	2.574185	0.2934564	0.1898768			
cyp519B1	-1.530613	-0.0315717	-2.0903	-0.46777			
dhkM	-1.093486	-0.2435697	-1.133067	0.6109032			
helE	-1.852413	-0.6698536	-1.463802	-0.829516			
msh3	-1.306654	N/A	-1.719728	N/A			
fhkB	-1.343576	-0.2811606	0.0209237	-0.605068			
DDB_G0280133	-1.650033	N/A	-1.285565	N/A			
roc06	N/A	N/A	N/A	2.936912			
DDB_G0278909	1.179399	4.262155	-0.15216	0.665758			
DDB_G0278455	-1.230314	-0.3639531	-1.362427	0.9059943			
DDB_G0277245	-0.04124185	1.061576	0.4321434	2.099223			
glnA1	-0.4248572	N/A	-2.352784	N/A			
ifkB	-1.809725	N/A	-1.707573	N/A			
abcH3	N/A	4.089957	0.7982794	N/A			
abcG18	-1.72422	-0.8910095	-1.991038	-1.011898			
DDB_G0275535	-0.3654164	N/A	-2.08598	N/A			
fncM	N/A	3.823905	N/A	N/A			
cyp508A2-2	N/A	6.205196	N/A	2.3677527			
cyp508A2-1	N/A	4.528547	N/A	0.6685828			
pckA	-2.039979	N/A	-0.735185	N/A			
abcA7	N/A	5.051061	N/A	N/A			
gdt8	-1.385653	-0.7555652	-0.666456	-0.9002			
act26	-1.51934	N/A	-1.010742	N/A			
tbck	-1.649732	N/A	-0.691086	N/A			

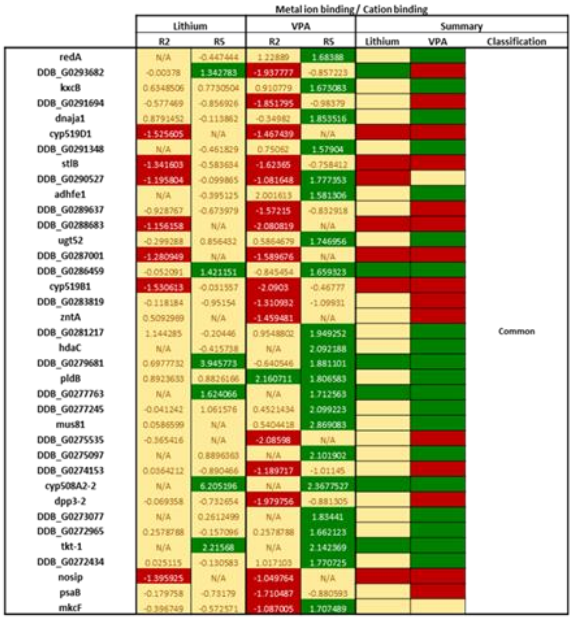

Metal ion binding / Cation binding

	Lithium		VPA		Summary		
	R2	R5	R2	R5	Lithium	VPA	Classification
redA	N/A	-0.447444	1.22889	1.68388			
DDB_G0293682	-0.00378	1.342783	-1.937777	-0.857223			
kxcB	0.6348506	0.7730504	-0.910779	1.675083			
DDB_G0291694	-0.577469	-0.856926	-1.851795	-0.98379			
dnaja1	0.8791452	-0.113862	-0.34982	1.853516			
cyp519D1	-1.525605	N/A	-1.467439	N/A			
DDB_G0291348	N/A	-0.461829	0.75062	1.57904			
stlB	-1.341603	-0.583634	-1.62365	-0.758413			
DDB_G0290527	-1.195804	-0.099865	-1.081648	1.777353			
adhfe1	N/A	-0.395125	2.001613	1.581306			
DDB_G0289637	-0.928767	-0.673979	-1.57215	-0.832918			
DDB_G0288683	-1.156358	N/A	-2.080819	N/A			
ugt52	-0.299288	0.856432	0.5864679	1.746956			
DDB_G0287001	-1.280949	N/A	-1.589676	N/A			
DDB_G0286459	-0.052091	1.421151	-0.845454	1.659323			
cyp519B1	-1.530613	-0.031557	-2.0903	-0.46777			
DDB_G0283819	-0.118184	-0.95154	-1.310982	-1.09931			
zntA	0.5092989	N/A	-1.459481	N/A			
DDB_G0281217	1.144285	-0.20446	0.9548802	1.949252			Common
hdaC	N/A	-0.415738	N/A	2.092188			
DDB_G0279681	0.6977732	3.945773	-0.640546	1.881101			
pldB	0.8923633	0.8826166	2.160711	1.806583			
DDB_G0277763	N/A	1.624066	N/A	1.712563			
DDB_G0277245	-0.041242	1.061576	0.4521434	2.099223			
mus81	0.0586599	N/A	0.5404418	2.869083			
DDB_G0275535	-0.365416	N/A	-2.08598	N/A			
DDB_G0275097	N/A	0.8896363	N/A	2.101902			
DDB_G0274153	0.0364212	-0.890466	-1.189717	-1.01145			
cyp508A2-2	N/A	6.205196	N/A	2.3677527			
dpp3-2	-0.069358	-0.732654	-1.979756	-0.881305			
DDB_G0273077	N/A	0.2612499	N/A	1.83441			
DDB_G0272965	0.2578788	-0.157096	0.2578788	1.662123			
tkt-1	N/A	2.21568	N/A	2.142369			
DDB_G0272434	0.025115	-0.130583	1.017103	1.770725			
nosip	-1.395925	N/A	-1.049764	N/A			
psaB	-0.179758	-0.78179	-1.710487	-0.880593			
mkcF	-0.396749	-0.572571	-1.087005	1.707489			

Hydrolase activity

	Lithium		VPA		Summary		
	R2	R5	R2	R5	Lithium	VPA	Classification
dcd3A	-1.468441	N/A	-1.624471	N/A			
pdx2	0.6256419	1.375534	0.9386771	1.905933			Common
oplah	-0.333335	-0.950092	-1.889815	-1.060622			
hdaC	N/A	-0.415738	N/A	2.092188			

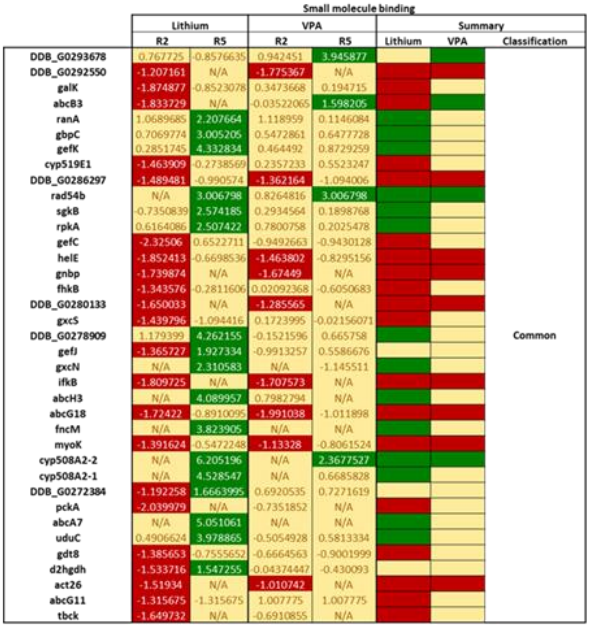

Small molecule binding

	Lithium		VPA		Summary		
	R2	R5	R2	R5	Lithium	VPA	Classification
DDB_G0293678	0.767725	-0.8576635	0.942451	3.945877			
DDB_G0292550	-1.207161	N/A	-1.775367	N/A			
galK	-1.874877	-0.8523078	0.3473668	0.194715			
abcB3	-1.833729	N/A	-0.03522065	1.598205			
ranA	1.0689685	2.207664	1.118959	0.1146084			
gbpC	0.7069774	3.005205	0.5472861	0.6477728			
gefK	0.2851745	4.332834	0.464492	0.8729259			
cyp519E1	-1.463909	-0.2738569	0.2357233	0.5523247			
DDB_G0286297	-1.489481	-0.990574	-1.362164	-1.094006			
rad54b	N/A	3.006798	0.8264816	3.006798			
sgkB	-0.7350839	2.574185	0.2934564	0.1898768			
rpkA	0.6164086	2.507422	0.7800758	0.2025478			
gefC	-2.32506	0.6522711	-0.9492663	-0.9430128			
helE	-1.852413	-0.6698536	-1.463802	-0.8295156			
gnbp	-1.739874	N/A	-1.67449	N/A			
fhkB	-1.343576	-0.2811606	0.0209237	-0.6050683			
DDB_G0280133	-1.650033	N/A	-1.285565	N/A			
gxcS	-1.439796	-1.094416	0.1723995	-0.0215607			
DDB_G0278909	1.179399	4.262155	-0.1521596	0.665758			Common
gefJ	-1.365727	1.927334	-0.9913257	0.5586676			
gxcN	N/A	2.310583	N/A	-1.145511			
ifkB	-1.809725	N/A	-1.707573	N/A			
abcH3	N/A	4.089957	0.7982794	N/A			
abcG18	-1.72422	-0.8910095	-1.991038	-1.011898			
fncM	N/A	3.823905	N/A	N/A			
myoK	-1.391624	-0.5472248	-1.13328	-0.8061524			
cyp508A2-2	N/A	6.205196	N/A	2.3677527			
cyp508A2-1	N/A	4.528547	N/A	0.6685828			
DDB_G0272384	-1.192258	1.6663995	0.6920535	0.7271619			
pckA	-2.039979	N/A	-0.7351852	N/A			
abcA7	N/A	5.051061	N/A	N/A			
uduC	0.4906624	3.978865	-0.5054928	0.5813334			
gdt8	-1.385653	-0.7555652	-0.6664563	-0.9001999			
d2hgdh	-1.533716	1.547255	-0.04374447	-0.430093			
act26	-1.51934	N/A	-1.010742	N/A			
abcG11	-1.315675	-1.315675	1.007775	1.007775			
tbck	-1.649732	N/A	-0.6910855	N/A			

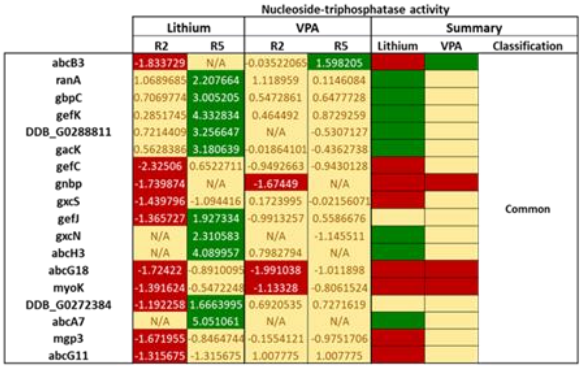

Nucleoside-triphosphatase activity

	Lithium		VPA		Summary		
	R2	R5	R2	R5	Lithium	VPA	Classification
abcB3	-1.833729	N/A	-0.03522065	1.598205			
ranA	1.0689685	2.207664	1.118959	0.1146084			
gbpC	0.7069774	3.005205	0.5472861	0.6477728			
gefK	0.2851745	4.332834	0.464492	0.8729259			
DDB_G0288811	0.7214409	3.256647	N/A	-0.5307127			
gacK	0.5628386	3.180639	-0.01864101	-0.4362738			
gefC	-2.32506	0.6522711	-0.9492663	-0.9430128			
gnbp	-1.739874	N/A	-1.67449	N/A			
gxcS	-1.439796	-1.094416	0.1723995	-0.0215607			Common
gefJ	-1.365727	1.927334	-0.9913257	0.5586676			
gxcN	N/A	2.310583	N/A	-1.145511			
abcH3	N/A	4.089957	0.7982794	N/A			
abcG18	-1.72422	-0.8910095	-1.991038	-1.011898			
myoK	-1.391624	-0.5472248	-1.13328	-0.8061524			
DDB_G0272384	-1.192258	1.6663995	0.6920535	0.7271619			
abcA7	N/A	5.051061	N/A	N/A			
mgp3	-1.671955	-0.8464744	-0.1554121	-0.9751706			
abcG11	-1.315675	-1.315675	1.007775	1.007775			

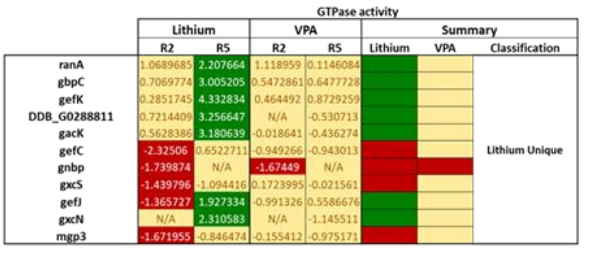

GTPase activity

	Lithium		VPA		Summary		
	R2	R5	R2	R5	Lithium	VPA	Classification
ranA	1.0689685	2.207664	1.118959	0.1146084			
gbpC	0.7069774	3.005205	0.5472861	0.6477728			
gefK	0.2851745	4.332834	0.464492	0.8729259			
DDB_G0288811	0.7214409	3.256647	N/A	-0.530713			
gacK	0.5628386	3.180639	-0.018641	-0.436274			
gefC	-2.32506	0.6522711	-0.949266	-0.943013			Lithium Unique
gnbp	-1.739874	N/A	-1.67449	N/A			
gxcS	-1.439796	-1.094416	0.1723995	-0.021561			
gefJ	-1.365727	1.927334	-0.991326	0.5586676			
gxcN	N/A	2.310583	N/A	-1.145511			
mgp3	-1.671955	-0.846474	-0.155412	-0.975171			

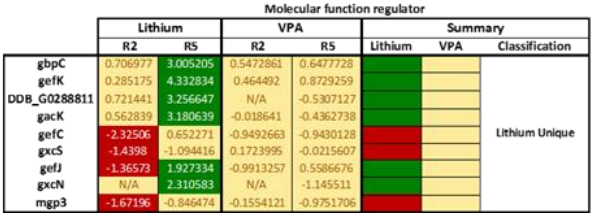

Molecular function regulator

	Lithium		VPA		Summary		
	R2	R5	R2	R5	Lithium	VPA	Classification
gbpC	0.706977	3.005205	0.5472861	0.6477728			
gefK	0.285175	4.332834	0.464492	0.8729259			
DDB_G0288811	0.721441	3.256647	N/A	-0.5307127			
gacK	0.562839	3.180639	-0.018641	-0.4362738			
gefC	-2.32506	0.652271	-0.9492663	-0.9430128			Lithium Unique
gxcS	-1.4398	-1.094416	0.1723995	-0.0215607			
gefJ	-1.36573	1.927334	-0.9913257	0.5586676			
gxcN	N/A	2.310583	N/A	-1.145511			
mgp3	-1.67196	-0.846474	-0.1554121	-0.9751706			

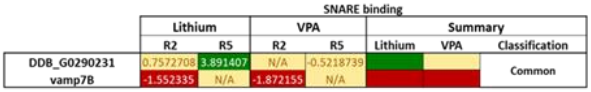

SNARE binding

	Lithium		VPA		Summary		
	R2	R5	R2	R5	Lithium	VPA	Classification
DDB_G0290231	0.7572708	3.891407	N/A	-0.5218739			Common
vamp7B	-1.552335	N/A	-1.872155	N/A			

Oxygen binding / Oxidoreductase activity

	Lithium		VPA		Summary		
	R2	R5	R2	R5	Lithium	VPA	Classification
cyp519D1	-1.525605	N/A	-1.467439	N/A			
cyp519E1	-1.463909	-0.273857	0.2357233	0.5523247			
cyp519B1	-1.530613	-0.031557	-2.0903	-0.46777			Common
cyp508A2-2	N/A	6.205196	N/A	2.3677527			
cyp508A2-1	N/A	4.528547	N/A	0.6685828			

Figure continues on next page.

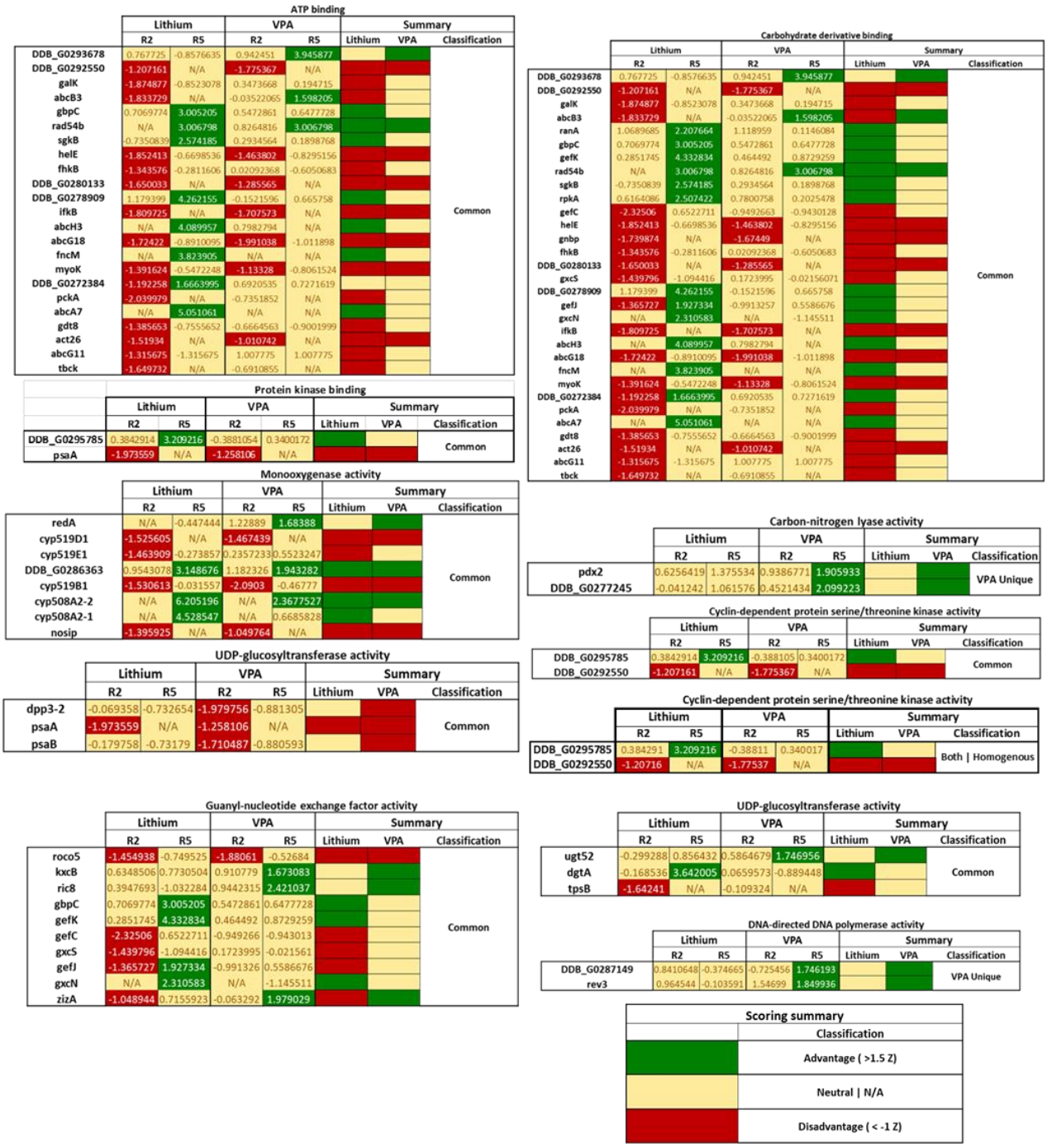

Figure 4.22. Summary tables for the Molecular function GO terms. The genes causing an overrepresentation of the molecular function GO terms are labelled advantaged or disadvantaged, dependent on which lithium or VPA gene list they came from. By comparing every gene within an individual GO term, each term was then classified as either lithium unique, VPA unique or common between the two. Figure over pages 165 - 166.

Biological Process

Galactose metabolic process

	Lithium		VPA		Summary		
	R2	R5	R2	R5	Lithium	VPA	Classification
galE	1.115735	-0.182016	0.5494504	1.840635			Common
uppA	0.2903293	3.943353	0.5670426	N/A			
galK	-1.874877	-0.852308	0.3473668	0.194715			

Lysosomal transport / Endosome transport / Vacuolar transport

	Lithium		VPA		Summary		
	R2	R5	R2	R5	Lithium	VPA	Classification
lvsA	-1.276369	N/A	-1.265752	N/A			Common
lvsB	-1.354181	-0.749941	-1.197717	-0.895562			
vamp7B	-1.552335	N/A	-1.872155	N/A			

Monosaccharide metabolic process / Hexose metabolic process

	Lithium		VPA		Summary		
	R2	R5	R2	R5	Lithium	VPA	Classification
galK	-1.874877	-0.8523078	0.3473668	0.194715			Common
uppA	0.2903293	3.943353	0.5670426	N/A			
ugt52	-0.2992881	0.856432	0.5864679	1.746956			
galE	1.115735	-0.1820162	0.5494504	1.840635			
pckA	-2.039979	N/A	-0.7351852	N/A			

Trehalose metabolic process

	Lithium		VPA		Summary		
	R2	R5	R2	R5	Lithium	VPA	Classification
tpsB	-1.64241	N/A	-0.109324	N/A			Common
treh	-0.039951	N/A	2.000342	1.023592			

Flavonoid metabolic process / Flavonoid biosynthetic process

	Lithium		VPA		Summary		
	R2	R5	R2	R5	Lithium	VPA	Classification
stlB	-1.341603	-0.583634	-1.62365	-0.758412			Common
ugt52	-0.299288	0.856432	0.5864679	1.746956			

Exogenous drug catabolic process / Response to xenobiotic stimulus

	Lithium		VPA		Summary		
	R2	R5	R2	R5	Lithium	VPA	Classification
cyp519D1	-1.525605	N/A	-1.467439	N/A			Common
cyp519E1	-1.463909	-0.2738569	0.2357233	0.5523247			
cyp519B1	-1.530613	-0.03155717	-2.0903	-0.4677698			
cyp508A2-2	N/A	6.205196	N/A	2.3677527			
cyp508A2-1	N/A	4.528547	N/A	0.6685828			

Positive regulation of cellular component movement

	Lithium		VPA		Summary		
	R2	R5	R2	R5	Lithium	VPA	Classification
gbpC	0.7069774	3.005205	0.5472861	0.6477728			Common
myoK	-1.391624	-0.547225	-1.13328	-0.806152			

Response to endoplasmic reticulum stress

	Lithium		VPA		Summary		
	R2	R5	R2	R5	Lithium	VPA	Classification
npl4	0.7267871	5.351291	0.4927343	-0.193456			Lithium Unique
DDB_G0280773	0.6894355	2.742758	0.739519	-0.938663			

Positive regulation of transport

	Lithium		VPA		Summary		
	R2	R5	R2	R5	Lithium	VPA	Classification
rpkA	0.6164086	2.507422	0.7800758	0.2025478			Common
pldB	0.8923633	0.8826166	2.160711	1.806583			
myoK	-1.391624	-0.547225	-1.13328	-0.806152			

Fucosylation

	Lithium		VPA		Summary		
	R2	R5	R2	R5	Lithium	VPA	Classification
fut2	0.4274135	2.857088	0.1184251	0.4528376			Lithium Unique
fut11	N/A	4.318534	N/A	N/A			

Cellular ketone metabolic process

	Lithium		VPA		Summary		
	R2	R5	R2	R5	Lithium	VPA	Classification
stlB	-1.341603	-0.583634	-1.62365	-0.7584119			Common
gloB1	-1.337601	-0.804476	-0.676368	-0.9405356			

Positive regulation of phagocytosis

	Lithium		VPA		Summary		
	R2	R5	R2	R5	Lithium	VPA	Classification
rpkA	0.6164086	2.507422	0.7800758	0.2025478			Common
myoK	-1.391624	-0.547225	-1.13328	-0.806152			

Cellular response to nitrogen starvation / Cellular response to nitrogen levels

	Lithium		VPA		Summary		
	R2	R5	R2	R5	Lithium	VPA	Classification
atg6A	N/A	3.088	N/A	N/A			Lithium Unique
DDB_G0283753	0.6446504	4.0707	0.0607	N/A			

Positive regulation of Ras protein signal transduction

	Lithium		VPA		Summary		
	R2	R5	R2	R5	Lithium	VPA	Classification
ric8	0.3947693	-1.032284	0.9442315	2.421037			Common
gbpC	0.7069774	3.005205	0.5472861	0.6477728			

Rac protein signal transduction / Regulation of hydrolase activity

	Lithium		VPA		Summary		
	R2	R5	R2	R5	Lithium	VPA	Classification
roco5	-1.454938	-0.7495251	-1.88061	-0.5268398			Common
kxcB	0.6348506	0.7730504	0.910779	1.673083			
ric8	0.3947693	-1.032284	0.9442315	2.421037			
gbpC	0.7069774	3.005205	0.5472861	0.6477728			
gefK	0.2851745	4.332834	0.464492	0.8729259			
gacL	N/A	0.8209318	N/A	1.595797			
DDB_G0288811	0.7214409	3.256647	N/A	-0.5307127			
gacK	0.5628386	3.180639	-0.01864101	-0.4362738			
gefC	-2.32506	0.6522711	-0.9492663	-0.9430128			
gxcS	-1.439796	-1.094416	0.1723995	-0.02156071			
gefJ	-1.365727	1.927334	-0.9913257	0.5586676			
gxcN	N/A	2.310583	N/A	-1.145511			
gacI	1.002443	-0.549904	0.9304808	1.593318			
zizA	-1.048944	0.7155923	-0.06329197	1.979029			
mgp3	-1.671955	-0.8464744	-0.1554121	-0.9751706			
ctnA	0.4564887	-0.03635404	1.292408	1.999835			

Carbohydrate metabolic process

	Lithium		VPA		Summary		
	R2	R5	R2	R5	Lithium	VPA	Classification
galK	-1.874877	-0.8523078	0.3473668	0.194715			Common
uppA	0.2903293	3.943353	0.5670426	N/A			
ugt52	-0.2992881	0.856432	0.5864679	1.746956			
dgtA	-0.1685357	3.642005	0.06595726	-0.8894482			
nagC	0.2651472	2.951569	0.1805738	-0.8013799			
tpsB	-1.64241	N/A	-0.1093241	N/A			
fut2	0.4274135	2.857088	0.1184251	0.4528376			
iliG	-0.6143557	1.0448154	0.8033868	1.879022			
treh	-0.03995068	N/A	1.023592	2.000342			
DDB_G0282715	-0.6501752	N/A	-1.133052	N/A			
DDB_G0278551	-0.1774525	-1.011152	-1.790179	-1.074322			
DDB_G0278171	N/A	1.489852	N/A	1.930047			
DDB_G0276439	0.5516761	N/A	1.428752	2.773156			
galE	1.115735	-0.1820162	0.5494504	1.840635			
ctnA	0.4564887	-0.03635404	1.292408	1.999835			
pckA	-2.039979	N/A	-0.7351852	N/A			
fut11	N/A	4.318534	N/A	N/A			

Sorocarp morphogenesis

	Lithium		VPA		Summary		
	R2	R5	R2	R5	Lithium	VPA	Classification
stlB	-1.341603	-0.583634	-1.62365	-0.758412			Common
abcG18	-1.72422	-0.89101	-1.991038	-1.011898			
psaA	-1.973559	N/A	-1.258106	N/A			
atg6A	N/A	3.088092	N/A	N/A			

Organic hydroxy compound biosynthetic process

	Lithium		VPA		Summary		
	R2	R5	R2	R5	Lithium	VPA	Classification
stlB	-1.341603	-0.583634	-1.62365	-0.758412			Common
ugt52	-0.299288	0.856432	0.5864679	1.746956			
pdx2	0.6256419	1.375534	0.9386771	1.905933			

Endosome organization

	Lithium		VPA		Summary		
	R2	R5	R2	R5	Lithium	VPA	Classification
abcG18	-1.72422	-0.8910095	-1.991038	-1.011898			Common
lvsA	-1.276369	N/A	-1.265752	N/A			

Chaperone-mediated protein folding

	Lithium		VPA		Summary		
	R2	R5	R2	R5	Lithium	VPA	Classification
ric8	0.3947693	-1.032284	0.9442315	2.421037			Common
DDB_G0278455	-1.230314	-0.363953	-1.362427	0.5059942			

Pyridine-containing compound metabolic process

	Lithium		VPA		Summary		
	R2	R5	R2	R5	Lithium	VPA	Classification
pdx2	0.6256419	1.375534	0.9386771	1.905933			Common
ctnA	0.4564887	-0.036354	1.292408	1.999835			
tkt-1	N/A	2.21568	N/A	2.142369			

Secondary metabolite biosynthetic process

	Lithium		VPA		Summary		
	R2	R5	R2	R5	Lithium	VPA	Classification
stlB	-1.341603	-0.583634	-1.62365	-0.758412			Common
DDB_G0286363	0.9543078	3.148676	1.182326	1.943282			

Figure continues on next page.

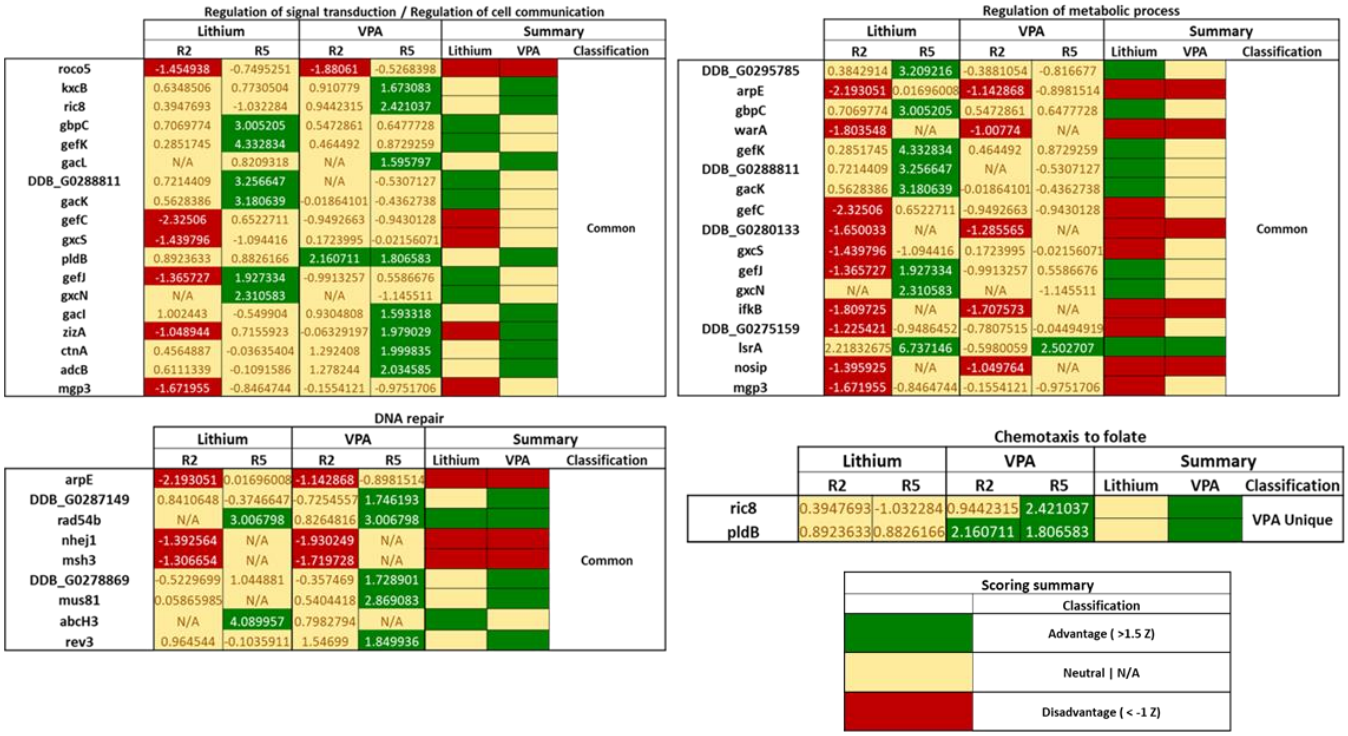

Figure 4.23. Summary tables for the biological process GO terms. The genes causing an overrepresentation of the biological process GO terms are labelled advantaged or disadvantaged, dependent on which lithium or VPA gene list they came from. By comparing every gene within an individual GO term, each term was then classified as either lithium unique, VPA unique or common between the two. Figure over pages 167 - 168.

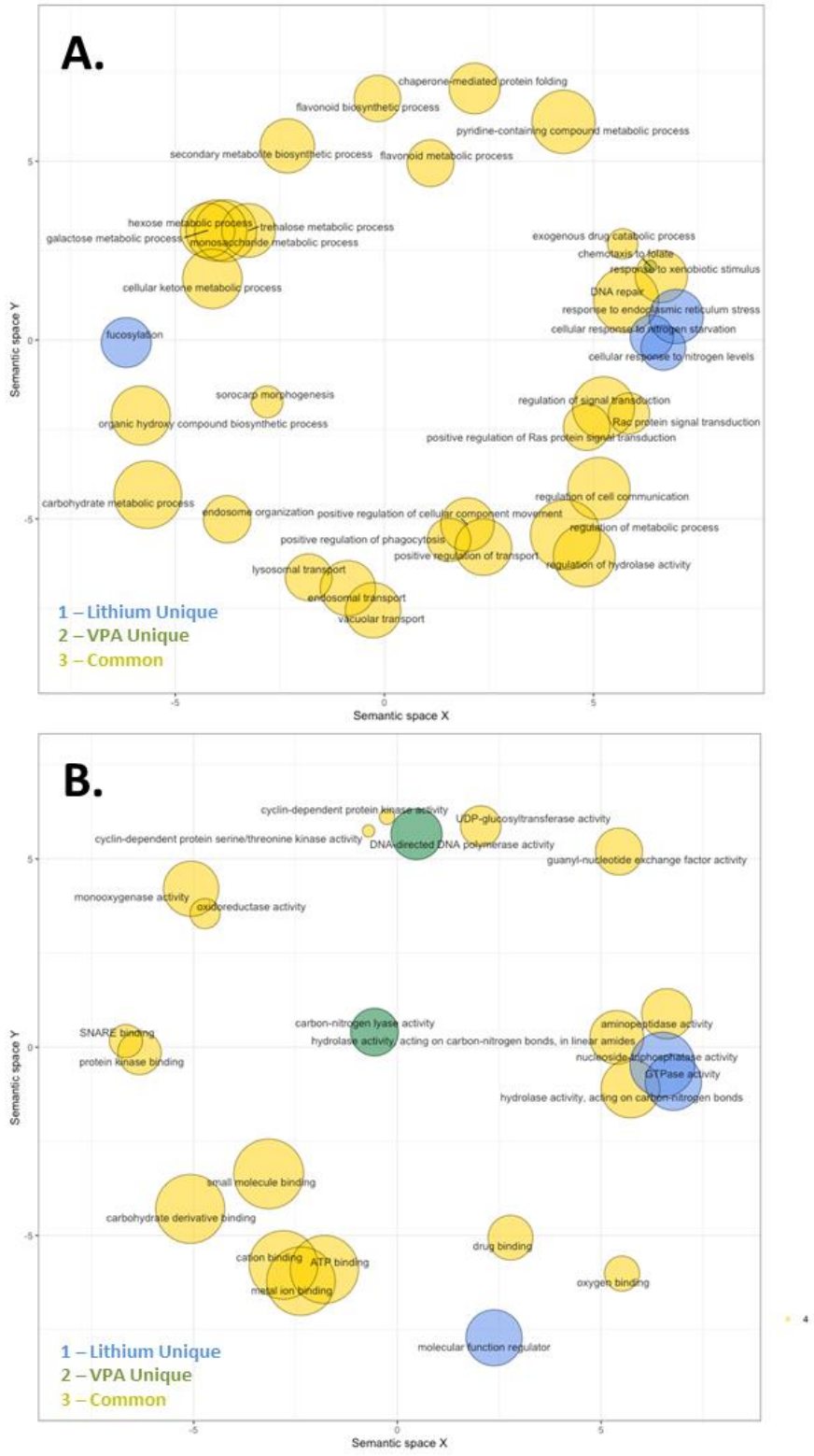

Figure 4.24. False coloured scatterplots of the significantly over-enriched biological process and molecular function GO terms. The refined, combined GO terms from the lithium, VPA and 'combined' GO term analysis were plotted on semantic space using the REVIGO tool (238). GO terms with biological similarities are plotted closer together. The size of each plot represents the biological complexity of the term, with larger plots representing 'broader' terms. Plots are false coloured: blue for uniquely lithium, green for uniquely VPA, gold for common **A.** Scatterplot for the Biological Process category. **B.** Scatterplot for the Molecular Function category.

4.4.8 Gene ontology (GO) analysis reveals key biological processes affected by lithium and VPA toxicity

By genetically phenotyping and using GO term analysis, we were able to identify a strong mechanistic tie between lithium and VPA. Global gene analysis has allowed for the biological processes disrupted by toxic compounds to be identified. Furthermore, the majority of the biological process and molecular function GO terms were represented by genes from both screens. This suggests that lithium and VPA toxicity affects common aspects of cellular biology. Furthermore, the GO term analysis clustered the terms into discreet groupings, suggesting that separate biological processes and pathways are commonly affected by both compounds. Using our Biological Processes GO terms we categorised them into key groups using the GO term hierarchy tree. We found that the 34 BP GO terms were clustered on four discreet branches of the Biological Processes GO term tree (data not shown) (238). Using the biological process terminology that the four branches represented, we named them: ‘metabolism’, ‘stress response’, ‘signal transduction’ and ‘vesicular’ (Figure 4.25). When the four categories were false coloured over the scatterplot, these key biological processes by which lithium and VPA mediate their toxic effects can be visualised (Figure 4.25).

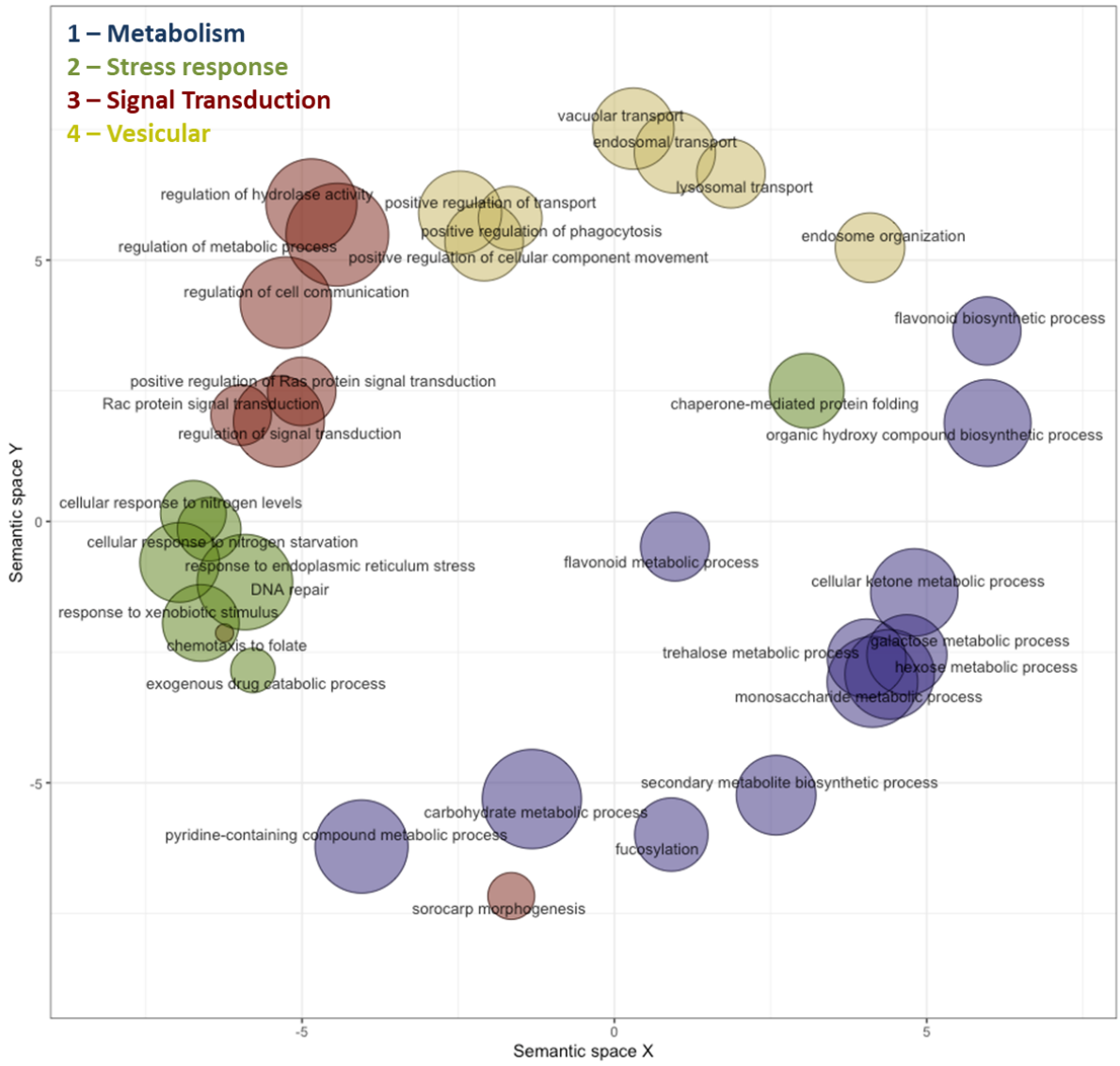

Figure 4.25. False coloured scatterplots of the significantly over-enriched biological process GO terms. The refined, combined biological process GO terms from the lithium, VPA and 'combined' GO term analysis were plotted on semantic space using the REVIGO tool (238). GO terms with biological similarities are plotted closer together. The size of each plot represents the biological complexity of the term, with larger plots representing 'broader' terms. Plots are false coloured for our broad mechanistic categories: blue for 'metabolism', green for 'stress response', red for 'signal transduction' and gold for 'vesicular'.

4.4.9 Lithium and VPA mediate cellular toxicity via common biological processes

Our analysis has revealed that the biological process GO terms clustered together and thus could be classified under broad umbrella terms: ‘signal transduction’, ‘stress response’, ‘vesicular’ and ‘metabolism’ (Figure 4.25). Furthermore, our GO term analysis has also shown that individually the majority of terms were comprised of genes coming from both the lithium and VPA screens (Figures 4.22, 4.23). Together, these data suggest that our broad categories represent the shared pathways and mechanisms by which both lithium and VPA mediate toxicity. The largest category of biological process GO terms is represented by the ‘metabolism’ group (Figure 4.25). All of the ‘metabolism’ classified GO terms were comprised of genes from both the lithium and VPA screens. Despite the large number of GO terms, many of the same genes were underlying the significant enrichment of the terms (Table 4.6). The most significant metabolism GO term was ‘galactose metabolism’, with three of the four enzymes in the Leloir pathway in our gene lists. The Leloir pathway is ubiquitous among eukaryotes where it functions to covert galactose into metabolically active glucose-6-phosphate (239). In order to gain further insight, we determined whether the three galactose metabolism genes were advantaged or disadvantaged and where they were located on the Leloir pathway (239) (Figure 4.26). Firstly, we found that all three genes (galK, uppA, galE) in the Leloir pathway, were within one enzymatic reaction of the metabolite glucose-1-phosphate (Figure 4.26). Glucose-1-phosphate (and Glucose-6-phosphate) are the metabolic precursors for the de-novo synthesis of inositol (Figure 1.7). Lithium and VPA are both known to attenuate inositol-based signalling pathways, causing a depletion of available inositol and its subsequent signalling inositol phosphates. Secondly, galK, uppA and galE were advantaged or disadvantaged (in either the lithium or VPA screens) dependant on whether they caused a bottleneck that would increase or decrease the availability of glucose-1-phosphate (Figure 4.26). For example, the uppA mutant is lithium advantaged, presumably as it converts glucose-1-phosphate into UDP-glucose, thus reducing glucose-1-phosphate levels needed for the de-novo synthesis of inositol (Figure 4.26). Conversely, the galK mutant is lithium disadvantaged, which could be because it prevents the conversion of galactose into glucose-1-phosphate (Figure 4.26). Interestingly, genes from other common lithium and VPA metabolism GO terms: tpsB, treh (‘Trehalose metabolism’) and pckA, were also found to be metabolic enzymes that were within one enzymatic reaction of either glucose-1-phosphate or glucose-6-phosphate (data not shown). Together, this suggests that these metabolic changes indirectly affect inositol levels, further demonstrating the commonality between lithium and VPA mediated toxicity.

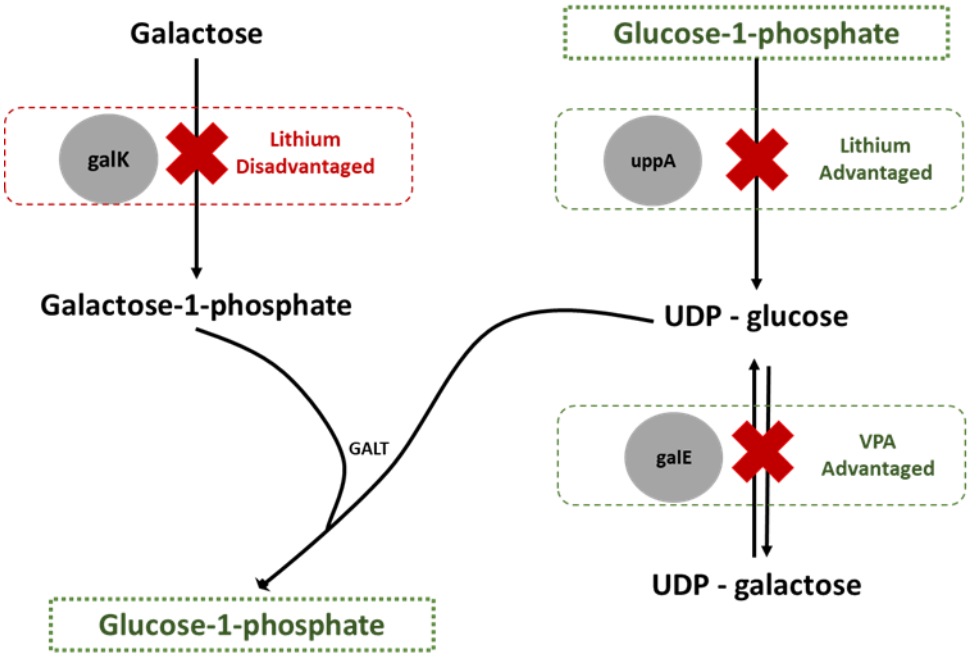

Figure 4.26. Lithium and VPA genes are closely linked on the galactose metabolic pathway. A schematic of the Leloir pathway with the identified lithium and VPA advantaged and disadvantaged genes highlighted. Figure adapted from (240).

In *D. discoideum* the exposure of lithium or VPA causes a depletion of the inositol derived signalling molecule, PIP_3. PIP_3 is critical signalling molecule required for macropinocytosis, the biological process by which cells uptake fluid and the primary method by which cells growing in our screens take up nutrients (80). Macropinocytosis requires the formation of macropinocytic cups, which form due to membrane bound signalling patches of PIP_3, active-ras and active-rac proteins (80). These patches recruit downstream activators to trigger actin polymerisation and, finally, fluid uptake. Our classification of 'signal transduction' GO terms contained terms 'rac' and 'ras' protein signal transduction (Figure 4.25). We therefore firstly assessed whether cellular fluid uptake is affected by both the lithium and VPA doses used in our screens.

Previously, exposure to 1 mM VPA (same dose as our screen) has been reported reduce PIP_3 production and fluid uptake rate in *D. discoideum* (241). Lithium treatment in *D. discoideum* has also been reported suppress PIP_3 signalling, although effects on fluid uptake rates have never been tested (171). Therefore, we firstly assessed whether the concentration of lithium or VPA used in our REMI-Seq screens affects fluid uptake. Fluid uptake was measured in a REMI-grid control cell line after 24h lithium or VPA

incubation using the fluid uptake assay reported by Williams and Kay (2018) (Figure 4.27) (242). As expected, the VPA doses we tested significantly reduced cellular fluid uptake (Figure 4.27 B). The concentration of lithium used in the screen also significantly reduced cellular fluid uptake (Figure 4.27 A). These results confirm that the suppression of fluid uptake rate is a common toxicological effect of both lithium and VPA at our screen doses.

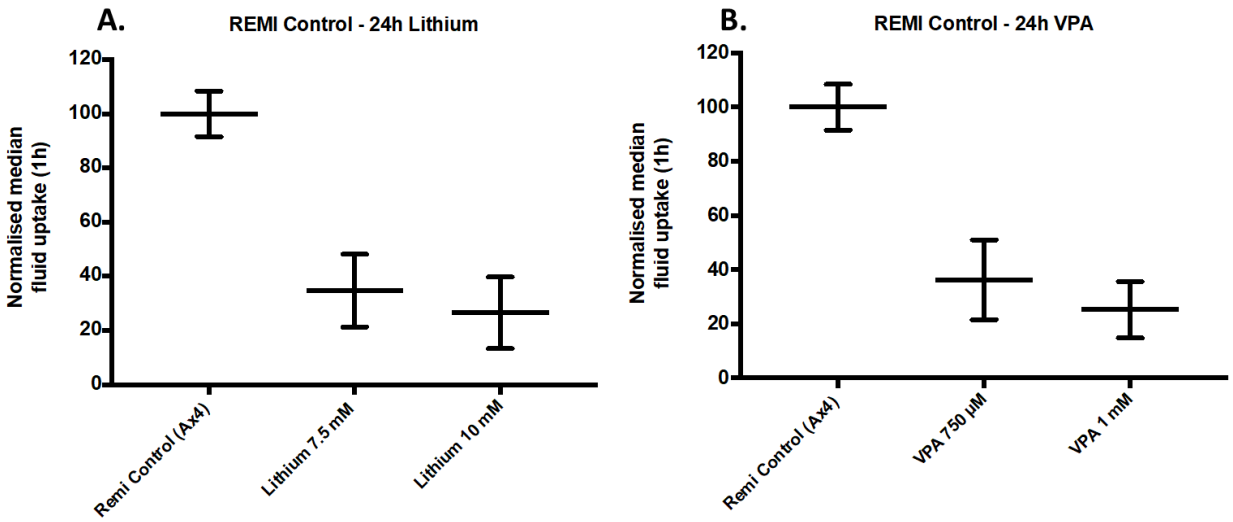

Figure 4.27. Lithium and VPA treatment significantly reduced cellular fluid uptake. REMI-control (Ax4) cell line was grown in log phase for 23 hours in a 24 well plate in the presence of either lithium or VPA. Fluid uptake was measured in the 24th hour (in the continued presence of either lithium or VPA using a modified version of Williams and Kay's HTP flow cytometry assay (242) (Methods section 6.10). Median fluorescent of cells was measured and normalised to the non-drug control. Data represents 9 biological replicates, mean ± SD. **A.** 7.5- and 10 mM LiCl cause a significant reduction in cellular fluid uptake. **B.** 750 µM and 1 mM VPA cause a significant reduction in cellular fluid uptake.

Next, we tested whether mutants from the signal transduction GO category significantly impacted on cellular fluid uptake. We selected 6 lithium mutants and 8 VPA mutants from the regulation of signal transduction GO term (a GO term in the signal transduction category) (Figure 4.28). 6 of the mutants were disadvantaged and 8 were advantaged. Fluid uptake was assessed in the selected mutants after 24h of treatment of 7.5- and 10 mM lithium or 750 µM and 1 mM VPA. All fluid uptake assay results for the lithium and VPA signal transduction mutants can be found in appendix figure A7.4. Examples are shown in figure 4.28 A, 4.28 B: the lithium disadvantage mutant, gefC, takes up significantly less fluid than the control at 7.5- and 10 mM ($p=0.0224$, $p=0.0093$); conversely, VPA advantage mutant, pldB, uptakes significantly more fluid (Figure 4.28 A, 4.28 B). Using the difference in mean fluid uptake between 7.5 mM lithium or 1 mM

VPA and the control a fluid uptake score was calculated (Figure 4.28 C). During lithium and VPA treatment the signal transduction mutants were generally found to uptake fluid at significant different rates compared to the control (Figure 4.28 C). Out of the signal transduction mutants tested, only zizA tested in lithium did not exhibit a significant change in fluid uptake (Figure 4.28 C). Furthermore, 2 lithium advantaged mutants (gacK, gbpC) had a significant reduction in fluid uptake (Figure 4.28 C). In total 13 out of the 14 signal transduction mutants (93%) exhibited a significant change in fluid uptake in comparison to the control (Figure 4.28 C). Additionally, 11 out of the 14 mutants (79%) took up less or more fluid dependant on whether they were disadvantaged and advantaged, respectively. These results suggest that the majority of the signal transduction mutants may modulate their resistance or sensitivity to lithium and VPA toxicity via changes to macropinocytosis. This effect appears to be specific to the signal transduction class of mutants. When we selected 10 mutants from the 'stress response' and 'metabolism' classifications of GO terms, only 2 of the mutants displayed a significant change in fluid uptake in comparison to the control (Figure 4.28 D). Therefore, in summary, 13 out of the 14, signal transduction GO term mutants displayed significantly changes in macropinocytosis; in contrast to only 2 out of the 10 tested 'metabolism and stress response' mutants (Figure 4.28).

These results suggest that lithium and VPA are mediating aspects of their toxicity via macropinocytosis, via common biological processes and mechanisms and is likely due to changes in phosphoinositol and ras/rac signalling pathways.

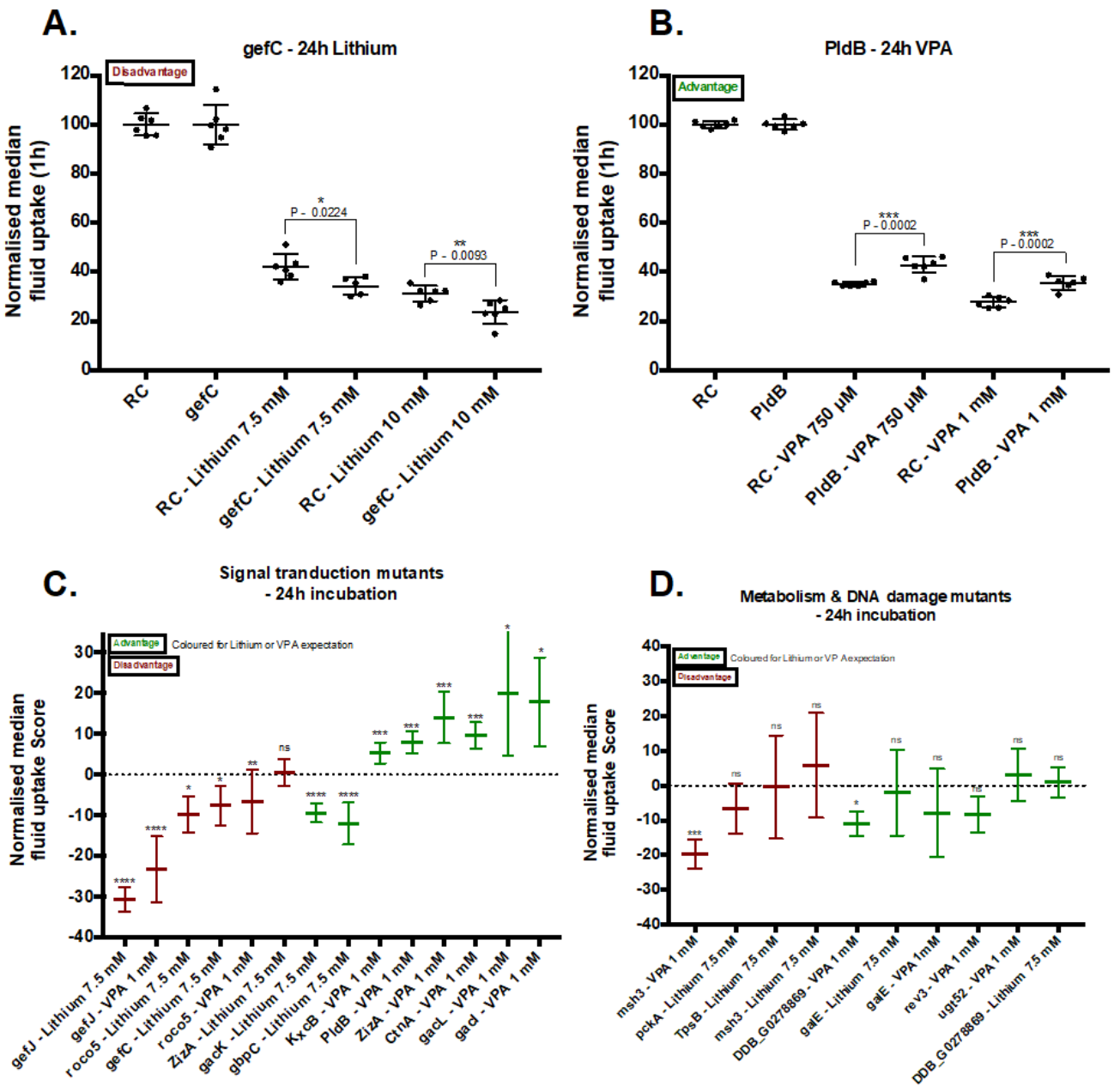

Figure 4.28. Defects in macropinocytosis are specific to mutants from signal transduction classified GO terms. REMI-control (Ax4) cell line and lithium or VPA screens mutants were grown in log phase for 23 hours in a 24 well plate in the presence of either lithium or VPA. Fluid uptake was measured in the 24th hour (in the continued presence of either lithium or VPA using a modified version of Williams and Kay's HTP flow cytometry assay (242) (Methods section 6.10). Median fluorescent of cells was measured and normalised to the non-drug control. A fluid uptake score is calculated between the difference in mean fluid uptake between 7.5 mM lithium or 1 mM VPA and the control. Data represents 2 biological replicates, mean ± SD. **A & B.** Lithium disadvantage mutant gefC and VPA advantaged mutant pldB, uptake significantly less or more fluid respectively. **C.** Fluid uptake score for lithium and VPA signal transduction GO term mutants. **D.** Fluid uptake score for lithium and VPA metabolism and stress response GO term mutants.

4.5 Chapter discussion

In this chapter we investigated the potential of *D. discoideum* forward genetics method, REMI-Seq, to interrogate and compare the mechanisms by which different teratogenic compounds act. We performed proof of principle screens for two teratogenic compounds, lithium and VPA. These are both mood stabilising and teratogenic compounds, which are thought to mediate their cellular effects through unique and common mechanisms (243). We hypothesised that the REMI-Seq parallel phenotyping method could be used to identify genetic loci responsible for key toxicity events associated with both compounds.

Our proof of principle experiments with lithium and VPA illustrate that REMI-Seq could provide an effective method for teratogen evaluation and comparison. They reveal a significant overlap between gene lists associated with toxicity to lithium and VPA (Figure 4.16). Consequently, by comparing toxicity mediating genes from novel compounds to lists of genes from characterised teratogenic compounds, common genetic markers of teratogenic phenotypes could be identified. Furthermore, as researchers develop new bio-active compounds it will allow them to quickly establish whether all compounds in the same class will have adverse developmentally toxic effects; whether specific chemical structure(s) result in developmental toxicity and whether the teratogenic effects are a result of off-target events (1). This would greatly expedite the development process as it would allow new compounds to be flagged as teratogenic very early in their development (1).

The methods employed here provide a quantitative measure of the effects of each gene on toxicity. Overwhelmingly, the mutants which exhibited the greatest advantage or disadvantage on one compound were also found in the top or bottom 25 % of the other screen. (Figure 4.19). When a strict threshold was applied, often mutants were not found to be significantly enrichened in both screens. However, experimental data shows that this is due to the fact that the cut off used precluded their identification (Figure 4.18). In fact, the most significantly advantaged or disadvantaged mutants on one compound tended to have a weaker advantaged or disadvantaged phenotype in the other compound (Figure 4.20). Our data thus suggests that the mechanisms of action shared between the compounds are greater than previously reported (149). Furthermore, our results suggest that even though lithium and VPA may initiate cellular toxicity in different ways, the downstream effects converge onto the same pathways.

The second aim of this chapter was to test whether REMI-Seq could be used to identify the biological processes disrupted by teratogenic compounds. We found that GO term analyses uncovered molecular functions and biological processes affected by both compounds (Section 4.4.7). This revealed many GO terms could be classified under the umbrella terms: ‘signal transduction’, ‘stress response’, ‘vesicular’ or ‘metabolism’ (Section 4.4.8).

One of the key biological process GO terms within the ‘stress response’ category was DNA repair (Table 4.6). The DNA repair term was comprised of nine genes from the lithium and VPA screens (Table 4.6). VPA has previously been reported to induce double stranded DNA breaks in multiple model systems including: yeast, preimplantation mouse embryos, and *in vivo* rat testing (244–246). It has been suggested that this is due to the inhibition of HDACs, which in turn results in the mis-expression of double strand repair factors (247). Unrepaired DNA damage has also been associated with the failure of neural tube closure in VPA treated mice and rats, an outcome associated with an increase in congenital neural traits, including autism-like behaviours (246). Our results thus support the idea that the DNA damage/repair effects of VPA exposure at therapeutic concentrations plays a major role in the cellular toxicity of the compound and is a potential mechanism for its teratogenic effects. In contrast, few studies have been conducted on the effects of lithium on DNA repair. Recently, lithium has been reported to provide protection to DNA damage *in vitro*, albeit at concentrations significantly lower than used in our REMI-Seq screen (248). However, the results from our forward genetics screen suggest that at a high concentration (7.5 mM), DNA repair may also be a key biological process affected by lithium. Interestingly, a G2 cell cycle arrest is reported in mouse renal cells (both *in vitro* and *in vivo*) after treatment of high doses of lithium (10 mM) (249). However, whether this affect was a response to DNA damage was not investigated. Future research will be required to understand the extent to which high lithium doses may interact with DNA repair. As genes in major DNA repair mechanisms were found to be significantly disadvantaged in high doses of lithium (Figure 4.23) it will be important to determine if this is directly due to lithium exposure. Previously, fluorescently tagging key DNA repair proteins has been used to indirectly measure DNA damage induction in *D. discoideum* (250). However, as lithium exposure may change the expression profiles of DNA repair genes and thus cause DNA damage, a direct measure of DNA damage such as a comet assay or H2A.X antibody marker may be more appropriate (251). Furthermore, it would be interesting to investigate whether a low dose

lithium does provide DNA damage protection to *D. discoideum* cells when co-treated with DNA damaging agents, as reported in other model systems.

The second umbrella GO term category is ‘vesicular’, which encompasses a range of GO terms that relate to intracellular membrane bound processes, including: vesicular transport, endosome transport and vacuolar transport. The vesicular based GO terms comprise a small number of overlapping, significantly enriched genes (Figure 4.25). Three of these genes (lvsA, lvsB and Vamp7b) are associated with the function of the *D. discoideum* contractive vacuole (252). However, lvsA and lvsB have also been demonstrated to be functionally important in endosome organisation and lysosome maturation in *D. discoideum,* respectively (253,254). lvsB is a close homolog of LYST (lysosomal-trafficking regulator) and mutations in LYST cause Chediak-Higashi syndrome, a rare and often fatal disease characterised by impaired lysosome transport (255). Recently, the attenuation of autophagy (a process in which lysosome maturation and trafficking is critical) has emerged as an important area of research on the cellular effects of both lithium and VPA (256–261). The autophagy-lysosome pathway functions to digest and recycle a range of intracellular targets, including abnormal organelles, long-lived proteins and protein aggregates (262). A reduction in the autophagy-lysosome pathway and the subsequent increase in protein aggregations is a major factor behind both Parkinson’s and Alzheimer’s diseases (263). Interestingly, lithium, VPA and another mood stabiliser carbamazepine have been found to induce autophagy (263). This has led lithium and VPA to be investigated as possible neuroprotective drugs (263). The induction of autophagy by lithium is caused by a reduction in IP_3 signalling, which is due to a reduction in free inositol (264) (Figure 1.7). As VPA and carbamazepine also impact on the inositol cycle it is suspected that they also induce the autophagy-lysosome pathway via a similar mechanism. Although more research is required to clarify the link between lysosome trafficking, autophagy and inositol derived signalling, the genes behind the ‘vesicular’ GO term category may relate to the common inositol depletion mechanism of lithium and VPA. It is therefore interesting to note that the top VPA resistant mutant (DDB_G0293258), was found to contain a myotubularin-like phosphatase domain ($p = <0.000001$) (Data not shown). Myotubularin-like family proteins are cellular phosphatases, with myotubularin functioning to dephosphorylate PI(3)P and $PI(2,5)P_2$, recycling them back into phosphatidylinositol (PI) (265). Additionally, another one of the top VPA resistant genes, hdaC, contains a FYVE domain near the N terminus. FYVE domains are small binding modules that recognise phosphatidylinositol 3-phosphate (PI(3)P). It is thus interesting that a mutant with an ablated protein, which contains domains related to deacetylation and PI(3)P, was found

to be strongly resistant to VPA. PI(3)P is an intracellular membrane bound signalling molecule that plays a critical role in membrane trafficking (266). PI(3)P plays an important signalling role in lysosome formation and maturation as well as in the autophagic process (266). Early autophagosomes are highly enriched in PI(3)P, which functions to recruit a wide range of FYVE domain containing proteins to the specialised vesical (267). PI(3)P is synthesised from phosphatidylinositol (PI), an important intermediate of the inositol phosphate biosynthetic cycle (Figure 1.7).

Lithium and VPA are both known to affect the inositol cycle (Section 1.4.5, Figure 1.7). Consistent with this idea, the majority of 'metabolism genes' enriched from either screen are enzymes in metabolic pathways that directly impact on the synthesis of glucose-1-phosphate or glucose-6-phosphate. Both glucose-1-phosphate and glucose-6-phosphate are metabolic precursors in the synthesis of inositol (Figure 1.7). For example, the most significant metabolism GO term was 'galactose metabolism', with three of the four enzymes in the Leloir pathway in our gene lists. The Leloir pathway functions to convert galactose in glucose-1-phosphate, which itself can be further modified into glucose-6-phosphate (239). The three genes were found in both the lithium and VPA screens, suggesting that this process mediates resistance and sensitivity to the toxic effects of both compounds (Figure 4.26). However, future research will be required to understand the extent to which these metabolic changes affect inositol levels, and to what extent it impacts their teratogenicity. The first objective would be to link the metabolism mutants from our lithium and VPA screens to inositol homeostasis. Firstly, by using colorimetric enzymatic assays to measure the intracellular levels of glucose-1-phosphate and glucose-6-phosphate in the different metabolic mutants after treatment with lithium and VPA. An increase or decrease in free glucose-1-phosphate and/or glucose-6-phosphate in the different metabolic mutants would support our hypothesis that changes in these metabolites could impact on de novo inositol synthesis. Secondly, by measuring whether the key phosphoinoistol signalling molecules affected by lithium and VPA treatment such as PIP_3, have significantly changed abundance in the metabolic mutants' background (171,241).

The final GO term category is 'signal transduction', which encompasses a range of GO terms that include broad terms such as 'Regulation of signal transduction/Regulation of cell communication' and more specific terms including 'rac protein signal transduction' and 'ras protein signal transduction' (Table 4.6). Unlike other GO term categories (which were defined by a small number of overlapping genes) the signal transduction GO terms were comprised of a much larger number of genes (Table 4.6). Many of these genes are

associated with ‘ras’ or ‘rac’ protein signal transduction. Furthermore, we found that a significant number of the mutants from this category significantly affected macropinocytosis (Figure 4.27). Macropinocytosis is the process by which cells take up fluid and is therefore the primary method for axenically grown *D. discoideum* to gain nutrients (242). For cells to form macropinocytic cups a complex signalling network is required to direct actin polymerisation (80). Macropinocytic cups are formed around patches of PIP_3 on the cell membrane, which recruit activators of the Arp2/3 complex, ultimately triggering actin polymerisation in a ring shape (80). However, activated small G-proteins, Ras and Rac also co-localise at patches of $PIP_{3,}$ which together with their activators (GEFs) and inhibitors (GAPs) are essential for PIP_3 signalling and thus macropinocytosis (80). We find that both lithium and VPA cause a significant reduction in fluid uptake rates, presumably due to the depletion of PIP_3 as previously reported for VPA (156). Changes in activity of Ras and Rac proteins (and their associated activators and repressors) provides a mechanism by which the rate of macropinocytosis is controlled in *D. discoideum.* In fact, axenic strains used in *D. discoideum* research are only viable due to the deletion of a RasGAP (repressor), NF1, which causes larger and more frequent Ras/ PIP_3 patches and increases fluid uptake 20-fold (268). Consistent with this idea we find that 11 out of the 14 signal transduction mutants affected fluid uptake (Figure 4.27 C). This suggests that changes in these Ras and Rac proteins leads to changes in macropinocytosis that mediate resistance or sensitivity to the toxic effects of both compounds. Our data suggests that lithium and VPA can be used to interrogate the complex signalling mechanisms needed for cells to up take fluid. However, more work is required to uncover the toxicological mechanistic link between lithium and VPA mediated reduction in PIP_3 and macropinocytosis in *D. discoideum*.

4.5.1 The effects of Lithium and VPA on Wnt signalling may explain teratogenic heart defects caused by both compounds

The most enriched mutant in the lithium screen had an insertion in a gene named loser A (lsrA), which also confers resistance to VPA (Tables A7.3, A7.4). LsrA was originally identified in a REMI screen identifying genes that affect stalk/spore fate choice (269). LsrA mutant cells form significantly more stalk cells in chimeric and clonal development. LsrA encodes a nulp1-like basic helix-loop-helix family transcription factor (bHLH), which is most similar to the human bHLH gene, TCF25 (269,270). TCF family transcription factors are ubiquitous major endpoint mediators of Wnt signalling (271). Lithium is a direct inhibitor of GSK3, a major component of many different signalling pathways and a core component of canonical Wnt signalling (272). Recent work on the *Drosophila* TCF25 homolog, dNULP1, shows it acts as a cofactor in developmental Wnt

signalling pathways and is essential for femur development and embryo survival (273). The *D. discoideum* genome has previously been shown to contain GSK3 and β-catenin homologs, however, transcription factor components associated with the Wnt signalling pathway have not been reported (274). With the discovery of a TCF/LEF transcription factor homolog in our lithium screen, we propose that lithium's direct impact on Wnt signalling in *D. discoideum* may be more analogous to its toxic effects in higher eukaryotes than previously thought (274). In light of this, it is interesting to note that the fifth highest ranked lithium advantage mutant had an insertion in fslE (Table A7.3), which encodes one of twenty-five reported frizzled-like receptors in the *D. discoideum* genome (274). Although frizzled proteins are a diverse class of receptors, they are also well known to play a role in Wnt signalling (275).

It is also interesting to note that ablation to LsrA also confers resistance to VPA (Table A7.4). This suggests that LsrA function may link the effects of lithium and VPA. One reason for this may be due to one the best characterised cellular targets of VPA, HDAC inhibition (176). Indeed, the fifth most abundant VPA resistant mutant had an insertion in hdaC, a gene with a histone deacetylase catalytic domain (Table A7.4). However, there may be a link between TCF/LEF transcription factors and HDACS. This is because TCF/LEF transcription factors can act as transcriptional activators or repressors. In the context of Wnt signalling, the presence of Wnt ligands activates β-catenin, causing it to translocate into the nucleus. β-catenin then binds to TCFs, activating the transcription factor and initiating a transcriptional switch towards gene expression. TCF regulation of transcriptional switching is mediated via the regulation of histone modifications, with gene repression caused by the recruitment of HDACs. Therefore, the similar lithium and VPA toxicity resistance exhibited by a lsrA mutant could be explained by both GSK3 attenuation of Wnt signalling and the gene expression mediation by HDACs recruitment to specific genes.

We noted that the human lsrA homolog, TCF25, is expressed during early human embryonic development with especially high expression in heart tissue where it plays a role in embryonic heart development (276). Moreover, Wnt signalling activity has widely being shown to play an important role in early heart development (277). This is interesting as heart defects (specifically Abstein's anomaly) are the most prevalent teratogenic abnormalities caused by lithium (278,279). Heart defects and cardiovascular defects are also one of the most consistent adverse outcomes presented in foetal valproate syndrome (172). In fact, specific heart defects associated with lithium teratogenicity, such as Abstein's anomaly, are also common after VPA exposure. As

lithium and VPA both result in heart defects and the loss of a Wnt signalling component, LsrA, confers toxicity resistant to both compounds, raises an interesting mechanistic link between the two compounds. This observation suggests that teratogenic heart defects induced by lithium and VPA exposure could be due to alterations in TCF25 activity in developing heart tissue. Consequently, it would be interesting to determine which genes are directly regulated by lsrA and thus further investigate its role in mediating lithium and VPA toxicity.

4.5.2 Discussion summary

Overall, the forward genetic evaluation of the toxicological mechanisms of lithium and VPA in proof of principle REMI-Seq screens has validated the ability for *D. discoideum* to function as a genetic evaluation model. The results in this chapter have demonstrated how the mechanistic relationship between two compounds can be established using global genetic phenotyping. The results also identify the biological processes affected by both test compounds, providing a foundation from which to further characterise the teratogenic compounds in the future. Together with chapters 2 and 3, the results presented this chapter provides compelling evidence for the use of, and continued research into, *D. discoideum* as a model for the evaluation of teratogenic compounds.

Chapter 5 – Discussion

5.1 Introductory remarks

This study aimed to evaluate whether *D. discoideum* could predict, compare and understand the molecular mechanisms underlying developmental toxicity. The first objective was to develop new HTP assays in *D. discoideum* (Chapter 2) that could be used to assess toxicity. A cohort of test compounds was selected (Section 2.4.1) and evaluated using these HTP toxicity assays (Sections 3.4.3, 3.4.5). This allowed toxicity in *D. discoideum* to be compared to mammalian toxicity values, illustrating that it is broadly predictive of *in vivo* mammalian toxicity (Sections 3.4.8). The second objective was to assess the potential for *D. discoideum* genetics, specifically REMI-Seq genetic technology, to allow unbiased 'genetic phenotyping' (Chapter 4). Proof of principle screens were conducted on two teratogenic compounds, lithium and VPA. This revealed a variety of molecular and biological pathways affected by each compound. Furthermore, it revealed that the effects of these compounds are shared more extensively than previously thought. Together these studies illustrate the power of *D. discoideum* to function as a model system for the evaluation of teratogenic compounds.

5.2 Can *D. discoideum* provide a teratogen evaluation model that combines HTP analysis with biological complexity?

It has been suggested that the ideal alternative developmental toxicity model must have sufficient biological complexity to be predictive of mammalian *in vivo* toxicity (1). Yet, the ideal model system must also allow HTP screening, and thus be low cost. However, increased biological complexity (and therefore predictivity) generally decreases as throughput increases, and cost decreases. This dichotomy lies at the heart of alternative model system design and has led to two broad classes of model system: complex, whole organism-based systems and, simpler, cellular-based systems (1) (Section 1.2). This project was established in order to determine if *D. discoideum* could break this relationship; a HTP model with sufficiently high *in vivo* biological complexity. This first required new HTP growth and developmental toxicity assays to be optimised and validated (Sections 2.4.2, 2.4.3). The new toxicity assays were conceived to be HTP in an academic laboratory setting. However, they have the potential to be further scaled up for use in an industrial setting, allowing for an even greater number of compounds and doses to be assayed. For example, the time-lapse microscopy approach to constructing our growth assay (Section 2.4.2), in tandem with the application of multi-

welled plates and programable stage allowed us to process 32 conditions simultaneously using 96-well plate format. Under our standard assay conditions, cells are imaged for just 48 hours (Methods section 6.5) and image processing of a standard 96 well assay took approximately 2 to 3 h. Therefore, a typical workflow from initial cell culture setup to final data processing could be completed in less than 3 days. However, the HTP capacity and the data analysis turnaround time could be improved with future optimisations. The first consideration for increasing sample capacity would be to use plates with a greater number of wells. By simply optimising the assay to a 384-well plate format the capacity would increase 4-fold over our current 96-well setup. During the improvement of a HTP yeast growth assay the transition from a 96- to 384-well format was reported to produce identical growth curves (280). There is no reason to assume that this would not be possible in *D. discoideum*. Another key to increasing throughput comes through reducing all aspects of the protocol that require manual input. For example, despite using a programable microscope stage, we found that manual input of Z axis coordinates was need for most (if not all) wells before the start of an experiment. This process could take up to 30 minutes for a 96-well dish. A similar problem was reported during the development of a HTP growth assay for adherent human lung fibroblast cells (281), which like *D. discoideum* cells require a solid substratum to grow on. If this is made of agar it can be variable in height from well to well, thus making cell focussing difficult (281). Therefore, to facilitate HTP analysis (in a 384-well format) a autofocusing procedure was used to ensure imaging accuracy in every well, without the need for manual observation and input (281). Incorporating a similar autofocusing method into our HTP growth would clearly be required in order to scale up the process.

We also developed a FPR-based developmental toxicity assay that utilises fluorescent reporter strains to measure progression through development when challenged with toxic compounds (Section 2.4.3). Due to the quick 24-hour time period required for a complete laboratory *D. discoideum* development, our developmental toxicity assay under standard conditions could generate developmental toxicity data in under 2 days. To our knowledge this development assay is the most HTP that has been reported for *D. discoideum* and is a significant improvement over previous assays (132). Currently, our assay uses 6 reporter strains which were chosen because of their temporal developmental expression profile (Section 2.4.3). However, the assay is highly customable. New reporter strains that report on cell types or specific temporal periods of development, or even specific signalling pathways could be generated to further refine the assay, dependant on whether a broader or more targeted developmental toxicity survey is required. For example, a mouse embryonic stem cell assay for detecting

embryo toxicity has been improved by developing fluorescent reporters for components of signalling pathways required for cardiomyocyte differentiation and cardiac morphogenesis (70). A similar approach in *D. discoideum* using reporters for the major developmental signalling pathways associated with terminal cell differentiation would allow for a more targeted and thus precise readout of developmental toxicity. Moreover, in our current assay changes to *D. discoideum* cell type differentiation is assessed using a single prespore and prestalk marker (Figure 2.6). It therefore, currently only provides a broad readout for abnormal cell type differentiation. However, multiple subtypes of prestalk cell have been characterised (Figure 1.6). Furthermore, it is known that different signalling pathways function to create the subtypes of prestalk cells, with the signalling molecule DIF-1 essential for PstB cell differentiation but not PstO or PstA (92,282) (Figure 1.6). By using only cell type reporters in the FPR assay, this would align the model more closely to cell-based alternative model systems (Section 1.2.3) where cells are challenged to terminally differentiate in the presence of toxic compounds (283). However, a readout would be possible in 24h, which is significantly faster than the 6 to 10 days required for the mouse or human EST assays (64,70). Finally, by using one fluorescent reporter strain that reported on the completion of a fruiting body (Section 2.4.3), a binary developmental toxicity screen could be developed. This could be used for the preliminary screening of large compound libraries for an initial gauge of developmental toxicity potential.

The HTP development assay has readouts that do not require expertise in *D. discoideum* developmental morphology. An important consequence of this is that it should permit future harmonisation of *D. discoideum* developmental toxicity testing. This is important because one of the most problematic aspects of current zebrafish developmental toxicity research has been to unify and harmonise the guidelines for testing procedures and data scoring (53,185). A reason for these limitations in the zebrafish system is the inherent biological complexity of the model (210). This has led to scoring systems which require expert analysis (57,284,285). The FPR based assay reported in this thesis avoids this pitfall, as the developmental toxicity readouts are simpler and easier to interpret (Figure 3.9). In fact, they exhibited a 95 % success rate (Section 3.4.5) when compared to ‘expert’ observations of developmental toxicity.

One area that could improve the HTP potential of both assays would be to increase the level of automation of the assays themselves, as well as the analysis of the resulting data. Other alternative models for developmental toxicity testing (Introduced in section 1.2) such as zebrafish, whole rat embryo and mouse embryonic stem cell assays have

all been improved through automation (1,50,286) and the use of robotic platforms (287). In the last decade robotic systems capable of storing compound collections, incubating, counting and dispensing cells into multiwell plates and performing specific assay steps, have become broadly accessible for toxicity screening procedures (219,287). A wide range of toxicity assays have been adapted to robotic platforms, including: biochemical and cell-based assays. Cell-based robotic assays display a wide range of endpoints and measurements including: fluorescent reporter genes and cell growth or cell death, measured by fluorescence or cell counting (219,287). Although custom robotic platforms for cell-based growth assays are highly variable in setup, generally they can screen libraries of >300,000 compounds with up to a seven-point dilution series, using over >1000 multiwell plates (287). The use of a robotic platform to increase HTP capacity would thus allow both the *D. discoideum* growth and development assays to be implemented in industrial scale toxicity screening studies.

Data processing and analysis is perhaps the most time consuming and labour-intensive part of developmental toxicity screening in *D. discoideum.* Therefore, to increase its HTP potential, particular attention should be paid to automating these processes. For example, automated image analysis pipelines need to be generated for the growth toxicity assay. Furthermore, key readouts such a cell doubling time could be automatically extracted from the growth curves. In other research fields (such as microbial phenomics) where the ability of generate large quantities of data had outpaced the ability analyse the resulting data, automated software has been crucial (288). Furthermore, a machine learning algorithm could be used to identify recurrent patterns from the reporter strain data that match (previously characterised) specific adverse phenotypes (Section 2.5). For example, the use of fluorescent reporter data from compounds known to causes specific phenotypes (i.e. aggregation defects, stalled mounds etc.) could be used to teach a machine learning algorithm how to interpret the newly generated data. Furthermore, by establishing an automated, machine learning platform to analyse the results of the FPR assay, its accuracy may be improved, as subjective interpretation is replaced with automated procedures. Indeed, the use of machine learning (over subjective manual interpretation) has been demonstrated to significantly improve the ability to diagnose cancer prognosis based on imaging data (289). Consequently, future work in optimising the workflow and speed of growth and developmental toxicity evaluation in *D. discoideum* would allow for the system to be adopted into industrial use.

5.3 *D. discoideum* can predict mammalian toxicity values

D. discoideum development is relatively complex, with many morphological and signalling processes that are analogues to higher eukaryotic embryonic development (Section 1.3.2.5). It is generally thought that increased complexity increases toxicological predictivity (1). However, a modified mouse embryonic stem cell assay been reported to predict ~72 % *in vivo* teratogenicity against a test cohort of 65 compounds (71). Thus, despite the lower complexity of cell-based assays, toxicological predictivity can be high. These results suggest that whilst biological complexity is important, using a relevant readout from which to measure developmental toxicity is also critical. In fact, we find significant correlations between the *D. discoideum* and rat developmental toxicity data (Figure 3.12). These suggests that a models' level of developmental complexity is irrelevant as long as the genetic complexity is sufficient to allow toxicological predictivity across a range of targets and pathways (Section 1.3.1). In general, we found that a larger dose was required to cause growth toxicity (over developmental toxicity) in *D. discoideum* (Figure 3.10). However, none of the compounds we tested was significantly more or less toxic in growth or development (Figure 3.10). This result suggests that none of the compounds adversely affect biological processes and pathways that are specific to the developmental cycle (or vegetative growth). This is surprising as high depth transcriptomics has revealed that *D. discoideum* development is characterised by large scale gene expression changes at the start development, as developmental genes switch on and vegetative genes switch off (201). It is, however, possible that testing a greater number and range of test compounds may reveal developmentally toxic chemicals that do not affect cellular growth.

Alternative teratogen evaluation models need to predict mammalian toxicity. In this research, we used an observable toxicity threshold (NOAEL/LOAEL) to compare *in vivo* rat data to the equivalent values in *D. discoideum* for both growth and development (Section 3.1). This is because, LOAEL/NOAEL comparisons are considered reasonable in developmental toxicity comparative studies if the direct exposure to the test compound occurs during the major stages of organogenesis (185,221). In *D. discoideum,* it is appropriate to compare the consistent exposure of the test compounds throughout development to *in vivo* animal studies where exposure is persistent through all major stages of organogenesis (185,214). For this measure, rat toxicity data is most widely available and is therefore generally considered to represent the gold standard for any comparison to *in vivo* data (188). Rat data is thus the foundation for our study, and previous validations of alternative developmental toxicity models (20,41,44,185,290). We found that *D. discoideum* growth toxicity values significantly correlate with acute (LD_{50})

and repeat dose measures of rat toxicity (Figure 3.12). Furthermore, the rat fetal teratogenic measurements significantly correlated to the developmental toxicity threshold in *D. discoideum* (Figure 3.12). Collectively, these results provide compelling evidence that *D. discoideum* can predict mammalian developmental toxicity (20,132). The power of the results presented in this thesis are strengthened by the quantity of test compounds used in our analysis. Our assessment in *D. discoideum* was based on 27 teratogenic compounds. Our study is thus close in scale to later stage multi-institutional alignment studies in zebrafish assay development which use ~ 25 to 40 compounds (52,61,185). Furthermore, despite developing our own protocol for selecting test compounds, a large proportion overlap with chemicals used to validate other alternative models (1,290). Additionally, of the 10 non-teratogenic control compounds used in our research, a significant number have widely been used in the validative studies of other groups in different model systems (52,57). In this primary phase study into the potential of *D. discoideum,* our test cohort thus represents an excellent spectrum of chemicals, both toxicologically and structurally (Appendix table A7.1).

Our approach to alternative model validation was based on a strategy proposed by Daston *et al*, (2014) (221), which concluded that previous attempts to validate alternative model systems should not simply rely on their ability to classify compounds as teratogenic or non-teratogenic. Compound classification should also consider the dependence of developmental toxicity on exposure levels. Daston *et al* (2014) thus proposed testing a series of well characterised test compounds at positive and negative exposure doses. This approach aligns well with the work presented in this thesis. Interestingly, the developmental toxicity data for five teratogenic compounds used in this study and are also present on Daston *et al's* guideline list and their toxicity would have been correctly predicted.

5.4 The advantage of a genetic phenotype vs morphological phenotype

The morphological phenotype that arises in response to developmentally toxic compound exposure is the most commonly used method to monitor toxicity (218). Phenotypic analysis is also used in alternative teratogenic model systems, such as whole embryo-based models (zebrafish, xenopus, whole rat embryo). However, quantitative measurements of morphological changes are difficult and instead qualitative readouts are generally generated (1). Furthermore, toxicity may result in subtle phenotypes which are difficult to detect. Finally, entire categories of adverse phenotypic outcomes, such as adult behavioural changes, may not be possible to assess by traditional observation-

based assays (218). To address these problems, early research on zebrafish systems resulted in the development of scoring systems to quantitate phenotypic toxicity (57). More recently, research in zebrafish has focussed on the development of software which can automate and quantify the measurement of morphological change in teratogen treated embryos (210). However, despite these different approaches, the complex biological processes behind the simpler phenotypic scoring inevitably results in reductive (albeit quantitative) measurements of developmental toxicity. Furthermore, by only assessing the final adverse outcomes, it generally does not allow the molecular initiating events and subsequent events that mediate chemically induced toxicity to be considered. As a result, cell-based alterative models (such as mouse or human embryonic stem cell tests – Section 1.2.3) have been designed to allow quantitative measurement of developmental toxicity (283). However, this is facilitated by limiting developmental complexity and thus the number of endpoints measured (283). In human embryonic stem cell tests, developmental toxicity is quantified by measuring the effect of chemical exposure on the differentiation of myocardiocytes (64). However, such simplified readouts mean the resulting data is often insufficient to understand the underlying mechanisms of toxicity. Thus, these alternative developmental toxicity models are most suited to developmental toxicity screening rather than the characterisation of the underlying toxicity mechanisms.

As the number of novel chemicals and pharmacological classes increases, there is an increasing need to characterise the molecular on- and off-targets of these compounds. In addition, even though more new compounds are being synthesised each year, the amount of new annual registered chemical has remained static, largely due to late stage failures in toxicity compliance (1). As developmental toxicity testing accounts for the some of this compliance failure, the need for further studies of the targets and molecular mechanisms affected by compounds that fail or succeed in developmental toxicity testing procedures is critical. This need has led to an increased use of current alternative developmental toxicity models (especially zebrafish) for characterising mechanisms of developmental toxicity. It has also led to a newer field of study, known as toxicogenomics, that attempts to link toxicity (including developmental toxicity) with genetic data (291). In most systems, transcriptomics has become the most widely used method within this field. Gene expression changes induced by chemical-mediated teratogenicity are reported as a means to describe the mechanism by which specific chemicals cause defects (291). Generally, these studies can take two approaches: the targeted assessment of specific genes expression changes or global assessment of RNA expression changes (291). For example, after observing a range of heart and tail

malformations in perfluorooctaneesulfonate (a persistent environment pollutant) treated zebrafish embryos, Shi *et al*, hypothesised that an increase in apoptosis could explanation for phenotypes (292). qRT-PCR revealed increases in the expression of genes associated with DNA repair, which was indicative of chemical-induced DNA damage and subsequent increase in apoptosis (292). In addition, global RNA sequencing can now be used to identify large scale changes in transcription profiles after toxic chemical exposure, which in turn can be used to identify gene networks associated with toxic mechanisms of action. For example, Zheng et al (2018) used RNA-Seq to report that specific liver genes are differentially expressed after toxic iron sulphide treatment in zebrafish, again identifying enrichments in genes associated with DNA repair and oxidative stress (293). Such studies could be invaluable for toxicity characterisation and comparison, as they provide a transcriptional phenotype (rather than morphological) across a class of related compounds (294). This is illustrated by studies in which the developmental toxicity phenotypes and genome-wide transcriptomics profiles were compared across 16 teratogenic polycyclic aromatic hydrocarbons to identify genes specific to developmental toxicity phenotypes (294). However, despite the increased use of toxicogenomic studies there are many limitations. There are different study designs using a range of 'omics approaches in addition to transcriptomics, including genomics and metabolomics. This makes integrating toxicity MOA data from these studies into a useful and centralised database difficult.

Furthermore, toxicogenomics studies can only be carried on a smaller scale and are thus mainly suitable in academic research. For example, targeted studies require the adverse phenotypes to be characterised before toxicogenomic assessment and are thus low throughput. Global characterisation methods such as RNA sequencing also have limitations. The approach is costly, especially if large numbers of chemicals are to be tested, or if multiple time points are needed. Furthermore, these studies rely on gene expression changes being closely linked to chemical mediated toxicity. However, developmental failure will often result in highly pleiotropic changes in gene expression that are unrelated to the proximal effects of the compound. Finally, some toxic compounds have even been reported to result in minimal transcriptional changes (234).

The REMI-Seq approach described here provides an alternative to transcriptomics as a toxicogenomic tool. It generates an unbiased genetic 'phenotype' to evaluate developmental toxicity (Section 4.4). Although our REMI-Seq teratogen screen is not truly HTP, the relatively quick turnaround of ~ 6 weeks (from screen start to finalised data analysis) represents a significant improvement for target evaluation in comparison to

other alternative models (86). The use of *D. discoideum* forward genetics to evaluate the targets of teratogenic compounds is strengthened in two aspects: firstly, by the genetic complexity of the mutant pools; and, secondly, by the quantity of valid mammalian homologs in the *D. discoideum* genome. It contains over 17,000 insertional mutants in over 5,800 genes. The REMI-Seq assay is thus a robust method to evaluate the toxicological targets of teratogenic compounds. It allows for toxicogenomics to be conducted on more compounds than is currently possible, increasing the viability of evaluating compounds for developmental toxicity genetically.

To test the utility of a REMI-Seq approach, we evaluated the relationship between the effects of lithium and VPA. This approach allowed a genome wide assessment of each chemical's toxicity profile. Indeed, risk assessments for multiple mechanistically related compounds is seen as a critical challenge for the future of developmental toxicity evaluation (227). However, it is generally thought that only hypothesis-driven testing will allow such analyses to be low cost and high throughput (227). This is because hypothesis-driven testing uses existing toxicological information (227) which allows phenotypic outcomes or dosages to be chosen prior to testing. An increased molecular and genetic knowledge of teratogenic mechanisms across a large spectrum of chemical classes, together with appropriate HTP assays, will improve these approaches. Our results suggest that the *D. discoideum* based REMI-Seq assay can fulfil these toxicological needs. Firstly, we were able to establish a mechanistic relationship between lithium and VPA, compounds with well characterised commonality in mammalian biology (e.g. mood stabilising, teratogenic). Secondly, by characterising the targets and biological processes affected during lithium and VPA toxicity we are able to demonstrate how mechanistic knowledge required for hypothesis-driven testing could be acquired. This is exemplified by our use of GO term analysis to identify biological processes affect by lithium and VPA toxicity. Furthermore, we were able to use the identified biological processes to form hypothesises which could be experimentally tested (Section 4.4.9). As more compounds are screened using REMI-Seq, a library of key genetic loci associated with toxicity can be established. Ultimately, we envisage that genetic phenotyping could be used to identify compounds with an increased teratogenic risk prior to *in vivo* animal testing. This will require a greater number of compounds to be evaluated by REMI-seq. For this, tests with different members of the pharmacological compound class of mood stabilisers would provide good test compounds for a phase two study. For example, lamotrigine and carbamazepine are also mood stabilisers and teratogenic compounds. However, they structurally differ and are in a different pharmaceutical class to lithium and VPA. Indeed, the preliminary results of a lamotrigine

REMI-Seq screen resulted in the identification of different advantaged and disadvantaged mutants to those enriched by lithium or VPA (data not shown). It will thus be interesting to characterise these targets, as well as extend these studies to other mood stabilisers. For example, carbamazepine is an also anti-epileptic compound and thus may have more common on-target effects with VPA (152). Future studies should reveal that REMI-Seq can genetically phenotype toxic compounds and thus establish a method for globally evaluating teratogenic compounds.

5.6 Concluding remarks

We have performed a phase one study to demonstrate the potential of *D. discoideum* to function as a new alternative developmental toxicity evaluation model. Using a comprehensive set of test compounds, we have shown that both *D. discoideum* growth and developmental toxicity values significantly correlate to mammalian *in vivo* data for acute, repeat dose and developmental toxicity. Furthermore, we have established a significant relationship between the growth and developmental toxicity endpoints in *D. discoideum* and the rat model. For this, we developed custom HTP toxicity assays for *D. discoideum* that demonstrate the capacity for screening large libraries of compounds and highlight how the model could be adopted into industrial use. We also provide evidence that genetic phenotyping of developmental toxic compounds provides an important tool for toxicogenomics. Proof of principle forward genetic REMI-Seq screens on lithium and VPA, suggest this method can be used to provide a detailed, but unbiased, method for classifying toxic compounds. This allowed the mechanistic relationship between lithium and VPA to be better established, whilst simultaneously identifying the biological process and targets mediating their toxicity; highlighting future areas of research into their biological mechanisms of action. Together, these studies suggest that *Dictyostelium* provides a useful alternative model for developmental toxicology that should be subjected to secondary phase evaluation studies with larger sets of test compounds. Furthermore, the translation of this research into an industrial research setting would also require further optimisation and automation of the HTP assays we developed. Such future research would build upon the significant findings of this study and could place *D. discoideum* as a key player in the battery of alternative developmental toxicity evaluation assays. Introducing a new 3R's model for teratogenic compound evaluation.

Chapter 6 – Methods

6.1 *Dictyostelium* cell culture, storage and development

Unless specified otherwise, the *D. discoideum* strains used in this work were axenic strain 4 (Ax4) or strains derived from Ax4. DpoA single gene deletion strain and its parental Ax2 cell line were obtained from the Dictybase stock centre (295). All strains were grown in HL5 growth media (1% peptone, 0.72% yeast extract, 1.54% glucose) supplemented with Penicillin G, Streptomycin sulphate, folate and vitamin B12 or maintained on a lawn of *Klebsiella aerogenes* (*K.a*) on standard media plates (1% glucose, 1% peptone, 0.1% yeast extract, 2% agar). General growth, growth assays and experimental developments were all conducted at 22°C. All fluorescent strains containing an extrachromosomal expression vector were supplemented during growth with G418 (20 µg/ml), which was removed 48 hours prior to experimentation (84). All strains were experimentally used for approximately 4 weeks before new cells were revived from storage. Aliquots for all strains were stored in freezing media (45% HL5, 45% FBS, 10% DMSO) at -80°C.

For all developments exponentially growing cells from axenic media were harvested at a concentration between $5x10^5$/ml and $2x10^6$/ml and washed twice in KK2 buffer (16.1 mM KH2PO4, 3.7 mM K2HPO4). Cells were re-suspended in KK2 at a concentration of $4x10^7$/ml. For 96- and 24-well plate experiments, 100 µl or 1 ml of 1.5% KK2 agar per well was used for the developmental substratum. For 96- and 24-well plate experiments 5 µl or 20 µl of cell suspension was plated per well and spread evenly across the surface, respectively. All development plates were incubated in the dark at 22°C in a humid environment.

6.2 Test compounds

Test teratogenic and non-teratogenic compounds were selected in a multi-step process (Figure 2.1). The test compounds represent a range of different physical chemical properties and biological mechanisms of action. All compounds were procured from Sigma-Aldrich (Section 2.4.1). The experimentally required dilution was freshly prepared in the relevant solvent (Table 2.1) before each experiment.

6.3 Collection of *in vivo* mammalian toxicity datasets

In vivo rat toxicity data sets were collected for three endpoints: acute toxicity (LD_{50}), repeat dose toxicity and developmental toxicity (Rat foetal teratogenicity). For the oral administrative route 100% bioavailability was assumed. In order to allow for more comparative doses, if non-toxicity was reported for developmental toxicity in every published study the highest dose tested was used. All values were converted to molarity from mg / kg doses assuming that 1 kg of mammalian body weight is equivalent to 1 L (188).

Acute toxicity data was collected using LD_{50} values (215). In order to have consistency across the acute toxicity dataset only oral administrative values were collected. Values were obtained using the FDA drug registration label (296). Values were also collected from both ChemIDplus and the Hazardous Substances Data Bank (HSDB) (297). If there were any inconsistencies between values obtained from difference databases the lowest value was used. Rat repeat dose toxicity values were split into two datasets dependant on the dosing length of the study: 'subacute' for studies ≥ 7 - ≤ 28 days and 'subchronic' for studies 3 – 6 months. A literature search was conducted to collect the repeat dose toxicity values: with toxicity databases (ChemIDplus, Pubchem, Hazardous Substances Data Bank), research papers, FDA drug registration labels and manufacture's material safety data sheets and product monographs used in collecting the values. Where possible the NOAEL and LOAEL value defined in each studies observation was recorded. For the rat developmental toxicity endpoint, the LOAEL value for teratogenicity in rat foetus was collect for the test compounds. To maintain consistency in the dataset only oral administrative values were collected. LOAEL doses were collected for the developmental toxicity endpoint as not all studies achieve a NOAEL, increasing the consistency across the dataset. Values were obtained using the FDA drug registration label (296). Values were also obtained using a UK committee on toxicity report which contained toxicological information concerning some of the non-teratogenic control compounds (216).

6.4 Construction of the fluorescence plate reader assay reporter strains

Primers for genes (DDB_G0273495, DDB_G027957, DDB_G0273641, DDB_G0284529, DDB_G0286321, DDB_G0295685, DDB_G0290855, DDB_G0280847, DDB_G0270722, DDB_G0274335) were designed to amplified the promoter region from ~1Kb upstream of the genes to just within the coding region. The primers were designed to keep the sequence in reading frame. The forward and reverse primers were modified adding a XhoI and BglII restriction sites, respectively. For DDB_G0274335 a BamHI site as added to the reverse primer as the promoter region contained a BgIII site. The promoter regions were amplified by PCR and digested with the appropriate restriction enzymes. Extrachromosomal RFP expression plasmid, pDM324, was digested with XhoI and BglII/ BamHI (84). The amplified promoter fragments were then ligated into pDM324.

The pDM324 promoter constructs were transformed in Ax4 cells suspended in H50 buffer (50 mM Hepes, 50 mM KCl, 10 mM NaCl, 1 mM Mg_2SO_4, 5 mM $NaHCO_3$, 1 mM Na_2HPO_4, pH 7.0) at a concentration of $2x10^7$/ ml. 100 µl of cell suspension ($2x10^6$ cells) was added to a 0.1 cm GenePulser cuvette (Bio-Rad) together with 10 µg of DNA. The cuvettes were incubated on ice for 5 minutes, then electroporated twice with a 5 second recovery (925V, 25Ω, 25µF). After 24 hours the transformed cells were placed under G418 selection (10 µg/ml) for 7 days. The transformants were cloned out on *K. aerogenes* lawn SM plates and visually inspected for developmental fluorescence. Promoter constructs strains from genes, DDB_G0273495, DDB_G0273641, DDB_G0286321, DDB_G0280847, DDB_G0270722 and DDB_G0274335 were selected as aggregation, streaming, mound, slug, culminant and fruiting body reporter strains, respectively. An ecmA-RFP / Psa-GFP dual cell type reporter strain was kindly provided by Dr. William Salvidge. The construct was created by co-transformation of Ax4 with pDdGFP- PspA and pDdRFP-ecmAO. Positive co-transformants we manually inspected and cloned out on *K. aerogenes* lawn SM plates.

6.5 Semi-automated time lapse microscopy-based growth assay

Cells were grown in HL5 media and harvested during exponential growth at a concentration between $5x10^5$/ml and $2x10^6$/ml. Cells were resuspended in fresh HL5 media at concentrations of $1x10^4$ cells per ml with 100 µl or 1ml of suspension plated per well in either a 96 or 24 well, respectively. Plates were kept stationary for 20 minutes allowing cells to settle and attach to the base of the well. Cells were filmed at a 4x magnification using an Olympus IX71 microscope augmented with a programmable

automated stage (Prior). Films were shot with a frame rate of 7.5 minutes during early optimisation and 1 hour in all subsequent growth assays for either 24 or 48 hours. Growth assays conducted in a 24 well plates implemented three to five technical replicate films per well whilst 96 well plates assays were conducted using three replicate wells per treatment. Images from individual growth films were stacked and inverted using ImageJ software (Fuji). Cell number per frame over the whole of the inverted film was extracted using the 'trackmate' plug-in for ImageJ. Growth rate was assessed by calculation of the doubling rate between 8-24- or 8-48 hours dependant on the length of the assay. When growth rate was assessed with the addition of a test compound a maximum solvent concentration of 1% was used. For test compound toxicity profiling, doubling rates were normalised to the control and tested for significance using a one-way ANOVA test (GraphPad – Prism).

6.6 Fluorescence plate reader based developmental assay

All developments assayed were set up in 96 well plate format and with the exception of initial agar background signal optimisation, black opaque fluorescent 96 well 'visionplates' (4titude) were used and found to reduce background signal in all conditions tested. All test compounds were dissolved in the agar prior to developmental exposure, with a maximum solvent concentration of 0.5%. A Synergy H1 (Biotech) multi-mode plate reader was used to measure fluorescent signal as adjustable Z focus and the ability for a top-down read were technical features found essential to detecting a signal from developments. GFP and RFP signals were measured using 485/528, 532/610 excitation/emission wavelengths, respectively. Developments conducted within the plate reader were incubated at 22°C with readings taken every 2 hours. Background signal was defined as the signal detectable from a well containing only agar. Fluorescent reporter strain data was normalised to timepoint 0h. After every FPR assay, plates were manually inspected to assess whether the control developments had progressed normally.

6.7 Qualitative *D. discoideum* developmental toxicity assessment

A dose range was defined for each test compound using the NOAEL growth toxicity dose as a middle anchor dose. From this dose three doses, 5-, 25- and 125-fold lower were assayed and two, 5- and 25-fold higher doses. The developmental toxicity assessments were conducted from 24-well plates developments (Section 3.4.4) with duplicate wells for each dose assayed. The compounds were dissolved into the agar

prior to the experiment with a maximum solvent concentration of 0.5%. The developments were visually inspected after 4h, 8h, 12h, 16h, 20h, 24h and 48h (timings of the major stages of development). The experimental developments were repeated up to three times over different weeks with only consistent toxic phenotypes recorded. Doses that caused any discernible change in developmental progression in comparison to control developments (at any development stage) were considered developmentally toxic (Teratogenic). Representative images were recorded at the mound, slug and/or fruiting body stage using a Lecia MZ-16-FA dissecting microscope with a Hamamatsu camera and HCImageLive software.

6.8 REMI-Seq Screens

6.8.1 Screen protocol

REMI-Seq pools created by Gruitheit *et al* (2019) containing ~23,000 mutants were hatched and split in two 10cm tissue culture plates in standard HL5 media (86). The pool was briefly allowed to recover and proliferate for 24h with care taken not to bottleneck mutant growth. The pool was allowed to grow to confluency (~$3x10^6$/ml) before being split into 3 populations for setup of 7.5 mM lithium, 1 mM VPA and 1% DMSO screens. Each screen was conducted with 2 biological replicate populations. For each biological replicate (for each screen) 3 10cm tissue culture plates were seeded at $2x10^5$/ml and grown until confluency (~3.5 generations). At which point the 3 plates of each biological replicate were pooled, counted and reseeded into 3 new plates at $2x10^5$/ml. The remaining cells were frozen down into multiple aliquots. This process constituted a single round for the screens and was repeated 5 times (~18 generations).

6.8.2 DNA sample processing and sequencing

Genomic DNA was obtained from cells from both replicates of rounds 2 and 5 for the DMSO, lithium and VPA screens. Frozen pool samples (25µl suspension of $2.5x10^5$ cells) were thawed directly into 400µl of an overnight culture of *K.a* and plated on a SM plate. The cells were grown overnight at 22°C until a clearing plate had formed but before *D. discoideum* development structures had formed. Nuclei were collected from ~ $5x10^8$ cells per sample that had been washed 6 times in 4°C KK2 (removing residual *K.a* cells) and resuspended in 30 ml nuclei buffer (40 mM Tris, pH 7.8, 1.5% sucrose, 0.1 mM EDTA, 6 mM MgCl2, 40 mM KCl, 0.4% NP-40 substitute, 5 mM DTT). The suspension was centrifuged at 4,000 g for 30 min, 4°C. The supernatant was discarded leaving pellets. The pellets were suspended in EDTA to a final concentration of 100 mM before adding 10% sodium lauryl sarcosyl (SLS) mixing and incubating at 55°C for 20 mins. 4M

ammonium acetate (250 µl) was added and the mixture was centrifuged at 20,000 g for 15 min at 4°C. One volume of supernatant was added to 2 volumes of 100 % ethanol, mixed and centrifuged at 20,000 g for 10 min, 4°C, from which the supernatant was discarded. The pellets were washed with 70% ethanol, dried and suspended in 50 µl of 10 mM Tris pH 7.8, containing RNase A and RNase T1 (10 U/ml and 400 U/ml respectively, Ambion). Finally, the gDNA samples were visualised by electrophoresis on a 1% agarose gel.

Each gDNA sample was prepared specifically for REMI-Seq sequencing as described by Gruitheit *et al* (2019). Briefly, the samples were digested with MmeI and I-SceI excising a DNA fragment contain the junction of the gDNA and REMI insert. Indexed adapters (D7 & D5) were ligated to the digested DNA. Different combinations of D7 or D5 indices were used to tag the individual samples for each screen and biological replicate. The DNA fragments were amplified by PCR, using primers specific to the ligated adapters. The samples were separated by gel electrophoresis and the resulting 183 bp DNA fragments were excised and quantified using a Qubit 3.0 Fluorimeter (ThermoFisher). Sample from rounds 2 and 5 were sequenced separately using a Illumina NextSeq 500 Sequencer with a High Output Kit v2 (75 cycles).

6.8.3 Sequencing data processing and analysis between the mutant pools of the DMSO and VPA or lithium screens

Upon receiving the sequencing reads from the Illumina sequencer the data was processed for REMI-Seq analysis as described by Gruitheit *et al* (2019). Using the REMI-Seq analysis script created by Gruitheit *et al* (2019), when a vector sequence was detected in the sequencing data (for each sample) the 6 bp index sequence was extracted along with a genomic tag resulting in a 19/20 bp tag sequence. Each tag and index combination was counted and finally compared to a pre-computed lookup table (86). These raw read counts were normalised (making comparisons across samples possible) using the total number of reads per sample and the total number of reads per insertion point. Insertion points and tags that could not be uniquely assigned to one position were removed. The analysis script was run on the round 2 and round 5 samples, separately.

Following sequencing data processing, mutants were binned according to their mean normalised DMSO replicate read counts for the round 2 and round 5 samples (bin 100 = <100 reads, bin 1,000 = 100-1,000 reads, bin 10,000 = >1,000 reads). Next, the log fold-change values relative to DMSO replicate mean read count were calculated for

each insertion mutant. This was completed for both replicates of the lithium and VPA screen, for rounds 2 and 5. To allow comparisons of mutants between the DMSO and lithium or VPA screens, data was normalised to have a mean of 0 with a standard deviation of 1 for each of the 3 bins of mutants. Mutants with a Z-score >1.5 (Thus >1.5 standard deviations from the mean of each bin) in each biological replicate for the lithium or VPA screens were considered to have an advantage. Similarity, mutants with a Z-score < -1 biological replicate for the lithium or VPA screens were considered to have a disadvantage. Mutants with fewer than 100 read counts in the DMSO screen that dropped out were discounted from this analysis because the technical dropout rate for these mutants is very high (86). Mutants were removed from the significantly advantaged or disadvantaged lists if they were found to have gene inserts in tRNAs, pseudogenes or transposable genetic elements.

6.8.4 GO term analysis

GO term analysis was performed using the GSEAbase R package (237). A significance cut-off of p=0.05 was used for significantly overrepresented biological process and molecular function GO terms. Gene lists containing 173 lithium genes (round 2 disadvantaged & round 5 advantaged), 235 VPA genes (round 2 disadvantaged & round 5 advantaged) and both lists combined (376 genes), compared against a gene universe of genes from every mutant in the starting library and all detectable mutants in either round 2 or 5 of the screen. The universal gene list was also modified to remove all gene excluded from the reference lists (tRNAs, pseudogenes, transposable genetic elements and non-promoter intergenic insertions). After the GSEAbase analysis the significant GO terms for biological process and molecular function were simplified using the REVIGO tool (238). The redundancy of the GO terms for both the biological process and molecular function lists was calculated and >0.5 threshold used to remove the most redundant terms (238).

The over-represented genes underlying the significant biological process and molecular function GO terms were classified as either advantaged (>1), neutral or disadvantaged (<1), using the mean replicate z score from the lithium and VPA screens. Then the BP and MF GO terms were classified as either uniquely lithium, VPA or common, dependent on the classification of the genes underlying them. The GO terms classified as common, were subclassified as either heterogeneous or homogenous dependent on whether the individual genes within a GO term behaved differently or similarly in both compounds, respectively.

6.9 Growth competition assay

Collective pools of REMI-Seq mutants or individual REMI-Seq mutants from the REMI-Seq-Bank (86) were assessed by growth competition assay. Ax4-GFP cells and the competitor cells were grown in tissue culture conditions until they reached similar levels of confluency. At which point the cells were harvested, counted and mixed together 50:50 to a cell density of $2x10^5$/ml then seeded into duplicate wells in a 24-well plate. The mixed cell populations were assayed with the addition of 1% DMSO and 7.5 mM lithium or 1 mM VPA with two technical replicates per condition. Cells were allowed to grow together until confluency (~3.5 generations), mimicking the conditions of each of the REMI-Seq screens rounds but in a 24-well plate format. The relative proportion of GFP- labelled to unlabelled cells was scored at the start as well as the end each round of the competition assays by flow cytometry (Attune NxT Flow cytometer). The competitions were continued until either the labelled or unlabelled cells were at 100% or 6 rounds were completed. The Competition data was normalised to the expected starting frequency (50:50). The competitions were further normalised as a ratio of the test mutant to GFP labelled cells (0-1). For validation of the putative advantage and disadvantage mutants a competition fitness score was calculated. The difference between the normalised drug and the non-drug treated competitions at rounds 3 and 6 (or the final round tested) was used to calculate the competition fitness score.

Competition fitness score calculation:

Round 3. Drug treatment ratio ÷ No Drug ratio = x
Final Round. Drug treatment ratio ÷ No Drug ratio = y
$\text{Log}(x \times y)$

6.10 Fluid uptake assay

A fluid uptake assay was performed as described by Williams and Kay (2018), but modified to work in a 24-well plate format. REMI-Seq mutants from the REMI-Seq-Bank and a control REMI-Seq mutant with a neutral intergenic insertion were tested using the assay. For each condition assayed, $1x10^5$ axenically growing cells were plated in triplicate in the wells of a 24-well plate. After settling in the wells for 20 minutes, 7.5- or 10 mM lithium or 750 µM or 1 mM VPA was added to non-control cells and the plate was incubated at 22°C for 23 hours. After 23 hours the HL5 media was aspirated and the cells incubated for 1 hour with 0.5mg/ml TRITC-dextran (Sigma Aldritch). 5- or 10 mM lithium or 750 µM or 1 mM VPA was added to non-control cells during the incubation

period. After 1 hour the TRITC-dextran was aspirated, the cells quickly washed in cold KK2. After which the cells from each well were collected in 1 mL ice cold KK2 + 5mM sodium azide (preventing exocytosis). Median fluorescence intensity was measured by flow cytometry (Attune NxT Flow Cytometer). All values were normalised to each mutants control, with 2 independent biological replicates performed per strain. A T-test was used to assess significance in the fluid uptake difference between the Ax4 REMI control and mutants' normalised fluid uptake at each dose tested (GraphPad – Prism). A mutant fluid uptake score was calculated by subtracting the mutants normalised median fluid uptake value from the mean of the Ax4 REMI control at either the 7.5 mM lithium or 1 mM VPA treatment.

6.11 Primers and Plasmids

Primers

Aggregation reporter promoter (Figure 2.7)

DDB_G0273495 – Forward - CGC**CTCGAG**TGTGAATTTGTATCTGACATT

DDB_G0273495 – Reverse – CGC**AGATCT**ACTTTCACTTGTTATATCTATCAT

Streaming reporter promoter (Figure 2.7)

DDB_G0273641 – Forward - CGC**CTCGAG**GGTAATTCTCCACAAGGTAGT

DDB_G0273641 – Reverse - CGC**AGATCT**ATCAAAAGTTGTAGATATAATATCCAT

Mound reporter promoter (Figure 2.7)

DDB_G0286321 – Forward **-** CGC**CTCGAG**AGGTTTCAATATATCATTCAT

DDB_G0286321 – Reverse **-** CGC**AGATCT**ACCTATTAAATTAATTAATAATTTCAT

Slug reporter promoter (Figure 2.7)

DDB_G0280847 – Forward - CGC**CTCGAG**GGTTTATATTATAATCTAGAAAATATA

DDB_G0280847 – Reverse - CGC**AGATCT**AAACTTACAAAAGAGTGTCAT

Culminant reporter promoter (Figure 2.7)

DDB_G0270722 - Forward - CGC**CTCGAG**CTAAATATTAATATCATCCCCATT

DDB_G0270722 – Reverse - CGC**AGATCT**AACCAAAATTACTTTTATTATTTTCAT

Fruiting body reporter promoter (Figure 2.7)

DDB_G0274335 – Forward - CGC**CTCGAG**TTGAGCTCTCTCCACTGAAAT

DDB_G0274335 – Reverse - CGC**GGATCC**AGTGGTTTTAATTTGATTTAAATCCAT

Plasmids

pDM324 – Act-15-C-term-RFP - (84).

7 - Appendix

Table A.7.1 Structural and physical characteristics of the test compounds.

Number	Compound Name	Classification	Molecular Weight	Structural Complexity	Polar Surface Area	ClogP
1	**Methotrexate** hydrate	Teratogen	454.44	704	212	-0.53
2	**Pemetrexed**	Teratogen	427.41	748	187	-1.17
3	**Lamotrigine**	Teratogen	256.09	242	90.7	2.53
4	**Carbamazepine**	Teratogen	236.27	326	46.3	2.38
5	**Phenytoin** sodium	Teratogen	274.25	350	58.2	2.08
6	**Primidone**	Teratogen	218.25	279	58.2	0.88
7	**Valproic Acid** sodium	Teratogen	166.2	93.4	37.3	2.76
8	**Lithium** chloride	Teratogen	42.39	2	0	-
9	**Acitretin**	Teratogen	326.43	539	46.5	6.07
10	**13-*cis*-Retinoic Acid**	Teratogen	300.44	567	37.3	6.74
11	**Retinoic Acid**	Teratogen	300.44	567	37.3	6.74
12	**Bosentan** hydrate	Teratogen	569.63	839	155	4.17
13	**Sitaxentan** sodium	Teratogen	476.89	720	144	3.44
14	**Bexarotene**	Teratogen	348.48	551	37.3	8.19
15	**Cadmium Sulphate** monohydrate	Teratogen	208.47	62.2	88.6	6.07
16	**Hydroxyurea**	Teratogen	76.05	42.2	75.4	-1.8
17	**Cyclophosphamide** monohydrate	Teratogen	279.1	212	42.6	0.8
18	**Cisplatin**	Teratogen	300.05	2.8	2	-
19	**Lead (II) Acetate** trihydrate	Teratogen	379.34	25.5	83.3	-
20	**Clomifene** citrate salt	Teratogen	598.08	708	145	7.15
21	**Raloxifene** hydrochloride	Teratogen	510.04	655	98.2	6.86
22	**Finasteride**	Teratogen	372.54	678	58.2	3.01
23	**Vinclozolin**	Teratogen	286.11	391	46.6	-
24	**Diethylstilbestrol (DES)**	Teratogen	268.35	286	40.5	4.96
25	**Salicylic Acid**	Teratogen	138.12	133	57.5	2.19
26	**Nifedipine**	Teratogen	346.33	608	110	3.12
27	**Warfarin** sodium	Teratogen	330.31	508	66.4	2.9
28	**Metoclopramide** hydrochloride	Non-teratogen	336.26	300	67.6	2.23
29	**Cefotaxime** sodium	Non-teratogen	477.45	839	230	0.14
30	**Sulfasalazine**	Non-teratogen	398.39	657	150	3.99
31	**Ascorbic acid**	Non-teratogen	176.12	232	107	-1.76
32	**Acebutolol** hydrochloride	Non-teratogen	372.89	401	87.7	1.71
33	**Camphor**	Non-teratogen	152.23	217	17.1	2.18
34	**Citric acid**	Non-teratogen	192.12	227	132	-2
35	**Penicillin G** sodium	Non-teratogen	356.37	536	115	1.75
36	**Saccharin** sodium hydrate	Non-teratogen	205.17	303	71.6	-
37	**Metformin** hydrochloride	Non-teratogen	165.62	132	91.5	-1.43

Table A.7.2 Mammalian toxicity datasets.

Compound Name	Acute Toxicity - LD_{50}	Repeat dose – Subacute - NOAEL	Repeat dose – Subacute - LOAEL	Repeat dose – Subchronic - NOAEL	Repeat dose – Subchronic - LOAEL	Rat Fetal teratogenicity – LOAEL
Methotrexate	135 mg / kg	0.06 mg / kg / d – 28 days	5.6 mg / kg / d – 28 days	n/a	n/a	0.2 mg / kg / d
Pemetrexed	980 mg / kg	0.285 mg / kg / d – 2 weeks	0.85 mg / kg / d – 2 weeks	n/a	n/a	1 mg / kg / d
Lamotrigine	205 mg / kg	11.5 mg / kg / d – 3 weeks	46 mg / kg / d – 3 weeks	10 mg / kg / d – 13 weeks	30 mg / kg / d – 13 weeks	10 mg / kg / d
Carbamazepine	1957 mg / kg	> 100 mg / kg / d – 28 days	n/a	n/a	n/a	200 mg / kg / d
Phenytoin	1635 mg / kg	n/a	50 mg / kg / d – 3 weeks	300 ppm / d – 13 weeks	n/a	100 mg / kg / d
Primidone	1500 mg / kg	500 mg / kg / d – 2 weeks	900 mg / kg / d – 2 weeks	20 mg / kg / d – 14 weeks	40 mg / kg / d – 14 weeks	120 mg / kg / d
Valproic Acid	670 mg / kg	250 mg / kg / d – 2 weeks	500 mg / kg / d – 2 weeks	378 mg / kg / d – 6 months	400 mg / kg / d – 90 days	100 mg / kg / d
Lithium	1530 mg / kg	n/a	1.46 mEq / L serum – 30 days	12.8 mg / kg / d – 4 months	25.6 mg / kg / d – 4 months	100 mg / kg / d
Acitretin	4000 mg / kg	5 mg / kg / d – 4 weeks	10 mg / kg / d – 4 weeks	3 mg / kg / d – 13 weeks	n/a	15 mg / kg / d
13-*cis*-Retinoic Acid	4000 mg / kg	15 mg / kg / d – 4 weeks	n/a	40 mg / kg / d – 12 weeks	n/a	30 mg / kg / d
Retinoic Acid	2000 mg / kg	5 mg / kg / d – 28 days	15 mg / kg / d – 4 weeks	4 mg / kg / d – 13 weeks	14 mg / kg / d – 13 weeks	2.5 mg / kg / d
Bosentan	1000 mg / kg	200 mg / kg / d – 28 days	2000 mg / kg / d – 28 days	15 mg / kg / d – 13 weeks	45 mg / kg / d – 13 weeks	75 mg / kg / d
Sitaxentan	980 mg / kg	80 mg / kg / d – 4 weeks	120 mg / kg / d – 4 weeks	20 mg / kg / d – 13 weeks	50 mg / kg / d – 90 days	20 mg / kg / d
Bexarotene	1500 mg / kg	n/a	10 mg / kg / d – 4 weeks	n/a	5 mg / kg / d – 90 days	4 mg / kg / d
Cadmium Sulphate	280 mg / kg	10 mg / kg / d – 28 days	20 mg / kg / d – 28 days	3 mg / kg / d – 3 months	8.58 mg / kg / d – 12 weeks	0.5 mg / kg / d
Hydroxyurea	5000 mg / kg	50 mg / kg / d – 2 weeks	500 mg / kg / d – 2 weeks	n/a	n/a	180 mg / kg / d
Cyclophosphamide	100 mg / kg	n/a	280 mg / kg / d – 4 weeks	6 mg / kg / d – 12 weeks	12 mg / kg / d – 12 weeks	6.2 mg / kg / d
Cisplatin	25.8 mg / kg	n/a	n/a	n/a	1 mg / kg / d – 11 weeks	0.25 mg / kg / d
Lead (II) Acetate	450 mg / kg	n/a	60 mg / kg / d – 4 weeks	n/a	7.5 mg / kg / d – 14 weeks	120 mg / kg / d
Clomifene	5750 mg / kg	n/a	0.5 mg / kg / d – 11 days	n/a	n/a	8 mg / kg / d
Raloxifene	> 5000 mg / kg	10 mg / kg / d – 4 weeks	n/a	25 mg / kg / d – 6 months	n/a	1 mg / kg / d
Finasteride	418 mg / kg	n/a	3 mg / kg / d – 2 weeks	80 mg / kg / d – 12 weeks	n/a	0.3 mg / kg / d
Vinclozolin	>10000 mg / kg	66 mg / kg / d – 4 weeks	180 mg / kg / d – 28 days	4 mg / kg / d – 3 months	22 mg / kg / d – 3 months	25 mg / kg / d
Diethylstilbestrol	3000 mg / kg	20 ug / kg / d – 3 weeks	40 ug / kg / d – 3 weeks	n/a	n/a	10 mg / kg / d
Salicylic Acid	891 mg / kg	n/a	646.5 mg / kg / d – 28 days	50 mg / kg / d – 17 weeks	500 mg / kg / d – 17 weeks	200 mg / kg / d
Nifedipine	1022 mg / kg	50 mg / kg / d – 4 weeks	n/a	100 mg / kg / d – 13 weeks	n/a	10 mg / kg / d
Warfarin	59 mg / kg	1 mg / kg / d – 21 days	2 mg / kg / d – 7 days	n/a	0.077 mg / kg / d – 13 weeks	0.16 mg / kg / d
Metoclopramide	750 mg / kg	n/a	n/a	100 mg / kg / d – 13 weeks	n/a	n/a
Cefotaxime	20000 mg / kg	300 mg / kg / d – 30 days	1000 mg / kg / d – 30 days	400 mg / kg / d – 13 weeks	800 mg / kg / d – 13 weeks	> 1200 mg / kg / d
Sulfasalazine	15600 mg / kg	600 mg / kg / d – 28 days	n/a	200 mg / kg / d	500 mg / kg /d	> 200 mg / kg / d
Ascorbic acid	11900 mg / kg	100,000 mg / kg / d – 14 days	n/a	10,000 mg / kg / d – 10 weeks	27.3 g/ kg / d – 10 weeks	n/a
Acebutolol	980 mg / kg	> 500 mg / kg / d – 14 days	n/a	75 mg / kg / d – 13 weeks	225 mg / kg / d – 13 weeks	> 1000 mg / kg / d
Camphor	>10000 mg / kg	1000 mg / kg / d – 7 days	2000 mg / kg / d – 7 days	n/a	464 mg / kg / d	> 1000 mg / kg / d
Citric acid	3000 mg / kg	4000 mg / kg / d – 2 weeks	9300 mg / kg / d – 2 weeks	n/a	n/a	> 2500 mg / kg / d
Penicillin G	>2000 mg / kg	2400 mg / kg / d – 2 weeks	n/a	750 mg / kg / d – 13 weeks	1500 mg / kg / d – 13 weeks	n/a
Saccharin	14200 mg / kg	30,000 mg / kg / d – 4 weeks	n/a	20000 ppm / d – 13 weeks	n/a	n/a
Metformin	1000 mg / kg	200 mg / kg / d – 2 weeks	1000 mg / kg / d – 2 weeks	200 mg / kg / d – 13 weeks	600 mg / kg / d – 13 weeks	> 600 mg / kg / d

Figure A.7.1 Qualitative toxicity descriptions and pictures. Figure over pages 206 – 221.

1. Methotrexate						
Dose	**40 nM**	**200 nM**	**1 µM**	***5 µM***	**25 µM**	**125 µM**
Aggregation 4h	Normal	Normal	Normal	Normal	Normal	Normal
Streaming 8h	Normal	Normal	Normal	Some loose streams | Mainly a lawn of aggregation minus	Aggregation minus | Some delayed loose mounds	Aggregation minus
Mound 14h	Normal	Normal	Normal	Hetrogenous development progression | Mounds still forming.	Lawn of aggregation minus | Some mounds forming.	Lawn of aggregation minus | Some mounds forming.
Slug 16h	Normal	Normal	Delayed slug formation ~2h.	Delayed slug formation | Some mounds still have streams.	Some small mounds in a lawn of aggregation minus	Few small mounds in a lawn of aggregation minus
Culminate mound 20h	Normal	Normal	Small Mound structures | Delayed slug formation	Smaller Mound structures | Delayed slug formation	Mostly streaming into stalled mounds | Few micro slugs.	Lawn of aggregation minus | Few micro slugs | Some culminant mounds
Fruiting body 24h	Normal	Normal	Hetrogenous development progression | Mounds, streaming, some slugs | Some micro fruiting bodies	Hetrogenous development progression | Mounds, streaming, some slugs | Some micro fruiting bodies	Majority of structures are mounds | Some have small stream arms | Some micro fruiting bodies	Lawn of aggregation minus | Some mounds forming | Some micro fruiting bodies
48 h	Normal	Normal	Normal	~25% of fruiting bodies are very tall | Thin stalks and small sporeheads	~50% of fruiting bodies are very tall | Thin stalks and small sporeheads	~50% of fruiting bodies are very tall | Thin stalks and small sporeheads

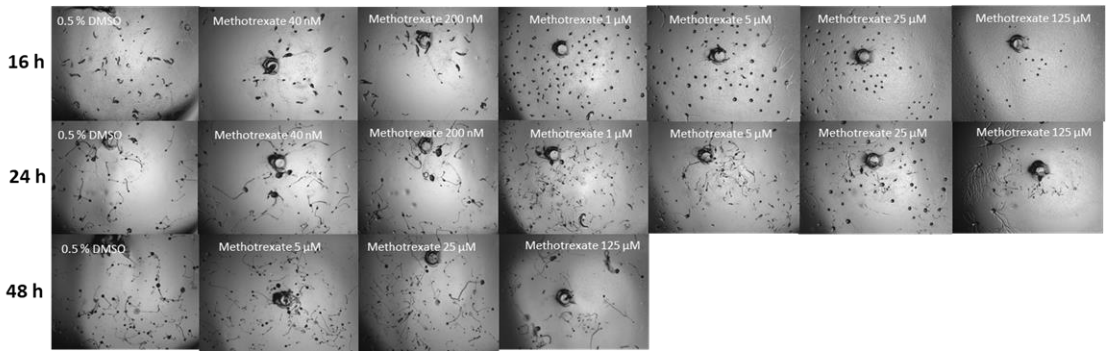

2. Pemetrexed					
Dose	**96 nM**	**480 nM**	**2.4 µM**	***12 µM***	**60 µM**
Aggregation 4h	Normal	Normal	Normal	Normal	Normal
Streaming 8h	Normal	Normal	Delayed Streaming | Irregular shaped stream arms	Delayed Streaming | Irregular shaped stream arms	Delayed Streaming | Irregular shaped stream arms
Mound 15h	Normal	Normal	Lawn of aggregation minus | Delayed mound formation | Some streaming | Some normal mounds	Lawn of aggregation minus | Delayed mound formation | Some streaming | Some normal mounds	Lawn of aggregation minus | Delayed mound formation | Some streaming | Some normal mounds
Slug 16h	Normal	Normal	Lawn of aggregation minus | Some normal mounds	Lawn of aggregation minus | Some normal mounds	Lawn of aggregation minus | normal mounds
Culminate mound 20h	Normal	Normal	Hetrogenous development progression | Lawn of aggregation minus | Loose mounds | Some culminant mounds	Hetrogenous development progression | Lawn of aggregation minus | Loose mounds | Some culminant mounds	Hetrogenous development progression | Lawn of aggregation minus | Loose mounds | Some culminant mounds
Fruiting body 24h	Normal	Normal	Mainly small fruiting bodies | Some aggregation defected cells | Some stalled mounds	Mainly mounds with streaming mounds | Some aggregation defect cells | A few micro fruiting bodies	Mainly mounds with streaming | Some aggregation defect cells | A few micro fruiting bodies
48 h	Normal	Normal	Very Tall fruiting bodies ~ 2-3x normal height | Thin stalks and very small sporeheads	Very Tall fruiting bodies ~ 2-3x normal height | Thin stalks and very small sporeheads	Very Tall fruiting bodies ~ 2-3x normal height | Thin stalks and very small sporeheads

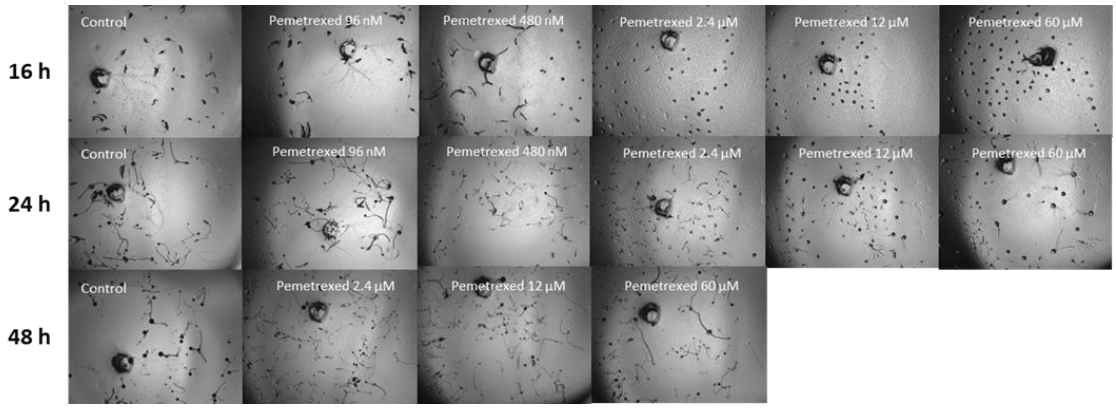

3. Lamotrigine				
Dose	1.6 µM	8 µM	40 µM	*200 µM*
Aggregation 4h	Normal	Normal	Normal	Normal
Streaming 8h	Normal	Normal	Normal	Normal
Mound 15h	Normal	Normal	Normal	Normal
Slug 16h	Normal	Normal	Normal	Normal
Culminate mound 20h	Normal	Normal	Normal	Normal
Fruiting body 24h	Normal	Normal	Normal	Normal
48 h	Normal	Normal	Normal	Normal

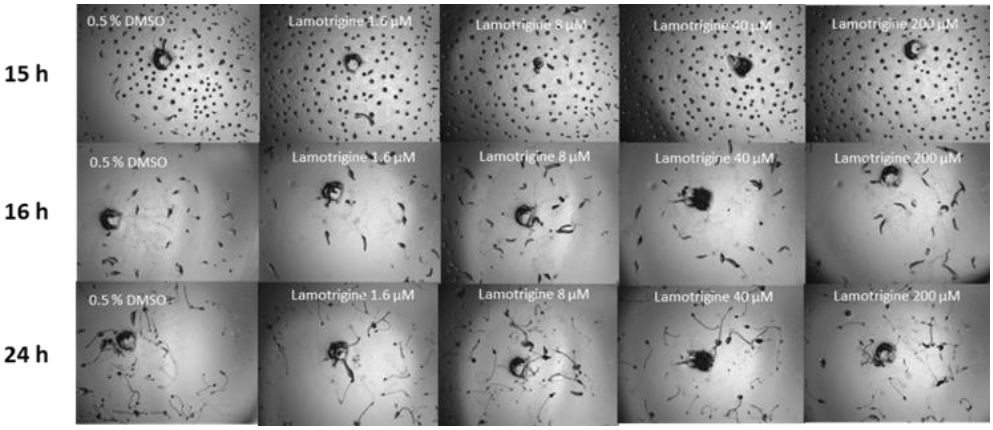

4. Carbamazepine					
Dose	2.4 µM	12 µM	60 µM	*300 µM*	1.5 mM
Aggregation 4h	Normal	Normal	Normal	Normal	Normal
Streaming 8h	Normal	Normal	Normal	Normal	Aggregation delay (NB. Crystals)
Mound 15h	Normal	Normal	Normal	Normal	Large mounds (NB. Crystals)
Slug 16h	Normal	Normal	Normal	Delayed Slug formation | All mounds	Large stalled mounds (NB. Crystals)
Culminate mound 20h	Normal	Normal	Normal	Delayed Slug formation | All mounds	Stalled mounds | Some streaming (NB. Crystals)
Fruiting body 24h	Normal	Normal	Normal fruiting bodies | Some small stalled mounds	Maily stalled mounds | Some streaming | Some slug formation	Stalled mounds | Some slug formation (NB. Crystals)
48 h	Normal	Normal	Normal	Normal	Normal

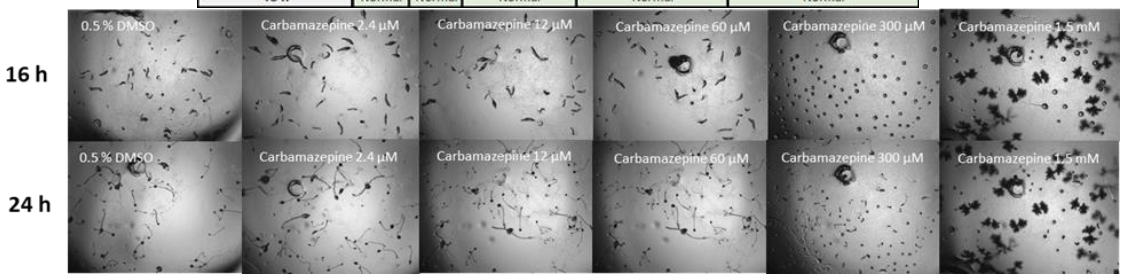

5. Phenytoin				
Dose	2.4 µM	12 µM	60 µM	*300 µM*
Aggregation 4h	Normal	Normal	Normal	Normal
Streaming 8h	Normal	Normal	Normal	Normal
Mound 15h	Normal	Normal	Normal	Normal
Slug 16h	Normal	Normal	Normal	Normal
Culminate mound 20h	Normal	Normal	Normal	Normal
Fruiting body 24h	Normal	Normal	Normal	Normal
48 h	Normal	Normal	Normal	Normal

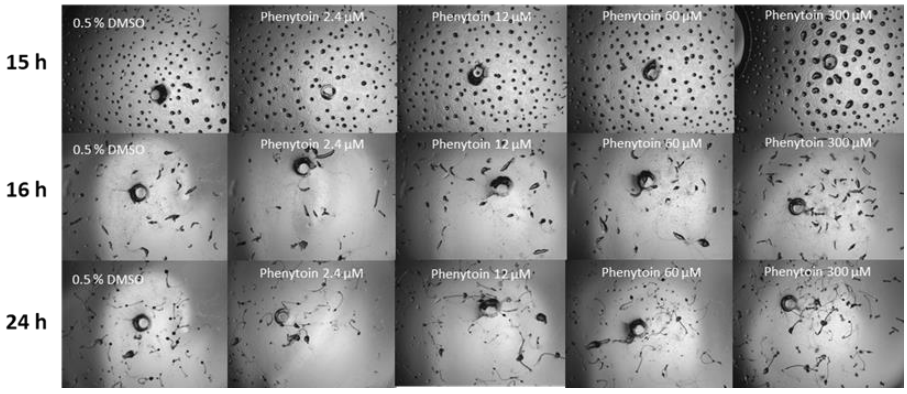

6. Primidone				
Dose	16 µM	80 µM	400 µM	*2 mM*
Aggregation 4h	Normal	Normal	Normal	Normal
Streaming 8h	Normal	Normal	Normal	Normal
Mound 15h	Normal	Normal	Normal	Normal
Slug 16h	Normal	Normal	Normal	Normal
Culminate mound 20h	Normal	Normal	Normal	Normal
Fruiting body 24h	Normal	Normal	Normal	Normal
48 h	Normal	Normal	Normal	Normal

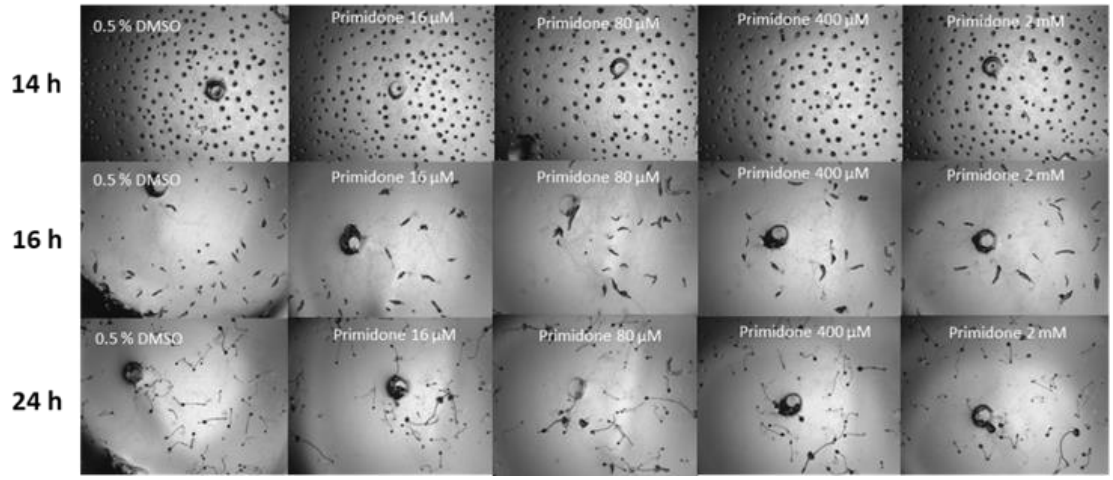

7. Valproic acid						
Dose	800 nM	4 µM	20 µM	*100 µM*	500 µM	2.5 mM
Aggregation 4h	Normal	Normal	Normal	Normal	Normal	Loose pools of cells (Dead?)
Streaming 8h	Normal	Normal	Normal	Normal	Delayed streaming	Aggregation minus
Mound 14h	Normal	Normal	Normal	Large mounds	Large mounds	Loose pools of cells (Dead?)
Slug 16h	Normal	Normal	Normal	Slugs form and migrate at correct time | Slugs are long and thin	Lawn of aggregation minus | Some loose stalled mounds	Aggregation minus
Culminate mound 20h	Normal	Normal	Normal	Extended slug migration	Loose flat mounds	Aggregation minus
Fruiting body 24h	Normal	Normal	Normal	Hetrogenous development progression | Slugs and fruiting bodies	Loose flat mounds	Aggregation minus
48 h	Normal	Normal	Normal	Normal	Some stalled mounds | Very small, short fruiting bodies | Very short stalks	Loose pools of cells (Dead?)

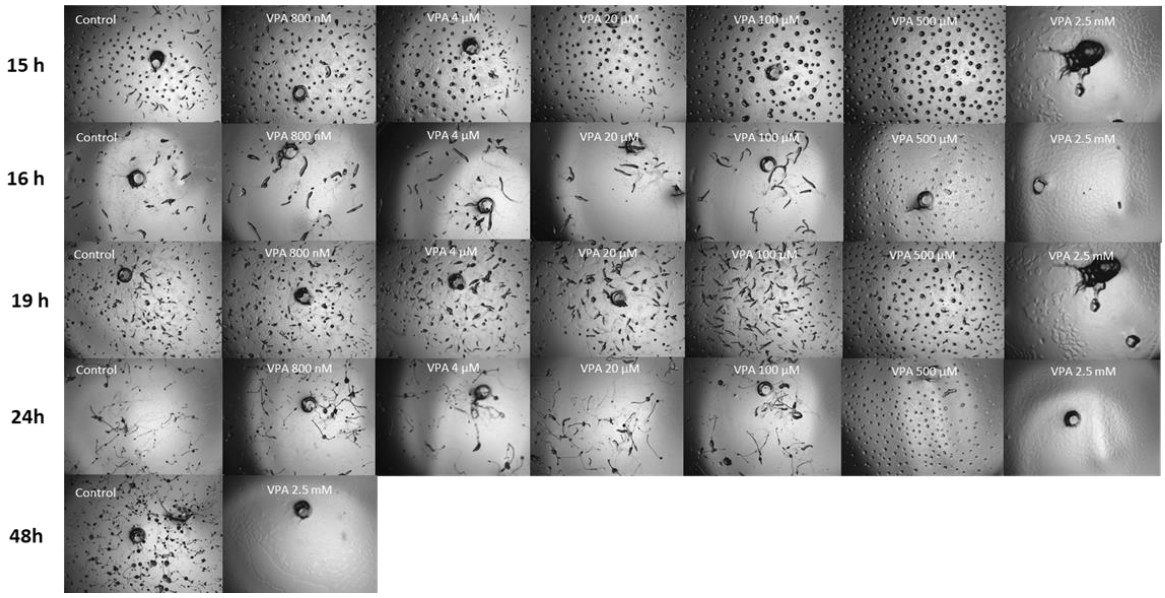

8. Lithium					
Dose	40 µM	200 µM	1 mM	*5 mM*	25 mM
Aggregation 4h	Normal	Normal	Normal	Normal	Normal
Streaming 8h	Normal	Normal	Normal	Aggregation defect | Micro mounds	Aggregation minus
Mound 14h	Normal	Normal	Normal	Lawn of aggregation minus | Many irregular small mounds	Aggregation minus
Slug 18h	Normal	Normal	Mounds and late slugs | Smaller structures	Lawn of aggregation minus | Many micro mounds	Loose pools of cells (Dead?)
Culminate mound 20h	Normal	Normal	Hetrogenous development progression | Extended slug migration	Lawn of aggregation minus | Many micro mounds	Loose pools of cells (Dead?)
Fruiting body 24h	Normal	Normal	Hetrogenous development progression | Many slugs | Small fruiting bodies	Many micro mounds	Loose pools of cells (Dead?)
48 h	Normal	Normal	Small fruiting bodies | Smaller spore heads	Many micro mounds | Few tiny fruiting bodies	Loose pools of cells (Dead?)

24h

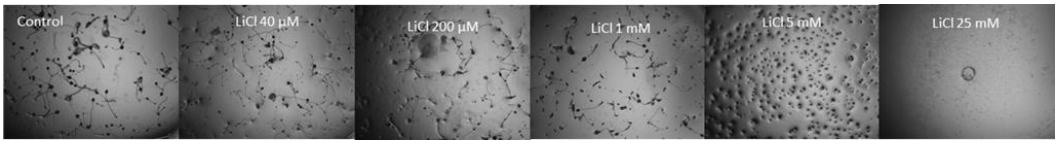

9. Acitretin					
Dose	220 nM	1.1 µM	5.5 µM	*27.5 µM*	137.5 µM
Aggregation 4h	Normal	Normal	Normal	Normal	Normal
Streaming 8h	Normal	Normal	Normal	Normal	Normal
Mound 15h	Normal	Normal	Normal	Normal	Normal
Slug 18h	Normal	Delayed slug formation ~ 2h	Delayed slug formation ~ 2h	Delayed slug formation ~ 2h	Delayed slug formation ~ 2h
Culminate mound 20h	Normal	Hetrogenous development progression | Emerging slugs | Some Small culminates mounds	Hetrogenous development progression | Emerging slugs | Some Small culminates mounds	Hetrogenous development progression | Emerging slugs | Some Small culminates mounds	Hetrogenous development progression | Emerging slugs | Some Small culminates mounds
Fruiting body 24h	Normal	Some stalled mounds | Smaller and normal fruiting bodies	Loose mounds | Some stalled mounds | Some micro fruiting bodies	Loose mounds | Some stalled mounds | Some micro fruiting bodies	Loose mounds | Some stalled mounds | Some micro fruiting bodies
48 h	Normal	Normal	Normal	Normal	Normal

15 h

18 h

24 h

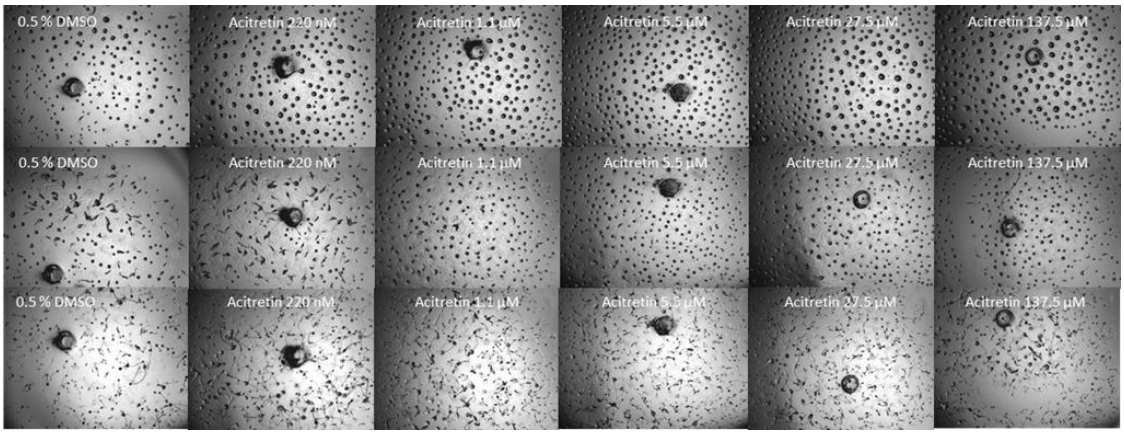

10. 13-cis-retinoic acid					
Dose	**140 nM**	**700 nM**	**3.5 µM**	***17.5 µM***	**87.5 µM**
Aggregation 4h	Normal	Normal	Normal	Normal	Normal
Streaming 8h	Normal	Normal	Normal	Normal	Breaking streams
Mound 15h	Normal	Normal	Normal	Normal	Normal
Slug 20h	Normal	Normal	Delayed slug formation ~ 4h	Delayed slug formation ~ 4h	Delayed slug formation ~ 4h
Culminate mound 20h	Normal	Normal	Delayed slug formation | Formed slugs have trailing rear | Small culminant mounds	Delayed slug formation | Formed slugs have trailing rear | Small culminant mounds	Delayed slug formation | Formed slugs have trailing rear | Small culminant mounds
Fruiting body 24h	Normal	Some smaller fruiting bodies	Loose mounds | Some stalled mounds | Micro fruiting bodies	Loose mounds | Some stalled mounds | Micro fruiting bodies	Loose mounds | Some stalled mounds | Micro fruiting bodies
48 h	Normal	Normal	Normal	Increased number of smaller fruiting bodies	Increased number of smaller fruiting bodies

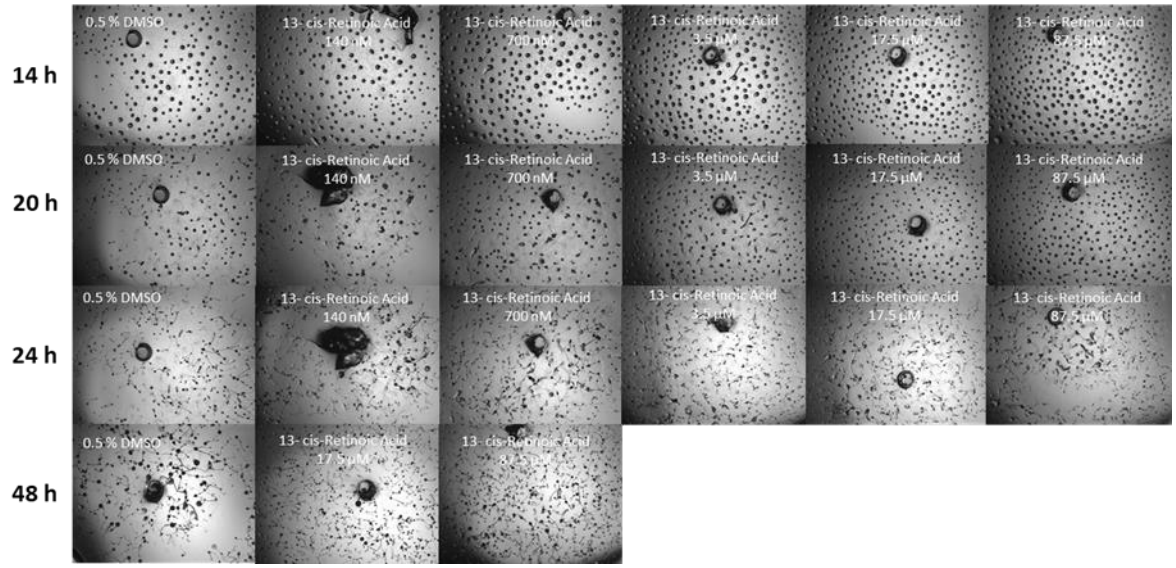

11. Retinoic acid						
Dose	**80 nM**	**400 nM**	**2 µM**	***10 µM***	**50 µM**	**250 µM**
Aggregation 4h	Normal	Normal	Normal	Normal	Normal	Normal
Streaming 8h	Normal	Normal	Normal	Normal	Normal	Normal
Mound 14h	Normal	Normal	Normal	Normal	Normal	Normal
Slug 20h	Normal	Normal	Delayed slug formation ~ 4h	Delayed slug formation ~ 4h	Delayed slug formation ~ 4h	Delayed slug formation ~ 4h
Culminate mound 20h	Normal	Normal	Delayed slug formation ~ 4h | Slugs emerging ~ 20h	Delayed slug formation ~ 4h | Slugs emerging ~ 20h	Delayed slug formation ~ 4h | Small culminant mounds | Slugs that have formed have a trailing rear	Delayed slug formation ~ 4h | Small culminant mounds | Slugs that have formed have a trailing rear
Fruiting body 24h	Normal	Normal	Loose mounds | Some stalled mounds | Micro fruiting bodies	Loose mounds | Some stalled mounds | Micro fruiting bodies	Loose mounds | Some stalled mounds | Micro fruiting bodies	Loose mounds | Some stalled mounds | Micro fruiting bodies
48 h	Normal	Normal	Normal	Normal	Normal	Normal

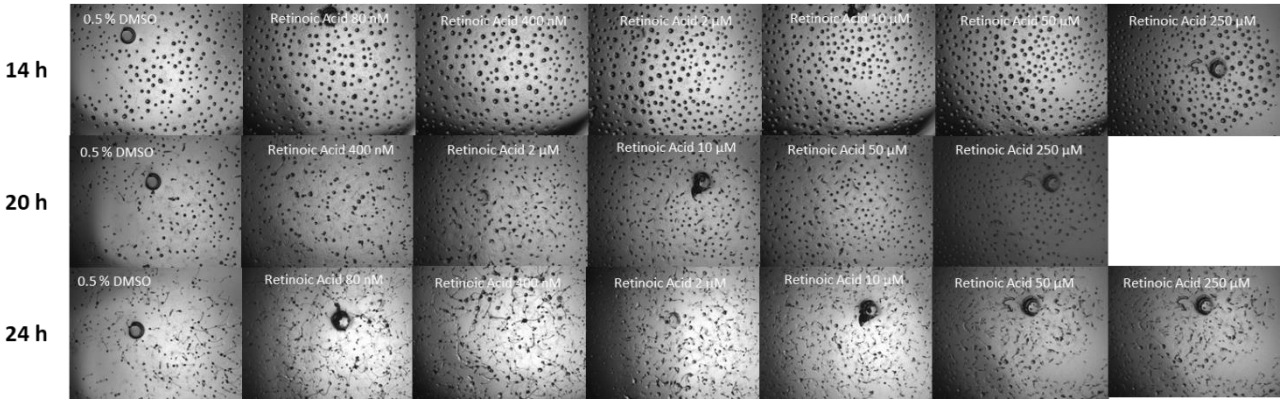

12. Bosentan					
Dose	**960 nM**	**4.8 µM**	**24 µM**	***120 µM***	**600 µM**
Aggregation 4h	Normal	Normal	Normal	Normal	Normal
Streaming 8h	Normal	Normal	Normal	Normal	Normal
Mound 15h	Normal	Normal	Normal	Normal	Greater number of generally smaller mounds
Slug 19h	Normal	Normal	Normal	Normal	Normal slug formation | All slugs are very small |The smallest mounds are stalled
Culminate mound 20h	Normal	Normal	Normal	Normal	Few very small slugs | Stalled mounds some have a small tip
Fruiting body 24h	Normal	Normal	Normal	Normal	Delayed culminatant mound formation |Extended slug migration | Stalled mounds | Very small slugs
48 h	Normal	Normal	Normal	Normal	No fruiting bodies | Streaming cells | Small tight stalled mounds

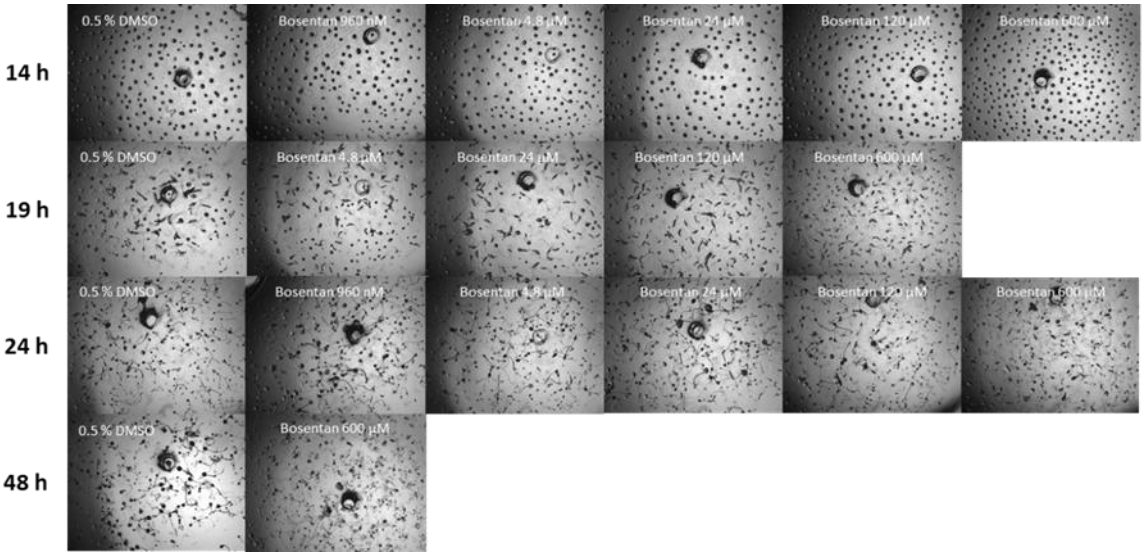

13. Sitaxentan				
Dose	**3.2 µM**	**16 µM**	**80 µM**	**400 µM**
Aggregation 4h	Normal	Normal	Normal	Normal
Streaming 8h	Normal	Delayed streaming ~ 3h	Delayed streaming ~ 3h	Delayed streaming ~ 3h
Mound 14h	Normal	Normal	Fewer larger mounds	Slightly larger mounds | Loose around the edge of the mound | Irregular shaped
Slug 17h	Normal	Normal	Fewer larger mounds | Delayed slug formation	Lawn of aggregation minus | Fewer larger mounds | Delayed slug formation
Culminate mound 20h	Normal	Normal	Extended slug migration | Larger slugs	Extended slug migration | Larger slugs
Fruiting body 24h	Normal	Normal	Delayed culmination by ~ 2h	Delayed culmination | Cumination and early extention at 24h
48 h	Normal	Normal	Normal	Normal

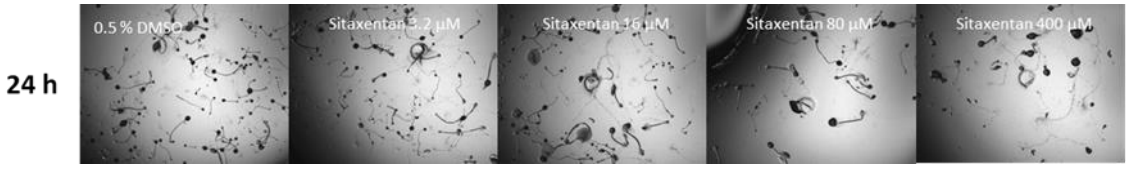

14. Bexarotene					
Dose	**40 nM**	**200 nM**	**1 µM**	***5 µM***	**25µM**
Aggregation 4h	Normal	Normal	Normal	Normal	Normal
Streaming 8h	Normal	Normal	Normal	Normal	Normal
Mound 15h	Normal	Normal	Normal	Normal	Normal
Slug 19h	Normal	Normal	Normal	Normal	Normal
Culminate mound 20h	Normal	Normal	Normal	Hetrogenous development progression | Mounds and C. mounds	Hetrogenous development progression | Mounds and C. mounds
Fruiting body 24h	Normal	Normal	Normal	Hetrogenous development progression | Stalled mounds | Normal fruiting bodies	Hetrogenous development progression | Stalled mounds | Normal fruiting bodies
48 h	Normal	Normal	Normal	Normal	Normal

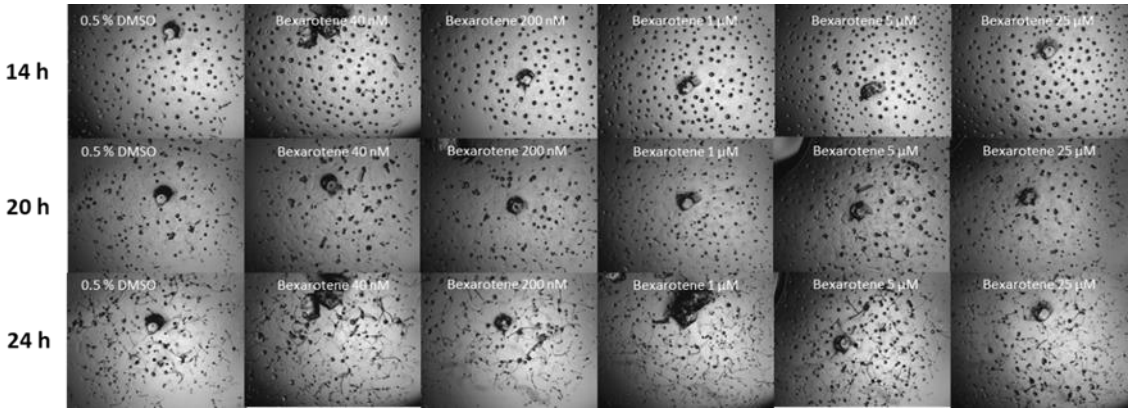

15. Cadmium sulphate					
Dose	**120 nM**	**600 nM**	**3 µM**	***15 µM***	**75 µM**
Aggregation 4h	Normal	Normal	Normal	Normal	Loose puddles (Dead)
Streaming 8h	Normal	Normal	Normal	Many small short streams	Dead
Mound 14h	Normal	Normal	Large loose mounds	Large loose flat mounds. Some have sunk	Dead
Slug 19h	Normal	Normal	Delayed slug formation	Large loose flat mounds. Some have sunk	Dead
Culminate mound 20h	Normal	Normal	Hetrogenous development progression | Mounds slugs and culminant mounds	Large loose flat mounds. Some have sunk	Dead
Fruiting body 24h	Normal	Normal	Normal	Many stalled mounds | Small loose puddles of cells | Few Slugs	Dead
48 h	Normal	Normal	Normal	Many stalled mounds | Normal fruiting bodies	Dead

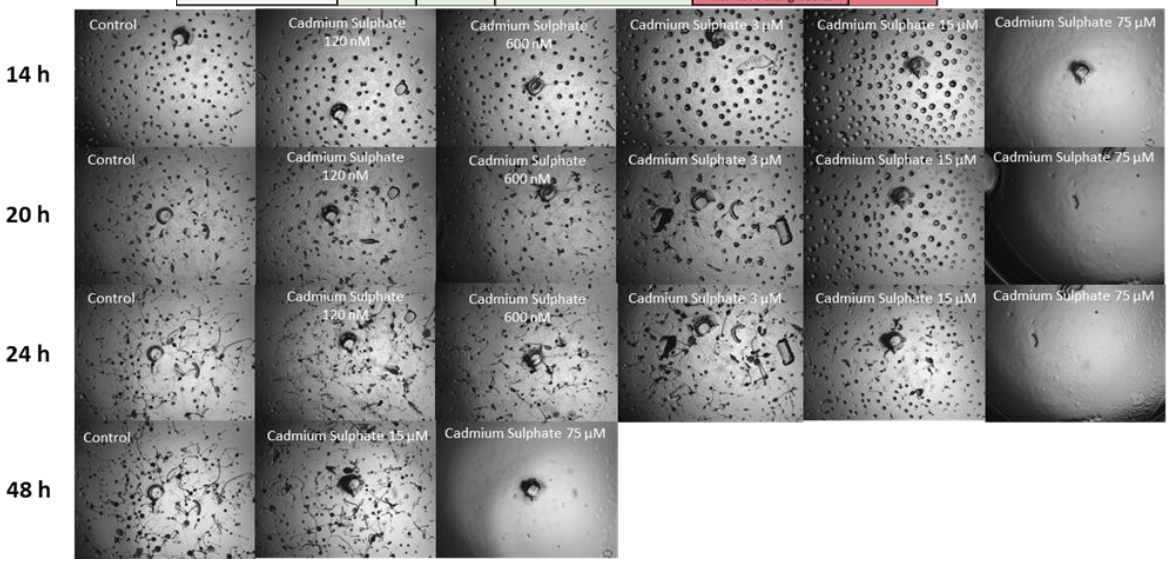

16. Hydroxyurea						
Dose	**1.6 µM**	**8 µM**	**40 µM**	***200 µM***	**1 mM**	**5 mM**
Aggregation 4h	Normal	Normal	Normal	Normal	Normal	Normal
Streaming 8h	Normal	Normal	Normal	Normal	Normal	Normal
Mound 14h	Normal	Normal	Normal	Normal	Normal	Extended streaming time | Broken stream arms visable
Slug 18h	Normal	Normal	Normal	Normal	Hetrogenous development progression | Loose lawn of aggregation defect	Hetrogenous development progression | Loose lawn of aggregation defect | Stalled mounds | Slugs are long with trailing rears
Culminate mound 20h	Normal	Normal	Normal	Normal	Hetrogenous development progression | Mounds slugs and culminant mounds	Extended slug migration | Long thin slugs with trailing rears | Some slugs splitting into two
Fruiting body 24h	Normal	Normal	Normal	Normal	Hetrogenous development progression | Stalled mounds | Taller fruiting bodies | Extended stalks	Loose piles of aggreagtion minus cells | Some small short fruiting bodies | Large basel disc and lower stalk
48 h	Normal	Normal	Normal	Normal	Normal	Some localised aggreagtion defect cells | Few stalled mounds | Short fruiting bodies

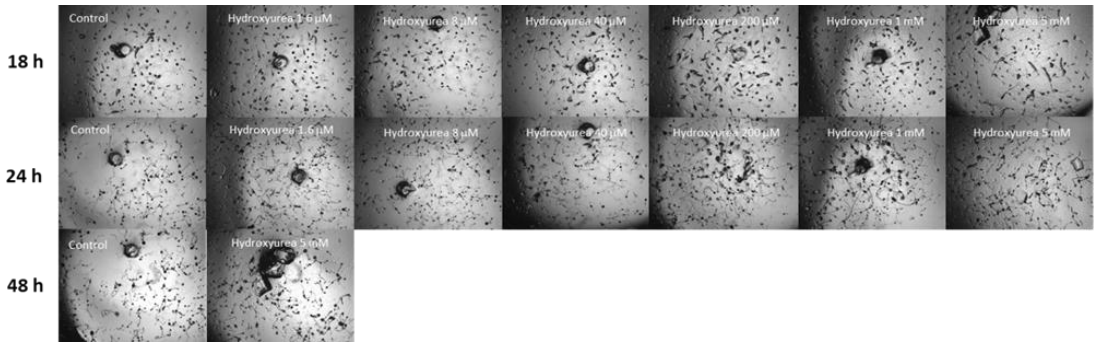

17. Cyclophosphamide			
Dose	**200 µM**	**1 mM**	**5 mM**
Aggregation 4h	Normal	Normal	Normal
Streaming 8h	Normal	Some larger mounds | Short stream mounds	Some larger mounds | Short stream mounds
Mound 14h	Normal	Some larger mounds | Short stream mounds	Some larger mounds | Short stream mounds
Slug 17h	Normal	Normal	Smaller short slugs
Culminate mound 20h	Normal	Normal	Normal
Fruiting body 24h	Normal	Normal	Normal
48 h	Normal	Normal	Normal

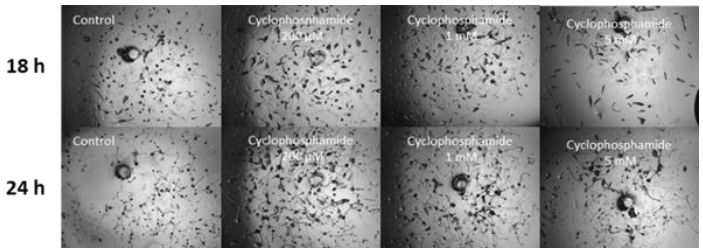

18. Cisplatin				
Dose	**240 nM**	**1.2 µM**	**6 µM**	***30 µM***
Aggregation 4h	Normal	Normal	Normal	Normal
Streaming 8h	Normal	Normal	Normal	Normal
Mound 15h	Normal	Normal	Normal	Normal
Slug 16h	Normal	Normal	Normal	Longer larger slugs
Culminate mound 20h	Normal	Normal	Normal	Hetrogenous development progression | Slugs and culminant mounds
Fruiting body 24h	Normal	Normal	Normal	Hetrogenous development progression | Slugs and fruiting bodies
48 h	Normal	Normal	Normal	Normal

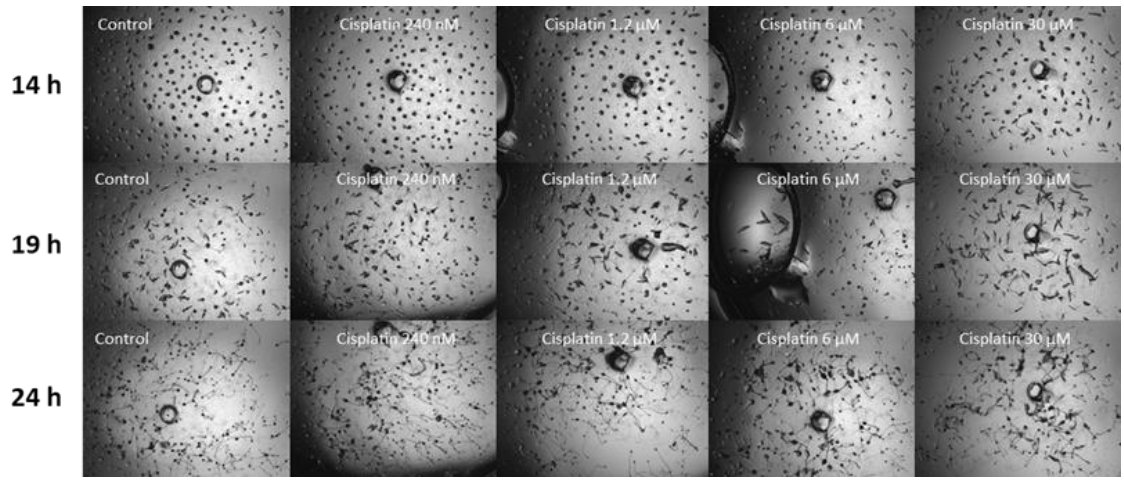

19. Lead acetate						
Dose	**1.6 µM**	**8 µM**	**40 µM**	***200 µM***	**1 mM**	**5 mM**
Aggregation 4h	Normal	Normal	Normal	Normal	Normal	Normal
Streaming 8h	-	-	-	-	-	-
Mound 14h	Normal	Normal	Very loose mounds | Some latent streaming arms | Irregular stream arms	Very loose mounds | Some latent streaming arms | Irregular stream arms	Very loose mounds | Edge of mounds falling away	Aggregation minus
Slug 17h	Normal	Normal	Normal	Normal	Some loose stalled mounds | Normal slugs	Aggregation minus
Culminate mound 20h	Normal	Normal	Extended slug migration	Extended slug migration | Slugs have a long visable tail	Loose stalled mounds | Fingers from loose mounds which are collapsing	Aggregation minus
Fruiting body 24h	Normal	Normal	Normal	Tall fruiting bodies | Smaller sporehead	Sparse fruiting bodies | Tall with smaller sporeheads | Loose stalled mounds	Aggregation minus
48 h	Normal	Normal	Normal	Tall fruiting bodies	Sparse fruiting bodies | Tall with smaller sporeheads | 50% of structures are loose stalled mounds	Aggregation minus

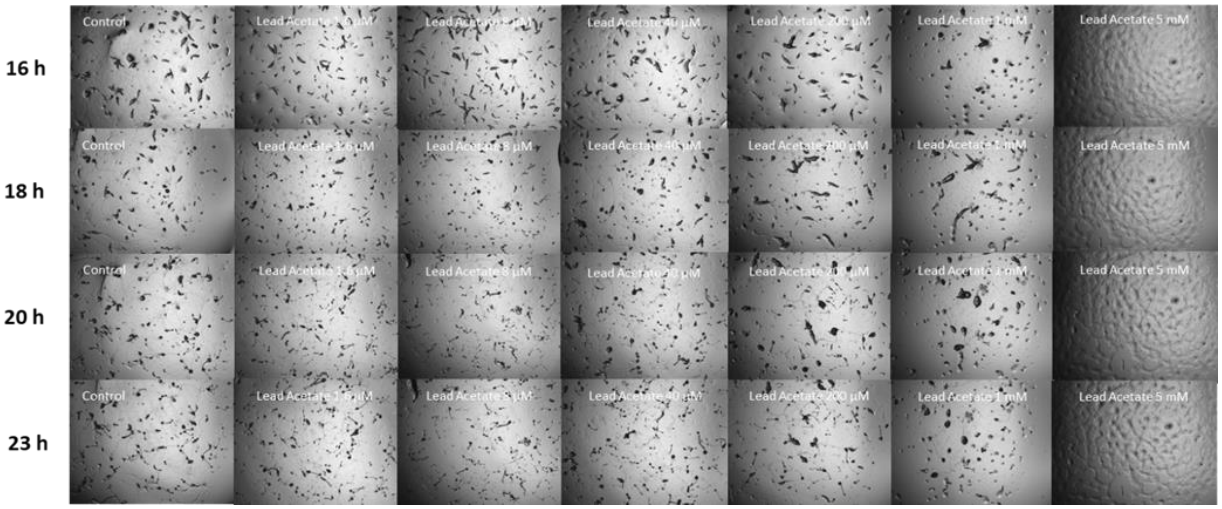

20. Clomifene						
Dose	**2 nM**	**10 nM**	**50 nM**	***250 nM***	**1.25 µM**	**6.25 µM**
Aggregation 4h	Normal	Normal	Normal	Normal	Normal	Normal
Streaming 8.5h	Normal	Normal	Normal	Normal	Normal	Normal
Mound 14h	Normal	Normal	Normal	Normal	Normal	Increase numbers of micro mounds | Other mounds look normal
Slug 20h	Normal	Normal	Normal	Normal	Delayed slug formation	Loose puddles of cells | Delayed slug formation | Many small stalled mounds
Culminate mound 20h	Normal	Normal	Normal	Normal	Many smaller slugs | Some stalled mounds | Few culminant mounds	Many small stalled mounds | Some small slugs
Fruiting body 24h	Normal	Normal	Normal	Normal	Some stalled mounds | Sparse fruiting bodies | Some thin fruiting bodies	Many stalled mounds | Loose puddles of cells | Some shorter fruiting bodies
48 h	Normal	Normal	Normal	Normal	Many stalled mounds | Loose puddles of cells | Some normal fruiting bodies	Many stalled mounds | Loose puddles of cells | Some normal fruiting bodies

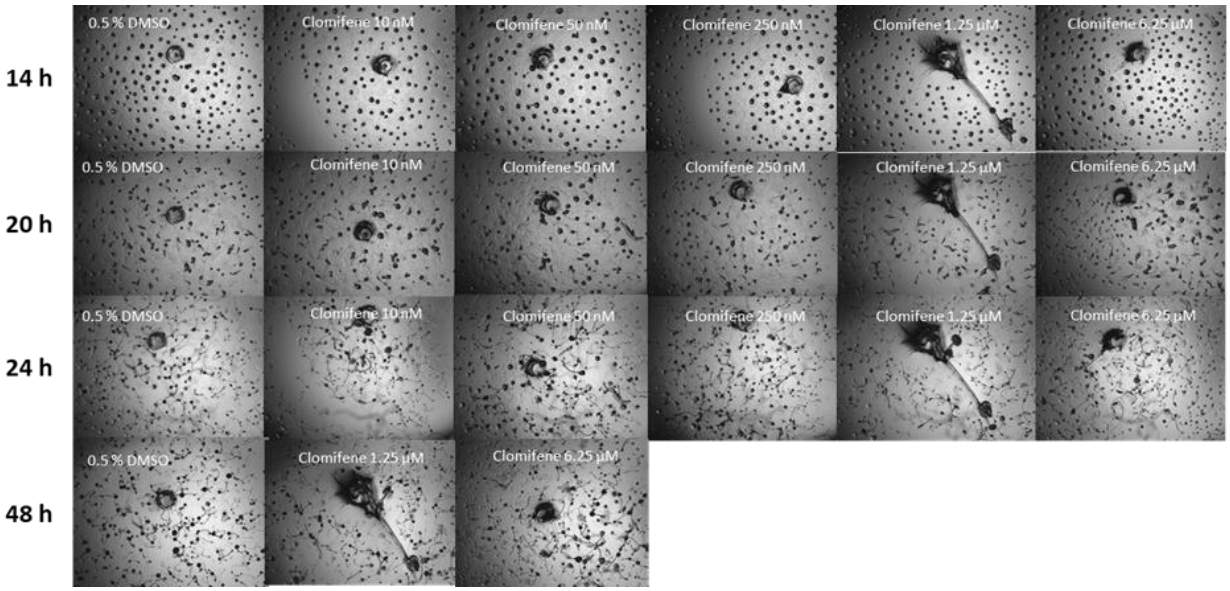

21. Raloxifene						
Dose	**160 nM**	**800 nM**	**4 µM**	***20 µM***	**100 µM**	**500 µM**
Aggregation 4h	Normal	Normal	Normal	Normal	Normal	Normal
Streaming 8.5h	Normal	Normal	Short wide streams	Delayed streaming	Delayed streaming	Aggregation minus
Mound 14h	Normal	Normal	Normal	Extremely large irregular shaped mounds	Lawn of aggregation minus | Delayed streaming | Short wide streams | Some very large mounds	Aggregation minus
Slug 20h	Normal	Normal	Normal	Delayed slug formation	Delayed slug formation | All mounds some loose mounds	Aggregation minus
Culminate mound 20h	Normal	Normal	Normal	Late slug migration	Delayed slug formation | All mounds some loose mounds	Aggregation minus
Fruiting body 24h	Normal	Normal	Normal	Sparse smaller fruiting bodies	Delayed slug formation | All mounds some loose mounds | Few slugs formed	Aggregation minus
48 h	Normal	Normal	Normal	Normal	Many stalled mounds | Some normal fruiting bodies	Aggregation minus

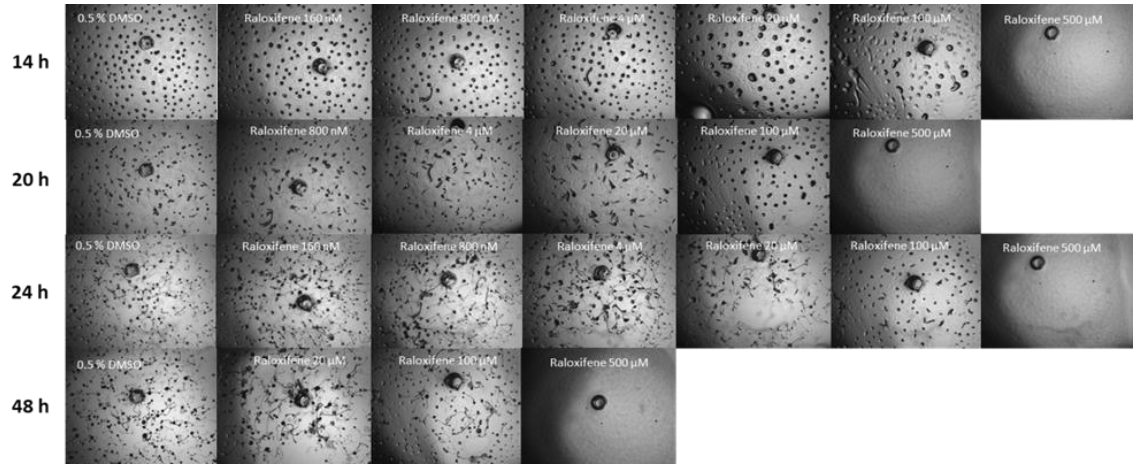

22. Finasteride						
Dose	**600 nM**	**3 µM**	**15 µM**	***75 µM***	**375 µM**	**1.875 mM**
Aggregation 4h	Normal	Normal	Normal	Normal	Normal	Normal
Streaming 8.5h	Normal	Normal	Normal	Large mounds forming streams	Delayed streaming	Normal (Crystals)
Mound 14h	Normal	Normal	Some larger mounds	Large mounds forming	Extremely large mounds with visable streams	Lawn of aggregation defect cells | Large mounds (Crystals)
Slug 18h	Normal	Hetrogenous development progression | Mounds and slugs	Delayed slug formation	Delayed slugs| Large mounds | Few slugs	Large loose mounds| Still streams	Crystals
Culminate mound 20h	Normal	Hetrogenous development progression | Mounds slugs and culminant mounds	Hetrogenous development progression | Mounds slugs and culminant mounds	All culminant mounds are large	Still streaming | Stalled mounds large and small	Crystals
Fruiting body 24h	Normal	Some stalled mounds | Normal looking fruiting bodies	Some stalled mounds | Normal looking fruiting bodies	Many stalled mounds | Normal looking fruiting bodies	Still streaming | Stalled mounds large and small	Crystals
48 h	Normal	Normal	Normal	Normal	Few piles of loose cells | Fruiting bodies normal	Crystals

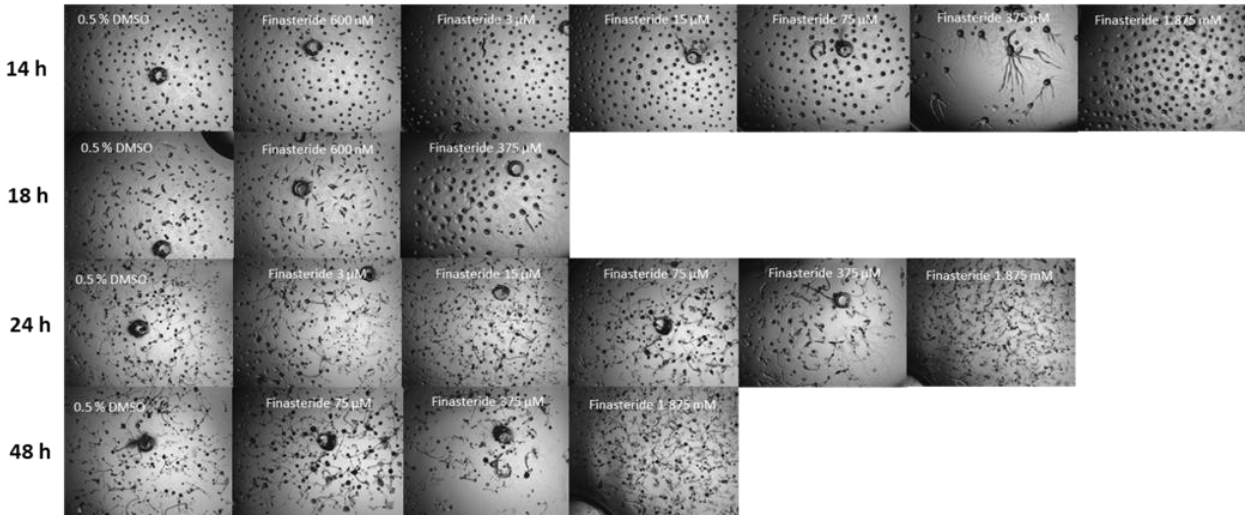

23. Vinclozolin						
Dose	**80 nM**	**400 nM**	**2 µM**	***10 µM***	**50 µM**	**250 µM**
Aggregation 4h	Normal	Normal	Normal	Normal	Normal	Normal
Streaming 8.5h	Normal	Normal	Normal	Normal	Large stream arms | Many arms have detached	Large stream arms | Many arms have detached
Mound 14h	Normal	Normal	Normal	Large mounds	Large mounds	Large mounds
Slug 18h	Normal	Normal	Normal	Delayed slug formation	Delayed slug formation	Delayed slug formation
Culminate mound 20h	Normal	Normal	Normal	Delayed slug formation	Delayed slug formation	Delayed slug formation
Fruiting body 24h	Normal	Normal	50 / 50 Structures Fruiting bodies | Stalled mounds	50 / 50 Structures Fruiting bodies | Stalled mounds | Fruiting bodies are smaller	50 / 50 Structures Fruiting bodies | Stalled mounds | Fruiting bodies are smaller	50 / 50 Structures Fruiting bodies | Stalled mounds | Fruiting bodies are smaller
48 h	Normal	Normal	Normal	Smaller fruiting bodies	Smaller fruiting bodies	Smaller fruiting bodies

24 h

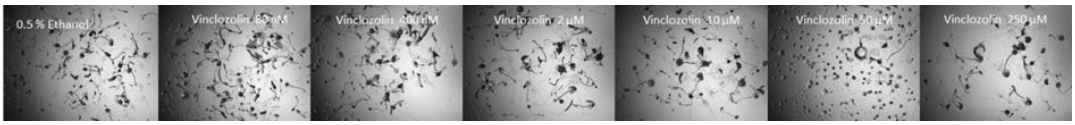

24. Diethylstilbestrol (DES)						
Dose	**80 nM**	**40 nM**	**200 nM**	***1 µM***	**5 µM**	**25 µM**
Aggregation 4h	Normal	Normal	Normal	Normal	Normal	Normal
Streaming 8h	Normal	Normal	Normal	Many short streams | Increase streaming speed	Many short streams | Increase streaming speed	Delayed stream formation
Mound 14h	Normal	Normal	Normal	Slightly larger mounds | Irregular shape	Many large mounds | Irregular shape	Large loose iregular shaped mounds| Broken streams | Puddles of cells around the mounds
Slug 19h	Normal	Normal	Normal	Hetrogenous development progression | Mounds slugs and large ammount of aggregation minus cells	Irregular shaped mounds | Loose puddles around the mound	Irregular shaped mounds | Loose puddles around the mound
Culminate mound 20h	Normal	Normal	Normal	Hetrogenous development progression | Mounds slugs and large ammount of aggregation minus cells	Many large loose stalled mounds	Irregular shaped mounds | Loose puddles around the mound
Fruiting body 24h	Normal	Normal	Normal	50 / 50 Structures Fruiting bodies | Stalled mounds	Many small loose puddles of cells | Stalled mounds | Few fruiting bodies	Irregular shaped mounds | Loose puddles around the mound
48 h	Normal	Normal	Normal	Normal	Stalled loose mounds | Some fruiting bodies	Many stalled loose mounds | Some thin fruiting bodies

14 h

19 h

48 h

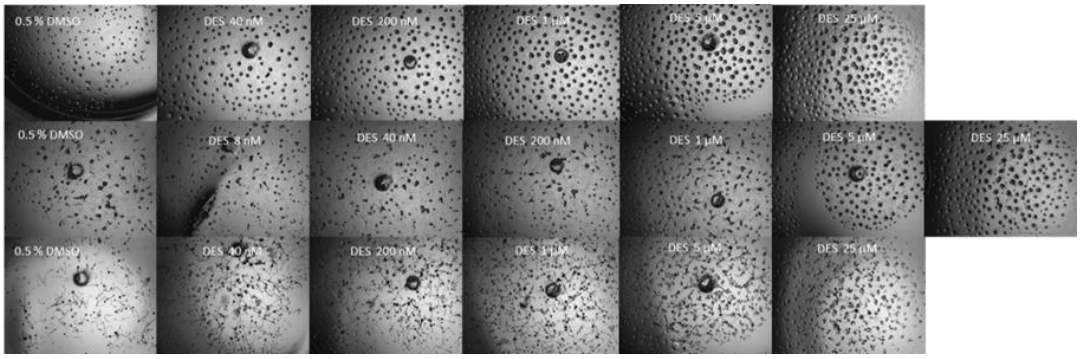

25. Salicylic acid				
Dose	**24 µM**	**120 µM**	**600 µM**	***3 mM***
Aggregation 4h	Normal	Normal	Normal	Normal
Streaming 8h	Normal	Normal	Shorter wide streaming arms	Delayed streaming | Shorter wide streaming arms
Mound 15h	Normal	Normal	Normal	Larger mounds
Slug 19h	Normal	Normal	Normal	Delayed slug formation
Culminate mound 20h	Normal	Normal	Hetrogenous development progression | Mounds slugs and culminant mounds	Delayed slug formation
Fruiting body 24h	Normal	Normal	Hetrogenous development progression | Mounds slugs and fruiting bodies	Slug migration at 24h
48 h	Normal	Normal	Normal	Normal

15 h

18 h

48 h

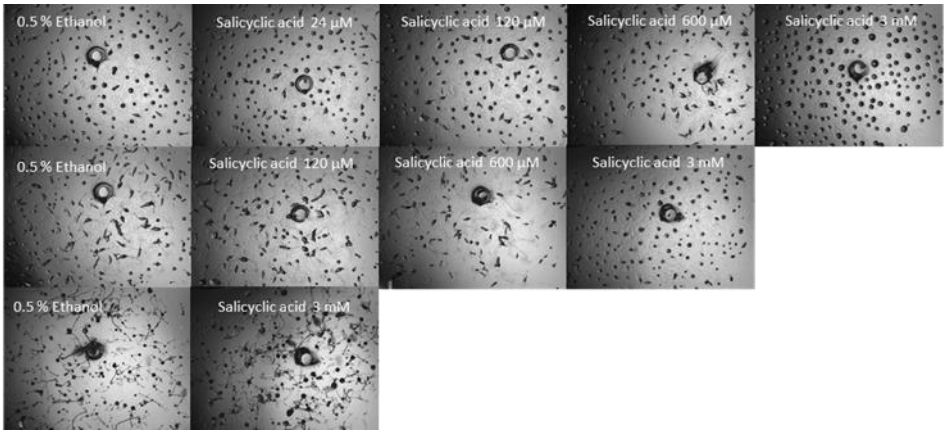

26. Nifedipine						
Dose	**200 nM**	**1 µM**	**5 µM**	***25 µM***	**125 µM**	**625 µM**
Aggregation 4h	Normal	Normal	Normal	Normal	Aggregation minus	Crystals (Dead)
Streaming 8h	Normal	Normal	Normal	Delayed streaming	Aggregation minus	Crystals (Dead)
Mound 14h	Normal	Normal	Normal	Many loose mounds | Close together	Aggregation minus	Crystals (Dead)
Slug 19h	Normal	Normal	Normal	Many loose mounds | Close together	Aggregation minus	Crystals (Dead)
Culminate mound 20h	Normal	Normal	Normal	Many loose mounds | Close together	Aggregation minus	Crystals (Dead)
Fruiting body 24h	Normal	Normal	Normal	Many stalled mounds | Few slugs | 50/50 loose and tight mounds	Aggregation minus	Crystals (Dead)
48 h	Normal	Normal	Normal	Many loose stalled mounds | A few thin fruiting bodies | Small sporehead	Aggregation minus	Crystals (Dead)

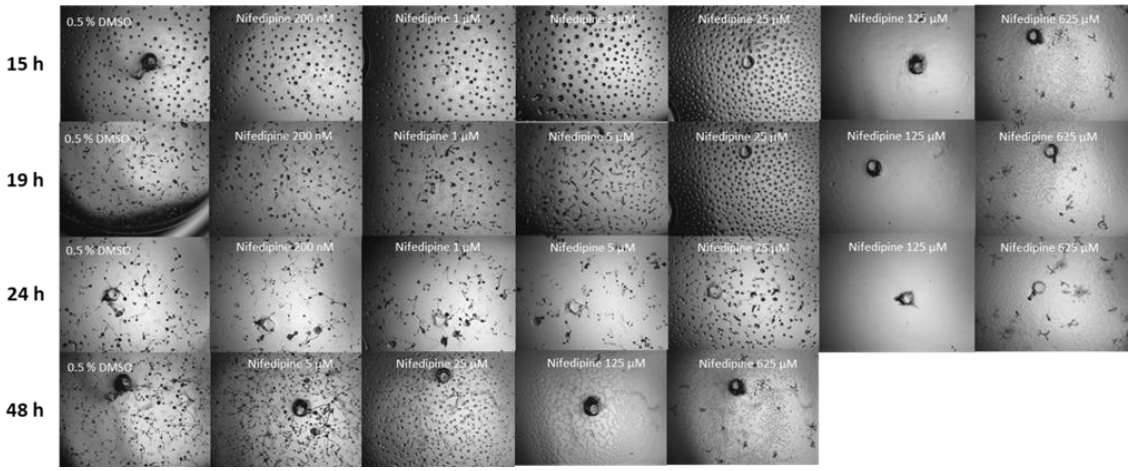

27. Warfarin					
Dose	**3.2 µM**	**16 µM**	**80 µM**	***400 µM***	**2 mM**
Aggregation 4h	Normal	Normal	Normal	Normal	Dead
Streaming 8h	Normal	Normal	Normal	Irregular width of stream arms	Dead
Mound 14h	Normal	Normal	Normal	Many irregular shapped mounds	Dead
Slug 18h	Normal	Normal	Hetrogenous development progression | Mounds slugs and culminant mounds	Delayed slugs | Large mounds | Slugs are fat and short	Dead
Culminate mound 20h	Normal	Normal	Hetrogenous development progression | Mounds slugs and culminant mounds	Delayed slugs | Large mounds | Slugs are fat and short	Dead
Fruiting body 24h	Normal	Normal	Sparse fruiting bodies | Collapsed fruiting bodies | Some stalled mounds	Large mounds | Irregular shape | Some small slugs	Dead
48 h	Normal	Normal	Normal	Normal fruiting bodies | 25% of structures are stalled mounds	Dead

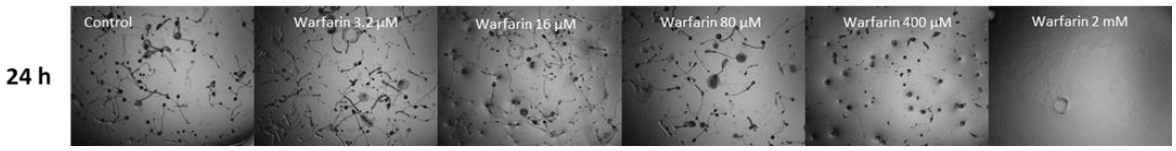

28. Metoclopramide				
Dose	12 µM	60 µM	300 µM	*1.5 mM*
Aggregation 4h	Normal	Normal	Normal	Normal
Streaming 8h	Normal	Normal	Normal	Normal
Mound 14h	Normal	Normal	Normal	Slighly larger mounds | Irregular shaped mound
Slug 19h	Normal	Normal	Normal	Hetrogenous development progression | Extended slug migration
Culminate mound 20h	Normal	Normal	Normal	Hetrogenous development progression | Extended slug migration
Fruiting body 24h	Normal	Normal	Normal	Normal
48 h	Normal	Normal	Normal	Normal

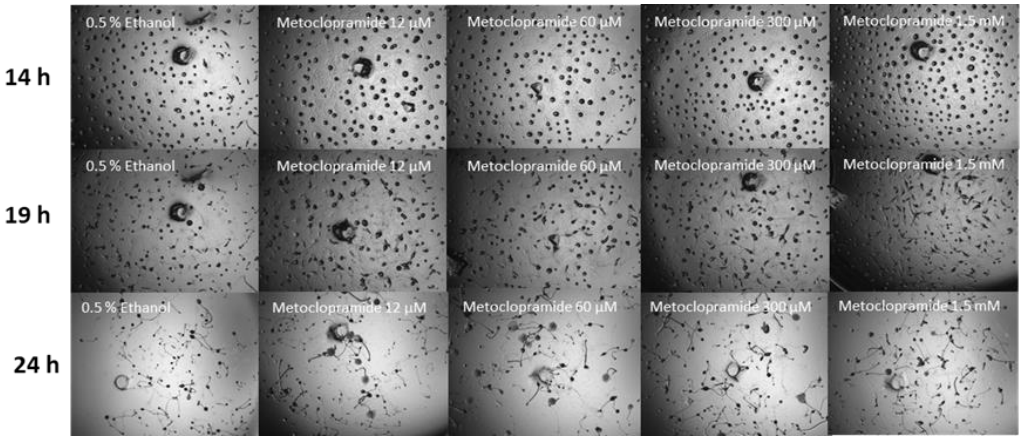

29. Cefotaxime			
Dose	80 µM	400 µM	2 mM
Aggregation 4h	Normal	Normal	Normal
Streaming 8h	Normal	Normal	Normal
Mound 14h	Normal	Normal	Normal
Slug 19h	Normal	Normal	Normal
Culminate mound 20h	Normal	Normal	Normal
Fruiting body 24h	Normal	Normal	Normal
48 h	Normal	Normal	Normal

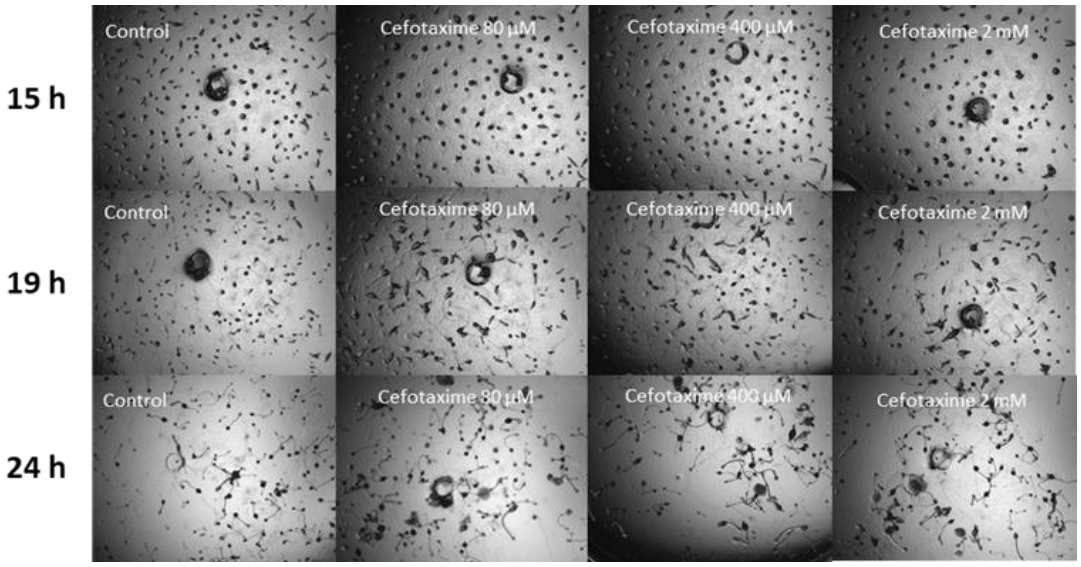

30. Sulfasalazine				
Dose	8 µM	40 µM	200 µM	*1 mM*
Aggregation 4h	Normal	Normal	Normal	Normal
Streaming 8h	Normal	Normal	Normal	Aggregation minus lawn | Micro streams forming
Mound 14h	Normal	Normal	Larger mounds | Irregular shaped mound | Lawn of early aggregation minus	Larger mounds | Irregular shaped mound | Lawn of early aggregation minus
Slug 19h	Normal	Normal	Hetrogenous development progression | Streaming | loose mounds | slugs | culminant mounds	Extremely hetrogenous development progression | Streaming | loose mounds | slugs | culminant mounds
Culminate mound 20h	Normal	Normal	Hetrogenous development progression | Streaming | loose mounds | slugs | culminant mounds	Extremely hetrogenous development progression | Streaming | loose mounds | slugs | culminant mounds
Fruiting body 24h	Normal	Normal	Hetrogenous development progression | Many stalled mounds and fruiting bodies	Large loose mounds
48 h	Normal	Normal	Hetrogenous development progression | Stalled mounds | collapsed fruiting bodies	Many large loose mounds | Few fruiting bodies

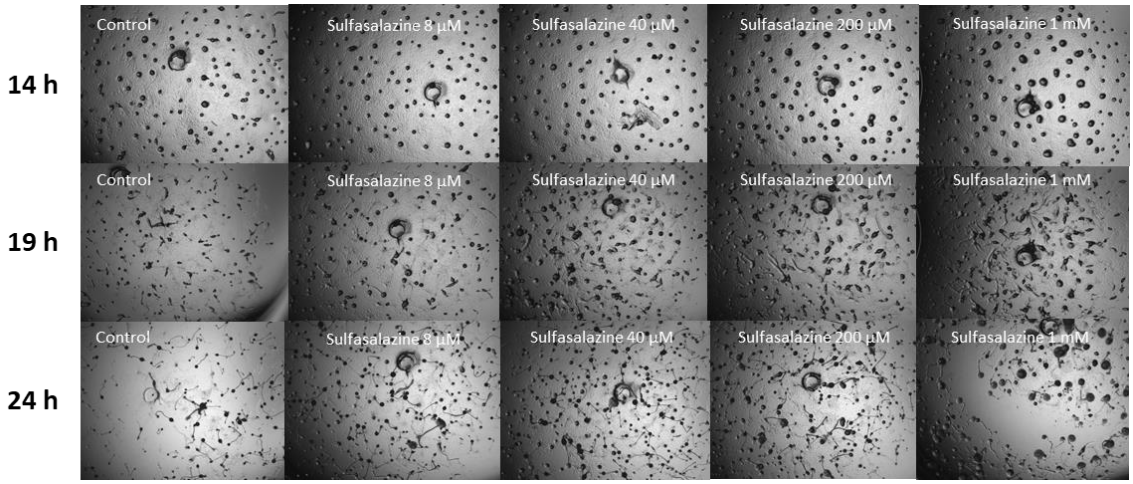

31. Ascorbic acid				
Dose	40 µM	200 µM	1 mM	*5 mM*
Aggregation 4h	Normal	Normal	Normal	Normal
Streaming 8h	Normal	Normal	Normal	Normal
Mound 14h	Normal	Normal	Normal	Normal
Slug 18h	Normal	Normal	Normal	Hetrogenous development progression | Slugs and culminant mounds | One mound with 2 tips
Culminate mound 20h	Normal	Normal	Normal	Hetrogenous development progression | Slugs and culminant mounds
Fruiting body 24h	Normal	Normal	Normal	Hetrogenous development progression | Sparse smaller fruiting bodies | Some long thin slugs | Slugs trailing rear
48 h	Normal	Normal	Normal	Larger sporeheads

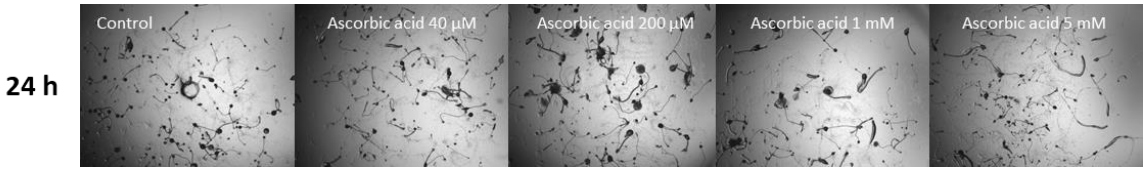

32. Acebutolol					
Dose	**9.6 µM**	**48 µM**	**240 µM**	***1.2 mM***	**6 mM**
Aggregation 4h	Normal	Normal	Normal	Normal	Normal
Streaming 8h	Normal	Normal	Normal	Normal	Normal
Mound 14h	Normal	Normal	Normal	Normal	Normal
Slug 18h	Normal	Normal	Normal	Hetrogenous development progression	Multiple slug coming from the same mound
Culminate mound 20h	Normal	Normal	Normal	Hetrogenous development progression	Extended slug migration
Fruiting body 24h	Normal	Normal	Normal	Hetrogenous development progression	Hetrogenous development progression | Slugs and culminant mounds
48 h	Normal	Normal	Normal	Normal	10 % of fruiting bodies are twisted

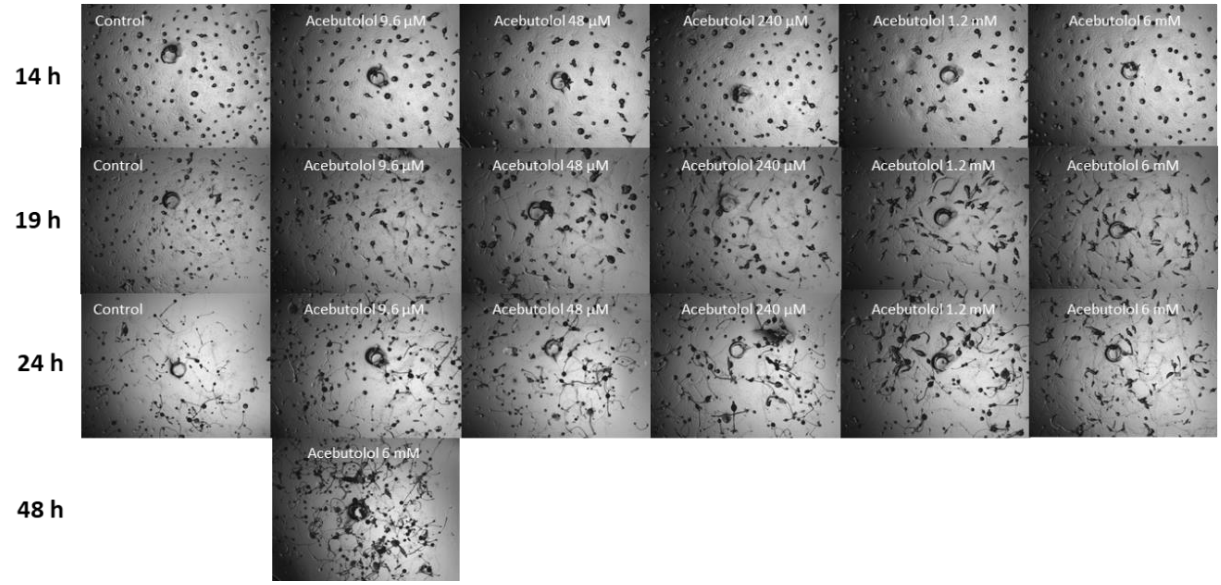

33. Camphor				
Dose	**24 µM**	**120 µM**	**600 µM**	***3 mM***
Aggregation 4h	Normal	Normal	Normal	Normal
Streaming 8h	Normal	Normal	Normal	Normal
Mound 14h	Normal	Normal	Normal	Normal
Slug 18h	Normal	Normal	Normal	Normal
Culminate mound 20h	Normal	Normal	Normal	Normal
Fruiting body 24h	Normal	Normal	Normal	Normal
48 h	Normal	Normal	Normal	Normal

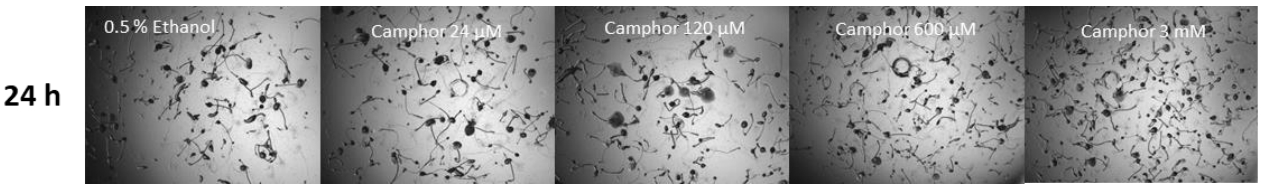

34. Citric acid						
Dose	**16 µM**	**80 µM**	**400 µM**	***2 mM***	**10 mM**	**50 mM**
Aggregation 4h	Normal	Normal	Normal	Normal	Dead	Dead
Streaming 8h	Normal	Normal	Normal	Large loose streams | Thick steam arms	Dead	Dead
Mound 14h	Normal	Normal	Normal	Larger mounds	Dead	Dead
Slug 19h	Normal	Normal	Normal	Very large, long thin slugs| Rear of the slugs can be left behind |Loose puddles of cells	Dead	Dead
Culminate mound 20h	Normal	Normal	Normal	Hetrogenous development progression | Rear of the slugs can be left behind | Loose puddles of cells	Dead	Dead
Fruiting body 24h	Normal	Normal	Normal	Hetrogenous development progression | Sparse fruiting bodies| Loose puddles of cells	Dead	Dead
48 h	Normal	Normal	Normal	Normal	Dead	Dead

24 h

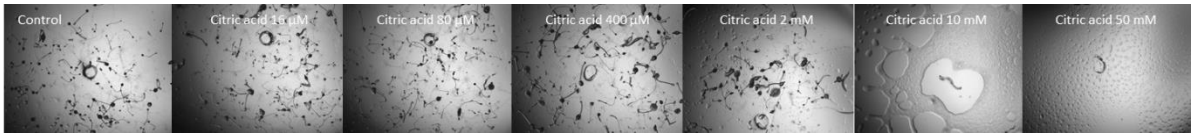

35. Penicillin G				
Dose	**96 µM**	**480 µM**	**2.4 mM**	***12 mM***
Aggregation 4h	Normal	Normal	Normal	Normal
Streaming 8h	Normal	Normal	Normal	Normal
Mound 14h	Normal	Normal	Normal	Normal
Slug 18h	Normal	Normal	Normal	Normal
Culminate mound 20h	Normal	Normal	Normal	Normal
Fruiting body 24h	Normal	Normal	Normal	Normal
48 h	Normal	Normal	Normal	Normal

24 h

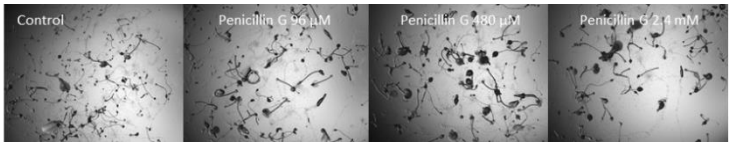

36. Saccharin				
Dose	**280 µM**	**1.4 mM**	**7 mM**	***35 mM***
Aggregation 4h	Normal	Normal	Normal	Normal
Streaming 8h	Normal	Normal	Some aggregation minus cells | Streaming delay | Uneven stream arms	Aggregation minus | Delayed streaming
Mound 14h	Normal	Normal	Normal	Delayed mounds | Manily lawn of aggregation minus cells | Few normal mounds
Slug 18h	Normal	Normal	Delayed slug formation	Some stalled mounds | Manily lawn of aggregation minus cells | Few delayed slugs
Culminate mound 20h	Normal	Normal	Normal	Some stalled mounds | Manily lawn of aggregation minus cells | Few delayed slugs
Fruiting body 24h	Normal	Normal	Normal	Some stalled mounds | Manily lawn of aggregation minus cells | Few delayed slugs
48 h	Normal	Normal	Normal	-

24 h

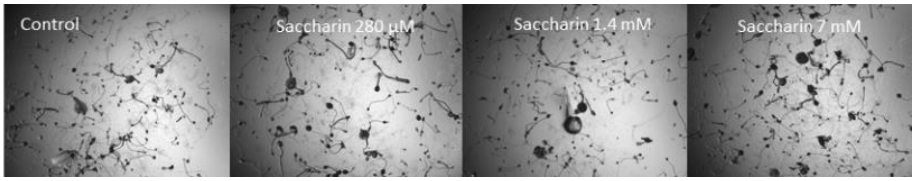

37. Metformin				
Dose	**40 µM**	**200 µM**	**1 mM**	***5 mM***
Aggregation 4h	Normal	Normal	Normal	Normal
Streaming 8h	Normal	Normal	Normal	Normal
Mound 14h	Normal	Normal	Normal	Normal
Slug 18h	Normal	Normal	Normal	Normal
Culminate mound 20h	Normal	Normal	Normal	Normal
Fruiting body 24h	Normal	Normal	Normal	Normal
48 h	Normal	Normal	Normal	Normal

24 h

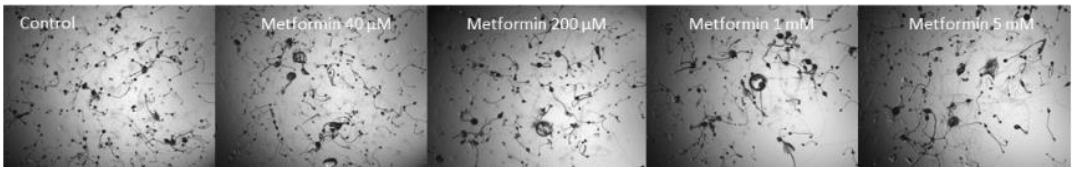

Figure A.7.2 Quantitative FPR data. **Figure over pages 222 – 231.**

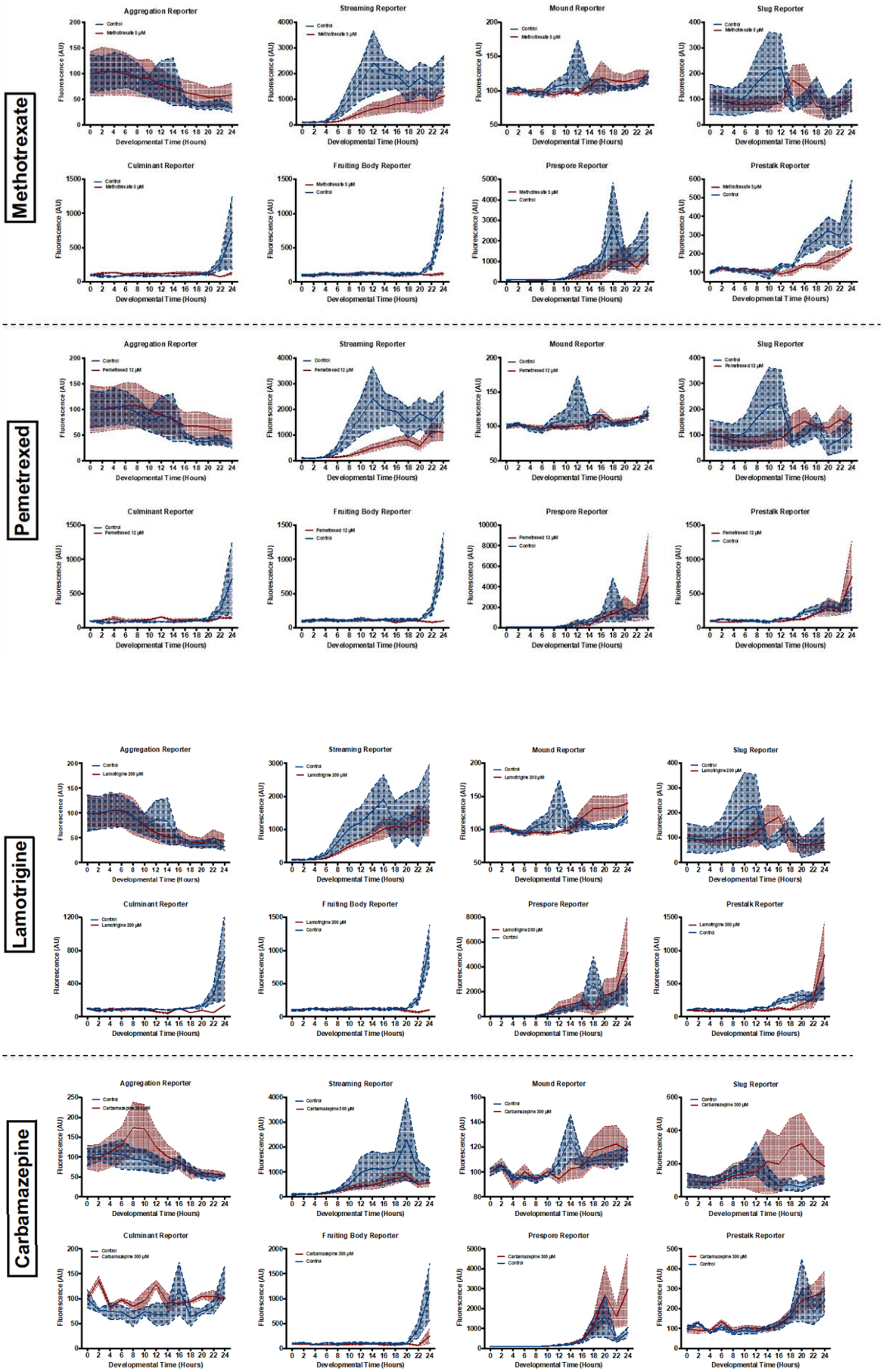

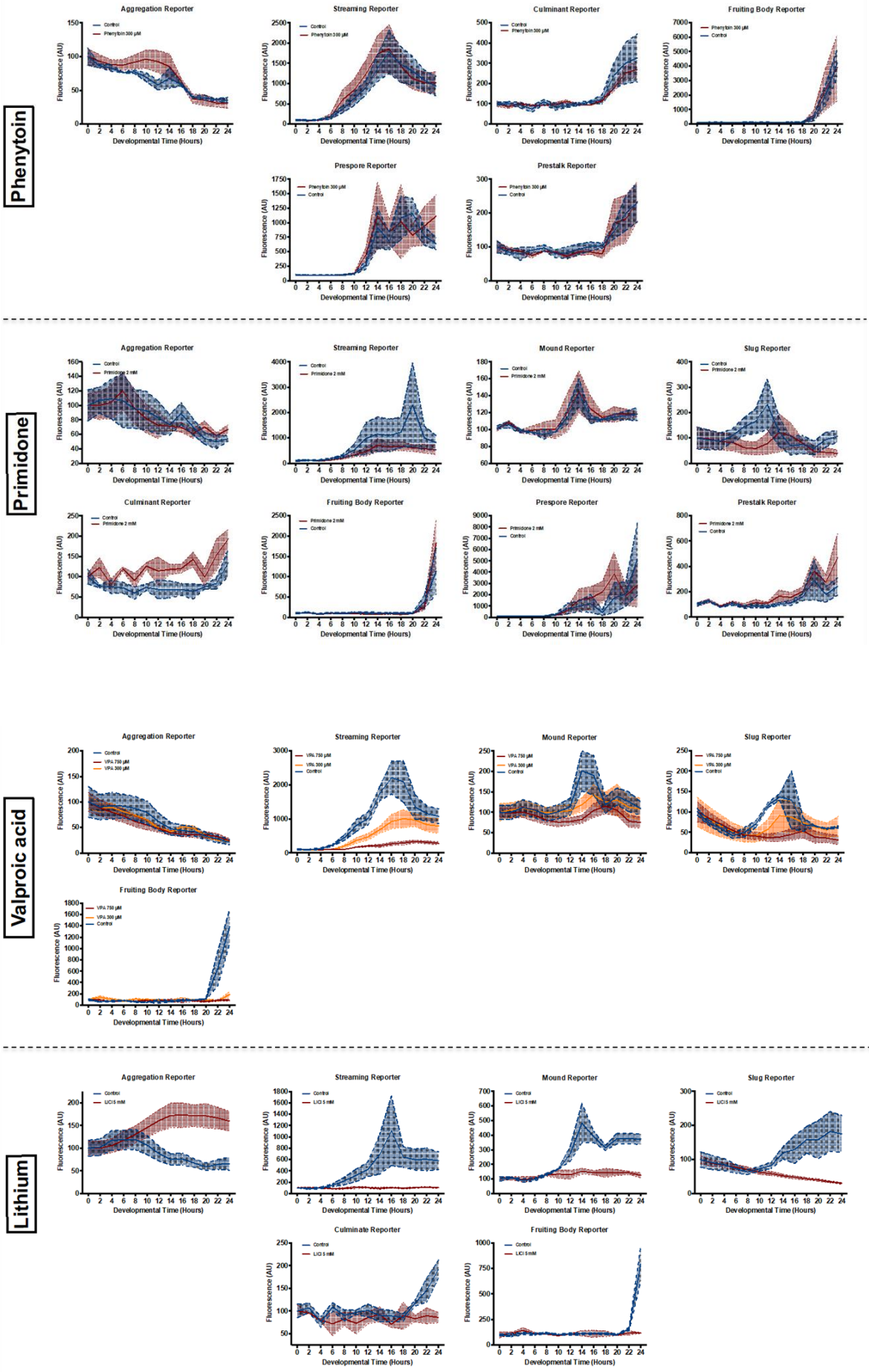
Phenytoin
Aggregation Reporter
Streaming Reporter
Culminant Reporter
Fruiting Body Reporter
Prespore Reporter
Prestalk Reporter
Primidone
Aggregation Reporter
Streaming Reporter
Mound Reporter
Slug Reporter
Culminant Reporter
Fruiting Body Reporter
Prespore Reporter
Prestalk Reporter
Valproic acid
Aggregation Reporter
Streaming Reporter
Mound Reporter
Slug Reporter
Fruiting Body Reporter
Lithium
Aggregation Reporter
Streaming Reporter
Mound Reporter
Slug Reporter
Culminate Reporter
Fruiting Body Reporter
Fluorescence (AU)
Developmental Time (Hours)

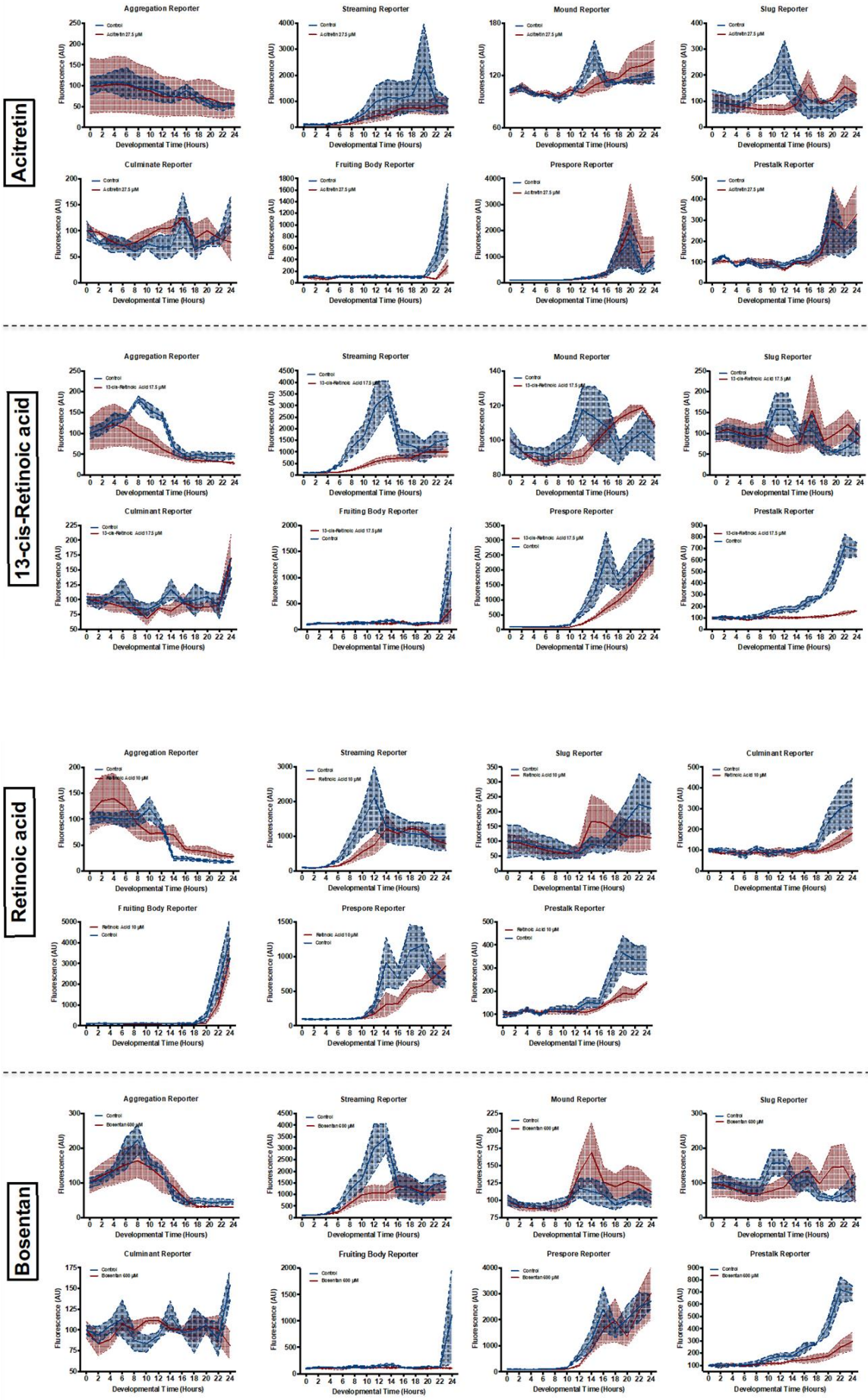
Acitretin
Aggregation Reporter
Streaming Reporter
Mound Reporter
Slug Reporter
Culminate Reporter
Fruiting Body Reporter
Prespore Reporter
Prestalk Reporter
13-cis-Retinoic acid
Culminant Reporter
Retinoic acid
Bosentan
Fluorescence (AU)
Developmental Time (Hours)
Control

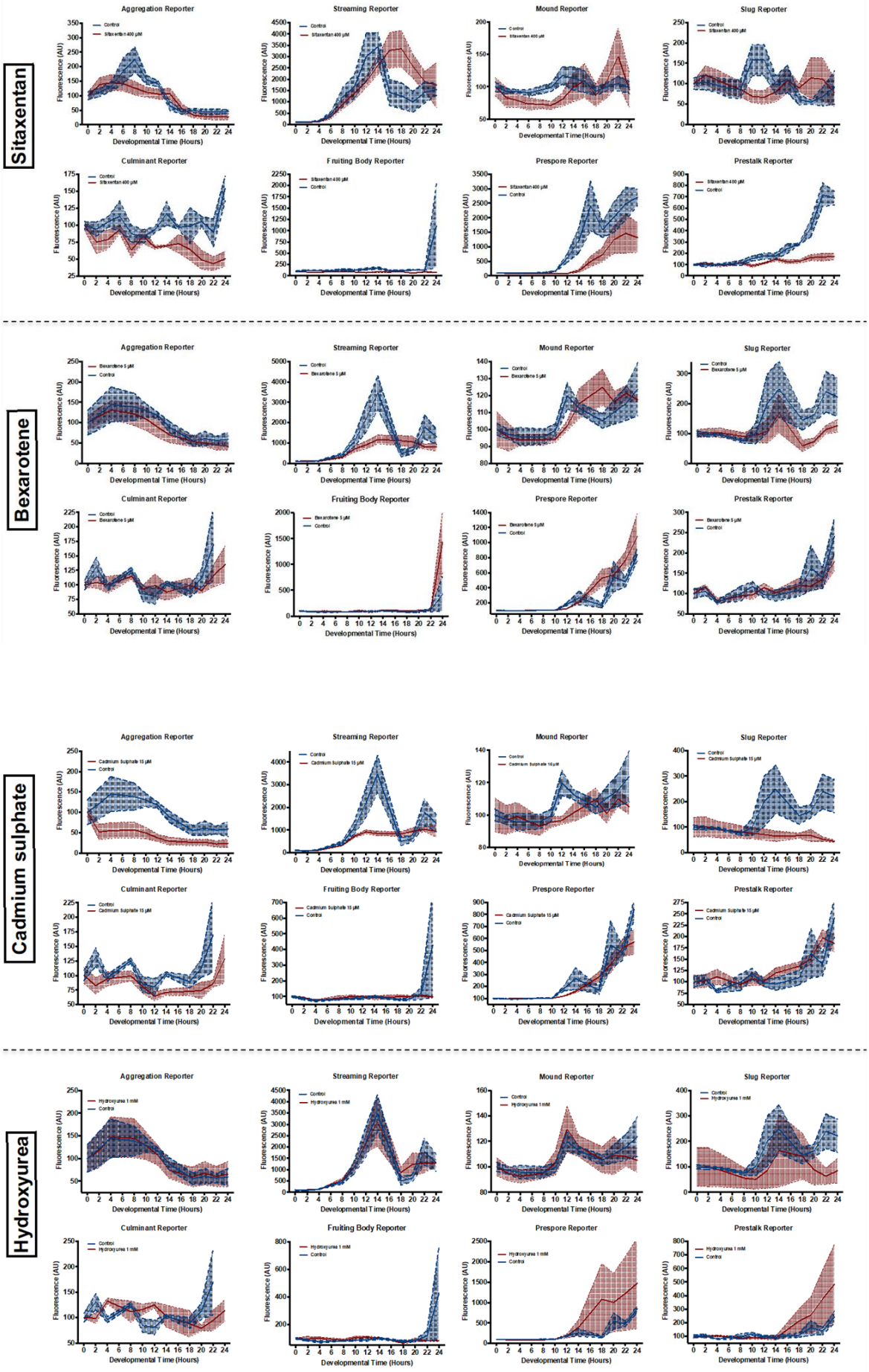
Sitaxentan
Aggregation Reporter
Streaming Reporter
Mound Reporter
Slug Reporter
Culminant Reporter
Fruiting Body Reporter
Prespore Reporter
Prestalk Reporter
Bexarotene
Cadmium sulphate
Hydroxyurea
Fluorescence (AU)
Developmental Time (Hours)

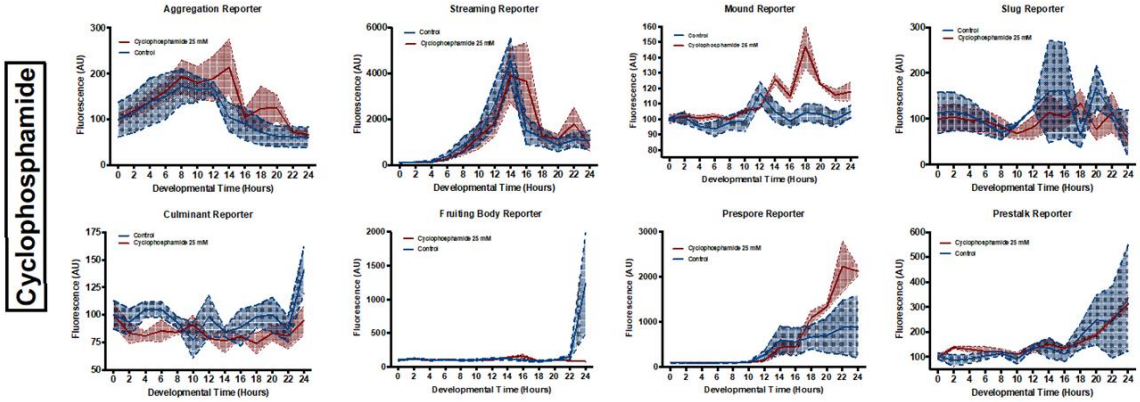
Cyclophosphamide
Aggregation Reporter
Streaming Reporter
Mound Reporter
Slug Reporter
Culminant Reporter
Fruiting Body Reporter
Prespore Reporter
Prestalk Reporter
Fluorescence (AU)
Developmental Time (Hours)
Control
Cyclophosphamide 25 mM

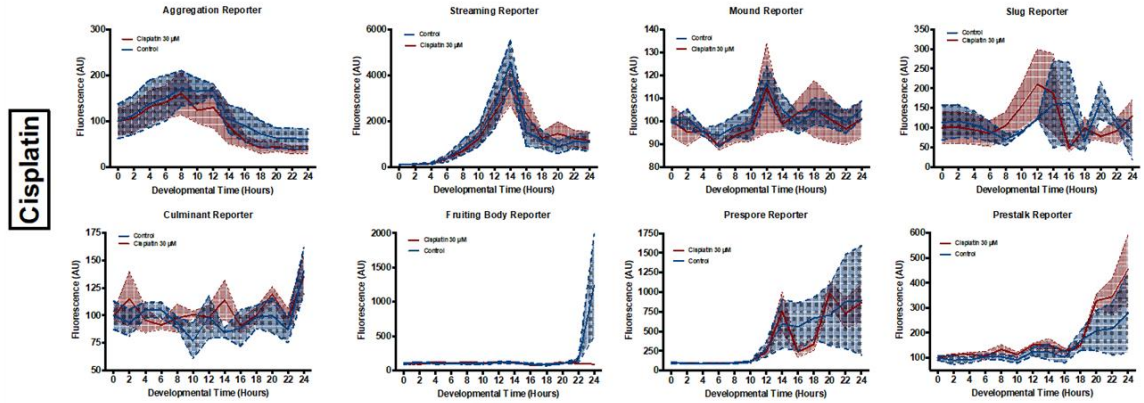
Cisplatin
Aggregation Reporter
Streaming Reporter
Mound Reporter
Slug Reporter
Culminant Reporter
Fruiting Body Reporter
Prespore Reporter
Prestalk Reporter
Fluorescence (AU)
Developmental Time (Hours)
Control
Cisplatin 30 µM

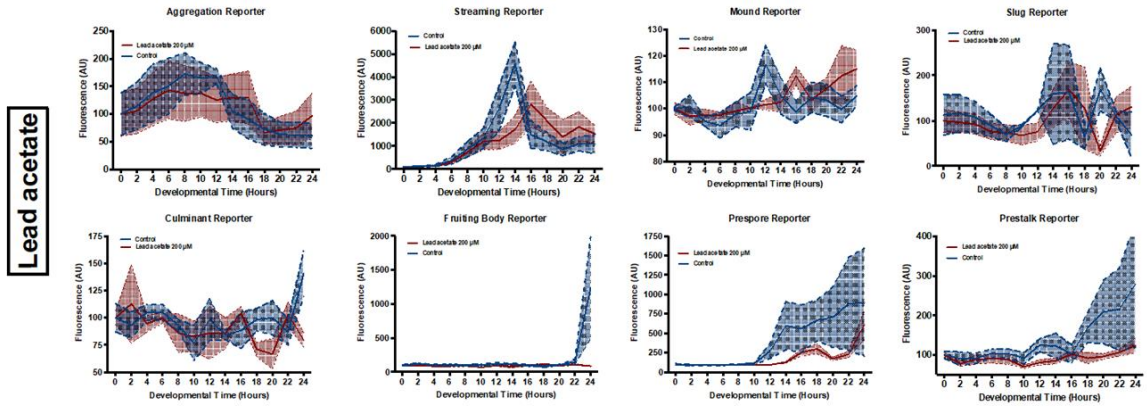
Lead acetate
Aggregation Reporter
Streaming Reporter
Mound Reporter
Slug Reporter
Culminant Reporter
Fruiting Body Reporter
Prespore Reporter
Prestalk Reporter
Fluorescence (AU)
Developmental Time (Hours)
Control
Lead acetate 200 µM

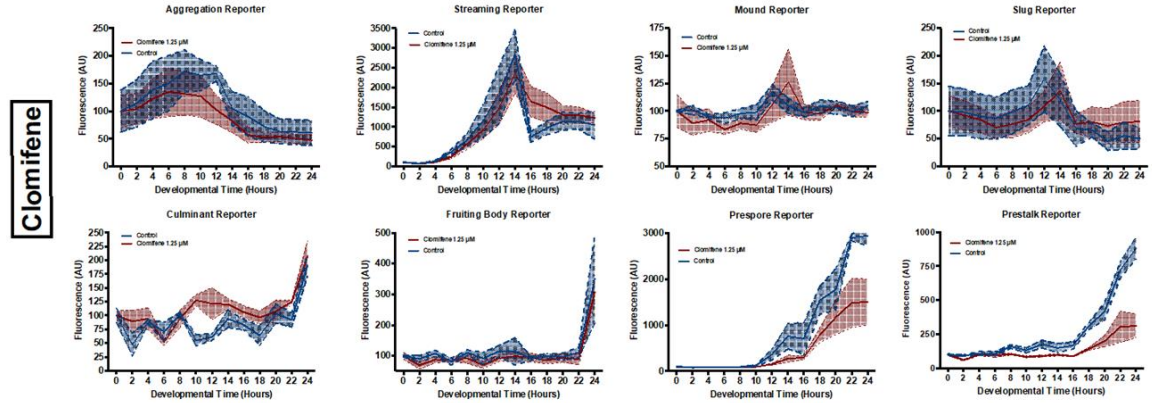
Clomifene
Aggregation Reporter
Streaming Reporter
Mound Reporter
Slug Reporter
Culminant Reporter
Fruiting Body Reporter
Prespore Reporter
Prestalk Reporter
Fluorescence (AU)
Developmental Time (Hours)
Control
Clomifene 1.25 µM

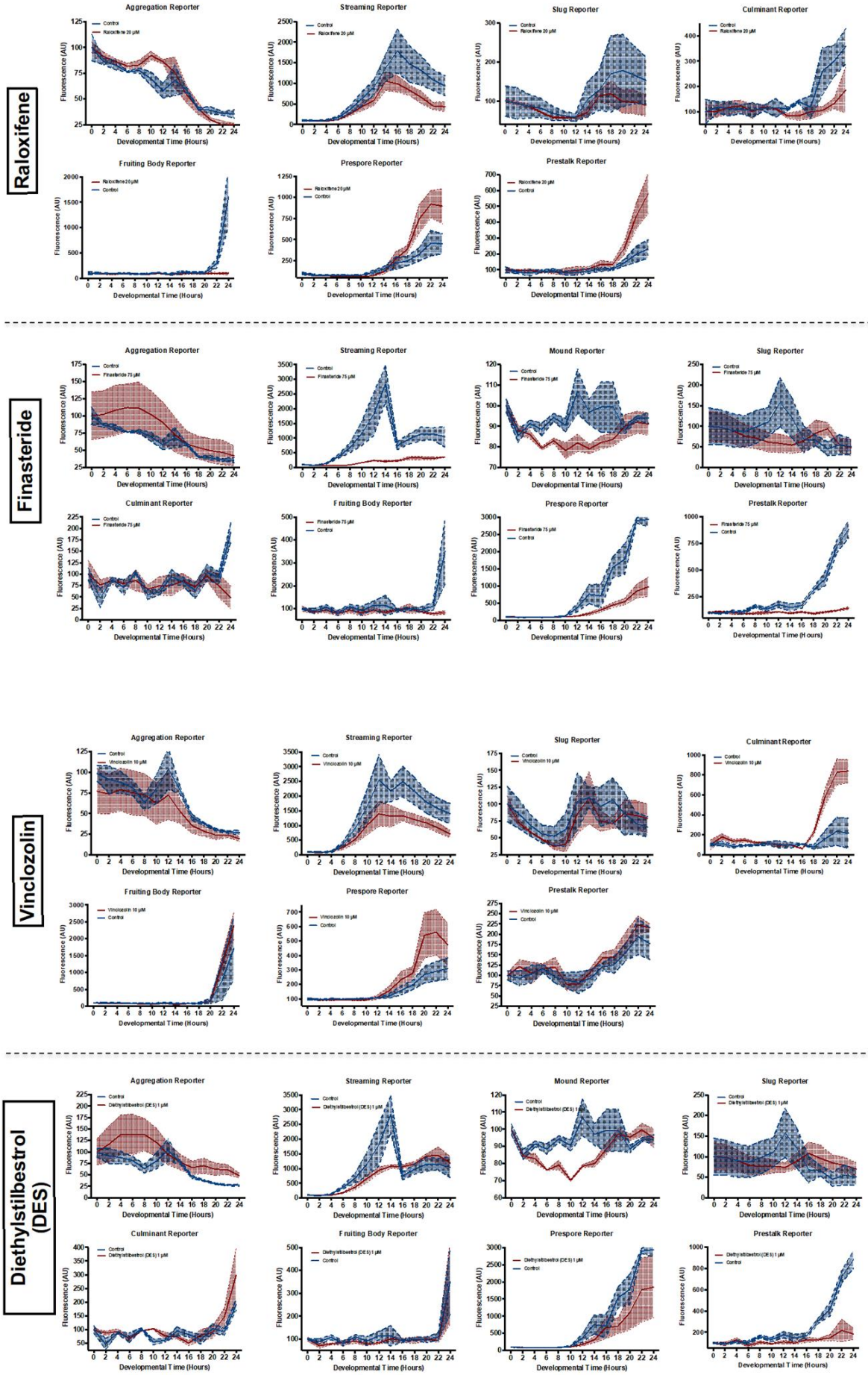
Raloxifene
Aggregation Reporter
Streaming Reporter
Slug Reporter
Culminant Reporter
Fruiting Body Reporter
Prespore Reporter
Prestalk Reporter
Finasteride
Aggregation Reporter
Streaming Reporter
Mound Reporter
Slug Reporter
Culminant Reporter
Fruiting Body Reporter
Prespore Reporter
Prestalk Reporter
Vinclozolin
Aggregation Reporter
Streaming Reporter
Slug Reporter
Culminant Reporter
Fruiting Body Reporter
Prespore Reporter
Prestalk Reporter
Diethylstilbestrol (DES)
Aggregation Reporter
Streaming Reporter
Mound Reporter
Slug Reporter
Culminant Reporter
Fruiting Body Reporter
Prespore Reporter
Prestalk Reporter
Fluorescence (AU)
Developmental Time (Hours)

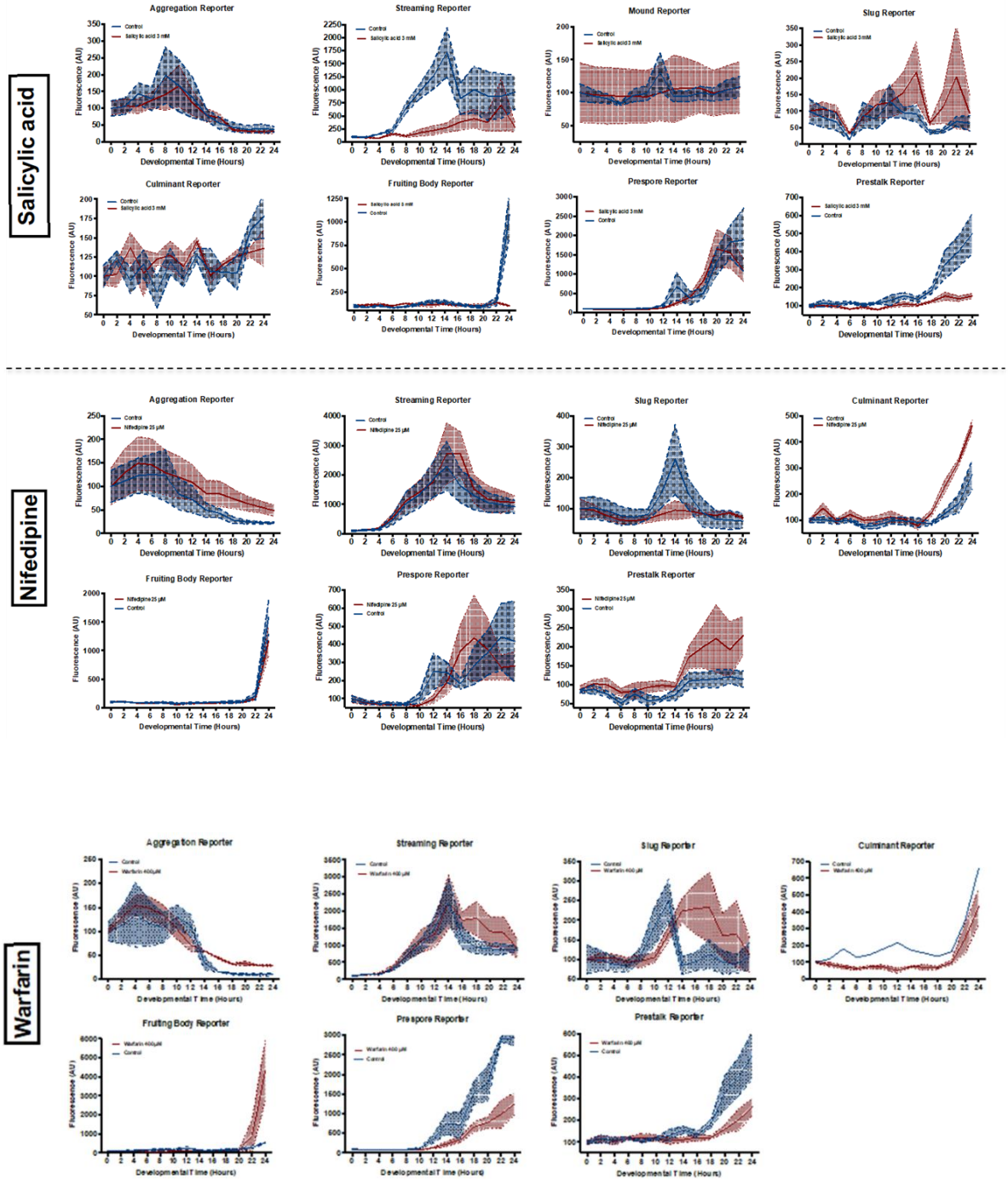
Salicylic acid
Aggregation Reporter
Streaming Reporter
Mound Reporter
Slug Reporter
Culminant Reporter
Fruiting Body Reporter
Prespore Reporter
Prestalk Reporter
Control
Salicylic acid 3 mM
Fluorescence (AU)
Developmental Time (Hours)
Nifedipine
Aggregation Reporter
Streaming Reporter
Slug Reporter
Culminant Reporter
Fruiting Body Reporter
Prespore Reporter
Prestalk Reporter
Control
Nifedipine 25 µM
Fluorescence (AU)
Developmental Time (Hours)
Warfarin
Aggregation Reporter
Streaming Reporter
Slug Reporter
Culminant Reporter
Fruiting Body Reporter
Prespore Reporter
Prestalk Reporter
Control
Warfarin 400 µM
Fluorescence (AU)
Developmental Time (Hours)

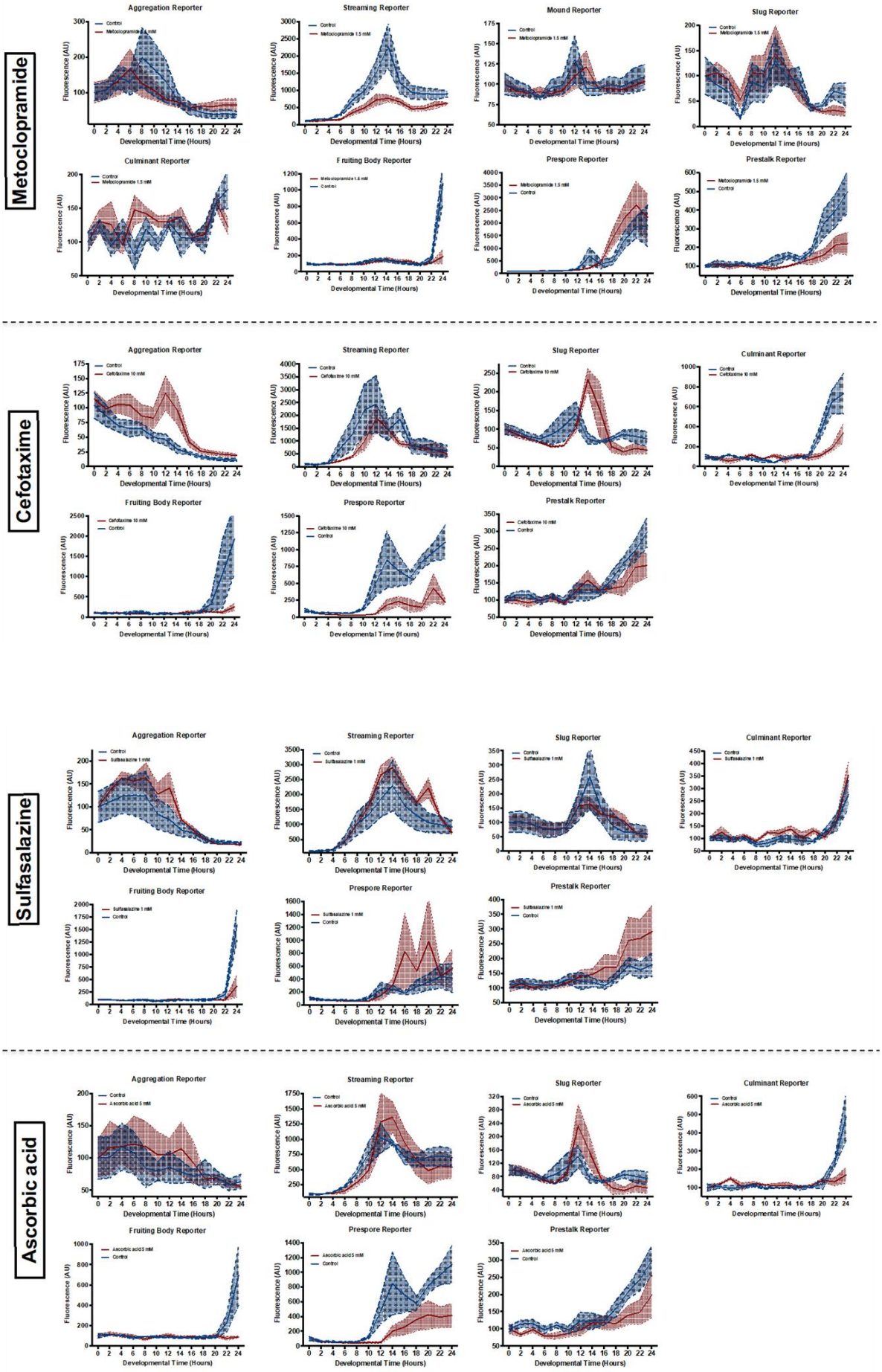
Metoclopramide
Aggregation Reporter
Streaming Reporter
Mound Reporter
Slug Reporter
Culminant Reporter
Fruiting Body Reporter
Prespore Reporter
Prestalk Reporter
Control
Metoclopramide 1.5 mM
Fluorescence (AU)
Developmental Time (Hours)
Cefotaxime
Aggregation Reporter
Streaming Reporter
Slug Reporter
Culminant Reporter
Fruiting Body Reporter
Prespore Reporter
Prestalk Reporter
Control
Cefotaxime 10 mM
Fluorescence (AU)
Developmental Time (Hours)
Sulfasalazine
Aggregation Reporter
Streaming Reporter
Slug Reporter
Culminant Reporter
Fruiting Body Reporter
Prespore Reporter
Prestalk Reporter
Control
Sulfasalazine 1 mM
Fluorescence (AU)
Developmental Time (Hours)
Ascorbic acid
Aggregation Reporter
Streaming Reporter
Slug Reporter
Culminant Reporter
Fruiting Body Reporter
Prespore Reporter
Prestalk Reporter
Control
Ascorbic acid 5 mM
Fluorescence (AU)
Developmental Time (Hours)

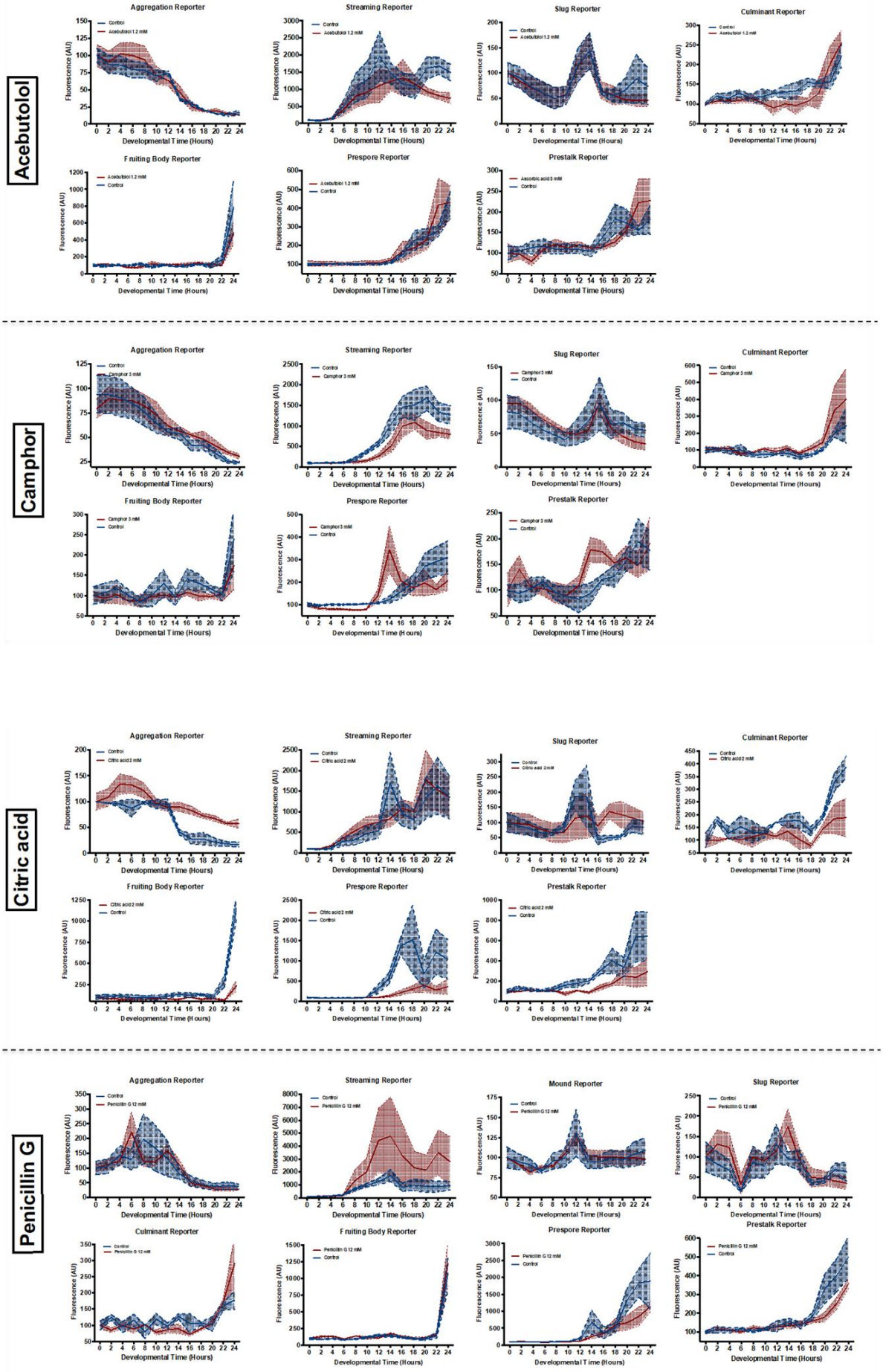
Acebutolol
Aggregation Reporter
Streaming Reporter
Slug Reporter
Culminant Reporter
Fruiting Body Reporter
Prespore Reporter
Prestalk Reporter
Camphor
Aggregation Reporter
Streaming Reporter
Slug Reporter
Culminant Reporter
Fruiting Body Reporter
Prespore Reporter
Prestalk Reporter
Citric acid
Aggregation Reporter
Streaming Reporter
Slug Reporter
Culminant Reporter
Fruiting Body Reporter
Prespore Reporter
Prestalk Reporter
Penicillin G
Aggregation Reporter
Streaming Reporter
Mound Reporter
Slug Reporter
Culminant Reporter
Fruiting Body Reporter
Prespore Reporter
Prestalk Reporter
Fluorescence (AU)
Developmental Time (Hours)

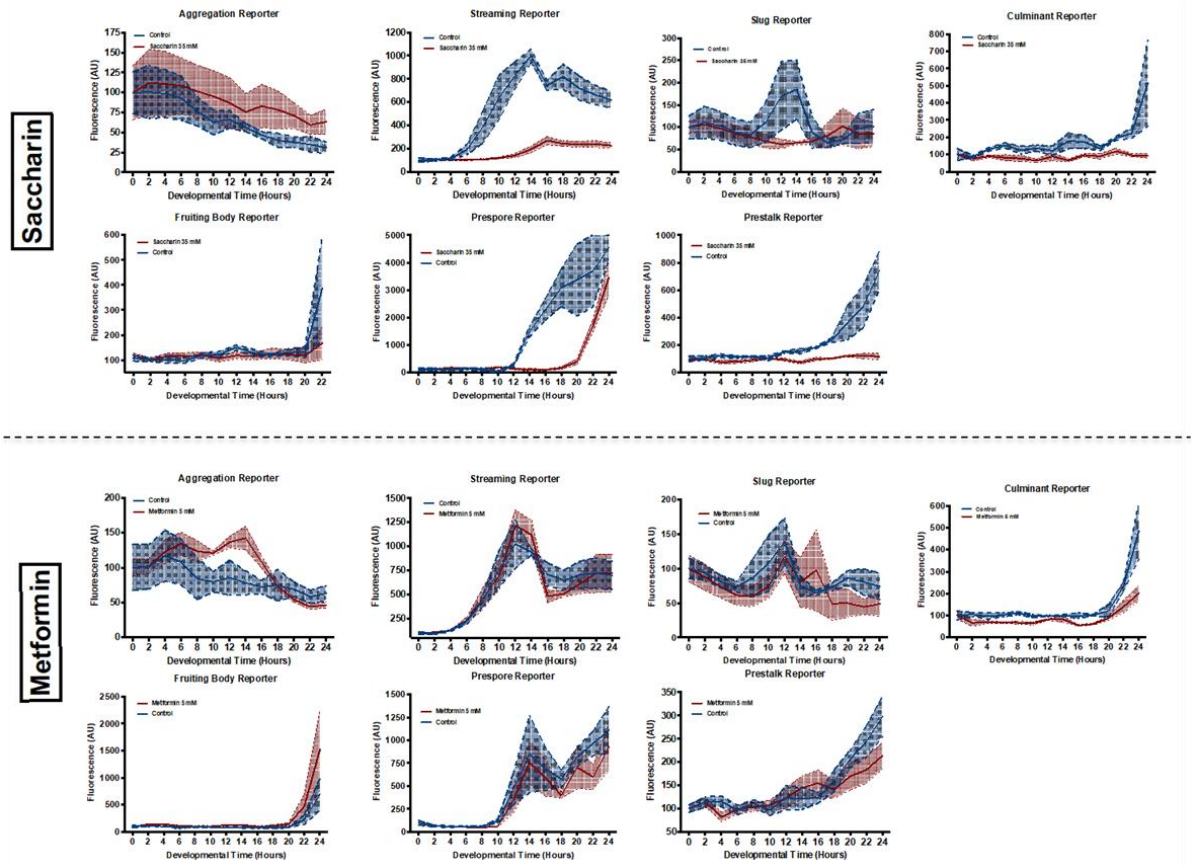
Saccharin
Aggregation Reporter
Streaming Reporter
Slug Reporter
Culminant Reporter
Fruiting Body Reporter
Prespore Reporter
Prestalk Reporter
Fluorescence (AU)
Developmental Time (Hours)
Control
Saccharin 35 mM

Metformin
Aggregation Reporter
Streaming Reporter
Slug Reporter
Culminant Reporter
Fruiting Body Reporter
Prespore Reporter
Prestalk Reporter
Fluorescence (AU)
Developmental Time (Hours)
Control
Metformin 5 mM

Table A.7.3 Significantly advantaged and disadvantaged lithium mutant lists.

Screen Rank	Mutant ID	Gene name	Screen behaviour	Mean Norm. Lithium readcount	Mean Norm. DMSO readcount
1	DDB0232429_4757950_CATG	**lsrA**	Advantage	183,726	1
2	DDB0232429_3582544_CATG	**cyp508A2-2**	Advantage	146,460	1
3	DDB0232429_2449245_CATG	**cyp508A2-1**	Advantage	104,823	1
4	DDB0232431_2254100_GATC	**DDB_G0284721**	Advantage	75,817	1
5	DDB0232432_1291047_CATG	**fslE**	Advantage	22,851	844
6	DDB0232432_3833313_CATG	**DDB_G0290231**	Advantage	11,039	21
7	DDB0232431_2254316_CATG	**DDB_G0284721**	Advantage	9,961	1
8	DDB0232432_3828004_GATC	**npl4**	Advantage	9,621	101
9	DDB0232429_4761262_GATC	**DDB_G0274981**	Advantage	7,119	1
10	DDB0232429_198220_CATG	**abcA7**	Advantage	5,317	1
11	DDB0232431_310315_CATG	**DDB_G0283213**	Advantage	4,915	133
12	DDB0232432_576570_GATC	**DDB_G0287701**	Advantage	4,433	117
13	DDB0232430_4004024_GATC	**DDB_G0281069**	Advantage	4,361	1.71
14	DDB0232433_250962_CATG	**DDB_G0291394**	Advantage	4,034	9.63
15	DDB0232431_4536258_CATG	**DDB_G0295785**	Advantage	4,015	39.8
16	DDB0232433_2102124_GATC	**DDB_G0292822**	Advantage	3,853	1
17	DDB0232431_4796593_GATC	**DDB_G0286655**	Advantage	3,292	1
18	DDB0232433_3248329_GATC	**DDB_G0293678**	Advantage	3,225	330
19	DDB0232432_2441760_GATC	**DDB_G0289167**	Advantage	3,041	72.7
20	DDB0232431_3452953_GATC	**DDB_G0285767**	Advantage	2,705	27.8
21	DDB0232430_2441210_GATC	**DDB_G0279681**	Advantage	2,605	291
22	DDB0232430_1381840_CATG	**DDB_G0278909**	Advantage	2,309	159
23	DDB0232431_1314786_GATC	**pks22**	Advantage	2,167	145
24	DDB0232429_5746977_CATG	**DDB_G0275861**	Advantage	2,093	93
25	DDB0232432_1384902_CATG	**dgtA**	Advantage	1,821	358
26	DDB0232431_2876457_GATC	**rad54b**	Advantage	1,666	793
27	DDB0232431_32004_GATC	**DDB_G0282945**	Advantage	1,535	1
28	DDB0232428_3870542_GATC	**DDB_G0269920**	Advantage	1,491	98.7
29	DDB0232428_4218470_GATC	**uduC**	Advantage	1,315	124
30	DDB0232428_1639788_GATC	**fut11**	Advantage	1,283	1
31	DDB0232428_201627_CATG	**DDB_G0267458**	Advantage	1,176	1
32	DDB0232432_4730363_GATC	**gefK**	Advantage	1,102	1
33	DDB0232428_1513759_GATC	**DDB_G0268130**	Advantage	991	56.4
34	DDB0232428_512372_CATG	**tgrO2**	Advantage	941	1.15
35	DDB0232431_2257802_GATC	**DDB_G0284625**	Advantage	779	42.6
36	DDB0232429_5592392_GATC	**abcH3**	Advantage	699	1
37	DDB0232431_1051000_GATC	**DDB_G0283753**	Advantage	659	1
38	DDB0232432_3439242_CATG	**uppA**	Advantage	607	1
39	DDB0232428_1606976_CATG	**pslA**	Advantage	551	1
40	DDB0232429_6503513_GATC	**DDB_G0276251**	Advantage	545	1
41	DDB0232431_4361009_GATC	**DDB_G0286363**	Advantage	496	252
42	DDB0232432_451305_GATC	**nagC**	Advantage	430	283
43	DDB0232429_4113372_GATC	**fncM**	Advantage	428	1
44	DDB0232430_3726010_GATC	**DDB_G0280773**	Advantage	426	407
45	DDB0232428_285956_CATG	**DDB_G0267532**	Advantage	410	1
46	DDB0232431_1784417_CATG	**ppil2**	Advantage	409	313
47	DDB0232429_7229564_CATG	**gxcN**	Advantage	365	703
48	DDB0232432_2007050_GATC	**DDB_G0288811**	Advantage	359	138
49	DDB0232430_6008658_CATG	**DDB_G0282621**	Advantage	357	179
50	DDB0232431_3915798_CATG	**DDB_G0285991**	Advantage	348	387
51	DDB0232430_176856_CATG	**DDB_G0278029**	Advantage	327	177
52	DDB0232432_209965_GATC	**DDB_G0287457**	Advantage	325	1
53	DDB0232433_1395449_GATC	**DDB_G0292288**	Advantage	303	3.06
54	DDB0232430_1729999_CATG	**DDB_G0279181**	Advantage	302	338
55	DDB0232429_904131_CATG	**DDB_G0271836**	Advantage	296	248
56	DDB0232432_4962097_CATG	**gbpC**	Advantage	293	179
57	DDB0232433_78426_CATG	**ranA**	Advantage	287	692
58	DDB0232432_503101_GATC	**DDB_G0287665**	Advantage	285	156
59	DDB0232431_1023266_CATG	**rpkA**	Advantage	280	406
60	DDB0232431_2469721_GATC	**fut2**	Advantage	274	214
61	DDB0232428_3768988_GATC	**DDB_G0269870**	Advantage	274	1
62	DDB0232431_2087044_GATC	**sgkB**	Advantage	273	353
63	DDB0232432_3985783_GATC	**DDB_G0290337**	Advantage	270	288
64	DDB0232431_5295981_GATC	**DDB_G0287075**	Advantage	268	797
65	DDB0232432_4407329_GATC	**DDB_G0290635**	Advantage	249	1
66	DDB0232431_3822777_GATC	**gacK**	Advantage	242	108
67	DDB0232433_2666181_CATG	**psiQ**	Advantage	240	1
68	DDB0232430_2652375_CATG	**DDB_G0279897**	Advantage	240	138

Table continue on next page

69	DDB0232431_2253599_CATG	**DDB_G0284721**	Advantage	234	1
70	DDB0232432_149608_CATG	**DDB_G0287439**	Advantage	233	184
71	DDB0232428_4212179_GATC	**DDB_G0270100**	Advantage	229	519
72	DDB0232428_4002502_CATG	**DDB_G0270700**	Advantage	222	226
73	DDB0232428_436600_CATG	**DDB_G0267620**	Advantage	205	1.25
74	DDB0232428_516204_CATG	**tgrO3**	Advantage	164	2.38
75	DDB0232429_424314_GATC	**DDB_G0271482**	Advantage	97	1.53
76	DDB0232428_4268550_GATC	**atg6A**	Advantage	92	1

1	DDB0232429_3834387_GATC	**DDB_G0274349**	Disadvantage	118	1026
2	DDB0232430_6246367_CATG	**gefC**	Disadvantage	1	155
3	DDB0232430_2522165_GATC	**DDB_G0279759**	Disadvantage	1.54	228
4	DDB0232431_1314786_GATC	**pks22**	Disadvantage	233	1601
5	DDB0232430_1482339_GATC	**DG2033**	Disadvantage	1	140
6	DDB0232429_3947362_CATG	**DDB_G0274807**	Disadvantage	1	138
7	DDB0232433_715037_CATG	**arpE**	Disadvantage	1.35	160
8	DDB0232428_850496_GATC	**DDB_G0267784**	Disadvantage	1.47	170
9	DDB0232431_1128561_CATG	**DDB_G0283807**	Disadvantage	1	119
10	DDB0232433_3101030_CATG	**DDB_G0293592**	Disadvantage	1	116
11	DDB0232433_2213310_GATC	**DDB_G0292884**	Disadvantage	1.47	161
12	DDB0232428_2428552_CATG	**DDB_G0269270**	Disadvantage	1	112
13	DDB0232428_2429439_GATC	**DDB_G0269270**	Disadvantage	1	110
14	DDB0232431_2332196_GATC	**expl2**	Disadvantage	1	108
15	DDB0232432_4405812_CATG	**DDB_G0290635**	Disadvantage	203	1246
16	DDB0232429_7415677_GATC	**ifkB**	Disadvantage	1.40	146
17	DDB0232428_1236441_GATC	**DDB_G0267984**	Disadvantage	1	107
18	DDB0232431_488761_CATG	**tgrI1**	Disadvantage	1	104
19	DDB0232428_3353533_CATG	**DDB_G0269700**	Disadvantage	1	104
20	DDB0232429_810278_CATG	**pckA**	Disadvantage	1.63	143
21	DDB0232429_1938067_GATC	**DDB_G0272696**	Disadvantage	1.49	131
22	DDB0232429_215324_CATG	**DDB_G0271250**	Disadvantage	1.05	100
23	DDB0232429_1417104_GATC	**DDB_G0272386**	Disadvantage	2.03	161
24	DDB0232429_5474335_GATC	**DDB_G0275375**	Disadvantage	3.03	239
25	DDB0232428_3841778_GATC	**DDB_G0270994**	Disadvantage	1.82	158
26	DDB0232432_772122_GATC	**DDB_G0287825**	Disadvantage	1.63	127
27	DDB0232430_1177585_GATC	**DDB_G0278787**	Disadvantage	1.35	107
28	DDB0232429_6027834_CATG	**DDB_G0275911**	Disadvantage	1.47	118
29	DDB0232428_1291192_CATG	**DDB_G0268008**	Disadvantage	3.49	243
30	DDB0232433_1203444_CATG	**galK**	Disadvantage	1.63	109
31	DDB0232430_5314879_GATC	**DDB_G0281949**	Disadvantage	3.42	179
32	DDB0232429_4859882_CATG	**DDB_G0274617**	Disadvantage	2.17	150
33	DDB0232433_3353669_CATG	**DDB_G0293810**	Disadvantage	3.9	173
34	DDB0232429_3700672_GATC	**DDB_G0274041**	Disadvantage	2.06	118
35	DDB0232433_671809_CATG	**abcB3**	Disadvantage	3.46	192
36	DDB0232429_7415097_CATG	**ifkB**	Disadvantage	3.77	177
37	DDB0232431_856910_GATC	**DDB_G0283577**	Disadvantage	2.34	123
38	DDB0232432_3020799_GATC	**DDB_G0289609**	Disadvantage	2.65	141
39	DDB0232432_5010304_CATG	**warA**	Disadvantage	3.35	163
40	DDB0232432_766231_CATG	**DDB_G0287821**	Disadvantage	2.34	118
41	DDB0232430_396463_GATC	**DDB_G0278173**	Disadvantage	2.76	130
42	DDB0232429_3941938_CATG	**DDB_G0274739**	Disadvantage	1.91	103
43	DDB0232433_90893_GATC	**DDB_G0291301**	Disadvantage	3.05	136
44	DDB0232430_963365_CATG	**DDB_G0278489**	Disadvantage	3.05	135
45	DDB0232429_1992739_GATC	**DDB_G0272923**	Disadvantage	6.54	395
46	DDB0232429_7379269_GATC	**DDB_G0276989**	Disadvantage	6.48	225
47	DDB0232432_2121780_CATG	**psiI**	Disadvantage	2.34	113
48	DDB0232430_4748476_GATC	**DDB_G0281639**	Disadvantage	2.73	157
49	DDB0232431_1344003_GATC	**DDB_G0283943**	Disadvantage	2.58	122
50	DDB0232429_7566707_CATG	**DDB_G0276879**	Disadvantage	4.32	167
51	DDB0232429_5759285_GATC	**abcG18**	Disadvantage	2.30	113
52	DDB0232432_2640184_GATC	**DDB_G0289321**	Disadvantage	3.49	138
53	DDB0232430_6204463_GATC	**tmem104**	Disadvantage	5.18	275
54	DDB0232428_3171960_GATC	**mgp3**	Disadvantage	5.08	224
55	DDB0232430_1603449_GATC	**DDB_G0279089**	Disadvantage	5.44	217
56	DDB0232430_2996118_CATG	**DDB_G0280133**	Disadvantage	3.35	127
57	DDB0232428_794911_GATC	**tbck**	Disadvantage	6.22	295
58	DDB0232431_2738369_GATC	**DDB_G0284975**	Disadvantage	2.65	108
59	DDB0232428_3758804_CATG	**DDB_G0270978**	Disadvantage	3.28	144
60	DDB0232433_2908514_CATG	**DDB_G0293456**	Disadvantage	3.28	118
61	DDB0232428_3885193_CATG	**DDB_G0269928**	Disadvantage	3.56	150
62	DDB0232433_640517_CATG	**DDB_G0295483**	Disadvantage	3.98	161

Table continue on next page

63	DDB0232433_2530423_GATC	**DDB_G0293116**	Disadvantage	5.09	147
64	DDB0232428_2537262_CATG	**DDB_G0270480**	Disadvantage	2.93	105
65	DDB0232433_3188567_CATG	**ponA**	Disadvantage	3.56	117
66	DDB0232432_4172240_CATG	**DDB_G0290647**	Disadvantage	4.74	133
67	DDB0232429_7680814_GATC	**vamp7B**	Disadvantage	2.46	104
68	DDB0232428_2682884_CATG	**d2hgdh**	Disadvantage	3.70	111
69	DDB0232428_4147743_GATC	**DDB_G0270060**	Disadvantage	6.93	269
70	DDB0232428_3826898_CATG	**act26**	Disadvantage	4.21	171
71	DDB0232428_4001650_GATC	**DDB_G0270002**	Disadvantage	4.12	140
72	DDB0232431_133939_GATC	**maoD**	Disadvantage	4.06	152
73	DDB0232428_3992048_GATC	**DDB_G0269994**	Disadvantage	3.63	130
74	DDB0232431_4322695_GATC	**DDB_G0286297**	Disadvantage	8.55	325
75	DDB0232432_621826_GATC	**DDB_G0287735**	Disadvantage	5.86	177
76	DDB0232431_4464463_GATC	**cyp519E1**	Disadvantage	8.86	253
77	DDB0232429_7701248_GATC	**DDB_G0277185**	Disadvantage	3.49	114
78	DDB0232428_2874280_CATG	**DDB_G0270540**	Disadvantage	5.32	190
79	DDB0232430_2912184_GATC	**gxcS**	Disadvantage	4.05	122
80	DDB0232428_2940237_CATG	**nosip**	Disadvantage	8.15	272
81	DDB0232429_3959817_GATC	**DDB_G0274575**	Disadvantage	7.45	246
82	DDB0232428_3724722_CATG	**gdt8**	Disadvantage	4.65	141
83	DDB0232429_4415022_CATG	**DDB_G0274907**	Disadvantage	4.95	127
84	DDB0232430_205598_GATC	**gefJ**	Disadvantage	6.60	209
85	DDB0232429_5620434_CATG	**DDB_G0275789**	Disadvantage	5.55	174
86	DDB0232429_673715_GATC	**lvsB**	Disadvantage	4.43	131
87	DDB0232430_971449_CATG	**DDB_G0278499**	Disadvantage	7.71	239
88	DDB0232428_1449186_GATC	**DDB_G0268096**	Disadvantage	11.80	363
89	DDB0232430_3551949_GATC	**DDB_G0280599**	Disadvantage	6.33	185
90	DDB0232432_4653610_GATC	**stlB**	Disadvantage	4.79	137
91	DDB0232432_213441_CATG	**forC**	Disadvantage	6.09	182
92	DDB0232431_3631840_GATC	**gloB1**	Disadvantage	9.99	250
93	DDB0232432_2520447_GATC	**DDB_G0289231**	Disadvantage	14.34	423
94	DDB0232428_3033225_CATG	**abcG11**	Disadvantage	4.71	133
95	DDB0232429_3801274_CATG	**fslH**	Disadvantage	10.13	288
96	DDB0232432_2239937_GATC	**DDB_G0289017**	Disadvantage	4.64	130
97	DDB0232430_566805_GATC	**DDB_G0278253**	Disadvantage	6.44	170
98	DDB0232430_965656_GATC	**DDB_G0278491**	Disadvantage	5.96	167
99	DDB0232428_2211176_CATG	**DDB_G0269014**	Disadvantage	7.38	197
100	DDB0232429_5205353_CATG	**DDB_G0275159**	Disadvantage	12.11	292
101	DDB0232433_1643921_GATC	**DDB_G0292550**	Disadvantage	11.16	273
102	DDB0232429_1408837_CATG	**DDB_G0272384**	Disadvantage	14.53	347
103	DDB0232432_2120881_GATC	**psiI**	Disadvantage	10.59	249
104	DDB0232428_246397_GATC	**DDB_G0267504**	Disadvantage	7.57	159

Table A.7.4 Significantly advantaged and disadvantaged VPA mutant lists.

Screen Rank	Mutant ID	Gene name	Screen behaviour	Mean Norm. VPA readcount	Mean Norm. DMSO readcount
1	DDB0232433_2615619_GATC	**DDB_G0293258**	Advantage	73,730	1,467
2	DDB0232433_1060701_GATC	**ric8**	Advantage	9,511	82.5
3	DDB0232431_810420_GATC	**DDB_G0283551**	Advantage	7,276	397
4	DDB0232428_218219_GATC	**DDB_G0267494**	Advantage	6,569	933
5	DDB0232430_3091994_GATC	**hdaC**	Advantage	5,724	761
6	DDB0232430_1252700_GATC	**DDB_G0278945**	Advantage	5,018	795
7	DDB0232429_4035058_GATC	**DDB_G0274825**	Advantage	4,835	1
8	DDB0232429_3895022_GATC	**DG1124**	Advantage	4,772	134
9	DDB0232429_5917468_GATC	**med26**	Advantage	4,322	541
10	DDB0232429_7801157_GATC	**DDB_G0277245**	Advantage	3,089	369
11	DDB0232429_933295_GATC	**gmppA**	Advantage	3,044	77.7
12	DDB0232429_2359007_CATG	**tkt-1**	Advantage	2,901	323
13	DDB0232431_1844853_GATC	**iliG**	Advantage	2,771	585
14	DDB0232430_6319727_GATC	**DDB_G0282861**	Advantage	2,653	836
15	DDB0232429_5298862_GATC	**zizA**	Advantage	2,329	417
16	DDB0232429_7800554_GATC	**DDB_G0277245**	Advantage	2,313	1
17	DDB0232431_4361009_GATC	**DDB_G0286363**	Advantage	1,812	252
18	DDB0232432_1073765_CATG	**DDB_G0288121**	Advantage	1,763	213
19	DDB0232429_3895130_GATC	**DG1124**	Advantage	1,735	159
20	DDB0232429_466628_CATG	**DDB_G0271510**	Advantage	1,570	800
21	DDB0232430_2441210_GATC	**DDB_G0279681**	Advantage	1,460	291
22	DDB0232432_3380395_GATC	**DDB_G0289901**	Advantage	1,340	102
23	DDB0232428_3056743_CATG	**DDB_G0269128**	Advantage	1,328	678
24	DDB0232430_2125293_CATG	**pldB**	Advantage	1,320	378
25	DDB0232432_1071186_GATC	**DDB_G0288121**	Advantage	1,289	355
26	DDB0232431_1844857_GATC	**iliG**	Advantage	1,262	264
27	DDB0232430_4065471_GATC	**gpt10**	Advantage	1,222	1
28	DDB0232432_1604694_GATC	**DDB_G0288493**	Advantage	1,174	340
29	DDB0232433_2557774_GATC	**kxcB**	Advantage	1,173	469
30	DDB0232428_224467_GATC	**DDB_G0267496**	Advantage	1,152	527
31	DDB0232428_3104096_GATC	**pks2**	Advantage	1,134	33
32	DDB0232428_4223056_GATC	**mkcF**	Advantage	1,115	418
33	DDB0232432_886974_CATG	**DDB_G0287955**	Advantage	1,115	182
34	DDB0232428_3751703_CATG	**sigJ**	Advantage	1,090	175
35	DDB0232431_466488_GATC	**DDB_G0283289**	Advantage	1,081	328
36	DDB0232430_395199_CATG	**DDB_G0278171**	Advantage	1,057	205
37	DDB0232429_4693338_GATC	**adcB**	Advantage	1,046	134
38	DDB0232428_264740_GATC	**dhx57**	Advantage	1,004	319
39	DDB0232429_5495413_GATC	**tacc**	Advantage	976	101
40	DDB0232432_1802820_GATC	**ugt52**	Advantage	968	321
41	DDB0232433_254553_GATC	**DDB_G0291396**	Advantage	964	224
42	DDB0232431_310315_CATG	**DDB_G0283213**	Advantage	942	133
43	DDB0232428_1013757_CATG	**DDB_G0267872**	Advantage	931	210
44	DDB0232431_807178_CATG	**DDB_G0283595**	Advantage	887	439
45	DDB0232429_635029_CATG	**DDB_G0271550**	Advantage	874	323
46	DDB0232431_1355783_GATC	**mybU**	Advantage	868	107
47	DDB0232429_3894327_CATG	**DG1124**	Advantage	842	1
48	DDB0232429_650862_CATG	**tgrK2**	Advantage	825	326
49	DDB0232430_4231738_GATC	**DDB_G0281217**	Advantage	804	158
50	DDB0232429_2366488_GATC	**fslJ-1**	Advantage	802	235
51	DDB0232429_7687785_GATC	**DDB_G0277177**	Advantage	799	3.93
52	DDB0232432_1072832_CATG	**DDB_G0288121**	Advantage	787	115
53	DDB0232430_1313606_CATG	**DDB_G0278869**	Advantage	783	278
54	DDB0232431_138085_CATG	**DDB_G0283067**	Advantage	778	278
55	DDB0232431_2254100_GATC	**DDB_G0284721**	Advantage	775	1
56	DDB0232429_1946310_GATC	**DDB_G0272670**	Advantage	765	269
57	DDB0232430_95042_CATG	**DDB_G0277895**	Advantage	762	246
58	DDB0232429_7568360_GATC	**dcx**	Advantage	727	151
59	DDB0232433_102111_CATG	**DDB_G0294555**	Advantage	712	101
60	DDB0232429_2679954_CATG	**DDB_G0273189**	Advantage	705	3.10
61	DDB0232429_1735865_CATG	**DDB_G0272470**	Advantage	693	1
62	DDB0232431_747978_GATC	**treh**	Advantage	684	119
63	DDB0232429_3807776_CATG	**ctnA**	Advantage	681	118
64	DDB0232429_4638083_CATG	**DDB_G0274637**	Advantage	678	1
65	DDB0232430_4065461_GATC	**gpt10**	Advantage	675	1
66	DDB0232429_4438041_CATG	**DDB_G0274481**	Advantage	657	51.01
67	DDB0232430_3577527_CATG	**arrJ**	Advantage	656	334
68	DDB0232433_1784186_GATC	**DDB_G0292714**	Advantage	655	255

Table continue on next page

69	DDB0232431_5382361_CATG	**DDB_G0287149**	Advantage	655	213
70	DDB0232429_1232016_CATG	**DDB_G0272100**	Advantage	652	40.3
71	DDB0232429_5253432_CATG	**galE**	Advantage	648	152
72	DDB0232433_2868713_CATG	**DDB_G0293424**	Advantage	628	1
73	DDB0232429_3226823_GATC	**DDB_G0273647**	Advantage	626	1.94
74	DDB0232433_3583065_GATC	**redA**	Advantage	611	241
75	DDB0232432_3463025_GATC	**DDB_G0289937**	Advantage	601	209
76	DDB0232433_191952_GATC	**smp3**	Advantage	599	243
77	DDB0232429_4757950_CATG	**lsrA**	Advantage	575	1
78	DDB0232429_5263006_GATC	**gacI**	Advantage	564	288
79	DDB0232430_3031416_CATG	**DDB_G0280157**	Advantage	558	273
80	DDB0232431_3392608_CATG	**DDB_G0285567**	Advantage	556	105
81	DDB0232432_1362679_CATG	**pdx2**	Advantage	555	110
82	DDB0232432_3991635_CATG	**DDB_G0290371**	Advantage	546	220
83	DDB0232429_6449707_GATC	**ddcB**	Advantage	542	1
84	DDB0232433_965522_CATG	**DDB_G0291938**	Advantage	540	140
85	DDB0232428_403267_CATG	**DDB_G0267602**	Advantage	539	1
86	DDB0232429_2647099_CATG	**DDB_G0273077**	Advantage	529	121
87	DDB0232433_559640_CATG	**dnaja1**	Advantage	528	135
88	DDB0232432_3840236_GATC	**nhe4**	Advantage	514	112
89	DDB0232429_487963_GATC	**rev3**	Advantage	512	133
90	DDB0232432_3881923_GATC	**ctdspl2**	Advantage	508	101
91	DDB0232428_1104665_GATC	**DDB_G0268386**	Advantage	503	142
92	DDB0232428_4624308_CATG	**DDB_G0270774**	Advantage	493	210
93	DDB0232430_66908_GATC	**DDB_G0277961**	Advantage	489	32.1
94	DDB0232430_4064509_CATG	**gpt10**	Advantage	488	1
95	DDB0232431_5320495_CATG	**pks24**	Advantage	483	130
96	DDB0232428_920510_GATC	**DDB_G0267820**	Advantage	479	15.1
97	DDB0232432_4216222_GATC	**DDB_G0290527**	Advantage	474	132
98	DDB0232430_2806501_GATC	**DDB_G0279979**	Advantage	473	3.32
99	DDB0232430_1840328_CATG	**DDB_G0279255**	Advantage	470	116
100	DDB0232429_7496604_CATG	**DDB_G0277095**	Advantage	469	194
101	DDB0232433_160016_CATG	**DDB_G0291348**	Advantage	466	247
102	DDB0232429_671474_CATG	**lvsB**	Advantage	461	1
103	DDB0232429_1571152_GATC	**DDB_G0272280**	Advantage	453	187
104	DDB0232432_83379_CATG	**DDB_G0287277**	Advantage	440	100
105	DDB0232432_4603498_GATC	**mybO**	Advantage	437	226
106	DDB0232429_1569678_GATC	**DDB_G0272434**	Advantage	436	139
107	DDB0232430_2100525_GATC	**roco6**	Advantage	435	1
108	DDB0232430_4986041_CATG	**DDB_G0281793**	Advantage	435	201
109	DDB0232431_4825971_CATG	**DDB_G0286675**	Advantage	434	134
110	DDB0232432_2715642_GATC	**DDB_G0289385**	Advantage	433	125
111	DDB0232430_2652375_CATG	**DDB_G0279897**	Advantage	433	138
112	DDB0232429_3896724_CATG	**DG1124**	Advantage	430	1
113	DDB0232428_3160745_CATG	**DDB_G0269620**	Advantage	423	205
114	DDB0232429_2868208_CATG	**psiG-1**	Advantage	420	228
115	DDB0232432_3672683_CATG	**adhfe1**	Advantage	418	220
116	DDB0232429_2642834_GATC	**DDB_G0273295**	Advantage	416	3.57
117	DDB0232430_5541716_CATG	**DDB_G0282225**	Advantage	409	168
118	DDB0232432_3048284_GATC	**DDB_G0289627**	Advantage	408	1
119	DDB0232431_466452_CATG	**DDB_G0283289**	Advantage	407	128
120	DDB0232431_4378499_CATG	**DDB_G0286459**	Advantage	403	143
121	DDB0232431_3409669_CATG	**DDB_G0285583**	Advantage	403	208
122	DDB0232428_4255945_GATC	**DDB_G0271034**	Advantage	402	170
123	DDB0232430_436791_GATC	**DDB_G0278627**	Advantage	396	100
124	DDB0232430_2280895_CATG	**DDB_G0279573**	Advantage	395	180
125	DDB0232429_3799568_CATG	**fslH**	Advantage	387	107
126	DDB0232429_2444171_CATG	**DDB_G0272807**	Advantage	376	160
127	DDB0232429_7010466_GATC	**mus81**	Advantage	375	1
128	DDB0232430_1393749_GATC	**DDB_G0278915**	Advantage	353	1
129	DDB0232429_1946967_GATC	**DDB_G0272965**	Advantage	343	146
130	DDB0232428_3353308_CATG	**DDB_G0269700**	Advantage	339	1
131	DDB0232432_4725477_GATC	**gacL**	Advantage	338	24.5
132	DDB0232429_8472987_GATC	**DDB_G0277763**	Advantage	318	117
133	DDB0232430_5420288_GATC	**DDB_G0282121**	Advantage	300	149
134	DDB0232429_6953594_GATC	**DDB_G0276439**	Advantage	290	1
135	DDB0232429_1469840_CATG	**DDB_G0272402**	Advantage	264	2.14
136	DDB0232431_3775288_GATC	**rpl18a**	Advantage	240	1.79
137	DDB0232429_3582544_CATG	**cyp508A2-2**	Advantage	232	1
138	DDB0232429_8148731_CATG	**DDB_G0277475**	Advantage	219	1.15
139	DDB0232429_5062066_GATC	**DDB_G0275097**	Advantage	165	1.38
140	DDB0232429_2294729_CATG	**DDB_G0273027**	Advantage	114	2.58

Table continue on next page

1	DDB0232431_1314786_GATC	**pks22**	Disadvantage	164	1,601
2	DDB0232433_2140723_CATG	**DDB_G0292962**	Disadvantage	46.1	1,308
3	DDB0232430_5288703_CATG	**pks21**	Disadvantage	285	1,022
4	DDB0232428_3521811_CATG	**cnrI**	Disadvantage	24.4	860
5	DDB0232431_4244611_CATG	**ponB**	Disadvantage	24.4	568
6	DDB0232429_5495413_GATC	**tacc**	Disadvantage	24.9	542
7	DDB0232429_6797542_CATG	**DDB_G0276531**	Disadvantage	14.6	417
8	DDB0232431_1155412_CATG	**DDB_G0283819**	Disadvantage	14.2	397
9	DDB0232433_2012546_GATC	**tgrG1**	Disadvantage	13.9	372
10	DDB0232428_3121109_GATC	**lvsA**	Disadvantage	12.2	365
11	DDB0232432_745429_GATC	**DDB_G0287807**	Disadvantage	12	363
12	DDB0232429_4911229_GATC	**DDB_G0274153**	Disadvantage	13.6	358
13	DDB0232433_1791110_GATC	**DDB_G0292574**	Disadvantage	11	351
14	DDB0232430_5727535_GATC	**dhkM**	Disadvantage	14.6	350
15	DDB0232431_4322695_GATC	**DDB_G0286297**	Disadvantage	9.39	325
16	DDB0232428_3934265_GATC	**DDB_G0269962**	Disadvantage	10.4	313
17	DDB0232430_3028022_CATG	**DDB_G0280157**	Disadvantage	8.82	281
18	DDB0232430_6204463_GATC	**tmem104**	Disadvantage	8.07	275
19	DDB0232433_1643921_GATC	**DDB_G0292550**	Disadvantage	7.55	273
20	DDB0232428_2940237_CATG	**nosip**	Disadvantage	13.1	272
21	DDB0232431_5190371_CATG	**DDB_G0287001**	Disadvantage	5.93	243
22	DDB0232433_3331014_CATG	**DDB_G0349347**	Disadvantage	8.6	242
23	DDB0232433_3252686_CATG	**DDB_G0293682**	Disadvantage	3.5	237
24	DDB0232433_2689922_CATG	**DDB_G0293216**	Disadvantage	7.48	237
25	DDB0232430_4626668_GATC	**vinB**	Disadvantage	3.57	236
26	DDB0232432_4998859_GATC	**DDB_G0291101**	Disadvantage	2.78	234
27	DDB0232431_2483087_CATG	**DDB_G0284785**	Disadvantage	2.5	231
28	DDB0232428_4615258_CATG	**DDB_G0270310**	Disadvantage	10.1	220
29	DDB0232430_1603449_GATC	**DDB_G0279089**	Disadvantage	9.07	217
30	DDB0232430_3822066_CATG	**DDB_G0280873**	Disadvantage	9.76	214
31	DDB0232431_2683376_GATC	**oplah**	Disadvantage	2.51	214
32	DDB0232429_7452850_CATG	**glnA1**	Disadvantage	1.11	208
33	DDB0232433_615661_GATC	**DDB_G0291694**	Disadvantage	3.75	202
34	DDB0232430_905875_CATG	**DDB_G0278455**	Disadvantage	5.8	201
35	DDB0232433_1851738_GATC	**phdG**	Disadvantage	7.88	200
36	DDB0232429_1642818_GATC	**DDB_G0272456**	Disadvantage	3.61	200
37	DDB0232429_3465954_CATG	**DDB_G0273835**	Disadvantage	5.43	197
38	DDB0232429_4196223_CATG	**DDB_G0274549**	Disadvantage	7.68	192
39	DDB0232429_7463260_GATC	**DDB_G0276839**	Disadvantage	4.09	191
40	DDB0232430_6192176_GATC	**DDB_G0282715**	Disadvantage	7.85	187
41	DDB0232433_1354404_GATC	**DDB_G0349138**	Disadvantage	6.35	184
42	DDB0232428_4900587_CATG	**DDB_G0270446**	Disadvantage	5.43	183
43	DDB0232433_2270821_GATC	**DDB_G0292916**	Disadvantage	4.69	183
44	DDB0232430_1061482_CATG	**DDB_G0278551**	Disadvantage	3.05	182
45	DDB0232429_7224194_CATG	**expl5**	Disadvantage	4.9	182
46	DDB0232433_2212750_GATC	**DDB_G0292884**	Disadvantage	5.42	181
47	DDB0215018_91183_CATG	**DDB_G0294196**	Disadvantage	6.72	180
48	DDB0232432_4670457_GATC	**DDB_G0290855**	Disadvantage	4.33	178
49	DDB0232429_7415097_CATG	**ifkB**	Disadvantage	3.66	177
50	DDB0232431_5089038_GATC	**DDB_G0286925**	Disadvantage	6.17	177
51	DDB0232431_886066_CATG	**DDB_G0283629**	Disadvantage	4.23	176
52	DDB0232429_673482_CATG	**lvsB**	Disadvantage	4.63	173
53	DDB0232428_850496_GATC	**DDB_G0267784**	Disadvantage	4.27	170
54	DDB0232430_566805_GATC	**DDB_G0278253**	Disadvantage	6.97	170
55	DDB0232432_2160306_GATC	**DDB_G0288943**	Disadvantage	3.25	168
56	DDB0232429_6933213_GATC	**DDB_G0276429**	Disadvantage	7.15	168
57	DDB0232430_965656_GATC	**DDB_G0278491**	Disadvantage	2.78	167
58	DDB0232429_7984860_CATG	**rgn**	Disadvantage	5.58	167
59	DDB0232429_4157354_GATC	**abcA5**	Disadvantage	6.56	164
60	DDB0232433_1741945_CATG	**DDB_G0292494**	Disadvantage	7.5	163
61	DDB0232429_3113028_GATC	**dpp3-2**	Disadvantage	1.63	163
62	DDB0232428_3731272_GATC	**psaB**	Disadvantage	3.64	162
63	DDB0232432_3177964_GATC	**DDB_G0289733**	Disadvantage	1	162
64	DDB0232433_715037_CATG	**arpE**	Disadvantage	6.81	160
65	DDB0232433_392932_GATC	**abcC7**	Disadvantage	5.93	158
66	DDB0232430_4748476_GATC	**DDB_G0281639**	Disadvantage	4.1	157
67	DDB0232432_2511718_CATG	**adcF**	Disadvantage	3.16	156
68	DDB0232431_3972404_GATC	**ubqP**	Disadvantage	2.84	156
69	DDB0232432_1529364_CATG	**DDB_G0288433**	Disadvantage	3.92	154
70	DDB0232432_1443128_GATC	**roco5**	Disadvantage	1.99	145
71	DDB0232431_2232925_GATC	**DDB_G0284615**	Disadvantage	2.14	142

Table continue on next page

72	DDB0232432_3020799_GATC	**DDB_G0289609**	Disadvantage	3.26	141
73	DDB0232430_1482339_GATC	**DG2033**	Disadvantage	4.17	140
74	DDB0232430_4201584_GATC	**DDB_G0281207**	Disadvantage	2.23	138
75	DDB0232432_4653610_GATC	**stlB**	Disadvantage	3.75	137
76	DDB0232431_3525212_CATG	**mrkB**	Disadvantage	4.44	135
77	DDB0232432_3349504_GATC	**DDB_G0289839**	Disadvantage	3.05	135
78	DDB0232428_3813384_GATC	**kcnma1**	Disadvantage	3.55	135
79	DDB0232432_3035820_CATG	**DDB_G0289637**	Disadvantage	3.16	134
80	DDB0232429_3242592_GATC	**vatD-2**	Disadvantage	1	133
81	DDB0232433_445254_GATC	**rrpB**	Disadvantage	3.47	132
82	DDB0232428_3599691_GATC	**DDB_G0270962**	Disadvantage	1	131
83	DDB0232429_673715_GATC	**lvsB**	Disadvantage	4.93	131
84	DDB0232432_2239937_GATC	**DDB_G0289017**	Disadvantage	1.99	130
85	DDB0232429_3666303_CATG	**fslJ-2**	Disadvantage	2.11	128
86	DDB0232429_3129589_GATC	**DDB_G0273573**	Disadvantage	3.9	127
87	DDB0232432_4940094_CATG	**DDB_G0291065**	Disadvantage	3.67	126
88	DDB0232429_5871284_CATG	**DDB_G0275535**	Disadvantage	1.03	124
89	DDB0232431_856910_GATC	**DDB_G0283577**	Disadvantage	1	123
90	DDB0232433_940915_GATC	**argJ**	Disadvantage	3.56	122
91	DDB0232428_3813231_GATC	**kcnma1**	Disadvantage	1	122
92	DDB0232432_1812136_CATG	**DDB_G0288683**	Disadvantage	1.02	122
93	DDB0232431_1555185_GATC	**cyp519B1**	Disadvantage	1	120
94	DDB0232432_1388514_CATG	**dcd3A**	Disadvantage	2.79	119
95	DDB0232429_4995666_GATC	**DDB_G0275245**	Disadvantage	2.43	116
96	DDB0232431_581277_GATC	**DDB_G0283379**	Disadvantage	2.87	115
97	DDB0232431_3718204_GATC	**DDB_G0285851**	Disadvantage	2.87	114
98	DDB0232429_5759285_GATC	**abcG18**	Disadvantage	1.11	113
99	DDB0232431_1324699_GATC	**pks23**	Disadvantage	4.74	112
100	DDB0232432_4917779_GATC	**DDB_G0291025**	Disadvantage	1.02	112
101	DDB0232433_324063_CATG	**cyp519D1**	Disadvantage	3.3	111
102	DDB0232430_1142430_GATC	**cstf1**	Disadvantage	1.2	108
103	DDB0232428_2537262_CATG	**DDB_G0270480**	Disadvantage	1	105
104	DDB0232429_7511786_CATG	**DDB_G0277103**	Disadvantage	2.34	104
105	DDB0232429_7680814_GATC	**vamp7B**	Disadvantage	1.29	104
106	DDB0232431_488761_CATG	**tgrl1**	Disadvantage	3.65	104
107	DDB0232428_3353533_CATG	**DDB_G0269700**	Disadvantage	2.96	104
108	DDB0232430_4810124_GATC	**msh3**	Disadvantage	1.81	103
109	DDB0232432_2975301_CATG	**DDB_G0289591**	Disadvantage	1	101
110	DDB0232433_622716_GATC	**DDB_G0295705**	Disadvantage	1	101
111	DDB0232429_8390177_GATC	**DDB_G0277729**	Disadvantage	1.73	100

Figure A.7.3 Growth competition fitness assays for mutant validation.

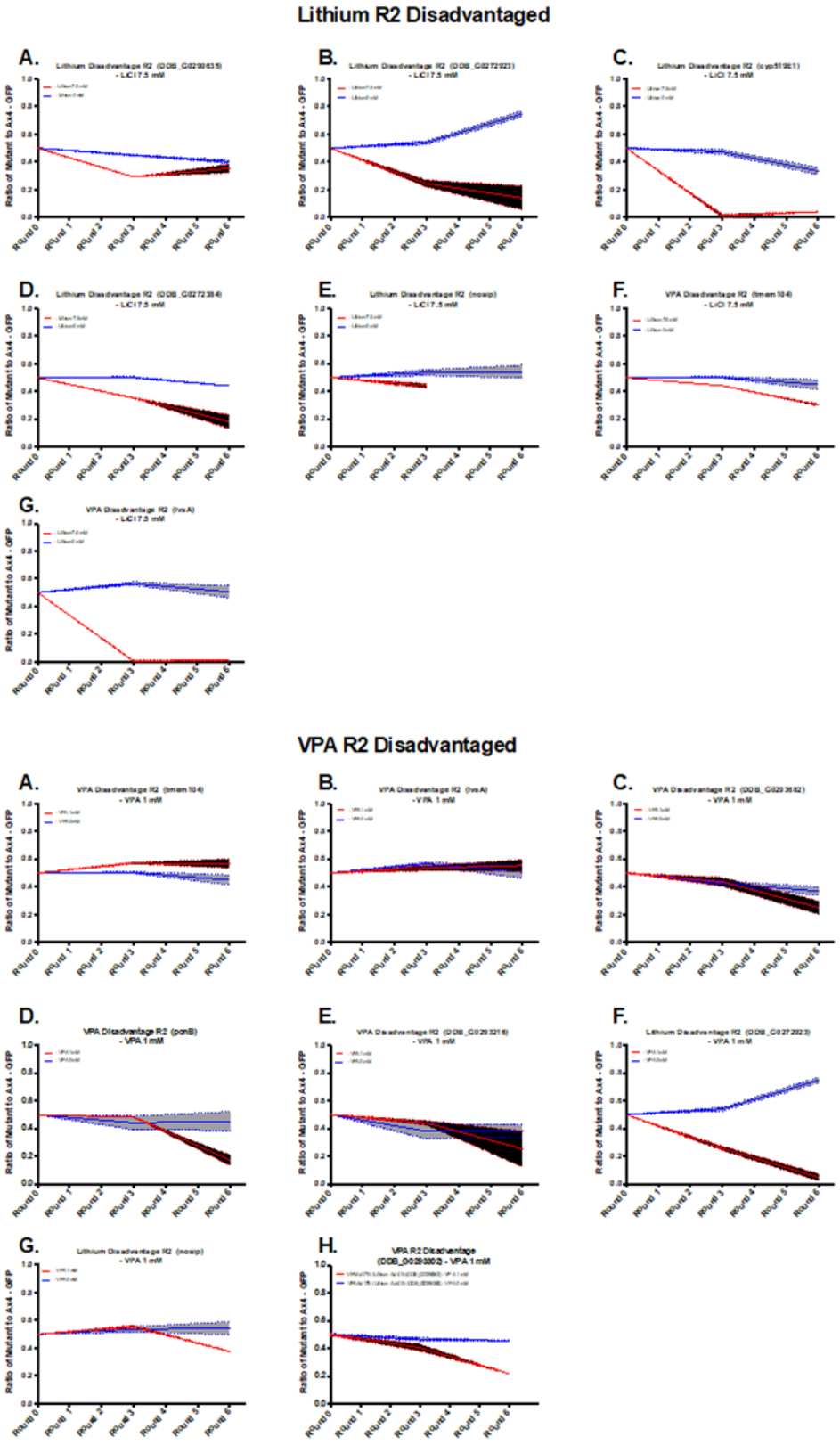

Lithium R5 Advantaged

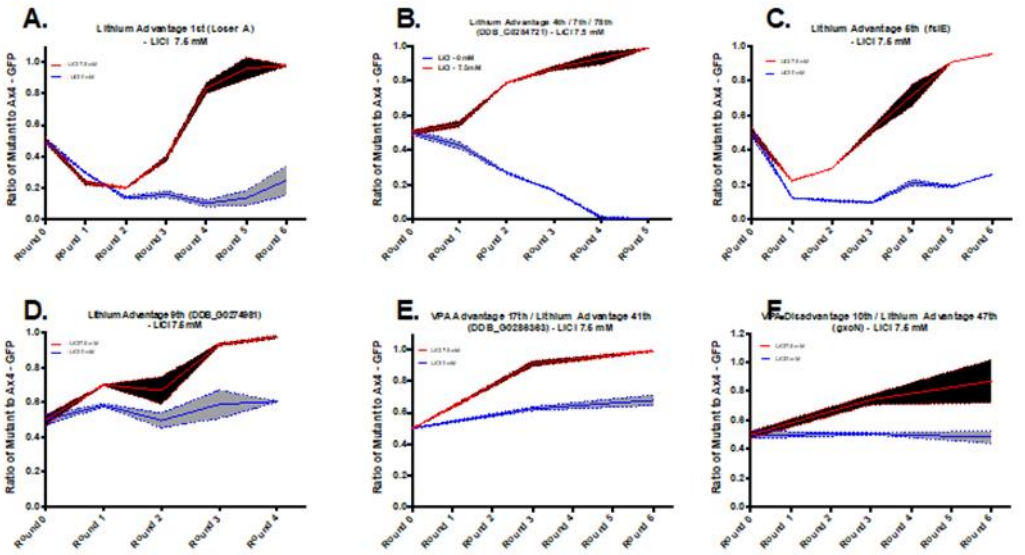

VPA R5 Advantaged

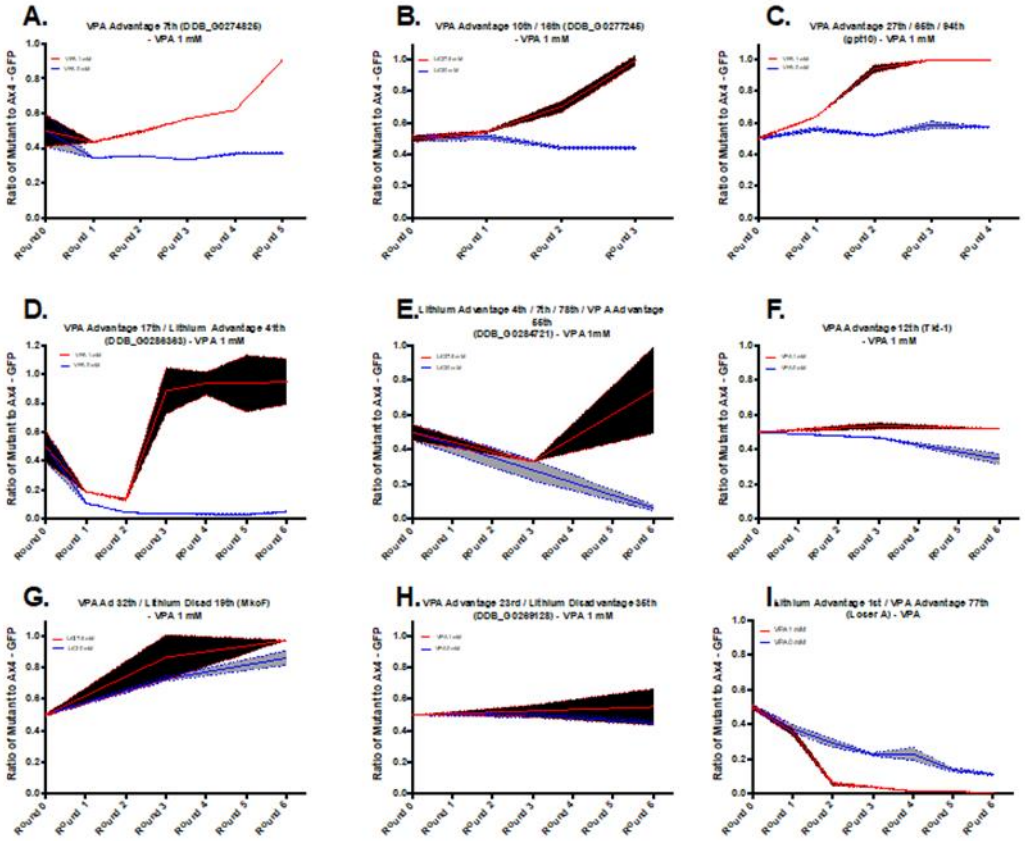

Lithium & VPA R2 Advantaged

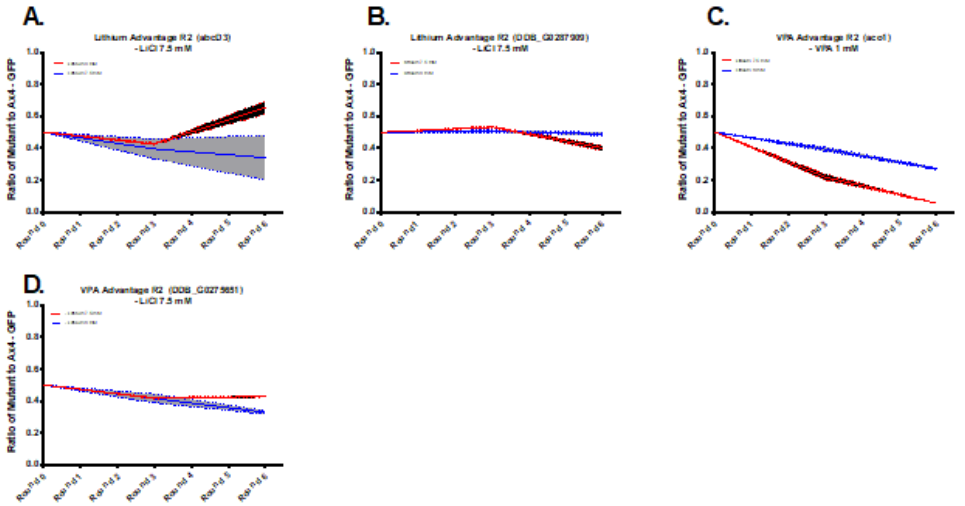

Lithium & VPA R5 Disadvantaged

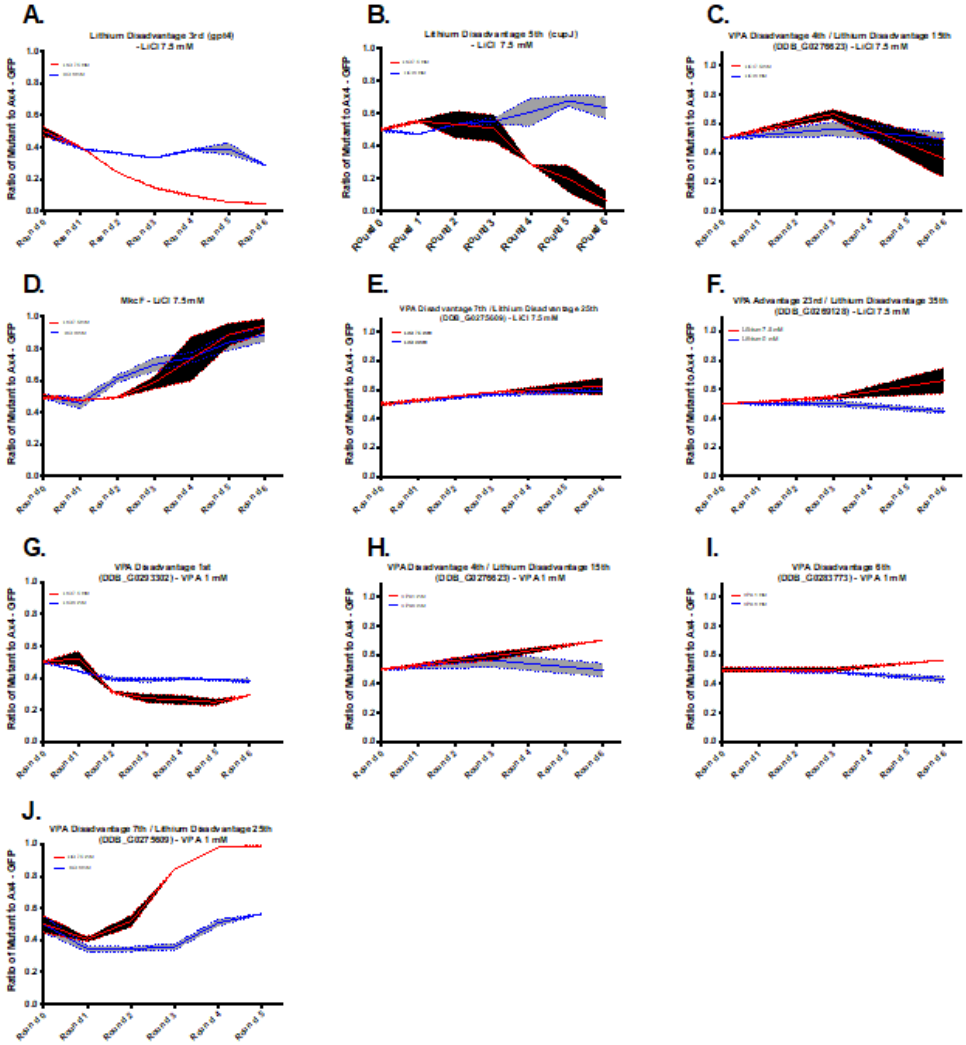

Figure A.7.4 Fluid uptake experiments.

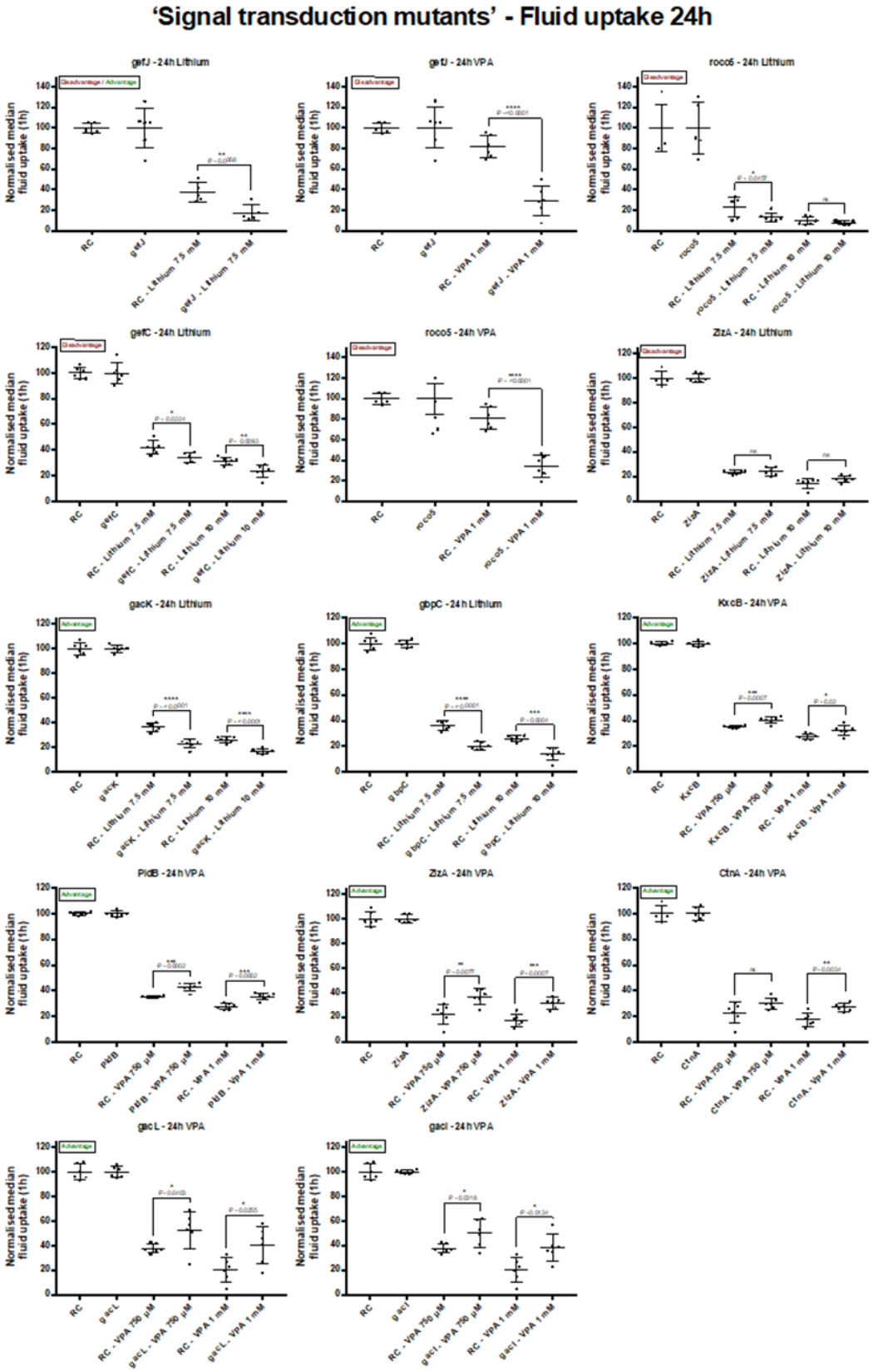

‘Metabolism & DNA damage mutants’ - Fluid uptake 24h

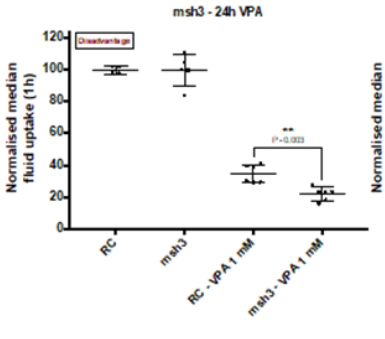

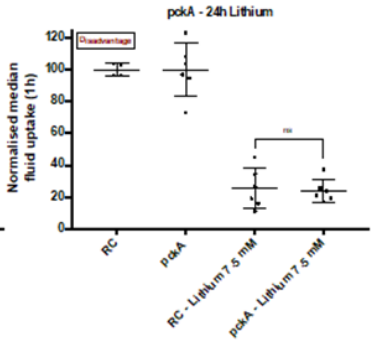

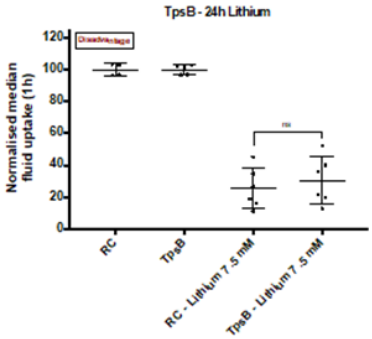

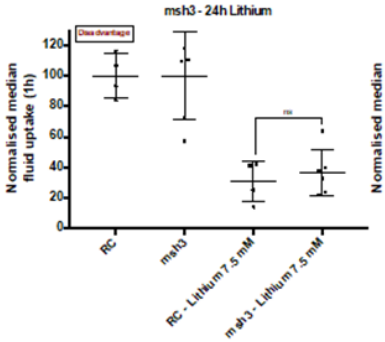

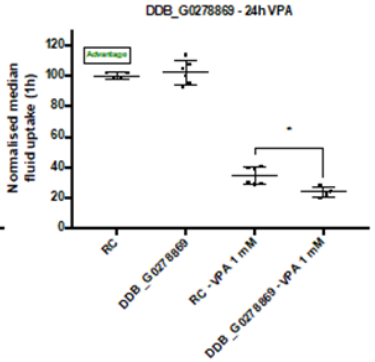

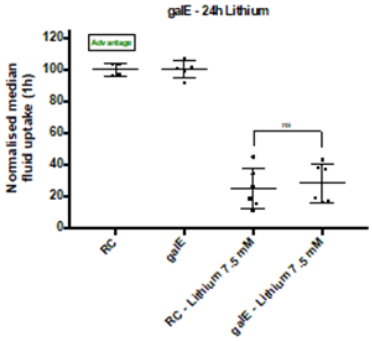

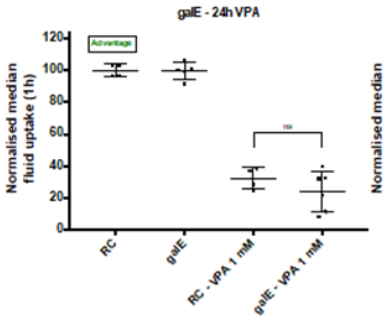

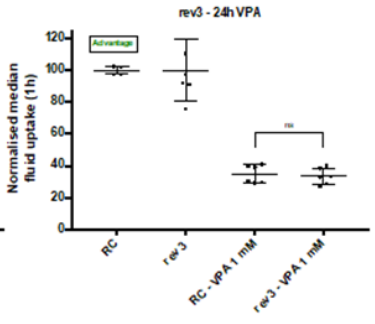

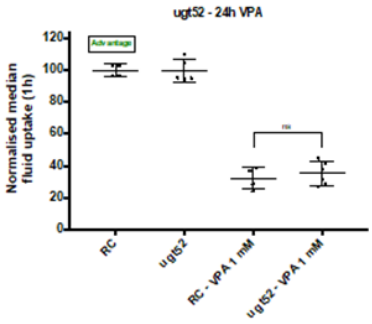

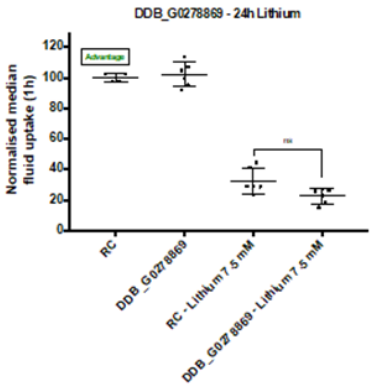

References

1. Brannen KC, Chapin RE, Jacobs AC, Green ML. Alternative Models of Developmental and Reproductive Toxicity in Pharmaceutical Risk Assessment and the 3Rs. ILAR J [Internet]. 2016 Dec 4 [cited 2019 Apr 12];57(2):144–56. Available from: https://academic.oup.com/ilarjournal/article-lookup/doi/10.1093/ilar/ilw026

2. Beekhuijzen M. The era of 3Rs implementation in developmental and reproductive toxicity (DART) testing: Current overview and future perspectives. Reprod Toxicol [Internet]. 2017 Sep 1 [cited 2019 Apr 8];72:86–96. Available from: https://www.sciencedirect.com/science/article/pii/S0890623817301703

3. Guengerich FP, MacDonald JS. Applying mechanisms of chemical toxicity to predict drug safety. Chem Res Toxicol [Internet]. 2007 Mar [cited 2019 Apr 4];20(3):344–69. Available from: http://www.ncbi.nlm.nih.gov/pubmed/17302443

4. Horder T. History of Developmental Biology. Encycl Life Sci [Internet]. 2010 [cited 2019 Mar 19]; Available from: www.els.net

5. Scientific Frontiers in Developmental Toxicology and Risk Assessment [Internet]. Scientific Frontiers in Developmental Toxicology and Risk Assessment. 2000 [cited 2019 Mar 27]. Available from: http://www.nap.edu/catalog/9871.html

6. Beckwith JB. A Hitchhiker's guide to the older literature of descriptive teratology. Am J Med Genet Part A [Internet]. 2007 Dec 15 [cited 2019 Mar 27];143(24):2862–7. Available from: http://www.ncbi.nlm.nih.gov/pubmed/18000901

7. Warren KR. A Review of the History of Attitudes Toward Drinking in Pregnancy. Alcohol Clin Exp Res [Internet]. 2015 Jul [cited 2019 Mar 27];39(7):1110–7. Available from: http://www.ncbi.nlm.nih.gov/pubmed/26137906

8. Hale F. The relation of vitamin A to anophthalmos in pigs. Am J Ophthalmol [Internet]. 1935 Dec 1 [cited 2019 Mar 31];18(12):1087–93. Available from: https://www.sciencedirect.com/science/article/pii/S0002939435905633

9. Ujházy E, Mach M, Navarová J, Brucknerová I, Dubovický M. Teratology - Past, present and future. Interdiscip Toxicol [Internet]. 2012 [cited 2019 Mar 18];5(4):163–8. Available from: www.intertox.sav.sk

10. NELSON MM, EVANS HM. Pteroylglutamic acid and reproduction in the rat. J Nutr [Internet]. 1949 May 1 [cited 2019 Mar 31];38(1):11–24. Available from: https://academic.oup.com/jn/article/38/1/11/4725546

11. GIROUD A, MARTINET M. Fentes de palais chez l'embryon de rat par hypervitaminose A. C R Seances Soc Biol Fil [Internet]. 1954 Nov [cited 2019 Mar 31];148(21–22):1742–3. Available from: http://www.ncbi.nlm.nih.gov/pubmed/14365012

12. GIROUD A, TUCHMANN-DUPLESSIS H. Congenital abnormalities. Role of exogenous factors. Pathol Biol (Paris) [Internet]. 1962 Jan [cited 2019 Mar 31];10:119–51. Available from: http://www.ncbi.nlm.nih.gov/pubmed/13898942

13. Vargesson N. Thalidomide-induced teratogenesis: History and mechanisms. Birth Defects Res Part C - Embryo Today Rev [Internet]. 2015 Jun 1 [cited 2019 Mar 31];105(2):140–56. Available from: http://doi.wiley.com/10.1002/bdrc.21096

14. Vargesson N. Thalidomide-induced limb defects: Resolving a 50-year-old puzzle. BioEssays [Internet]. 2009 Dec 1 [cited 2019 Mar 31];31(12):1327–36. Available from: http://doi.wiley.com/10.1002/bies.200900103

15. Kim JH, Scialli AR. Thalidomide: The tragedy of birth defects and the effective treatment of disease. Toxicol Sci [Internet]. 2011 Jul 1 [cited 2019 Mar 31];122(1):1–6. Available from: https://academic.oup.com/toxsci/article/1672454/Thalidomide:

16. Ito T, Ando H, Handa H. Teratogenic effects of thalidomide: Molecular mechanisms. Cell Mol Life Sci [Internet]. 2011 May 5 [cited 2019 Mar 31];68(9):1569–79. Available from: http://link.springer.com/10.1007/s00018-010-0619-9

17. Bailey J, Knight A, Balcombe J. The future of teratology research is in vitro [Internet]. Vol. 19, Biogenic Amines. 2005 [cited 2019 Apr 6]. Available from: https://www.safermedicines.org/reports/teratology.pdf

18. Aston SA. Environment and Birth Defects (1973), by James G. Wilson. 2014 Jun 22 [cited 2019

Apr 6]; Available from: https://hpsrepository.asu.edu/handle/10776/7975

19. Alwan S, Chambers C. Identifying Human Teratogens: An Update. J Pediatr Genet [Internet]. 2015 [cited 2019 Apr 6];04(02):039–41. Available from: http://dx.doi.org/

20. Schumann J. Teratogen screening: State of the art [Internet]. Vol. 2, Avicenna Journal of Medical Biotechnology. 2010 [cited 2019 Apr 4]. Available from: https://www.ncbi.nlm.nih.gov/pmc/articles/PMC3558154/pdf/AJMB-2-115.pdf

21. Beedie SL, Mahony C, Walker HM, Chau CH, Figg WD, Vargesson N. Shared mechanism of teratogenicity of anti-angiogenic drugs identified in the chicken embryo model. Sci Rep [Internet]. 2016 [cited 2019 Apr 14];6:30038. Available from: http://www.ncbi.nlm.nih.gov/pubmed/27443489

22. D'Amato RJ, Loughnan MS, Flynn E, Folkman J. Thalidomide is an inhibitor of angiogenesis. Proc Natl Acad Sci U S A [Internet]. 1994 Apr 26 [cited 2019 Apr 23];91(9):4082–5. Available from: http://www.ncbi.nlm.nih.gov/pubmed/7513432

23. Vargesson N. Thalidomide-induced teratogenesis: History and mechanisms. Birth Defects Res Part C - Embryo Today Rev [Internet]. 2015 Jun [cited 2019 Apr 23];105(2):140–56. Available from: http://www.ncbi.nlm.nih.gov/pubmed/26043938

24. Garry VF, Truran P. Teratogenicity. Reprod Dev Toxicol [Internet]. 2017 [cited 2019 Apr 8];1167–81. Available from: http://dx.doi.org/10.1016/B978-0-12-804239-7.00062-7

25. Ali S, Aalders J, Richardson MK. Teratological effects of a panel of sixty water-soluble toxicants on zebrafish development. Zebrafish [Internet]. 2014 [cited 2019 Apr 6];11(2):129–41. Available from: www.zfin.org

26. Wilson JG. Present status of drugs as teratogens in man [Internet]. Vol. 7, Teratology. 1973 [cited 2019 Apr 7]. Available from: https://onlinelibrary.wiley.com/doi/pdf/10.1002/tera.1420070103

27. Nielsen E, Ostergaard G, Larsen JC. Toxicological Risk Assessment of Chemicals [Internet]. Toxicological Risk Assessment of Chemicals. Informa Healthcare; 2008 [cited 2019 Apr 8]. Available from: https://www.taylorfrancis.com/books/9781420006940

28. DeSesso JM. Future of developmental toxicity testing. Curr Opin Toxicol [Internet]. 2017 Apr [cited 2019 Apr 9];3:1–5. Available from: https://linkinghub.elsevier.com/retrieve/pii/S2468202017300220

29. Daston G, Piersma A, Attias L, Beekhuijzen M, Chen C, Foreman J, et al. Best practices for developmental toxicity assessment for classification and labeling. Reprod Toxicol. 2018 Sep 1;80:44–8.

30. Law R, Bozzo P, Koren G, Einarson A. FDA pregnancy risk categories and the CPS: Do they help or are they a hindrance? [Internet]. Vol. 56, Canadian Family Physician. 2010 [cited 2019 Apr 8]. Available from: www.motherisk.org

31. Pernia S, DeMaagd G. The New Pregnancy and Lactation Labeling Rule. P T [Internet]. 2016 Nov [cited 2019 Apr 8];41(11):713–5. Available from: http://www.ncbi.nlm.nih.gov/pubmed/27904304

32. Miyagawa M. Globally harmonized system of classification and labelling of chemicals (GHS) and its implementation in Japan [Internet]. Vol. 65, Nippon eiseigaku zasshi. Japanese journal of hygiene. 2010 [cited 2019 Apr 8]. 5–13 p. Available from: http://www.unece.org/fileadmin/DAM/trans/danger/publi/ghs/ghs_rev08/ST-SG-AC10-30-Rev8e.pdf

33. Bermas BL, Tassinari M, Clowse M, Chakravarty E. The new FDA labeling rule: impact on prescribing rheumatological medications during pregnancy. Rheumatology [Internet]. 2018 Jul 1 [cited 2020 Jan 20];57(suppl_5):v2–8. Available from: https://academic.oup.com/rheumatology/article/57/suppl_5/v2/5076144

34. Rovida C, Hartung T. Re-evaluation of animal numbers and costs for in vivo tests to accomplish REACH legislation requirements for chemicals - A report by the transatlantic think tank for toxicology (t4) [Internet]. Vol. 26, Altex. 2009 [cited 2019 Apr 9]. Available from: http://www.altex.ch/resources/altex_2009_3_187_208_Rovida.pdf

35. Hartung T, Rovida C. Chemical regulators have overreached. Nature [Internet]. 2009 Aug 27 [cited 2019 Apr 10];460(7259):1080–1. Available from: http://www.ncbi.nlm.nih.gov/pubmed/19713914

36. Tannenbaum J, Bennett BT. Russell and Burch's 3Rs then and now: The need for clarity in definition and purpose. J Am Assoc Lab Anim Sci [Internet]. 2015 Mar [cited 2019 Apr 11];54(2):120–32. Available from: http://www.ncbi.nlm.nih.gov/pubmed/25836957

37. Flint OP, Orton TC. An in vitro assay for teratogens with cultures of rat embryo midbrain and limb bud cells. Toxicol Appl Pharmacol [Internet]. 1984 Nov 1 [cited 2019 Apr 15];76(2):383–95.

Available from: https://www.sciencedirect.com/science/article/pii/0041008X84900206

38. New DA. Whole-embryo culture and the study of mammalian embryos during organogenesis. Biol Rev Camb Philos Soc [Internet]. 1978 Feb 1 [cited 2019 Apr 17];53(1):81–122. Available from: http://doi.wiley.com/10.1111/j.1469-185X.1978.tb00993.x

39. Lee HY, Inselman AL, Kanungo J, Hansen DK. Alternative models in developmental toxicology. Syst Biol Reprod Med [Internet]. 2012 [cited 2019 Apr 18];58(1):10–22. Available from: https://www.ncbi.nlm.nih.gov/pmc/articles/PMC6075688/pdf/nihms979422.pdf

40. Harris C. Rodent whole embryo culture. In: Methods in Molecular Biology [Internet]. 2012 [cited 2019 Apr 21]. p. 215–37. Available from: http://www.ncbi.nlm.nih.gov/pubmed/22669667

41. Zhang C, Cao J, Kenyon JR, Panzica-Kelly JM, Gong L, Augustine-Rauch K. Development of a Streamlined Rat Whole Embryo Culture Assay for Classifying Teratogenic Potential of Pharmaceutical Compounds. Toxicol Sci [Internet]. 2012 Jun 1 [cited 2019 Apr 18];127(2):535–46. Available from: https://academic.oup.com/toxsci/article-lookup/doi/10.1093/toxsci/kfs112

42. Genschow E, Spielmann H, Scholz G, Seiler A, Brown N, Piersma A, et al. The ECVAM international validation study on in vitro embryotoxicity tests: Results of the definitive phase and evaluation of prediction models. ATLA Altern to Lab Anim [Internet]. 2002 [cited 2019 Apr 18];30(2):151–76. Available from: http://www.ncbi.nlm.nih.gov/pubmed/11971753

43. Tonk ECM, Robinson JF, Verhoef A, Theunissen PT, Pennings JLA, Piersma AH. Valproic acid-induced gene expression responses in rat whole embryo culture and comparison across in vitro developmental and non-developmental models. Reprod Toxicol [Internet]. 2013 Nov [cited 2019 Apr 18];41:57–66. Available from: http://www.ncbi.nlm.nih.gov/pubmed/23811354

44. Robinson JF, Verhoef A, Pennings JLA, Pronk TE, Piersma AH. A comparison of gene expression responses in rat whole embryo culture and in vivo: Time-dependent retinoic acid-induced teratogenic response. Toxicol Sci [Internet]. 2012 [cited 2020 Oct 28];126(1):242–54. Available from: http://brainarray.mbni.

45. Miller-Pinsler L, Sharma A, Wells PG. Enhanced NADPH oxidases and reactive oxygen species in the mechanism of methanol-initiated protein oxidation and embryopathies in vivo and in embryo culture. Arch Toxicol [Internet]. 2016 Mar 1 [cited 2019 Apr 21];90(3):717–30. Available from: http://link.springer.com/10.1007/s00204-015-1482-0

46. Hughes A, Greene NDE, Copp AJ, Galea GL. Valproic acid disrupts the biomechanics of late spinal neural tube closure in mouse embryos. Mech Dev [Internet]. 2018 Feb 1 [cited 2019 Apr 21];149:20–6. Available from: https://www.sciencedirect.com/science/article/pii/S092547731730802X

47. Dimopoulou M, Verhoef A, van Ravenzwaay B, Rietjens IMCM, Piersma AH. Flusilazole induces spatio-temporal expression patterns of retinoic acid-, differentiation- and sterol biosynthesis-related genes in the rat Whole Embryo Culture. Reprod Toxicol [Internet]. 2016 Sep 1 [cited 2019 Apr 21];64:77–85. Available from: https://www.sciencedirect.com/science/article/pii/S0890623816300533

48. Augustine-Rauch K, Zhang CX, Panzica-Kelly JM. A Developmental Toxicology Assay Platform for Screening Teratogenic Liability of Pharmaceutical Compounds. Birth Defects Res Part B - Dev Reprod Toxicol [Internet]. 2016 [cited 2019 Apr 21];107(1):4–20. Available from: https://onlinelibrary.wiley.com/doi/pdf/10.1002/bdrb.21168

49. Görge G, Nagel R. Toxicity of lindane, atrazine, and deltamethrin to early life stages of zebrafish (Brachydanio rerio). Ecotoxicol Environ Saf [Internet]. 1990 Dec [cited 2019 Apr 19];20(3):246–55. Available from: http://www.ncbi.nlm.nih.gov/pubmed/1708710

50. Lantz-Mcpeak S, Guo X, Cuevas E, Dumas M, Newport GD, Ali SF, et al. Developmental toxicity assay using high content screening of zebrafish embryos. J Appl Toxicol [Internet]. 2015 Mar 1 [cited 2019 Apr 19];35(3):261–72. Available from: http://doi.wiley.com/10.1002/jat.3029

51. Kanungo J, Cuevas E, Ali S, Paule M. Zebrafish Model in Drug Safety Assessment. Curr Pharm Des [Internet]. 2014 [cited 2019 Apr 19];20(34):5416–29. Available from: http://www.ncbi.nlm.nih.gov/pubmed/24502596

52. Ball JS, Stedman DB, Hillegass JM, Zhang CX, Panzica-kelly J, Coburn A, et al. Fishing for teratogens: A consortium effort for a harmonized zebrafish developmental toxicology assay. Toxicol Sci [Internet]. 2014 May 1 [cited 2019 Apr 21];139(1):210–9. Available from: http://www.ncbi.nlm.nih.gov/pubmed/24496635

53. Beekhuijzen M, de Koning C, Flores-Guillén ME, de Vries-Buitenweg S, Tobor-Kaplon M, van de Waart B, et al. From cutting edge to guideline: A first step in harmonization of the zebrafish embryotoxicity test (ZET) by describing the most optimal test conditions and morphology scoring

system. Reprod Toxicol [Internet]. 2015 Aug 15 [cited 2019 Apr 21];56:64–76. Available from: http://www.ncbi.nlm.nih.gov/pubmed/26111580

54. Yamashita A, Inada H, Chihara K, Yamada T, Deguchi J, Funabashi H. Improvement of the evaluation method for teratogenicity using zebrafish embryos. J Toxicol Sci [Internet]. 2014 Jun [cited 2019 Apr 19];39(3):453–64. Available from: http://www.ncbi.nlm.nih.gov/pubmed/24849680

55. Ji C, Yan L, Chen Y, Yue S, Dong Q, Chen J, et al. Evaluation of the developmental toxicity of 2,7-dibromocarbazole to zebrafish based on transcriptomics assay. J Hazard Mater [Internet]. 2019 Apr 15 [cited 2019 Apr 21];368:514–22. Available from: https://www.sciencedirect.com/science/article/pii/S030438941930086X

56. Van den Bulck K, Hill A, Mesens N, Diekman H, De Schaepdrijver L, Lammens L. Zebrafish developmental toxicity assay: A fishy solution to reproductive toxicity screening, or just a red herring? Reprod Toxicol [Internet]. 2011 Sep [cited 2019 Apr 21];32(2):213–9. Available from: http://www.ncbi.nlm.nih.gov/pubmed/21704152

57. Brannen KC, Panzica-Kelly JM, Danberry TL, Augustine-Rauch KA. Development of a zebrafish embryo teratogenicity assay and quantitative prediction model. Birth Defects Res Part B - Dev Reprod Toxicol [Internet]. 2010 Feb [cited 2019 Apr 21];89(1):66–77. Available from: http://www.ncbi.nlm.nih.gov/pubmed/20166227

58. Panzica-Kelly JM, Zhang CX, Augustine-Rauch KA. Optimization and performance assessment of the chorion-off[Dechorinated] Zebrafish Developmental toxicity assay. Toxicol Sci [Internet]. 2015 Jul [cited 2019 Apr 19];146(1):127–34. Available from: http://www.ncbi.nlm.nih.gov/pubmed/25877614

59. Sipes NS, Padilla S, Knudsen TB. Zebrafish-As an integrative model for twenty-first century toxicity testing. Birth Defects Res Part C - Embryo Today Rev [Internet]. 2011 Sep 1 [cited 2019 Apr 19];93(3):256–67. Available from: http://doi.wiley.com/10.1002/bdrc.20214

60. Augustine-Rauch K, Zhang CX, Panzica-Kelly JM. In vitro developmental toxicology assays: A review of the state of the science of rodent and zebrafish whole embryo culture and embryonic stem cell assays. Birth Defects Res Part C - Embryo Today Rev [Internet]. 2010 [cited 2019 Apr 14];90(2):87–98. Available from: www.interscience.wiley.com

61. Gustafson AL, Stedman DB, Ball J, Hillegass JM, Flood A, Zhang CX, et al. Inter-laboratory assessment of a harmonized zebrafish developmental toxicology assay - Progress report on phase I. Reprod Toxicol [Internet]. 2012 Apr [cited 2019 Apr 21];33(2):155–64. Available from: http://www.ncbi.nlm.nih.gov/pubmed/22210281

62. Liu S, Yin N, Faiola F. Prospects and Frontiers of Stem Cell Toxicology. Stem Cells Dev [Internet]. 2017 Nov 1 [cited 2019 Apr 21];26(21):1528–39. Available from: https://www.liebertpub.com/doi/10.1089/scd.2017.0150

63. Spielmann H, Pohl I, Döring B, Liebsch M, Moldenhauer F. The Embryonic Stem cell Test, an in vitro embryotoxicity test using two permanent mouse cell lines: 3T3 fibroblasts and embryonic stem cells. In: In Vitro and Molecular Toxicology: Journal of Basic and Applied Research [Internet]. 1997 [cited 2019 Apr 20]. p. 119–27. Available from: http://www.springerlink.com/index/10.1007/978-3-7091-7500-2_69

64. Tandon S, Jyoti S. Embryonic stem cells: An alternative approach to developmental toxicity testing. J Pharm Bioallied Sci [Internet]. 2012 Apr [cited 2019 Apr 20];4(2):96–100. Available from: http://www.ncbi.nlm.nih.gov/pubmed/22557918

65. Yu R, Miyamura N, Okamoto-Uchida Y, Arima N, Ishigami-Yuasa M, Kagechika H, et al. A Modified Murine Embryonic Stem Cell Test for Evaluating the Teratogenic Effects of Drugs on Early Embryogenesis. PLoS One [Internet]. 2015 [cited 2019 Apr 20];10(12). Available from: https://journals.plos.org/plosone/article/file?id=10.1371/journal.pone.0145286&type=printable

66. Flamier A, Singh S, Rasmussen TP. A standardized human embryoid body platform for the detection and analysis of teratogens. Lako M, editor. PLoS One [Internet]. 2017 Feb 9 [cited 2019 Apr 23];12(2):e0171101. Available from: http://www.ncbi.nlm.nih.gov/pubmed/28182681

67. Flamier A, Singh S, Rasmussen TP. Use of Human Embryoid Bodies for Teratology. In: Current Protocols in Toxicology [Internet]. Hoboken, NJ, USA: John Wiley & Sons, Inc.; 2018 [cited 2019 Apr 20]. p. 13.13.1-13.13.14. Available from: http://doi.wiley.com/10.1002/cptx.38

68. Bremer S, Worth AP, Paparella M, Bigot K, Kolossov E, Fleischmann BK, et al. Establishment of an in vitro reporter gene assay for developmental cardiac toxicity. Toxicol Vitr [Internet]. 2001 Jun [cited 2019 Apr 23];15(3):215–23. Available from: http://www.ncbi.nlm.nih.gov/pubmed/11377094

69. Kolossov E, Fleischmann BK, Liu Q, Bloch W, Viatchenko-Karpinski S, Manzke O, et al. Functional characteristics of ES cell-derived cardiac precursor cells identified by tissue-specific expression of

the green fluorescent protein. J Cell Biol [Internet]. 1998 Dec 28 [cited 2019 Apr 23];143(7):2045–56. Available from: http://www.ncbi.nlm.nih.gov/pubmed/9864374

70. Suzuki N, Ando S, Yamashita N, Horie N, Saito K. Evaluation of novel high-throughput embryonic stem cell tests with new molecular markers for screening embryotoxic chemicals in vitro. Toxicol Sci [Internet]. 2011 Dec 1 [cited 2019 Apr 23];124(2):460–71. Available from: https://academic.oup.com/toxsci/article-lookup/doi/10.1093/toxsci/kfr250

71. Panzica-Kelly JM, Brannen KC, Ma Y, Zhang CX, Flint OP, Lehman-McKeeman LD, et al. Establishment of a molecular embryonic stem cell developmental toxicity assay. Toxicol Sci [Internet]. 2013 Feb 1 [cited 2020 Sep 8];131(2):447–57. Available from: https://academic.oup.com/toxsci/article/131/2/447/1641305

72. Worley KE, Rico-Varela J, Ho D, Wan LQ. Teratogen screening with human pluripotent stem cells. Integr Biol (United Kingdom) [Internet]. 2018 Sep 1 [cited 2019 Apr 21];10(9):491–501. Available from: http://www.ncbi.nlm.nih.gov/pubmed/30095839

73. Pellizzer C, Bremer S, Hartung T. Developmental toxicity testing from animal towards embryonic stem cells [Internet]. Vol. 22, Altex. 2005 [cited 2019 Apr 21]. Available from: http://www.altex.ch/resources/Altex_2005_2_047_057_Pellizzer.pdf

74. Bosgra S, Westerhout J. Interpreting in vitro developmental toxicity test battery results: The consideration of toxicokinetics. Reprod Toxicol [Internet]. 2015 Aug 1 [cited 2019 Apr 21];55:73–80. Available from: http://www.ncbi.nlm.nih.gov/pubmed/25462785

75. Williams JG. Dictyostelium finds new roles to model. Genetics [Internet]. 2010 Jul 1 [cited 2019 Feb 17];185(3):717–26. Available from: http://www.ncbi.nlm.nih.gov/pubmed/20660652

76. Fey P, Kowal AS, Gaudet P, Pilcher KE, Chisholm RL. Protocols for growth and development of Dictyostelium discoideum. Nat Protoc [Internet]. 2007 Jun 1 [cited 2019 Feb 6];2(6):1307–16. Available from: http://www.ncbi.nlm.nih.gov/pubmed/17545967

77. Raper KB, Smith NR. The Growth of Dictyostelium discoideum upon Pathogenic Bacteria1 [Internet]. Vol. 38, Journal of Bacteriology. 1939 [cited 2019 Feb 17]. Available from: http://jb.asm.org/

78. Artemenko Y, Lampert TJ, Devreotes PN. Moving towards a paradigm: common mechanisms of chemotactic signaling in Dictyostelium and mammalian leukocytes. Vol. 71, Cellular and molecular life sciences : CMLS. 2014. p. 3711–47.

79. Rivero F. Endocytosis and the Actin Cytoskeleton in Dictyostelium discoideum. Vol. 267, International Review of Cell and Molecular Biology. 2008. p. 343–97.

80. Williams TD, Paschke PI, Kay RR. Function of small GTPases in Dictyostelium macropinocytosis. Vol. 374, Philosophical Transactions of the Royal Society B: Biological Sciences. Royal Society Publishing; 2019.

81. Dunn JD, Bosmani C, Barisch C, Raykov L, Lefrançois LH, Cardenal-Muñoz E, et al. Eat prey, live: Dictyostelium discoideum as a model for cell-autonomous defenses. Vol. 8, Frontiers in Immunology. Frontiers Media S.A.; 2018.

82. Schaf J, Damstra-Oddy J, Williams RSB. Dictyostelium discoideum as a pharmacological model system to study the mechanisms of medicinal drugs and natural products. Int J Dev Biol [Internet]. 2019 [cited 2020 Jan 28];63(8-9–10):541–50. Available from: http://www.intjdevbiol.com/paper.php?doi=190228rw

83. Wiegand S, Kruse J, Gronemann S, Hammann C. Efficient generation of gene knockout plasmids for Dictyostelium discoideum using one-step cloning. Genomics. 2011 May;97(5):321–5.

84. Veltman DM, Akar G, Bosgraaf L, Van Haastert PJM. A new set of small, extrachromosomal expression vectors for Dictyostelium discoideum. Plasmid [Internet]. 2009 Mar [cited 2019 Apr 24];61(2):110–8. Available from: http://www.ncbi.nlm.nih.gov/pubmed/19063918

85. Kuspa A. Restriction enzyme-mediated integration (REMI) mutagenesis. Methods Mol Biol. 2006;346:201–9.

86. Gruenheit N, Baldwin A, Stewart B, Jaques S, Keller T, Parkinson K, et al. REMI-seq: Development of methods and resources for functional genomics in Dictyostelium. bioRxiv [Internet]. 2019 [cited 2019 May 30];582072. Available from: http://dx.doi.org/10.1101/582072

87. Sekine R, Kawata T, Muramoto T. CRISPR/Cas9 mediated targeting of multiple genes in Dictyostelium. Sci Rep. 2018 Dec 1;8(1).

88. Eichinger I, Pachebat JA, Glöckner G, Rajandream MA, Sucgang R, Berriman M, et al. The

genome of the social amoeba Dictyostelium discoideum. Nature [Internet]. 2005 May 5 [cited 2019 Feb 6];435(7038):43–57. Available from: http://www.ncbi.nlm.nih.gov/pubmed/15875012

89. Pray L. Eukaryotic Genome Complexity. Nat Educ [Internet]. 2008;1(2008):1–6. Available from: http://harths.edlioschool.com/ourpages/auto/2009/11/15/50863591/Article 1 Eukaryotic Genome Complexity.pdf

90. Payne SH, Loomis WF. Retention and loss of amino acid biosynthetic pathways based on analysis of whole-genome sequences. Eukaryot Cell [Internet]. 2006 Feb [cited 2019 May 11];5(2):272–6. Available from: http://www.ncbi.nlm.nih.gov/pubmed/16467468

91. Gomer RH, Jang W, Brazill D. Cell density sensing and size determination. Dev Growth Differ [Internet]. 2011 May 1 [cited 2019 May 11];53(4):482–94. Available from: http://doi.wiley.com/10.1111/j.1440-169X.2010.01248.x

92. Loomis WF. Cell signaling during development of Dictyostelium. Dev Biol [Internet]. 2014 Jul 1 [cited 2019 May 11];391(1):1–16. Available from: https://www.sciencedirect.com/science/article/pii/S0012160614001924

93. Taminato A, Bagattini R, Gorjão R, Chen G, Kuspa A, Souza GM. Role for YakA, cAMP, and protein kinase A in regulation of stress responses of Dictyostelium discoideum cells. Mol Biol Cell [Internet]. 2002 Jul [cited 2019 May 11];13(7):2266–75. Available from: http://www.ncbi.nlm.nih.gov/pubmed/12134067

94. Du Q, Kawabe Y, Schilde C, Chen Z, Schaap P. The Evolution of Aggregative Multicellularity and Cell–Cell Communication in the Dictyostelia. J Mol Biol [Internet]. 2015 Nov 20 [cited 2019 May 13];427(23):3722–33. Available from: http://www.ncbi.nlm.nih.gov/pubmed/26284972

95. Maeda M, Lu S, Shaulsky G, Miyazaki Y, Kuwayama H, Tanaka Y, et al. Periodic Signaling Controlled by an Oscillatory Circuit That Includes Protein Kinases ERK2 and PKA. Science (80-) [Internet]. 2004 May 7 [cited 2019 May 14];304(5672):875–8. Available from: http://www.ncbi.nlm.nih.gov/pubmed/15131307

96. Laub MT, Loomis WF. A molecular network that produces spontaneous oscillations in excitable cells of Dictyostelium. Mol Biol Cell [Internet]. 1998 Dec [cited 2019 May 14];9(12):3521–32. Available from: http://www.ncbi.nlm.nih.gov/pubmed/9843585

97. Gerhardt M, Walz M, Beta C. Signaling in chemotactic amoebae remains spatially confined to stimulated membrane regions. J Cell Sci [Internet]. [cited 2019 May 14]; Available from: http://jcs.biologists.org/content/joces/127/23/5115.full.pdf

98. Iranfar N, Fuller D, Loomis WF. Genome-wide expression analyses of gene regulation during early development of Dictyostelium discoideum. Eukaryot Cell [Internet]. 2003 [cited 2020 Jan 20];2(4):664–70. Available from: http://www.biology.ucsd.edu

99. Coates JC, Harwood AJ. Cell-cell adhesion and signal transduction during Dictyostelium development [Internet]. Vol. 114, Journal of Cell Science. 2001 [cited 2019 May 16]. Available from: http://jcs.biologists.org/content/joces/114/24/4349.full.pdf

100. Siegert F, Weijer CJ. Spiral and concentric waves organize multicellular Dictyostelium mounds. Curr Biol [Internet]. 1995 Aug 1 [cited 2019 May 16];5(8):937–43. Available from: http://www.ncbi.nlm.nih.gov/pubmed/7583152

101. Thompson CRL, Reichelt S, Kay RR. A demonstration of pattern formation without positional information in Dictyostelium. Dev Growth Differ [Internet]. 2004 Aug 1 [cited 2019 May 16];46(4):363–9. Available from: http://doi.wiley.com/10.1111/j.1440-169x.2004.00753.x

102. Chattwood A, Nagayama K, Bolourani P, Harkin L, Kamjoo M, Weeks G, et al. Developmental lineage priming in Dictyostelium by heterogeneous Ras activation. Elife [Internet]. 2013 Nov 26 [cited 2019 May 13];2:e01067. Available from: http://www.ncbi.nlm.nih.gov/pubmed/24282234

103. Gruenheit N, Parkinson K, Brimson CA, Kuwana S, Johnson EJ, Nagayama K, et al. Cell Cycle Heterogeneity Can Generate Robust Cell Type Proportioning. Dev Cell [Internet]. 2018 [cited 2019 Feb 6];47(4):494-508.e4. Available from: https://doi.org/10.1016/j.devcel.2018.09.023

104. Gross JD. Acidic Ca2+ stores, excitability, and cell patterning in Dictyostelium discoideum. Eukaryot Cell [Internet]. 2009 May [cited 2019 May 13];8(5):696–702. Available from: http://www.ncbi.nlm.nih.gov/pubmed/19252125

105. Kubohara Y, Arai A, Gokan N, Hosaka K. Pharmacological evidence that stalk cell differentiation involves increases in the intracellular Ca2+ and H+ concentrations in Dictyostelium discoideum. Dev Growth Differ [Internet]. 2007 Mar 30 [cited 2019 May 13];49(3):253–64. Available from: http://www.ncbi.nlm.nih.gov/pubmed/17394603

106. Thompson CRL, Kay RR. Cell-fate choice in Dictyostelium: Intrinsic biases modulate sensitivity to DIF signaling. Dev Biol [Internet]. 2000 [cited 2019 May 13];227(1):56–64. Available from: http://www.idealibrary.com

107. Weijer CJ, Duschl G, David CN. Dependence of cell-type proportioning and sorting on cell cycle phase in Dictyostelium discoideum [Internet]. Vol. VOL. 70, Journal of Cell Science. 1984 [cited 2019 May 17]. Available from: http://jcs.biologists.org/content/joces/70/1/133.full.pdf

108. Fukuzawa M. Control of prestalk-cell differentiation by transcription factors. Dev Growth Differ [Internet]. 2011 May 1 [cited 2019 May 16];53(4):538–47. Available from: http://doi.wiley.com/10.1111/j.1440-169X.2011.01269.x

109. Jang W, Gomer RH. Initial cell type choice in Dictyostelium. Eukaryot Cell [Internet]. 2011 Feb [cited 2019 May 17];10(2):150–5. Available from: http://www.ncbi.nlm.nih.gov/pubmed/21148754

110. Jermyn KA, Duffy KTI, Williams JG. A new anatomy of the prestalk zone in Dictyostelium. Nature [Internet]. 1989 Jul [cited 2019 May 17];340(6229):144–6. Available from: http://www.nature.com/articles/340144a0

111. Antolović V, Lenn T, Miermont A, Chubb JR. Transition state dynamics during a stochastic fate choice. Dev [Internet]. 2019 Jun 15 [cited 2019 May 17];146(12):dev173740. Available from: http://dev.biologists.org/content/146/12/dev173740.long

112. Berks M, Kay RR. Combinatorial control of cell differentiation by cAMP and DIF-1 during development of Dictyostelium discoideum. Development [Internet]. 1990 Nov [cited 2019 May 17];110(3):977–84. Available from: http://www.ncbi.nlm.nih.gov/pubmed/1965164

113. Loomis WF. Genetic control of morphogenesis in Dictyostelium. Dev Biol [Internet]. 2015 Jun 15 [cited 2019 May 17];402(2):146–61. Available from: http://www.ncbi.nlm.nih.gov/pubmed/25872182

114. Weijer CJ, Williams JG. Dictyostelium : Cell Sorting and Patterning . Encycl Life Sci [Internet]. 2009 [cited 2019 May 17]; Available from: www.els.net

115. Serafimidis I, Kay RR. New prestalk and prespore inducing signals in Dictyostelium. Dev Biol [Internet]. 2005 Jun 15 [cited 2019 May 17];282(2):432–41. Available from: http://www.ncbi.nlm.nih.gov/pubmed/15950608

116. Blanton RL, Fuller D, Iranfar N, Grimson MJ, Loomis WF. The cellulose synthase gene of Dictyostelium [Internet]. Vol. 97, Proceedings of the National Academy of Sciences of the United States of America. 2000 [cited 2019 May 17]. Available from: www.pnas.orgcgidoi10.1073pnas.040565697

117. Kim J, Ennis HL, Nguyen TH, Zhuang X, Luo J, Yao J, et al. Light-Directed Migration of D. discoideum Slugs in Microfabricated Confinements. Sens Actuators A Phys [Internet]. 2012 Dec 1 [cited 2019 May 17];188:312–9. Available from: http://www.ncbi.nlm.nih.gov/pubmed/24723742

118. Jermyn K, Traynor D, Williams J. The initiation of basal disc formation in Dictyostelium discoideum is an early event in culmination [Internet]. Vol. 122, Development. 1996 [cited 2019 May 17]. Available from: http://dev.biologists.org/content/develop/122/3/753.full.pdf

119. Jermyn KA, Williams JG. An analysis of culmination in Dictyostelium using prestalk and stalkspecific cell autonomous markers. Development. 1991;111(3):779–87.

120. Robinson V, Williams J. A marker of terminal stalk cell terminal differentiation in Dictyostelium. Differentiation [Internet]. 1997 May [cited 2019 May 17];61(4):223–8. Available from: http://www.ncbi.nlm.nih.gov/pubmed/9203345

121. Dickinson DJ, Nelson WJ, Weis WI. An epithelial tissue in Dictyostelium challenges the traditional origin of metazoan multicellularity. BioEssays [Internet]. 2012 Oct [cited 2019 May 17];34(10):833–40. Available from: http://www.ncbi.nlm.nih.gov/pubmed/22930590

122. West CM, Nguyen P, van der Wel H, Metcalf T, Sweeney KR, Blader IJ, et al. Dependence of stress resistance on a spore coat heteropolysaccharide in Dictyostelium. Eukaryot Cell [Internet]. 2009 Jan 1 [cited 2019 May 17];8(1):27–36. Available from: http://www.ncbi.nlm.nih.gov/pubmed/18996984

123. Chen ZH, Schaap P. The prokaryote messenger c-di-GMP triggers stalk cell differentiation in Dictyostelium. Nature [Internet]. 2012 Aug 5 [cited 2019 May 21];488(7413):680–3. Available from: http://www.ncbi.nlm.nih.gov/pubmed/22864416

124. Anjard C, Su Y, Loomis WF. The Polyketide MPBD Initiates the SDF-1 Signaling Cascade That Coordinates Terminal Differentiation in Dictyostelium. Eukaryot Cell [Internet]. 2011 Jul [cited 2019 May 21];10(7):956–63. Available from: http://ec.asm.org/lookup/doi/10.1128/EC.05053-11

125. Hopper NA, Harwood RJ, Bouzid S, Veron M, Williams JG. Activation of the prespore and spore cell pathway of Dictyostelium differentiation by cAMP-dependent protein kinase and evidence for its upstream regulation by ammonia. EMBO J [Internet]. 1993 Jun [cited 2019 May 21];12(6):2459–66. Available from: http://www.ncbi.nlm.nih.gov/pubmed/8508771

126. Fujimori T, Nakajima A, Shimada N, Sawai S. Tissue self-organization based on collective cell migration by contact activation of locomotion and chemotaxis. Proc Natl Acad Sci U S A [Internet]. 2019 Feb 19 [cited 2019 May 21];116(10):4291–6. Available from: http://www.ncbi.nlm.nih.gov/pubmed/30782791

127. Kay RR, L Thompson CR. Prespore cells make DIF-1 [Internet]. 2001 [cited 2019 May 22]. Available from: http://dev.biologists.org/content/develop/128/24/4959.full.pdf

128. Luciani MF, Song Y, Sahrane A, Kosta A, Golstein P. Early nucleolar disorganization in Dictyostelium cell death. Cell Death Dis [Internet]. 2017 Jan 5 [cited 2019 May 22];8(1):e2528–e2528. Available from: http://www.nature.com/articles/cddis2016444

129. Sforzini S, Dagnino A, Torrielli S, Dondero F, Fenoglio S, Negri A, et al. Use of highly sensitive sublethal stress responses in the social amoeba Dictyostelium discoideum for an assessment of freshwater quality. Sci Total Environ [Internet]. 2008 Jun 1 [cited 2019 May 28];395(2–3):101–8. Available from: http://www.ncbi.nlm.nih.gov/pubmed/18342359

130. Rodríguez-Ruiz A, Marigómez I, Boatti L, Viarengo A. Dictyostelium discoideum developmental cycle (DDDC) assay: A tool for Hg toxicity assessment and soil health screening. Sci Total Environ [Internet]. 2013 Apr 15 [cited 2019 May 14];450–451:39–50. Available from: http://www.ncbi.nlm.nih.gov/pubmed/23454908

131. Rodríguez-Ruiz A, Dondero F, Viarengo A, Marigómez I. Toxicity assessment of diesel- and metal-contaminated soils through elutriate and solid phase assays with the slime mold *Dictyostelium discoideum*. Environ Toxicol Chem [Internet]. 2016 Jun [cited 2019 May 14];35(6):1413–21. Available from: http://www.ncbi.nlm.nih.gov/pubmed/26450765

132. Dannat K, Tillner J, Winckler T, Weiss M, Eger K, Dingermann T. Effects of medicinal compounds on the differentiation of the eukaryotic microorganism Dictyostelium discoideum: Can this model be used as a screening test for reproductive toxicity in humans? [Internet]. Vol. 58, Pharmazie. 2003 [cited 2019 Mar 13]. Available from: http://www.nih.gov/science/models/

133. Williams RSB, Boeckeler K, Gräf R, Müller-Taubenberger A, Li Z, Isberg RR, et al. Towards a molecular understanding of human diseases using Dictyostelium discoideum. Vol. 12, Trends in Molecular Medicine. 2006. p. 415–24.

134. Loomis WF. A better way to discover gene function in the social amoeba Dictyostelium discoideum. Vol. 26, Genome Research. Cold Spring Harbor Laboratory Press; 2016. p. 1161–4.

135. Li G, Alexander H, Schneider N, Alexander S. Molecular basis for resistance to the anticancer drug cisplatin in Dictyostelium. Microbiology. 2000;146(9):2219–27.

136. Min J, Traynor D, Stegner AL, Zhang L, Hanigan MH, Alexander H, et al. Sphingosine Kinase Regulates the Sensitivity of Dictyostelium discoideum Cells to the Anticancer Drug Cisplatin. Eukaryot Cell [Internet]. 2005 [cited 2020 Jan 27];4(1):178–89. Available from: http://ec.asm.org/

137. Van Driessche N, Alexander H, Min J, Kuspa A, Alexander S, Shaulsky G. Global transcriptional responses to cisplatin in Dictyostelium discoideum identify potential drug targets [Internet]. Vol. 104, Proceedings of the National Academy of Sciences of the United States of America. 2007 [cited 2020 Jan 27]. Available from: www.pnas.org/cgi/content/full/

138. Cocorocchio M, Baldwin AJ, Stewart B, Kim L, Harwood AJ, Thompson CRL, et al. Curcumin and derivatives function through protein phosphatase 2A and presenilin orthologues in Dictyostelium discoideum. DMM Dis Model Mech. 2018 Jan 1;11(1).

139. Waheed A, Ludtmann MHR, Pakes N, Robery S, Kuspa A, Dinh C, et al. Naringenin inhibits the growth of Dictyostelium and MDCK-derived cysts in a TRPP2 (polycystin-2)-dependent manner. Br J Pharmacol. 2014;171(10):2659–70.

140. McQuade KJ, Nakajima A, Ilacqua AN, Shimada N, Sawai S. The Green Tea Catechin Epigallocatechin Gallate (EGCG) Blocks Cell Motility, Chemotaxis and Development in Dictyostelium discoideum. PLoS One. 2013 Mar 14;8(3).

141. Tariqul Islam AFM, Scavello M, Lotfi P, Daniel D, Haldeman P, Charest PG. Caffeine inhibits PI3K and mTORC2 in Dictyostelium and differentially affects multiple other cAMP chemoattractant signaling effectors. Mol Cell Biochem. 2019;

142. Perry CJ, Finch P, Müller-Taubenberger A, Leung K, Warren EC, Damstra-Oddy J, et al. A new mechanism for cannabidiol in regulating the one-carbon cycle and methionine levels in <scp>

Dictyostelium </scp> and in mammalian epilepsy models. Br J Pharmacol [Internet]. 2020 Jan 3 [cited 2020 Jan 28];bph.14892. Available from: https://onlinelibrary.wiley.com/doi/abs/10.1111/bph.14892

143. Grove JE, Brown RJ, Watts DJ. The Intracellular Target for the Antiresorptive Aminobisphosphonate Drugs in Dictyostelium discoideum Is the Enzyme Farnesyl Diphosphate Synthase. J Bone Miner Res [Internet]. 2010 Feb 18 [cited 2020 Jan 28];15(5):971–81. Available from: http://doi.wiley.com/10.1359/jbmr.2000.15.5.971

144. Ouertatani-Sakouhi H, Kicka S, Chiriano G, Harrison CF, Hilbi H, Scapozza L, et al. Inhibitors of Mycobacterium marinum virulence identified in a Dictyostelium discoideum host model. PLoS One. 2017 Jul 1;12(7).

145. Vieta E, Berk M, Schulze TG, Carvalho AF, Suppes T, Calabrese JR, et al. Bipolar disorders. Nat Rev Dis Prim [Internet]. 2018 Mar 8 [cited 2019 May 30];4:18008. Available from: http://www.nature.com/articles/nrdp20188

146. Grover S, Avasthi A. Mood stabilizers in pregnancy and lactation. Indian J Psychiatry [Internet]. 2015 Jul [cited 2019 May 30];57(Suppl 2):S308. Available from: http://www.ncbi.nlm.nih.gov/pubmed/26330649

147. Nguyen HTT, Sharma V, Mcintyre RS. Teratogenesis Associated with Antibipolar Agents. Adv Ther [Internet]. 2009 [cited 2019 Jun 11];26(3):281–94. Available from: http://clinicaltrials.gov

148. Klein PS, Melton DA. A molecular mechanism for the effect of lithium on development [Internet]. Vol. 93, Bipolar Disorder: The Science of Mental Health. 2019 [cited 2019 Jun 12]. Available from: https://www.pnas.org/content/pnas/93/16/8455.full.pdf

149. Yu W, Greenberg ML. Inositol depletion, GSK3 inhibition and bipolar disorder. Future Neurol [Internet]. 2016 May [cited 2019 Jun 4];11(2):135–48. Available from: http://www.ncbi.nlm.nih.gov/pubmed/29339929

150. Harwood AJ. Lithium and bipolar mood disorder: The inositol-depletion hypothesis revisited. Vol. 10, Molecular Psychiatry. 2005. p. 117–26.

151. Williams RSB, Eames M, Ryves WJ, Viggars J, Harwood AJ. Loss of a prolyl oligopeptidase confers resistance to lithium by elevation of inositol (1,4,5) trisphosphate. EMBO J [Internet]. 1999 May 17 [cited 2019 Nov 18];18(10):2734–45. Available from: http://emboj.embopress.org/cgi/doi/10.1093/emboj/18.10.2734

152. Williams RSB, Cheng L, Mudge AW, Harwood AJ. A common mechanism of action for three mood-stabilizing drugs. Nature [Internet]. 2002 May [cited 2019 Jun 18];417(6886):292–5. Available from: http://www.nature.com/articles/417292a

153. King J, Keim M, Teo R, Weening KE, Kapur M, McQuillan K, et al. Genetic control of lithium sensitivity and regulation of inositol biosynthetic genes. PLoS One [Internet]. 2010 Jun 17 [cited 2019 Jun 10];5(6):e11151. Available from: http://www.ncbi.nlm.nih.gov/pubmed/20567601

154. Kelly E, Sharma D, Wilkinson CJ, Williams RSB. Diacylglycerol kinase (DGKA) regulates the effect of the epilepsy and bipolar disorder treatment valproic acid in Dictyostelium discoideum. DMM Dis Model Mech. 2018 Sep 1;11(9).

155. Brown KM, Tracy DK. Lithium: The pharmacodynamic actions of the amazing ion. Ther Adv Psychopharmacol. 2013;3(3):163–76.

156. Teo R, King J, Dalton E, Ryves J, Williams RSB, Harwood AJ. PtdIns(3,4,5)P3 and inositol depletion as a cellular target of mood stabilizers. Biochem Soc Trans [Internet]. 2009 [cited 2020 Oct 26];37(5):1110–4. Available from: http://portlandpress.com/biochemsoctrans/article-pdf/37/5/1110/544054/bst0371110.pdf

157. Masuda CA, Xavier MA, Mattos KA, Galina A, Montero-Lomeli M. Phosphoglucomutase is an in vivo lithium target in yeast. J Biol Chem [Internet]. 2001 Oct 12 [cited 2019 Jun 11];276(41):37794–801. Available from: http://www.ncbi.nlm.nih.gov/pubmed/11500487

158. Shaltiel G, Shamir A, Shapiro J, Ding D, Dalton E, Bialer M, et al. Valproate decreases inositol biosynthesis. Biol Psychiatry. 2004 Dec 1;56(11):868–74.

159. Vaden DL, Ding D, Peterson B, Greenberg ML. Lithium and Valproate Decrease Inositol Mass and Increase Expression of the Yeast *INO1* and *INO2* Genes for Inositol Biosynthesis. J Biol Chem [Internet]. 2001 May 4 [cited 2019 Jun 11];276(18):15466–71. Available from: http://www.ncbi.nlm.nih.gov/pubmed/11278273

160. Ju S, Shaltiel G, Shamir A, Agam G, Greenberg ML. Human 1-D- *myo* -Inositol-3-phosphate Synthase Is Functional in Yeast. J Biol Chem [Internet]. 2004 May 21 [cited 2019 Jun

11];279(21):21759–65. Available from: http://www.ncbi.nlm.nih.gov/pubmed/15024000

161. Klein PS, Melton DA. A molecular mechanism for the effect of lithium on development. Proc Natl Acad Sci [Internet]. 1996 Aug 6 [cited 2019 Jun 5];93(16):8455–9. Available from: http://www.ncbi.nlm.nih.gov/pubmed/8710892

162. Ryves WJ, Harwood AJ. Lithium Inhibits Glycogen Synthase Kinase-3 by Competition for Magnesium. Biochem Biophys Res Commun [Internet]. 2001 Jan 26 [cited 2019 Jun 5];280(3):720–5. Available from: http://www.ncbi.nlm.nih.gov/pubmed/11162580

163. Hikasa H, Sokol SY. Wnt Signaling in Vertebrate Axis Specification. Cold Spring Harb Perspect Biol [Internet]. 2013 [cited 2019 Jun 12];5(1). Available from: https://www.ncbi.nlm.nih.gov/pmc/articles/PMC3579404/

164. Price KL, Kolatsi-Joannou M, Mari C, Long DA, Winyard PJD. Lithium induces mesenchymal-epithelial differentiation during human kidney development by activation of the Wnt signalling system. Cell Death Discov [Internet]. 2018 Dec 7 [cited 2019 Jun 13];4(1):13. Available from: http://www.nature.com/articles/s41420-017-0021-6

165. Soleimani M, Ghasemi N. Lithium Chloride can Induce Differentiation of Human Immortalized RenVm Cells into Dopaminergic Neurons. Avicenna J Med Biotechnol [Internet]. 2017 [cited 2019 Jun 13];9(4):176–80. Available from: http://www.ncbi.nlm.nih.gov/pubmed/29090066

166. Roux M, Dosseto A. From direct to indirect lithium targets: a comprehensive review of omics data. Metallomics [Internet]. 2017 Oct 18 [cited 2019 Jun 13];9(10):1326–51. Available from: http://xlink.rsc.org/?DOI=C7MT00203C

167. Hedgepeth CM, Conrad LJ, Zhang J, Huang H-C, Lee VMY, Klein PS. Activation of the Wnt Signaling Pathway: A Molecular Mechanism for Lithium Action. Dev Biol [Internet]. 1997 May [cited 2019 Jun 13];185(1):82–91. Available from: https://linkinghub.elsevier.com/retrieve/pii/S0012160697985523

168. Shaikh Qureshi WM, Latif ML, Parker TL, Pratten MK. Lithium carbonate teratogenic effects in chick cardiomyocyte micromass system and mouse embryonic stem cell derived cardiomyocyte – Possible protective role of myo-inositol. Reprod Toxicol [Internet]. 2014 Jul 1 [cited 2019 Jun 13];46:106–14. Available from: https://www.sciencedirect.com/science/article/pii/S0890623814000537#bib0090

169. MAEDA Y. Influence of Ionic Conditions on Cell Differentiation and Morphogenesis of the Cellular Slime Molds. Dev Growth Differ [Internet]. 1970 Oct 1 [cited 2019 Jun 13];12(3):217–27. Available from: http://doi.wiley.com/10.1111/j.1440-169X.1970.00217.x

170. Harwood AJ, Plyte SE, Woodgett J, Strutt H, Kay RR. Glycogen Synthase Kinase 3 Regulates Cell Fate in Dictyostelium [Internet]. Vol. 80, Cell. 1995 [cited 2019 Jun 13]. Available from: https://www.cell.com/cell/pdf/0092-8674(95)90458-1.pdf?_returnURL=https%3A%2F%2Flinkinghub.elsevier.com%2Fretrieve%2Fpii%2F0092867495904581%3Fshowall%3Dtrue

171. King JS, Teo R, Ryves J, Reddy J V., Peters O, Orabi B, et al. The mood stabiliser lithium suppresses PIP3 signalling in Dictyostelium and human cells. DMM Dis Model Mech [Internet]. 2009 [cited 2019 Jun 13];2(5–6):306–12. Available from: https://www.ncbi.nlm.nih.gov/pmc/articles/PMC2675811/

172. DiLiberti JH, Farndon PA, Dennis NR, Curry CJR. The fetal valproate syndrome. Am J Med Genet [Internet]. 1984 Nov [cited 2019 Jun 13];19(3):473–81. Available from: http://www.ncbi.nlm.nih.gov/pubmed/6439041

173. Phiel CJ, Zhang F, Huang EY, Guenther MG, Lazar MA, Klein PS. Histone Deacetylase is a Direct Target of Valproic Acid, a Potent Anticonvulsant, Mood Stabilizer, and Teratogen. J Biol Chem [Internet]. 2001 [cited 2019 Jun 6];276(39):36734–41. Available from: http://www.jbc.org/

174. Gottlicher M, Minucci S, Zhu P, Krämer OH, Schimpf A, Giavara S, et al. Valproic acid defines a novel class of HDAC inhibitors inducing differentiation of transformed cells. EMBO J [Internet]. 2001 Dec 17 [cited 2019 Jun 8];20(24):6969–78. Available from: http://www.ncbi.nlm.nih.gov/pubmed/11742974

175. Eyal S, Yagen B, Sobol E, Altschuler Y, Shmuel M, Bialer M. The Activity of Antiepileptic Drugs as Histone Deacetylase Inhibitors. Epilepsia [Internet]. 2004 Jul [cited 2019 Jun 8];45(7):737–44. Available from: http://www.ncbi.nlm.nih.gov/pubmed/15230695

176. Lloyd KA. A scientific review: Mechanisms of valproate-mediated teratogenesis. Biosci Horizons [Internet]. 2013 [cited 2019 Jun 17];6:2013. Available from: https://academic.oup.com/biohorizons/article-abstract/doi/10.1093/biohorizons/hzt003/302011

177. Hill DS, Wlodarczyk BJ, Palacios AM, Finnell RH. Teratogenic effects of antiepileptic drugs. Expert Rev Neurother [Internet]. 2010 [cited 2019 Jun 17];10(6):943–59. Available from: https://www.ncbi.nlm.nih.gov/pmc/articles/PMC2970517/pdf/nihms215086.pdf

178. Eikel D, Lampen A, Nau H. Teratogenic Effects Mediated by Inhibition of Histone Deacetylases: Evidence from Quantitative Structure Activity Relationships of 20 Valproic Acid Derivatives. Chem Res Toxicol [Internet]. 2006 Feb [cited 2019 Jun 17];19(2):272–8. Available from: http://www.ncbi.nlm.nih.gov/pubmed/16485903

179. Wiltse J. Mode of action: Inhibition of histone deacetylase, altering WNT-dependent gene expression, and regulation of beta-catenin - Developmental effects of valproic acid. Crit Rev Toxicol [Internet]. 2005 [cited 2019 Jun 17];35(8–9):727–38. Available from: http://www.ncbi.nlm.nih.gov/pubmed/16417040

180. Tillner J, Nau H, Winckler T, Dingermann T. Evaluation of the Teratogenic Potential of Valproic Acid Analogues in Transgenic Dictyostelium discoideum Strains. Toxicol Vitr [Internet]. 1998 Aug [cited 2019 Jun 17];12(4):463–9. Available from: https://linkinghub.elsevier.com/retrieve/pii/S0887233398000162

181. Walker SL, Ariga J, Mathias JR, Coothankandaswamy V, Xie X, Distel M, et al. Automated Reporter Quantification In Vivo: High-Throughput Screening Method for Reporter-Based Assays in Zebrafish. Karl MO, editor. PLoS One [Internet]. 2012 Jan 4 [cited 2019 May 28];7(1):e29916. Available from: http://www.ncbi.nlm.nih.gov/pubmed/22238673

182. Liao X-H, Kimmel AR. A Unique High-Throughput Assay to Identify Novel Small Molecule Inhibitors of Chemotaxis and Migration. Curr Protoc cell Biol [Internet]. 2017 Mar 3 [cited 2019 Jun 29];74:12.11.1-12.11.13. Available from: http://www.ncbi.nlm.nih.gov/pubmed/28256720

183. Paumgartten FJR. Influence of maternal toxicity on the outcome of developmental toxicity studies. J Toxicol Environ Heal - Part A Curr Issues. 2010 Jan;73(13–14):944–51.

184. Schardein JL. Approaches to defining the relationship of maternal and developmental toxicity. Teratog Carcinog Mutagen [Internet]. 1987 [cited 2019 Nov 8];7(3):255–71. Available from: http://doi.wiley.com/10.1002/tcm.1770070307

185. Cassar S, Beekhuijzen M, Beyer B, Chapin R, Dorau M, Hoberman A, et al. A multi-institutional study benchmarking the zebrafish developmental assay for prediction of embryotoxic plasma concentrations from rat embryo–fetal development studies. Reprod Toxicol. 2019 Jun 1;86:33–44.

186. Horzmann KA, Freeman JL. Making waves: New developments in toxicology with the zebrafish. Toxicol Sci [Internet]. 2018 May 1 [cited 2020 Jan 13];163(1):5–12. Available from: https://academic.oup.com/toxsci/article/163/1/5/4870163

187. Ducharme NA, Peterson LE, Benfenati E, Reif D, McCollum CW, Gustafsson JÅ, et al. Meta-analysis of toxicity and teratogenicity of 133 chemicals from zebrafish developmental toxicity studies. Reprod Toxicol. 2013 Nov;41:98–108.

188. Ducharme NA, Reif DM, Gustafsson JA, Bondesson M. Comparison of toxicity values across zebrafish early life stages and mammalian studies: Implications for chemical testing. Reprod Toxicol. 2015 Aug 1;55:3–10.

189. van Gelder MMHJ, van Rooij IALM, Miller RK, Zielhuis GA, de Jong-van den Berg LTW, Roeleveld N. Teratogenic mechanisms of medical drugs. Hum Reprod Update [Internet]. 2010 Jul 1 [cited 2019 Jun 30];16(4):378–94. Available from: http://www.ncbi.nlm.nih.gov/pubmed/20061329

190. REACH. No 1907/2006 of the European Parliament and of the Council of. 2006 [cited 2019 Nov 2]; Available from: https://eur-lex.europa.eu/legal-content/EN/TXT/PDF/?uri=CELEX:02006R1907-20190702&from=en

191. Hansen JM. Oxidative stress as a mechanism of teratogenesis. Birth Defects Res Part C Embryo Today Rev [Internet]. 2006 Dec [cited 2019 Jun 30];78(4):293–307. Available from: http://www.ncbi.nlm.nih.gov/pubmed/17315243

192. Wells PG, McCallum GP, Chen CS, Henderson JT, Lee CJJ, Perstin J, et al. Oxidative Stress in Developmental Origins of Disease: Teratogenesis, Neurodevelopmental Deficits, and Cancer. Toxicol Sci [Internet]. 2009 Mar [cited 2019 Jun 30];108(1):4–18. Available from: http://www.ncbi.nlm.nih.gov/pubmed/19126598

193. Knudsen TB, Kleinstreuer NC. Disruption of embryonic vascular development in predictive toxicology. Birth Defects Res Part C Embryo Today Rev [Internet]. 2011 Dec [cited 2019 Jun 30];93(4):312–23. Available from: http://www.ncbi.nlm.nih.gov/pubmed/22271680

194. Pajouhesh H, Lenz GR. Medicinal chemical properties of successful central nervous system drugs. NeuroRx [Internet]. 2005 Oct [cited 2019 Jun 27];2(4):541–53. Available from:

http://www.ncbi.nlm.nih.gov/pubmed/16489364

195. Cadena-Herrera D, Esparza-De Lara JE, Ramírez-Ibañez ND, López-Morales CA, Pérez NO, Flores-Ortiz LF, et al. Validation of three viable-cell counting methods: Manual, semi-automated, and automated. Biotechnol Reports. 2015 Jun 1;7:9–16.

196. Krediet CJ, DeNofrio JC, Caruso C, Burriesci MS, Cella K, Pringle JR. Rapid, Precise, and Accurate Counts of Symbiodinium Cells Using the Guava Flow Cytometer, and a Comparison to Other Methods. Moustafa A, editor. PLoS One [Internet]. 2015 Aug 20 [cited 2019 Jun 30];10(8):e0135725. Available from: https://dx.plos.org/10.1371/journal.pone.0135725

197. Tinevez JY, Perry N, Schindelin J, Hoopes GM, Reynolds GD, Laplantine E, et al. TrackMate: An open and extensible platform for single-particle tracking. Methods [Internet]. 2017 Feb 15 [cited 2019 Feb 13];115:80–90. Available from: https://www.sciencedirect.com/science/article/pii/S1046202316303346

198. Pastor N, Kaplan C, Domínguez I, Mateos S, Cortés F. Cytotoxicity and mitotic alterations induced by non-genotoxic lithium salts in CHO cells in vitro. Toxicol In Vitro [Internet]. 2009 Apr [cited 2019 Jun 30];23(3):432–8. Available from: http://www.ncbi.nlm.nih.gov/pubmed/19444924

199. Repetto G, Del Peso A, Sanz P, Repetto M. In vitro effects of lithium and nickel at different levels on Neuro-2a mouse neuroblastoma cells. Toxicol Vitr [Internet]. 2001 [cited 2019 Jun 30];15(4–5):363–8. Available from: http://www.ncbi.nlm.nih.gov/pubmed/11566564

200. Engel R, Van Haastert PJM, Visser AJWG. Spectral characterization ofDictyostelium autofluorescence. Microsc Res Tech [Internet]. 2006 Mar [cited 2019 Jun 30];69(3):168–74. Available from: http://www.ncbi.nlm.nih.gov/pubmed/16538623

201. Rosengarten RD, Santhanam B, Fuller D, Katoh-Kurasawa M, Loomis WF, Zupan B, et al. Leaps and lulls in the developmental transcriptome of Dictyostelium discoideum. BMC Genomics [Internet]. 2015 Dec 13 [cited 2019 Jun 30];16(1):294. Available from: http://www.biomedcentral.com/1471-2164/16/294

202. Mazo-Vargas A, Park H, Aydin M, Buchler NE. Measuring fast gene dynamics in single cells with time-lapse luminescence microscopy. Mol Biol Cell [Internet]. 2014 Nov 5 [cited 2019 Jun 30];25(22):3699–708. Available from: http://www.ncbi.nlm.nih.gov/pubmed/25232010

203. Hu L, Wu L, Xue Y, Zhu J, Shi H. An assay to determine the sensitive window of embryos to chemical exposure using Xenopus tropicalis. J Appl Toxicol [Internet]. 2016 May [cited 2019 Nov 2];36(5):685–91. Available from: http://www.ncbi.nlm.nih.gov/pubmed/26177576

204. Walmod PS, Berezin A, Gallagher HC, Gravemann U, Lepekhin EA, Belman V, et al. Automated in vitro screening of teratogens. Toxicol Appl Pharmacol. 2002 May 15;181(1):1–15.

205. Cocorocchio M, Ives R, Clapham D, Andrews PLR, Williams RSB. Research article bitter tastant responses in the amoeba Dictyostelium correlate with rat and human taste assays. ALTEX. 2016;33(3):225–36.

206. Napper AD, Motlekar N, de Almeida RA, Pavitt GD. Parallel High-Throughput Automated Assays to Measure Cell Growth and Beta-Galactosidase Reporter Gene Expression in the Yeast Saccharomyces cerevisiae. Curr Protoc Chem Biol [Internet]. 2011 Mar 1 [cited 2019 Nov 2];3(1):1–14. Available from: http://www.ncbi.nlm.nih.gov/pubmed/23836585

207. Alexander H, Vomund AN, Alexander S. Viability assay for Dictyostelium for use in drug studies. Biotechniques [Internet]. 2003 Sep 1 [cited 2020 Nov 10];35(3):464–70. Available from: https://www.future-science.com/doi/abs/10.2144/03353bm05

208. Min J, Sridevi P, Alexander S, Alexander H. Sensitive cell viability assay for use in drug screens and for studying the mechanism of action of drugs in Dictyostelium discoideum. Biotechniques [Internet]. 2006 Nov 21 [cited 2020 Nov 10];41(5):591–5. Available from: https://www.future-science.com/doi/10.2144/000112260

209. Dondero F, Jonsson H, Rebelo M, Pesce G, Berti E, Pons G, et al. Cellular responses to environmental contaminants in amoebic cells of the slime mould Dictyostelium discoideum. Comp Biochem Physiol - C Toxicol Pharmacol. 2006 Jun;143(2):150–7.

210. Teixidó E, Kießling TR, Krupp E, Quevedo C, Muriana A, Scholz S. Automated Morphological Feature Assessment for Zebrafish Embryo Developmental Toxicity Screens. Toxicol Sci [Internet]. 2019 [cited 2020 Jan 10];167(2):438–49. Available from: https://doi.org/10.5061/dryad.gv144d5

211. Wassermann AM, Camargo LM, Auld DS. Composition and applications of focus libraries to phenotypic assays. Vol. 5 JUN, Frontiers in Pharmacology. Frontiers Research Foundation; 2014.

212. Wu Y, Wang G. Machine learning based toxicity prediction: From chemical structural description to

transcriptome analysis. Int J Mol Sci. 2018 Aug 10;19(8).

213. Gad SC. Rodents model for toxicity testing and biomarkers. In: Biomarkers in Toxicology. Elsevier Inc.; 2014. p. 7–69.

214. Agency USEP. Guidelines for Developmental Toxicity Risk Assessment. Risk Assess Forum [Internet]. 1991 [cited 2019 Sep 24];56(EPA/600/FR-91/001):63798–826. Available from: http://www.epa.gov/raf/publications/guidelines-dev-toxicity-risk-assessment.htm

215. Erhirhie EO, Ihekwereme CP, Ilodigwe EE. Advances in acute toxicity testing: Strengths, weaknesses and regulatory acceptance. Interdiscip Toxicol. 2018;11(1):5–12.

216. Cot T, Loaels H. COMMITTEE ON TOXICITY OF CHEMICALS IN FOOD , CONSUMER PRODUCTS AND THE ENVIRONMENT Assessment of the adequacy of the 10-fold uncertainty factor to allow for interspecies variation in developmental toxicity. 2014 [cited 2019 Oct 10];1–27. Available from: https://cot.food.gov.uk/sites/default/files/cot/tox201417.pdf

217. Sura Alwan A, Bleyl SB, Brent RL, Chambers CD, Daston GP, Faustman EM, et al. Teratology Primer.

218. Parasuraman S. Toxicological screening. J Pharmacol Pharmacother. 2011 Apr;2(2):74–9.

219. Krewski D, Acosta D, Andersen M, Anderson H, Bailar JC, Boekelheide K, et al. Toxicity testing in the 21st century: A vision and a strategy. Vol. 13, Journal of Toxicology and Environmental Health - Part B: Critical Reviews. NIH Public Access; 2010. p. 51–138.

220. Daston GP, Chapin RE, Scialli AR, Piersma AH, Carney EW, Rogers JM, et al. A different approach to validating screening assays for developmental toxicity. Birth Defects Res Part B - Dev Reprod Toxicol [Internet]. 2010 Dec 1 [cited 2020 Feb 20];89(6):526–30. Available from: http://doi.wiley.com/10.1002/bdrb.20276

221. Daston GP, Beyer BK, Carney EW, Chapin RE, Friedman JM, Piersma AH, et al. Exposure-based validation list for developmental toxicity screening assays. Birth Defects Res Part B - Dev Reprod Toxicol [Internet]. 2014 Dec [cited 2020 Jan 9];101(6):423–8. Available from: http://doi.wiley.com/10.1002/bdrb.21132

222. Leconte I, Mouche I. Frog Embryo Teratogenesis Assay on Xenopus and Predictivity Compared with In Vivo Mammalian Studies. In 2013 [cited 2019 Nov 6]. p. 403–21. Available from: http://link.springer.com/10.1007/978-1-62703-131-8_29

223. Development SKBAC, Coefficient P, Although A. Application Note LogP—Making Sense of the Value [Internet]. Journal of Pharmaceutical Sciences. 2011 [cited 2019 Nov 3]. Available from: www.acdlabs.com

224. Yang NJ, Hinner MJ. Getting across the cell membrane: an overview for small molecules, peptides, and proteins. Vol. 1266, Methods in molecular biology (Clifton, N.J.). 2015. p. 29–53.

225. Serafimidis I, Bloomfield G, Skelton J, Ivens A, Kay RR. A new environmentally resistant cell type from Dictyostelium. Microbiology. 2007 Feb;153(2):619–30.

226. Nair A, Jacob S. A simple practice guide for dose conversion between animals and human. J Basic Clin Pharm. 2016;7(2):27.

227. Scialli AR, Daston G, Chen C, Coder PS, Euling SY, Foreman J, et al. RETHINKING DEVELOPMENTAL TOXICITY TESTING: EVOLUTION OR REVOLUTION? EPA Public Access. Birth Defects Res. 2018;110(10):840–50.

228. Raies AB, Bajic VB. In silico toxicology: computational methods for the prediction of chemical toxicity. Wiley Interdiscip Rev Comput Mol Sci. 2016 Mar 1;6(2):147–72.

229. Rudmann DG. On-target and off-target-based toxicologic effects. Toxicol Pathol. 2013;41(2):310–4.

230. Escher BI, Hackermüller J, Polte T, Scholz S, Aigner A, Altenburger R, et al. From the exposome to mechanistic understanding of chemical-induced adverse effects. Vol. 99, Environment International. Elsevier Ltd; 2017. p. 97–106.

231. Wittwehr C, Aladjov H, Ankley G, Byrne HJ, De Knecht J, Heinzle E, et al. How Adverse Outcome Pathways Can Aid the Development and Use of Computational Prediction Models for Regulatory Toxicology. Toxicol Sci [Internet]. 2017 [cited 2019 Dec 10];155(2):326–36. Available from: https://aopwiki.org/;

232. Browne P, Noyes PD, Casey WM, Dix DJ. Application of adverse outcome pathways to U.S. EPA's endocrine disruptor screening program. Environ Health Perspect [Internet]. 2017 [cited 2019 Dec

10];125(9). Available from: https://doi.org/10.1289/EHP1304.

233. Giacomini KM, Yee SW, Mushiroda T, Weinshilboum RM, Ratain MJ, Kubo M. Genome-wide association studies of drug response and toxicity: An opportunity for genome medicine. Vol. 16, Nature Reviews Drug Discovery. Nature Publishing Group; 2016. p. 1.

234. Sirci F, Napolitano F, Pisonero-Vaquero S, Carrella D, Medina DL, di Bernardo D. Comparing structural and transcriptional drug networks reveals signatures of drug activity and toxicity in transcriptional responses. npj Syst Biol Appl. 2017 Dec 1;3(1).

235. Terbach N, Shah R, Kelemen R, Klein PS, Gordienko D, Brown NA, et al. Identifying an uptake mechanism for the antiepileptic and bipolar disorder treatment valproic acid using the simple biomedical model Dictyostelium. J Cell Sci. 2011 Jul 1;124(13):2267–76.

236. Oliveros JC. Venny 2.1.0 [Internet]. An interactive tool for comparing lists with Venn's diagrams. . 2015 [cited 2020 Jan 24]. Available from: http://bioinfogp.cnb.csic.es/tools/venny/

237. GSEABase-package: Gene set enrichment data structures and methods in GSEABase: Gene set enrichment data structures and methods [Internet]. [cited 2019 Dec 6]. Available from: https://rdrr.io/bioc/GSEABase/man/GSEABase-package.html

238. Supek F, Bošnjak M, Škunca N, Šmuc T. Revigo summarizes and visualizes long lists of gene ontology terms. Gibas C, editor. PLoS One [Internet]. 2011 Jul 18 [cited 2019 Feb 15];6(7):e21800. Available from: https://dx.plos.org/10.1371/journal.pone.0021800

239. Holden HM, Rayment I, Thoden JB. Structure and Function of Enzymes of the Leloir Pathway for Galactose Metabolism. Vol. 278, Journal of Biological Chemistry. 2003. p. 43885–8.

240. Tang M, Etokidem E, Lai K. The leloir pathway of galactose metabolism - A novel therapeutic target for hepatocellular carcinoma. Anticancer Res [Internet]. 2016 Dec 1 [cited 2020 Mar 11];36(12):6265–71. Available from: http://www.ncbi.nlm.nih.gov/pubmed/27919945

241. Xu E, Müller-Taubenberger A, Adley KE, Pawolleck N, Lee VWY, Wiedemann C, et al. Attenuation of phospholipid signaling provides a novel mechanism for the action of valproic acid. Eukaryot Cell. 2007 Jun 1;6(6):899–906.

242. Williams T, Kay RR. High-throughput measurement of dictyostelium discoideum macropinocytosis by flow cytometry. J Vis Exp. 2018 Sep 10;2018(139).

243. Chiu C-T, Wang Z, Hunsberger JG, Chuang D-M. Therapeutic potential of mood stabilizers lithium and valproic acid: beyond bipolar disorder. Pharmacol Rev [Internet]. 2013 Jan [cited 2019 Jun 2];65(1):105–42. Available from: http://www.ncbi.nlm.nih.gov/pubmed/23300133

244. Desfossés-Baron K, Hammond-Martel I, Simoneau A, Sellam A, Roberts S, Wurtele H. Valproate inhibits MAP kinase signalling and cell cycle progression in S. cerevisiae. Sci Rep. 2016 Oct 26;6.

245. Lamparter C, Winn LM. Tissue-Specific Effects of Valproic Acid on DNA Repair Genes and Apoptosis in Postimplantation Mouse Embryos. Toxicol Sci [Internet]. 2014 Sep 1 [cited 2019 Dec 29];141(1):59–67. Available from: http://academic.oup.com/toxsci/article/141/1/59/2338108/TissueSpecific-Effects-of-Valproic-Acid-on-DNA

246. Servadio M, Manduca A, Melancia F, Leboffe L, Schiavi S, Campolongo P, et al. Impaired repair of DNA damage is associated with autistic-like traits in rats prenatally exposed to valproic acid. Eur Neuropsychopharmacol [Internet]. 2018 Jan 1 [cited 2019 Feb 28];28(1):85–96. Available from: https://www.sciencedirect.com/science/article/pii/S0924977X17320059?via%3Dihub#bib48

247. Roos WP, Krumm A. Survey and Summary: The multifaceted influence of histone deacetylases on DNA damage signalling and DNA repair. Vol. 44, Nucleic Acids Research. Oxford University Press; 2016. p. 10017–30.

248. Yang Y, Wu N, Tian S, Li F, Hu H, Chen P, et al. Lithium promotes DNA stability and survival of ischemic retinal neurocytes by upregulating DNA ligase IV. Cell Death Dis. 2016;7(11).

249. De Groot T, Alsady M, Jaklofsky M, Otte-Höller I, Baumgarten R, Giles RH, et al. Lithium causes G2 arrest of renal principal cells. J Am Soc Nephrol. 2014 Mar 1;25(3):501–10.

250. Miermont A, Antolović V, Lenn T, Nichols JME, Millward LJ, Chubb JR. The fate of cells undergoing spontaneous DNA damage during development. Dev [Internet]. 2019 [cited 2020 Mar 17];146(12). Available from: http://dev.biologists.org/lookup/doi/10.1242/dev.174268

251. Langie SAS, Azqueta A, Collins AR. The comet assay: past, present, and future. Front Genet [Internet]. 2015 Aug 13 [cited 2020 Mar 17];6(Aug):266. Available from: http://journal.frontiersin.org/Article/10.3389/fgene.2015.00266/abstract

252. Plattner H. Contractile vacuole complex-its expanding protein inventory. In: International Review of Cell and Molecular Biology. Elsevier Inc.; 2013. p. 371–416.

253. Gerald NJ, Siano M, De Lozanne A. The Dictyostelium LvsA protein is localized on the contractile vacuole and is required for osmoregulation. Traffic. 2002;3(1):50–60.

254. Kypri E, Falkenstein K, De Lozanne A. Antagonistic Control of Lysosomal Fusion by Rab14 and the Lyst-Related Protein LvsB. Traffic [Internet]. 2013 May [cited 2020 Jan 4];14(5):599–609. Available from: http://doi.wiley.com/10.1111/tra.12058

255. Shiflett SL, Kaplan J, Ward DMV. Chediak-Higashi Syndrome: A rare disorder of lysosomes and lysosome related organelles. Vol. 15, Pigment Cell Research. 2002. p. 251–7.

256. Motoi Y, Shimada K, Ishiguro K, Hattori N. Lithium and autophagy. Vol. 5, ACS Chemical Neuroscience. American Chemical Society; 2014. p. 434–42.

257. Thellung S, Corsaro A, Nizzari M, Barbieri F, Florio T. Autophagy activator drugs: A new opportunity in neuroprotection from misfolded protein toxicity. Vol. 20, International Journal of Molecular Sciences. MDPI AG; 2019.

258. Frej AD, Otto GP, Williams RSB. Tipping the scales: Lessons from simple model systems on inositol imbalance in neurological disorders. Vol. 96, European Journal of Cell Biology. Elsevier GmbH; 2017. p. 154–63.

259. Schiebler M, Brown K, Hegyi K, Newton SM, Renna M, Hepburn L, et al. Functional drug screening reveals anticonvulsants as enhancers of mTOR-independent autophagic killing of *Mycobacterium tuberculosis* through inositol depletion. EMBO Mol Med [Internet]. 2015 Feb 22 [cited 2020 Jan 4];7(2):127–39. Available from: https://onlinelibrary.wiley.com/doi/abs/10.15252/emmm.201404137

260. Wu S, Zheng S Di, Huang HL, Yan LC, Yin XF, Xu HN, et al. Lithium down-regulates histone deacetylase 1 (HDAC1) and induces degradation of mutant huntingtin. J Biol Chem [Internet]. 2013 [cited 2019 Mar 13];288(49):35604–16. Available from: http://www.jbc.org/

261. Sarkar S, Ph D. Sovan Sarkar, Ph.D. [Internet]. Vol. 2, Autophagy. 2014 [cited 2020 Jan 4]. Available from: http://www.landesbioscience.com/journals/autophagy/abstract.php?id=2387

262. Kenney DL, Benarroch EE. The autophagy-lysosomal pathway. Neurology. 2015 Aug 18;85(7):634–45.

263. Pan T, Kondo S, Le W, Jankovic J. The role of autophagy-lysosome pathway in neurodegeneration associated with Parkinson's disease. [cited 2020 Mar 11]; Available from: https://academic.oup.com/brain/article-abstract/131/8/1969/265065

264. Sarkar S, Floto RA, Berger Z, Imarisio S, Cordenier A, Pasco M, et al. Lithium induces autophagy by inhibiting inositol monophosphatase. J Cell Biol [Internet]. 2005 Sep 26 [cited 2020 Mar 11];170(7):1101–11. Available from: http://www.ncbi.nlm.nih.gov/pubmed/16186256

265. Hnia K, Vaccari I, Bolino A, Laporte J. Myotubularin phosphoinositide phosphatases: Cellular functions and disease pathophysiology. Vol. 18, Trends in Molecular Medicine. 2012. p. 317–27.

266. Marat AL, Haucke V. Phosphatidylinositol 3-phosphates—at the interface between cell signalling and membrane traffic. EMBO J. 2016 Mar 15;35(6):561–79.

267. Axe EL, Walker SA, Manifava M, Chandra P, Roderick HL, Habermann A, et al. Autophagosome formation from membrane compartments enriched in phosphatidylinositol 3-phosphate and dynamically connected to the endoplasmic reticulum. J Cell Biol. 2008 Aug 25;182(4):685–701.

268. Bloomfield G, Traynor D, Sander SP, Veltman DM, Pachebat JA, Kay RR. Neurofibromin controls macropinocytosis and phagocytosis in Dictyostelium. Elife [Internet]. 2015 Mar 27 [cited 2020 Mar 12];2015(4). Available from: http://www.ncbi.nlm.nih.gov/pubmed/25815683

269. Parkinson K, Buttery NJ, Wolf JB, Thompson CRL. A Simple Mechanism for Complex Social Behavior. Keller L, editor. PLoS Biol [Internet]. 2011 Mar 29 [cited 2019 Dec 22];9(3):e1001039. Available from: https://dx.plos.org/10.1371/journal.pbio.1001039

270. Skinner MK, Rawls A, Wilson-Rawls J, Roalson EH. Basic helix-loop-helix transcription factor gene family phylogenetics and nomenclature. Vol. 80, Differentiation. 2010. p. 1–8.

271. Cadigan KM, Waterman ML. TCF/LEFs and Wnt signaling in the nucleus. Cold Spring Harb Perspect Biol [Internet]. 2012 [cited 2019 Mar 15];4(11). Available from: www.cshperspectives.org

272. MacDonald BT, Tamai K, He X. Wnt/beta-catenin signaling: components, mechanisms, and diseases. Dev Cell [Internet]. 2009 Jul [cited 2019 Jun 6];17(1):9–26. Available from:

http://www.ncbi.nlm.nih.gov/pubmed/19619488

273. Zeng Q, Wan Y, Zhu P, Zhao M, Jiang F, Chen J, et al. The bHLH protein Nulp1 is essential for femur development via acting as a cofactor in Wnt signaling in Drosophila. Curr Mol Med. 2018 Feb 14;18.

274. Harwood AJ. Dictyostelium development: A prototypic Wnt pathway? In: Methods in Molecular Biology [Internet]. Humana Press, Totowa, NJ; 2008 [cited 2019 Feb 28]. p. 21–32. Available from: http://link.springer.com/10.1007/978-1-60327-469-2_2

275. Huang HC, Klein PS. The frizzled family: Receptor for multiple signal transduction pathways [Internet]. Vol. 5, Genome Biology. 2004 [cited 2020 Jan 4]. Available from: http://genomebiology.com/2004/5/7/234

276. Cai Z, Wang Y, Yu W, Xiao J, Li Y, Liu L, et al. hnulp1, a basic helix-loop-helix protein with a novel transcriptional repressive domain, inhibits transcriptional activity of serum response factor. Biochem Biophys Res Commun. 2006 May 12;343(3):973–81.

277. Tian Y, Cohen ED, Morrisey EE. The importance of Wnt signaling in cardiovascular development. In: Pediatric Cardiology. NIH Public Access; 2010. p. 342–8.

278. Cohen LS, Friedman JM, Jefferson JW, Johnson EM, Weiner ML. A reevaluation of risk of in utero exposure to lithium. JAMA [Internet]. 1994 Jan 12 [cited 2019 Jun 12];271(2):146–50. Available from: http://www.ncbi.nlm.nih.gov/pubmed/8031346

279. Giles JJ, Bannigan JG. Teratogenic and developmental effects of lithium. Curr Pharm Des [Internet]. 2006 [cited 2019 Jun 12];12(12):1531–41. Available from: http://www.ncbi.nlm.nih.gov/pubmed/16611133

280. Jung PP, Christian N, Kay DP, Skupin A, Linster CL. Protocols and programs for high-throughput growth and aging phenotyping in yeast. PLoS One. 2015 Mar 30;10(3).

281. Mih JD, Sharif AS, Liu F, Marinkovic A, Symer MM, Tschumperlin DJ. A multiwell platform for studying stiffness-dependent cell biology. PLoS One. 2011;6(5).

282. Thompson CRL, Kay RR. The role of DIF-1 signaling in Dictyostelium development. Mol Cell. 2000;6(6):1509–14.

283. Tandon S, Jyoti S. Embryonic stem cells: An alternative approach to developmental toxicity testing. J Pharm Bioallied Sci. 2012 Apr;4(2):96–100.

284. Weigt S, Huebler N, Strecker R, Braunbeck T, Broschard TH. Zebrafish (Danio rerio) embryos as a model for testing proteratogens. Toxicology. 2011 Mar 15;281(1–3):25–36.

285. Panzica-Kelly JM, Zhang CX, Danberry TL, Flood A, DeLan JW, Brannen KC, et al. Morphological score assignment guidelines for the dechorionated zebrafish teratogenicity assay. Birth Defects Res Part B - Dev Reprod Toxicol. 2010 Oct;89(5):382–95.

286. Pardo-Martin C, Chang TY, Koo BK, Gilleland CL, Wasserman SC, Yanik MF. High-throughput in vivo vertebrate screening. Nat Methods. 2010 Aug;7(8):634–6.

287. Michael S, Auld D, Klumpp C, Jadhav A, Zheng W, Thorne N, et al. A robotic platform for quantitative high-throughput screening. Vol. 6, Assay and Drug Development Technologies. Mary Ann Liebert, Inc.; 2008. p. 637–57.

288. Fernandez-Ricaud L, Kourtchenko O, Zackrisson M, Warringer J, Blomberg A. PRECOG: a tool for automated extraction and visualization of fitness components in microbial growth phenomics. BMC Bioinformatics [Internet]. 2016 Dec 23 [cited 2020 Mar 14];17(1):249. Available from: http://bmcbioinformatics.biomedcentral.com/articles/10.1186/s12859-016-1134-2

289. Dimitriou N, Arandjelović O, Harrison DJ, Caie PD. A principled machine learning framework improves accuracy of stage II colorectal cancer prognosis. npj Digit Med. 2018 Dec 2;1(1):1–9.

290. Fort DJ, Stover EL, Farmer DR, Lemen JK. Assessing the predictive validity of frog embryo teratogenesis assay-Xenopus (FETAX). Teratog Carcinog Mutagen [Internet]. 2000 [cited 2020 Jan 11];20(2):87–98. Available from: http://www.ncbi.nlm.nih.gov/pubmed/10679752

291. Alexander-Dann B, Pruteanu LL, Oerton E, Sharma N, Berindan-Neagoe I, Módos D, et al. Developments in toxicogenomics: Understanding and predicting compound-induced toxicity from gene expression data. Mol Omi. 2018;14(4):218–36.

292. Shi X, Du Y, Lam PKS, Wu RSS, Zhou B. Developmental toxicity and alteration of gene expression in zebrafish embryos exposed to PFOS. Toxicol Appl Pharmacol. 2008 Jul 1;230(1):23–32.

293. Zheng M, Lu J, Zhao D. Toxicity and Transcriptome Sequencing (RNA-seq) Analyses of Adult Zebrafish in Response to Exposure Carboxymethyl Cellulose Stabilized Iron Sulfide Nanoparticles. Sci Rep. 2018 Dec 1;8(1):1–11.

294. Shankar P, Geier MC, Truong L, McClure RS, Pande P, Waters KM, et al. Coupling genome-wide transcriptomics and developmental toxicity profiles in zebrafish to characterize polycyclic aromatic hydrocarbon (PAH) hazard. Int J Mol Sci [Internet]. 2019 [cited 2020 Feb 22];20(10). Available from: www.mdpi.com/journal/ijms

295. StockCenter [Internet]. [cited 2020 Feb 26]. Available from: http://dictybase.org/StockCenter/StockCenter.html

296. U.S. Food & Drug Administration. Drugs@FDA: FDA-Approved Drugs [Internet]. U.S. Food & Drug Administration. 2020 [cited 2020 Feb 25]. p. 1. Available from: https://www.accessdata.fda.gov/scripts/cder/daf/index.cfm

297. PubChem [Internet]. [cited 2020 Feb 25]. Available from: https://pubchem.ncbi.nlm.nih.gov/